

# **Radar satellite imagery for humanitarian response**

## **Bridging the gap between technology and application**

### **Dissertation**

der Mathematisch-Naturwissenschaftlichen Fakultät  
der Eberhard Karls Universität Tübingen  
zur Erlangung des Grades eines  
Doktors der Naturwissenschaften  
(Dr. rer. nat.)

vorgelegt von  
Andreas Braun  
aus Bad Saulgau

Tübingen  
2019

Gedruckt mit Genehmigung der Mathematisch-Naturwissenschaftlichen Fakultät der  
Eberhard Karls Universität Tübingen.

Tag der mündlichen Qualifikation:

26-07-2019

Dekan:

Prof. Dr. Wolfgang Rosenstiel

1. Berichterstatter:

Prof. Dr. Volker Hochschild

2. Berichterstatter:

Assoz. Prof. Dr. Stefan Lang



## Abstract

This work deals with radar satellite imagery and its potential to assist of humanitarian operations. As the number of displaced people annually increases, both hosting countries and relief organizations face new challenges which are often related to unclear situations and lack of information on the number and location of people in need, as well as their environments. It was demonstrated in numerous studies that methods of earth observation can deliver this important information for the management of crises, the organization of refugee camps, and the mapping of environmental resources and natural hazards. However, most of these studies make use of -high-resolution optical imagery, while the role of radar satellites is widely neglected. At the same time, radar sensors have characteristics which make them highly suitable for humanitarian response, their potential to capture images through cloud cover and at night in the first place. Consequently, they potentially allow quicker response in cases of emergencies than optical imagery.

This work demonstrates the currently unused potential of radar imagery for the assistance of humanitarian operations by case studies which cover the information needs of specific emergency situations. They are thematically grouped into topics related to population, natural hazards and the environment. Furthermore, the case studies address different levels of scientific objectives: The main intention is the development of innovative techniques of digital image processing and geospatial analysis as an answer on the identified existing research gaps. For this reason, novel approaches are presented on the mapping of refugee camps and urban areas, the allocation of biomass and environmental impact assessment. Secondly, existing methods developed for radar imagery are applied, refined, or adapted to specifically demonstrate their benefit in a humanitarian context. This is done for the monitoring of camp growth, the assessment of damages in cities affected by civil war, and the derivation of areas vulnerable to flooding or sea-surface changes. Lastly, to foster the integration of radar images into existing operational workflows of humanitarian data analysis, technically simple and easily-adaptable approaches are suggested for the mapping of rural areas for vaccination campaigns, the identification of changes within and around refugee camps, and the assessment of suitable locations for groundwater drillings.

While the studies provide different levels of technical complexity and novelty, they all show that radar imagery can largely contribute to the provision of a variety of information which is required to make solid decisions and to effectively provide help in humanitarian operations. This work furthermore demonstrates that radar images are more than just an alternative image source for areas heavily affected by cloud cover. In fact, what makes them valuable is their information content regarding the characteristics of surfaces, such as shape, orientation, roughness, size, height, moisture, or conductivity. All these give decisive insights about man-made and natural environments in emergency situations and cannot be provided by optical images

Finally, the findings of the case studies are put into a larger context, discussing the observed potential and limitations of the presented approaches. The major challenges are summarized which need be addressed to make radar imagery more useful in humanitarian operations in the context of upcoming technical developments. New radar satellites and technological progress in the fields of machine learning and cloud computing will bring new opportunities. At the same time, this work demonstrated the large need for further research, as well as for the collaboration and transfer of knowledge and experiences between scientists, users and relief workers in the field. It is the first extensive scientific compilation of this topic and the first step for a sustainable integration of radar imagery into operational frameworks to assist humanitarian work and to contribute to a more efficient provision of help to those in need.

## Kurzfassung

Die vorliegende Arbeit beschäftigt sich mit bildgebenden Radarsatelliten und ihrem potenziellen Beitrag zur Unterstützung humanitärer Einsätze. Die jährlich zunehmende Zahl an vertriebenen oder geflüchteten Menschen stellt sowohl Aufnahmeländer als auch humanitäre Organisationen vor große Herausforderungen, da sie oft mit unübersichtlichen Verhältnissen konfrontiert sind. Effektives Krisenmanagement, die Planung und Versorgung von Flüchtlingslagern, sowie der Schutz der betroffenen Menschen erfordern jedoch verlässliche Angaben über Anzahl und Aufenthaltsort der Geflüchteten und ihrer natürlichen Umwelt. Die Bereitstellung dieser Informationen durch Satellitenbilder wurde bereits in zahlreichen Studien aufgezeigt. Sie beruhen in der Regel auf hochaufgelösten optischen Aufnahmen, während bildgebende Radarsatelliten bisher kaum Anwendung finden. Dabei verfügen gerade Radarsatelliten über Eigenschaften, die hilfreich für humanitäre Einsätze sein können, allen voran ihre Unabhängigkeit von Bewölkung oder Tageslicht. Dadurch ermöglichen sie in Krisenfällen verglichen mit optischen Satelliten eine schnellere Reaktion.

Diese Arbeit zeigt das derzeit noch ungenutzte Potenzial von Radardaten zur Unterstützung humanitärer Arbeit anhand von Fallstudien auf, in denen konkrete Informationen für ausgewählte Krisensituationen bereitgestellt werden. Sie sind in die Themenbereiche Bevölkerung, Naturgefahren und Ressourcen aufgeteilt, adressieren jedoch unterschiedliche wissenschaftliche Ansprüche: Der Hauptfokus der Arbeit liegt auf der Entwicklung von innovativen Methoden zur Verarbeitung von Radarbildern und räumlichen Daten als Antwort auf den identifizierten Forschungsbedarf in diesem Gebiet. Dies wird anhand der Kartierung von Flüchtlingslagern zur Abschätzung ihrer Bevölkerung, zur Bestimmung von Biomasse, sowie zur Ermittlung des Umwelteinflusses von Flüchtlingslagern aufgezeigt. Darüber hinaus werden existierende oder erprobte Ansätze für die Anwendung im humanitären Kontext angepasst oder weiterentwickelt. Dies erfolgt im Rahmen von Fallstudien zur Dynamik von Flüchtlingslagern, zur Ermittlung von Schäden an Gebäuden in Kriegsgebieten, sowie zur Erkennung von Risiken durch Überflutung. Zuletzt soll die Integration von Radardaten in bereits existierende Abläufe oder Arbeitsroutinen in der humanitären Hilfe anhand technisch vergleichsweise einfacher Ansätze vorgestellt und angeregt werden. Als Beispiele dienen hier die radargestützte Kartierung von entlegenen Gebieten zur Unterstützung von Impfkampagnen, die Identifizierung von Veränderungen in Flüchtlingslagern, sowie die Auswahl geeigneter Standorte zur Grundwasserentnahme.

Obwohl sich die Fallstudien hinsichtlich ihres Innovations- und Komplexitätsgrads unterscheiden, zeigen sie alle den Mehrwert von Radardaten für die Bereitstellung von Informationen, um schnelle und fundierte Planungsentscheidungen zu unterstützen. Darüber hinaus wird in dieser Arbeit deutlich, dass Radardaten für humanitäre Zwecke mehr als nur eine Alternative in stark bewölkten Gebieten sind. Durch ihren Informationsgehalt zur Beschaffenheit von Oberflächen, beispielsweise hinsichtlich ihrer Rauigkeit, Feuchte, Form, Größe oder Höhe, sind sie optischen Daten überlegen und daher für viele Anwendungsbereiche im Kontext humanitärer Arbeit besonders.

Die in den Fallstudien gewonnenen Erkenntnisse werden abschließend vor dem Hintergrund von Vor- und Nachteilen von Radardaten, sowie hinsichtlich zukünftiger Entwicklungen und Herausforderungen diskutiert. So versprechen neue Radarsatelliten und technologische Fortschritte im Bereich der Datenverarbeitung großes Potenzial. Gleichzeitig unterstreicht die Arbeit einen großen Bedarf an weiterer Forschung, sowie an Austausch und Zusammenarbeit zwischen Wissenschaftlern, Anwendern und Einsatzkräften vor Ort. Die vorliegende Arbeit ist die erste umfassende Darstellung und wissenschaftliche Aufarbeitung dieses Themenkomplexes. Sie soll als Grundstein für eine langfristige Integration von Radardaten in operationelle Abläufe dienen, um humanitäre Arbeit zu unterstützen und eine wirksame Hilfe für Menschen in Not ermöglichen.

## Acknowledgements

This work would have not been possible without the support and contributions of many people. Although I cannot name all of them, I still try to name the ones which have had a large impact.

First of all, I want to thank Prof. Dr. Volker Hochschild who gave me the opportunity to work on a dissertation. It took me a considerable time to finish this thesis, but I could always count on his open door and advice regarding my studies and the various facets of academic work. At the same time, I was given the freedom to develop and pursue own ideas and I hope I could live up to the confidence which was placed in me.

Working within the Geoinformatics Group at the University of Tübingen was a pleasure and a great adventure. Although I worked on this topic on my own, I want to thank all my (former) colleagues for their support, interesting collaborations, lots of discussions, and a familiar atmosphere: Adel, Christian B., Christian S., Felix, Gebhard, Geraldine, Hans, Jan, Jeannine, Jörg, Michael, Niklas, Philipp, Silvia, and Zara. Special thanks go to Ted Cahill, a real fighter and all-time source for encouraging thoughts, who substantially contributed to make this thesis more readable.

I also want to thank my international colleagues, mostly from Z\_GIS Salzburg which initiated the research to this topic (within the projects EO4Humen and EO4HumEn+, funded by the Austrian Research Promotion Agency FWF) and invited us to participate: Thank you to Stefan, Dirk, Lorenz, Petra und Barbara, and also Elisabeth and Kristin from the German Aerospace Center (DLR) for the close and fruitful collaboration.

This kind of research is impossible without experts from the humanitarian domain. Most of all, I want to thank Edith Rogenhofer of Médecins Sans Frontières (MSF) Austria who always believed in the potential of radar imagery, even when I sometimes had doubts myself. I also thank Geraint Burrows of Groundwater Relief (GWR), Yann Rebois of the International Committee of the Red Cross (ICRC), and Bassam Qashqo of the Austrian Red Cross (ÖRK) for their interest in our work, lots of discussions, and interesting insights into humanitarian work. You guys do an amazing job!

As the amount of geospatial data grows larger every second, I think it is appropriate to acknowledge the work of thousands of enthusiasts who develop great algorithms and tools like Python, QGIS or SNAP, and anyone who strives to promote open source software and open access science.

I also want to express my deepest gratitude to my parents, the most kind and hardworking people I know, my two sisters, and of course my wife Julia, who all contribute to the comforting feeling of family and home. This also includes my dearest friends from Bad Saulgau and their growing families with whom I shared so much amazing times. The future is ours.

My sincere respect goes out to all the tireless workers in the humanitarian field, and basically any person which sacrifices their time and own safety to help people in need. These are the people who define what 'humanity' is about and I hope this thesis is a little contribution to support their work.

# Table of contents

Lists of figures, tables and abbreviations .....	VIII
<b>1 Introduction .....</b>	<b>1</b>
1.1 Background.....	1
1.2 Need for information .....	5
1.3 Current state of research and identified deficits .....	9
1.4 Questions, aims and structure of this thesis.....	14
<b>2 Radar imagery .....</b>	<b>18</b>
2.1 Basic principles.....	18
2.2 Characteristics of radar images.....	22
2.3 Data processing .....	31
2.4 Sensors, modes, and products.....	37
<b>3 Applications .....</b>	<b>39</b>
3.1 Mapping of refugee camps, infrastructures and their dynamics .....	39
3.1.1 Current state of research and challenges.....	39
3.1.2 High-resolution mapping of camps (Dadaab, Kenya) .....	42
3.1.3 High-resolution mapping of urban areas (Maiduguri, Nigeria) .....	49
3.1.4 Mapping camp growth at different spatial and temporal scales (Kutupalong, Bangladesh).....	55
3.1.5 Mapping rural settlements and infrastructures, (Guéckédou, Guinea & Gambella, South Sudan).....	64
3.1.6 Damage assessment in urban areas (Raqqqa, Syria) .....	71
3.2 Hydrological hazards.....	78
3.2.1 Current state of research and challenges.....	78
3.2.2 Analysis of sea level changes (Bhasan Char, Bangladesh).....	80
3.2.3 Flood mapping (Attapeu, Laos) .....	85
3.2.4 DEM generation for runoff modeling (Kutupalong, Bangladesh) .....	92
3.3 Exploration of resources and environmental monitoring .....	100
3.3.1 Current state of research and challenges.....	100
3.3.2 Groundwater exploration (Kidal, Mali).....	103
3.3.3 Environmental impact assessment (Djabal, Chad) .....	113
3.3.4 Estimation of biomass (Sénégal) .....	123
3.4 Summary of the most important results.....	131
<b>4 Conclusions .....</b>	<b>133</b>
4.1 Potential and limitations of radar data .....	133
4.2 Future challenges and developments .....	140
4.3 Final remarks .....	150
<b>References.....</b>	<b>152</b>
<b>Appendix.....</b>	<b>192</b>

*Note: For the sake of readability, the sub-sections of the chapters in part 2 and 4 are not listed.*

## Lists of figures, tables and abbreviations

### List of figures

Figure 1: Civilians fleeing from violence during the Nord-Kivu conflict in 2008 .....	1
Figure 2: Provision of medical care during the cholera outbreak in Zimbabwe 2008 .....	3
Figure 3: Dimensions of humanitarian aid.....	4
Figure 4: Humanitarian aid needs information .....	5
Figure 5: Kutupalong refugee camp, Bangladesh .....	7
Figure 6: Information needs of humanitarian action which can be met by geospatial technologies .....	8
Figure 7: Structure of this thesis .....	15
Figure 8: Conceptual representation of this thesis.....	16
Figure 9: Study areas used in this thesis .....	17
Figure 10: Side-looking geometry of a synthetic aperture radar (SAR) system.....	19
Figure 11: Relationship between radar backscatter and the configuration of the satellite .....	20
Figure 12: Principle of the synthetic aperture radar (SAR) .....	21
Figure 13: Angular naming conventions in the radar imaging system .....	21
Figure 14: Angular dependence of the radar backscatter coefficient.....	22
Figure 15: Comparison of very high resolution optical and radar imagery.....	23
Figure 16: Geometric distortions in radar images.....	23
Figure 17: Factors influencing backscatter intensity of a pixel .....	24
Figure 18: Different types of scattering mechanisms .....	24
Figure 19: Speckle and texture in radar images .....	26
Figure 20: Horizontal and vertical polarization of an electromagnetic wave .....	26
Figure 21: Polarimetric ALOS-2 image of the city of Maiduguri, Nigeria .....	28
Figure 22: Amplitude and phase of a microwave .....	28
Figure 23: Amplitude (left) and phase (right) information of a radar image .....	29
Figure 24: Principles of spaceborne radar interferometry.....	30
Figure 25: Real and imaginary part of the complex radar information and resulting intensity.....	31
Figure 26: Schematic steps of radiometric calibration of SAR images.....	32
Figure 27: Steps and value ranges of radiometric calibration of SAR images.....	33
Figure 28: Comparison of different filter techniques.....	35
Figure 29: Calibrated image in linear representation (left) and log scale (right).....	35
Figure 30: Effect of geometric terrain correction on areas with pronounced topography.....	36
Figure 31: Effect of geometric terrain correction on flat areas.....	37
Figure 32: SAR imaging modes: ScanSAR, StripMap and Spotlight .....	38
Figure 33: Sentinel-1 image of Mumbai, India, revealing different urban structures.....	41
Figure 34: Study area for dwelling estimates in Dadaab region, Kenya.....	42
Figure 35: Realizations of multi-looking of TerraSAR-X images for dwelling estimation.....	44
Figure 36: Workflow for dwelling estimation for camp Dagahaley, Kenya .....	45
Figure 37: Training (left) and prediction (right) of dwelling density of camp Dagahaley.....	46

Figure 38: Results for dwelling density estimates in Dagahaley, Kenya .....	47
Figure 39: Study area for dwelling density estimations in Nigeria .....	49
Figure 40: Generation of a digital surface model from TanDEM-X data in Maiduguri, Nigeria .....	51
Figure 41: Observed vs. predicted building density .....	52
Figure 42: Anisotropy (red), Alpha angle (green) and Entropy (blue) derived from ALOS-2 data .....	52
Figure 43: Building density for Maiduguri, Nigeria .....	53
Figure 44: Study area for the monitoring of camp growth, Bangladesh .....	55
Figure 45: RGB composite of Sentinel-1 images (left) and corresponding interpretation (right) .....	57
Figure 46: Forest change around Kutupalong between December 2016 and December 2017 .....	58
Figure 47: Temporal changes within camp Kutupalong as identified by VHR SAR color composites.....	59
Figure 48: Size of camp Kutupalong as identified in the Sentinel-1 RGB image.....	60
Figure 49: Spatial distribution of building changes in Kutupalong refugee camp .....	62
Figure 50: RGB composite of three TerraSAR-X images of the refugee camp Minawao, Cameroon .....	63
Figure 51: Study areas for the mapping of rural areas and infrastructures .....	64
Figure 52: Image enhancement by temporal averaging .....	67
Figure 53: Results of the mapping of rural settlements based on SAR images versus optical imagery ..	68
Figure 54: Areas prone to flooding as identified by the SAR RGB composite .....	69
Figure 55: Study area for damage assessment in Syria .....	71
Figure 56: Data sources for building damage assessment in Syria .....	72
Figure 57: Mean backscatter intensity, identified permanent scatterers.....	73
Figure 58: Number of changes identified by UNOSAT (blue) and in this study (black).....	74
Figure 59: Locations of changes identified by UNOSAT (A) and this study (B) .....	75
Figure 60: Change analysis for the Great Mosque, the Raqqa stadium, and the Old Bridge.....	76
Figure 61: Study area for the analysis of sea level changes in Bangladesh .....	80
Figure 62: Temporal statistics and thresholding for the SAR images of the two islands .....	81
Figure 63: Size of the islands because of sea level changes since 1991.....	82
Figure 64: Bhasan Char in 2015 (red), 2016 (green) and 2017 (blue).....	82
Figure 65: Accuracy of selected binary island classification of Bhasan Char (left) .....	83
Figure 66: Study area for flood mapping in Laos .....	85
Figure 67: Sentinel-1 images of the study area before and after the dam break on 24.07.2018.....	86
Figure 68: Schema of the hierarchical histogram splitting.....	87
Figure 69: Validation of flood mapping with various approaches for 25.07.2018 .....	88
Figure 70: Evolution of water masses during July 2018 in southeast Laos .....	91
Figure 71: Study area for elevation extraction in Bangladesh.....	92
Figure 72: Interferogram (top) and coherence (bottom) of TanDEM-X (left) and Sentinel-1 (right) .....	94
Figure 73: Raw interferogram (left), after multi-looking / filtering (middle), and unwrapping (right).....	95
Figure 74: Digital elevation model derived from TanDEM-X interferometry .....	96
Figure 75: Terrain profile of DEMs from TanDEM-X (blue) and SRTM (red) .....	96
Figure 76: Dwellings in camp Kutupalong (February 2018) .....	97
Figure 77: TWI based on SRTM (top) and TanDEM-X (bottom).....	97
Figure 78: Distance above local drainage based on SRTM (top) and TanDEM-X (bottom) [0-10 m].....	97

Figure 79: TWI derived from SRTM (x) and TanDEM-X (y) .....	98
Figure 80: Dwellings potentially vulnerable to flooding based on TanDEM-X InSAR DEM .....	98
Figure 81: Interferogram at an antenna mast in the refugee camp of Kutupalong .....	99
Figure 82: Study area for groundwater assessment in Mali .....	103
Figure 83: Work flow for the systematic derivation of potential water extraction sites .....	104
Figure 84: Data to assist groundwater exploration in Mali .....	106
Figure 85: Geology of Kidal in optical image, geological map and SAR image .....	107
Figure 86: Wadis as shown in the ALOS-2 coherency matrix representation .....	108
Figure 87: Hillshading of SRTM (30 m, left) and TanDEM-X (12.5 m, right) with detected lineaments .....	109
Figure 88: Suggested sites for groundwater drilling .....	111
Figure 89: Study area for the environmental impact assessment in Chad .....	113
Figure 90: Automatically selected training areas for the environmental impact assessment in Chad ....	115
Figure 91: Calculation of the weighted Natural Resource Depletion (NRDw) Index .....	117
Figure 92: Resulting map of weighted Natural Resource Depletion (NRDw) .....	117
Figure 93: Calculation of the variability $v$ of a grid cell .....	118
Figure 94: Spatial representation of weighted natural resource depletion (NRDw) .....	119
Figure 95: Overall weighted natural resource depletion (NRDw) and variability .....	120
Figure 96: Frequency distribution of grid cell variability within the study area .....	121
Figure 97: Study area for biomass estimates in Senegal .....	124
Figure 98: Selected relationships between AGB and radar measures .....	127
Figure 99: AGB maps produced by selected regression methods (Figure 98) .....	128
Figure 100: Change of backscatter intensity (TerraSAR-X ST) in Aleppo during the Syrian civil war .....	151
Figure 101: Temporal operation time of SAR satellite missions .....	198
Figure 102: Pre-processed TerraSAR-X image of Djabal refugee camp, eastern Chad .....	199
Figure 103: OpenStreetMap data in Maiduguri of different editing date .....	201
Figure 104: OpenStreetMap data in Maiduguri of different spatial completeness .....	201
Figure 105: Number of Sentinel-1 GRD products acquired in IW mode .....	202
Figure 106: Changes in camp Kutupalong identified by VHR SAR color composites .....	203
Figure 107: Accuracy map of the supervised forest classification for December 2016 and 2017 .....	204
Figure 108: Road infrastructure and flood extents for Gambella, Ethiopia .....	206
Figure 109: Polarimetric image of the rural areas around Guéckédou, Guinea .....	207
Figure 110: Topographic Map of Kutupalong as provided to MSF within EO4HumEn+ in 10/2017 .....	208

## List of tables

Table 1: Potential of earth observation for humanitarian application.....	9
Table 2: Number of looks for TerraSAR-X StripMap products and resulting spatial resolution.....	34
Table 3: Data sources for dwelling estimation in Dadaab region, Kenya.....	43
Table 4: Parameters for multi-looking the TerraSAR-X images for dwelling estimation.....	44
Table 5: Satellite data used for population monitoring in Maiduguri, Nigeria.....	50
Table 6: Feature space used for building density estimation in Maiduguri, Nigeria.....	51
Table 7: Accuracy assessment for building density estimations with different input data.....	51
Table 8: SAR images used for forest classification in Kutupalong, Bangladesh.....	58
Table 9: Accuracy of the SAR-based classification of forest changes between 2016 and 2018.....	61
Table 10: Number of building changes in Kutupalong refugee camp between 10/2017 and 08/2018.....	61
Table 11: Damage confidence and severity in the reference dataset for damage assessment in Syria.....	73
Table 12: Satellite data used for flood mapping in Laos.....	86
Table 13: Criteria for the selection of image tiles for thresholding.....	87
Table 14: Accuracy assessment for flood mapping in Laos.....	89
Table 15: Dwellings vulnerable to flooding based on TanDEM-X and SRTM elevation models.....	98
Table 16: Radar information used for groundwater assessment in Mali.....	105
Table 17: Satellite data used for the environmental impact assessment in Chad.....	114
Table 18: Target classes and criteria of training areas for impact assessment in Chad.....	115
Table 19: Accuracy Assessment for the environmental impact assessment in Chad.....	116
Table 20: Importance of selected LULC classes for the study area in eastern Chad.....	116
Table 21: Natural resources (NR) and natural resource depletion (NRDw) between 2007 and 2017.....	118
Table 22: Satellite data used for biomass estimations in Sénégal.....	125
Table 23: Correlation analysis between AGB and radar measures.....	126
Table 24: Case studies presented in this thesis.....	131
Table 25: Case studies rated according to information content, requirements and technical aspects....	132
Table 26: Potential and limitations of SAR images for humanitarian operations.....	139
Table 27: Survey on the degree of familiarity with different geospatial data sources.....	192
Table 28: Survey on the opinion of radar remote sensing in a humanitarian context.....	193
Table 29: Optional comments on the use of radar remote sensing in a humanitarian context.....	193
Table 30: Potential of radar imagery as seen by staff in the humanitarian domain.....	194
Table 31: Optional comments on the benefits of radar images.....	194
Table 32: Comparison of SAR imaging modes and their spatial properties.....	195
Table 33: Product levels of SAR imagery.....	200
Table 34: SAR-related capacity development in alphabetical order.....	209
Table 35: Acquisition costs for the tasking of VHR SAR images for the ten largest refugee camps.....	211

## List of terms and abbreviations

ACF	Action Contre la Faim (Action Against Hunger)
AGDC	Australian Geoscience Data Cube
ASI	Agenzia Spaziale Italiana
AVHRR	Advanced Very High-Resolution Radiometer
Beta0	radar brightness [dimensionless]
CC	Creative Commons
cm	centimeter(s)
CAS	Canadian Space Agency
CSG	CosmoSkyMed Second Generation
CSM	CosmoSkyMed
dB	decibel(s)
DEM	digital elevation model
DLR	Deutsches Zentrum für Luft- und Raumfahrt / German Aerospace Center
DSM	digital surface model
EOSDIS	Earth Observing System Data and Information System
EROS	Earth Resources Observation and Science Center
ESA	European Space Agency
ETM+	Enhanced Thematic Mapper Plus
EU	European Union
FFT	fast Fourier transformation
Gamma0	perpendicular backscatter coefficient of a radar target [dimensionless]
GB	gigabyte
GEE	Google Earth Engine
GLCM	grey-level co-occurrence matrix
GRD	ground range detected [image product]
GUF	Global Urban Footprint
ha	hectare(s)
Hispasat	Hispasat Servicios Estratégicos, Spain
HR	high resolution
ICRC	International Committee of the Red Cross
IEEE	Institute of Electrical and Electronics Engineers
InSAR	interferometric SAR
ISO	International Organization for Standardization
ISRO	Indian Space Research Organization
JEODPP	JRC Earth Observation Data and Processing Platform
JRC	Joint Research Centre, Brussels
KARI	Korea Aerospace Research Institute

kg	kilogram(s)
km	kilometer(s)
kml / kmz	keyhole markup language (kmz = compressed)
LiDAR	light detection and ranging
LP DAAC	Land Processes Distributed Active Archive Center
LULC	land-use and land cover
MB	megabyte
MHz	megahertz
NASA	National Aeronautics and Space Administration,
NASDA	National Space Development Agency
NBR	normalized burn ratio
NDVI	normalized difference vegetation index
NEX	NASA Earth Exchange
NGO	non-governmental organization
NRDw	weighted Natural Resource Depletion Index
NSIDC	National Snow and Ice Data Center
m	meter(s)
MITI	Ministry of International Trade and Industry
OCHA	Office for the Coordination of Humanitarian Affairs
OLI / TIRS	Operational Land Imager / Thermal Infrared Sensor
OSM	OpenStreetMap
PCA	principal component analysis
PDF	portable document format
PoSAR	polarimetric SAR
PS	persistent scatterer (also permanent scatterer)
PSI	persistent scatterer interferometry
radar	radio detection and ranging
RCM	Radarsat Constellation Mission
RCS	radar cross section
RGB	red/green/blue
RF	random forest
RMSE	root mean square error
SAR	synthetic aperture radar
Sigma0	backscatter coefficient of a radar target [dimensionless]
SIR-C/X-SAR	Spaceborne Imaging Radar-C/X-band Synthetic Aperture Radar
SLC	single look complex [image product]
SRTM	Shuttle Radar Topography Mission
STA	Science and Technology Agency
SWIR	short-wave infra-red

## Contents

t	ton(s)
TOA	top-of-atmosphere
TWI	topographic wetness index
UAV	unmanned aerial vehicle
UNHCR	United Nations High Commissioner for Refugees
UNITAR	United Nations Institute for Training and Research
UNOSAT	United Nations Operational Satellite Applications Programme
USGS	U.S. Geological Survey
UTM	Universal Transverse Mercator
VDN	vertical distance above local drainage network
VHR	very high resolution
VÖAW	Verlag der Österreichischen Akademie der Wissenschaften
WASH	water, sanitation and hygiene
WGS84	World Geodetic System 1984
WHO	World Health Organization
Z_GIS	Interfaculty department for geoinformatics, University of Salzburg

# 1 Introduction

## 1.1 Background

The world is currently witnessing the highest levels of forcibly displaced people ever recorded. In the year 2018, the United Nations High Commissioner for Refugees (UNHCR) reported over 68 million individuals being either internally displaced within their home country (40 million), refugees hosted by other states (25 million) or people seeking asylum (3 million, UNHCR 2018a). Despite being considered a global phenomenon, 85 % of the displaced people are in developing countries and over half of them are under the age of 18. Still, the 21st century is perceived as the most peaceful period in the history of mankind, at least concerning the frequency, size, and impact of currently experienced warfare (Pinker 2012). In contrast to this global situation, the number of displaced people has increased by 50 % during the last decade, because the security and livelihood of people is being threatened in manifold ways.

While warfare between two or more states has declined since World War II, many regions of the earth face conflicts within larger regions or along borders where societies of different ethnicity, religion or ideology converge. In 2018, two thirds of the currently displaced people came from the Syrian Arab Republic, Afghanistan, South Sudan, Myanmar, and Somalia – all countries with enormous social tensions which have turned into violence (UNHCR 2018b). And although this violence often comes from only small groups or is targeted against authorities and governments, it impacts innocent people who are forced to leave their homes, whereby women, children and elderly are particularly at special risk (Carlin 1990, Figure 1). At the same time, the search for safety and protection has become more dangerous (UNHCR 2018c).



*Figure 1: Civilians fleeing from violence during the Nord-Kivu conflict in 2008  
(Julian Harneis, published on [Flickr](#) under CC BY-SA 2.0)*

Along with armed conflicts which severely threaten the security of local populations, the consequences of climate change and environmental degradation are a substantial trigger for displacement. An increase of both frequency and severity of natural disasters resulting from

weather extremes, such as hurricanes, heavy rains and heat waves, is reported and related to the rise of global temperatures (Helmer & Hilhorst 2006; van Aalst 2006). In addition to this, some parts of the world show a higher susceptibility towards certain disasters, such as volcanism, landslides, and earthquakes (Peduzzi et al. 2009). They result in an increased vulnerability of the population, especially in countries of the Global South where poverty, missing protective measures, and limited mobility lead to reduced disaster resilience of whole communities (Harrison & Williams 2016). And while some parts of the world struggle with recurring storms and flooding, others suffer from hunger and famines, caused by severe droughts, scarcity of drinking water and crop failures (Falkenmark 1990; Goff & Crow 2014).

As a third point, many forms of human activity lead to imbalanced ecosystems, which again threaten livelihoods of whole regions: large-scale deforestation, one the most striking examples of over-exploitation of resources, not only destroys wildlife habitats and reduces carbon sequestration but also increases the risk of flash floods, soil erosion and land degradation (Bradshaw et al. 2007; Newell & Stavins 2000). Also environmental pollution and large-scale land investments deprive people of their livelihoods in many ways (Hunsberger et al. 2015; Westra 2013), giving rise to the term *environmental* or *climate refugees* (Bates 2002; Gemenne 2015).

The previously mentioned developments lead to an increasing demand for humanitarian action<sup>1</sup>, which necessitates material, medical and logistic assistance to people in need. This is provided by a wide range of actors, ranging from global institutions, such as the Office for the Coordination of Humanitarian Affairs (OCHA) of the United Nations, international non-governmental organizations (NGOs), such as the *International Committee of the Red Cross* (ICRC) or *Médecins Sans Frontières* (MSF), to national or regional organizations focusing certain aspects or areas. However, in contrast to its traditional principles of neutrality and impartiality, the intersections between humanitarian and politics have been increasingly debated during the last few decades (Weiss 1999). While some argue that humanitarian relief defines itself as neutral and solidary with anyone who needs help, others see chances in political involvement to provide assistance more effectively, or even to use humanitarian aid within a comprehensive strategy to influence conflicts (Bütthe et al. 2012). Regardless of these definitions, humanitarian relief has become an irreplaceable instrument and mechanism to care for people in miserable situations. Fields of work include:

- **Engineering** which involves the supply of electricity to displaced persons or areas which are remote or hit by disasters. Engineers also provide safe access to drinking water, establish telecommunication systems, develop solutions to handle waste and contaminated ground, as well as assist the planning, development, or restorations ranging from single dwellings to whole camp infrastructures in areas of crisis (Mitcham & Muñoz 2010)
- **Health**-related tasks include the provision of medical care, the application of pharmaceuticals, vaccinations or bandages to persons which are injured, sick or threatened by communicable diseases (Figure 2). Further tasks include psychological assistance to victims of crimes and violence, and the assessment of food security and supply systems to fight malnutrition in developing countries (Spiegel et al. 2010).
- On the side of **technology**, the collection, analysis, and transfer of data is necessary to manage the large amounts of information required within humanitarian operations. This involves the development of database infrastructures for demographic data on the people in need, but also environmental analyses on the availability of natural resources, such as drinking water or fire wood (Darcy & Hofman 2003). These topics are particularly relevant to the content of this thesis

---

<sup>1</sup> In this work the terms *humanitarian aid*, *action*, *response*, *operations* or *relief* are used interchangeably.

- **Management and administration:** A wide-ranging field of applications addresses the organization of humanitarian relief. The development of logistical solutions and supply chains is a key task for the provision of efficient and reliable help. It also involves coordination of staff and their daily work, managing financial resources and funds, as well as training and capacity development to initiate sustainable solutions where people can help themselves in the long term. (Akhtar et al. 2012; Smillie 2001).
- The field of **communication** is responsible for the outreach of humanitarian organizations' activities to maintain support from governments and other institutions and to develop strategies for transferring messages to the public across different kinds of media. It is important to draw the public's attention to the need for help in different parts of the world. Furthermore, transparent reporting ensures the ongoing support from donors.



*Figure 2: Provision of medical care during the cholera outbreak in Zimbabwe 2008  
(Médecins Sans Frontières, published on [Flickr](#) under CC BY-NC-SA 2.0)*

All these tasks require different levels of specialization: While food can be provided by almost any person willing to engage, medical services or disaster relief operations require highly specialized staff. Besides the diversity of its services, humanitarian aid has also a strong spatial component. Some challenges are of global nature, such as the establishment of food security and sustainable livelihoods in areas threatened by droughts or recurring threats, while others are highly focused on regional or even local phenomena, such as the suppression of ethnic minorities. And despite the fact that many NGOs act on an international level, their solutions have to be adapted to local circumstances and beneficiaries (Smirl 2008).

The third dimension of humanitarian relief addresses the period over which help has to be provided. It is closely related to the needs of the people in different situations, as well as to the situation before the conflict or incidence (Longley & Maxwell 2003). It strongly defines how humanitarian aid needs to be established, organized, and funded. It is understood that the challenges in cases of natural disasters or emergencies are mainly focusing upon the short-term security of people, while sustainable supply of food and medical care to displaced people in large refugee camps is rather a long-term task.

Already based on the three dimensions mentioned (degree of specialization, spatial component of the challenges, and temporal component of needs), humanitarian aid ranges within a complex field of challenges with nearly seamless transitions. This field is outlined in Figure 3 as an effort to capture the different aspects which must be considered when talking about humanitarian relief. Of course, it could be expanded by further dimensions, such as the expenses required to provide efficient help in different situations, the degree of complexity of the conflicts and the connectedness to administrative or political decisions. But this shall serve as a coarse outline when it comes to allocating different approaches presented in this thesis within a larger framework.

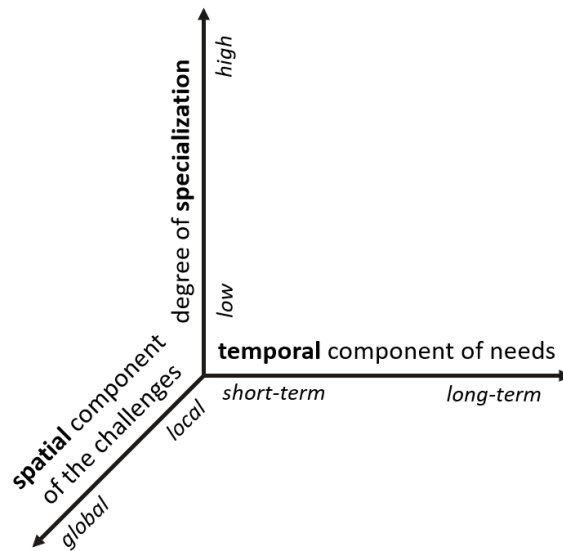


Figure 3: Dimensions of humanitarian aid

Besides secured funding and a well-trained devoted workforce, the availability of reliable and up-to-date information on the situation is one key requirement for successful humanitarian response and to cope with the challenges mentioned above. This requirement results from the need for quick and efficient response in cases of emergency, but also in crowded camps or other situations which are unclear to both the relief workers on the ground and in the coordination bureaus. This will be discussed at more detail in chapter 1.2.

Field surveys are the most straightforward method of assessing this information. However, their application is limited in numerous ways: Collecting data over large areas can be time-consuming and requires large numbers of staff. Especially in emergency situations, this time is often not available (Blackwell & Kaufman 2002). Furthermore, areas exist which are difficult to reach or even dangerous to work in (Fast 2014; Redwood-Campbell et al. 2014). Geospatial technologies have proven to be of significant help when it comes to data collection and management in humanitarian crises (Cowan 2014; MapAction 2011; Zlatanova & Li 2008). But they reach their limits when no spatial data are available (Verjee 2007).

To close this gap, remote sensing has become a valuable source of quick and reliable information retrieval covering large areas. Methods of digital image processing and interpretation are applied to images captured by satellites or aerial photography to characterize phenomena at the earth's surface and to monitor their dynamics with numerous applications in geology (van der Meer et al. 2012), agriculture (Atzberger 2013), vegetation and ecosystems (Xie et al. 2008), soils and landforms (Mulder et al. 2011), natural hazards and disasters (Joyce et al. 2009), urban areas and societies

(Patino & Duque 2013), as well as the mapping of landcover and its dynamics (Hansen & Loveland 2012; Joshi et al. 2016). Its use in a humanitarian context has been increasingly acknowledged (Lang et al. 2018), at first for the observation of crop systems and the management of water resources to ensure food security in drought-ridden regions (Bastiaanssen 1998; Thenkabail et al. 2010), but also in terms of damage assessment in disaster situations, such as flooding, volcanoes, and earthquakes (Dell'Acqua & Gamba 2012; Tralli et al. 2005; Yamazaki 2001). An extensive description of the current scientific progress is given in section 1.3.



Figure 4: Humanitarian aid needs information

Left: UNICEF planning water pumping for a refugee camp in Jordan (DFID, published on [Flickr](#) under CC BY 2.0)

Right: Coordination of the distribution of shelter kits in Lebanon (EU AID, published on [Flickr](#) under CC BY-SA 2.0)

Despite their large potential for humanitarian aid and disaster relief, the analysis of traditional optical satellite images is often limited by the presence of clouds and their shadows on the ground (Giles 2001; Pearce 1985; Wulder et al. 2008). This reduces their suitability for humanitarian applications which rely on the time-critical delivery of information, for example during emergency response (Boccardo & Tonolo 2015; Joyce et al. 2009). Furthermore, the development of operational services, that is the repeated application of procedures on data to receive consistently updated information, strongly relies on data which is not occasionally covered by clouds (Moser et al. 2017).

To overcome this constraint, sensors emitting microwaves have been developed which are able to penetrate atmospheric layers to image the earth's surface from space (Ulaby et al. 1981). Because of their wavelength, these signals are no longer dependent upon daylight which makes them a valuable source for the constant acquisition of images. Furthermore, these emitted signals are sensitive to surface characteristics of objects at the ground, which often reveals information on their properties which are complementary to the optical spectrum. All these advantages make them excellent for the assistance of humanitarian work, but yet, their application in this field is still limited because of data processing challenges and a lack of evidence for their use in practical examples (Braun & Hochschild 2017b). This thesis intends to demonstrate the potential of synthetic aperture radar (SAR, explained in detail in part 2) in a comprehensive set of humanitarian applications. The overall questions and aims are defined in chapter 1.4

## 1.2 Need for information

There are many ways to describe the variety of needs for information within the complex field of humanitarian response. As shown in Figure 3, the temporal component of the needs plays an

important role because it strongly defines what kind of help is of greatest importance at different stages of a crisis. Lang et al. (2018) distinguish between three main phases which are briefly introduced in the following.

#### **a) Pre-disaster and preparedness**

Before the outbreak of human conflicts or natural disasters which can potentially lead to humanitarian crises, it is important to know about the status-quo. The most frequently mentioned information in this context is the number of people living in a specific area, because it is directly related to the resources required to provide help for everyone in need (Darcy & Hofman 2003; MapAction 2011; Verjee 2007). Besides demographic baseline data, the condition of urban areas (Monaco 2014) and infrastructures (Verjee 2005) before their destruction in cases of earthquakes, floods, or armed conflicts is of crucial importance, because this baseline data is needed to estimate the severity of the impact. Thirdly, the state of the natural environment is a valuable indicator for the capacity of ecosystems and their vulnerability when impacted by natural disasters or a sudden increase in population (Langer et al. 2015).

However, as humanitarian aid is mainly oriented as a response to certain incidents or developments leading to critical situations, this aspect is easily neglected. Darcy & Hofman (2003) report that “in the aftermath of rapid-onset disasters, there is frequently an absence of adequate baseline data against which to measure the impact of the disaster” and first response is largely based on experience from previous cases, making it relatively ineffective.

In such situations, remote sensing can serve as an invaluable information source, because images collected by satellites are stored in archives which can be browsed for specific points in time. Thus, even if nothing is known about an area at the time of an incident, the archived imagery can still reveal much about its prior condition. These can then be compared to post-disaster images which are often provided free of charge by satellite image providers operating within international agreements (Jones et al. 2015).

Lastly, the aspect of early warning plays a role in humanitarian action when it comes to the prevention of escalating conflicts or natural events turning into a catastrophe (Lang et al. 2018). Observing developments which threaten the security of people reduce the number of people affected or the expected impact of the disaster. Again, remote sensing can be used to assess the risk which people are exposed to, this is often defined as the product of hazard and vulnerability (Darcy & Hofman 2003). Geospatial techniques can assist the prediction of famines by monitoring vegetation stress and crop systems from space, (Thenkabail et al. 2012) or the assessment of flood-prone areas in urban agglomerations and refugee camps (Jain et al. 2005).

#### **b) Crisis monitoring and humanitarian action**

After initial relief is provided in the case of emergencies, for example by medical care or the setup of relief camps, humanitarian work meets new challenges. As public institutions and basic services often collapsed in areas of crisis, the challenges are then to setup and consolidate daily working routines, and to ensure well-structured provision of care and accommodation (Weiss & Collins 2018). Concretely speaking, this includes the assessment of food security and nutrition, which is either provided based on locally available goods or from outside sources through logistical efforts. Knowledge on potential groundwater drilling sites or the spatial distribution of natural resources can support strategic decisions when it comes to the rapidly supplying the needs of large numbers of displaced persons (Davis & Lambert 2007). Furthermore, large gatherings of people always involve the risk of spreading communicable and waterborne diseases. Ensuring access to water,

sanitation and hygiene (WASH) can clearly reduce these risks, but also requires information on the local setting (Nicole 2015). That is, the number and demography of these people, the feasibility of technical solutions, and also the characteristics of the site. As stated in the WASH manual, “maps are particularly useful to analyze disease outbreak data (case mapping), and to determine gaps in WASH service coverage” (UNHCR 2018e).

The mapping of the camps and their environment is therefore of crucial interest to many relief workers because knowledge on population estimations and the spatial distribution of services can assist strategic decisions on supply, medical care, camp management and expansion, and makes relief work more effective. Davis & Lambert (2007) name factors for the identification of suitable sites for new refugee settlements, among others the area of potential sites, accessibility, topography, soil types, or proximity to existing settlements. These are based on mapping and a ranking of these factors which is to be defined by the users. And as reported by Xu et al. (2015), maps can even assist participatory community building in refugee camps.

Unlike permanent urban areas, refugee camps are constructed in cases of emergencies or even emerge at random locations when people are forcibly displaced from their homes (Hailey 2009). This can lead to circumstances in which authorities and relief workers lose control of the situation because of the multitude of scattered makeshift dwellings on unsteady ground, and lack of basic road networks or landmarks (Figure 5). Additional needs for information include energy supply, infrastructure management, waste disposal, logistics, civil protection, and land use (Papp & Barclay 2018; van den Noortgate & Maes 2010), which can be partly or fully provided by methods of remote sensing.



*Figure 5: Kutupalong refugee camp, Bangladesh  
(John Owens/VOA, public domain)*

### c) Medium-term and long-term effects and prospects

Although humanitarian action is mainly defined as short-term intervention to save lives or reduce human suffering, many argue that aspects of stability and sustainability have to be considered as well, once a critical situation is under control (Darcy & Hofman 2003; Tamminga 2011). Among the most evident tasks, the monitoring of populations, camp sizes and corresponding patterns

migrations in the region of operation (Ehrlich et al. 2009). The UNHCR handbook on emergencies declares constant population fluctuations as a major challenge in the long-term management of a camp and states “Knowing the size and profile of the refugee population is essential for an efficient and cost-effective operation” (UNHCR 2007).

And although the situation of the people should have improved when relocated to a reception or shelter camp, their vulnerability towards natural hazards or further violence is still high because of light construction materials, limited mobility and dense population patterns (Jansen 2008; Lischer 2005). Assessing these risks by mapping these threats and hazards is a key need for a secure and sustainable environment for displaced people (Verjee 2005).

Closely related to this task is the need for information on the natural environment around the camps and shelters. Not only can they serve as valuable sources for firewood, drinking water, and the gathering of food (Barbieri et al. 2017; Wilson 1992), but also it is necessary to monitor the ecosystems as these are reported to suffer under large-scale population flows (Suhrke 1994). The environmental impact of refugees was originally discussed by Jacobsen (1997) and Lonergan (1998), and Kakonge (2000) was one of the first to proclaim for the need for an impact assessment related to displaced persons. Also, Davis & Lambert (2007) list “environmental conditions” in their practical guide for relief workers as part of the health-related information to be collected. A survey among 21 persons involved in humanitarian action conducted by Z\_GIS Austria and MSF Austria affirmed a high demand on information related to environmental impact (Füreder & Rogenhofer 2014).

Lastly, the environment plays a role when it comes to the dismantling of camps and the recultivation of areas once occupied as makeshift camps. The WASH guidelines on camp closure name environmental degradation and contamination as points to remediate (UNHCR 2014) and the Global Camp Coordination and Camp Management Cluster suggests protection measures, such as access restrictions for conservation areas, the planting of trees and clean-up activities to care for minimum impact and the initiation of gentle transitions after dismantling of the camps (CCCM 2014).

Figure 6 summarizes the most important aspects of this chapter.

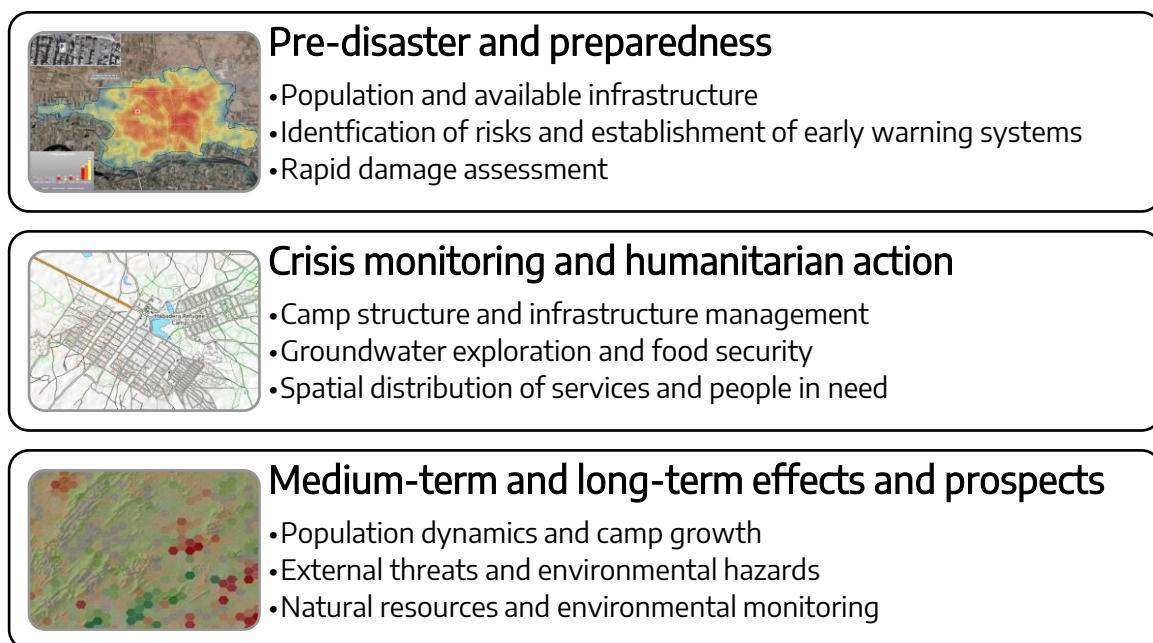


Figure 6: Information needs of humanitarian action which can be met by geospatial technologies  
Image sources from top to bottom: UNITAR (2017b), OpenStreetMap, and Braun & Hochschild (2017a)

### 1.3 Current state of research and identified deficits

As already indicated in the previous sections, methods of earth observation can be of large help in humanitarian crises of different spatial and temporal dimensions. This chapter briefly describes the scientific progress and recent advancements within this domain focusing special emphasis on the use of radar remote sensing. It serves as a framework for this thesis and prepares the definition of present gaps and challenges. More detailed descriptions of the respective fields of study are given at the beginning of each section in chapter 2.4.

Lang & Füreder (2015) identified five main benefits of remote sensing imagery in the field of humanitarian action, which are summarized in Table 1:

*Table 1: Potential of earth observation for humanitarian application  
Adapted from Lang & Füreder (2015)*

Asset	Potential for humanitarian action
Distance	Retrieval of information without accessing impassable terrain or dangerous sites Objective information source which provides an overview of situations Cost-effective method compared to data collection in the field (surveys, measurements)
Area & Detail	Control over the level of detail (spatial and temporal resolution) Uniform data over large areas High level of detail, if desired at the sub-meter scale
Time	Retrospective view on pre-disaster situations Monitoring of dynamics at regular intervals Remote sensing imagery for validation of information collected in the field
Availability & usability	Globally available data grants a consistent observation process Time-efficient and reliable data provision with fast and easy access Visual interpretation can be conducted by laymen

#### 1.3.1 Remote sensing for the mapping of unclear situations

As one of the first in this field, Kelly (1998) names remote sensing as a potential resource to provide an overview of refugee camps. He demonstrates how a video taken from an airplane helped to understand the location, size and condition of the displaced population in a camp in Liberia. When violent conflicts broke out in April 1996, humanitarian efforts were hampered by a lack of security and information, and safe access was not possible. As a further usefulness, he lists the counting of houses, the allocation of potential roads and landing sites, and the identification of crops which all helped operational and strategic planning for later relief. Based on the value of this information, the overall costs less than 6000 US dollars (for the camera and the rental and staff of the plane) were considered “a very good deal”. Also Beaudou et al. (1999) name “aerial videography and GIS” as an important tool for the development of a cartographic database for the refugee camp of Dadaab region in Kenya. Already in 1995, Gupta discussed the potential and risks of satellite imagery for international politics and mentions the opportunity to “filter fact from fiction in some types of eyewitness and government reports” (Gupta 1995).

In all of these studies mentioned, the main benefit is the quick, secure and reliable overview of an unclear setting for an effective preparation of humanitarian relief. While aerial imagery was considered superior because of its higher spatial resolution, the expenses of flight campaigns

remained. Fortunately, spaceborne imaging systems soon reached similar levels of detail and they gained importance in this domain: Einar Bjørgo can be considered a pioneer in this domain and introduced very high-resolution (VHR) satellites as a new source of information in humanitarian relief operations (Bjørgo 1999). He mentions cloud cover as a major challenge in time-critical situations, as well as the duration until an acquired image is cleared for commercial distribution, preprocessed, and disseminated to relief staff. Using multispectral images of the Russian satellite KVR-1000, he mapped camps, villages, roads, and water sources around the Qala en Nahal refugee settlement in southeast of Khartoum (Bjørgo 2000a) as well as the size and different infrastructures of Thailand's Site 2 refugee camps near the Thai-Kampuchean border (Bjørgo 2000b). He furthermore identified a statistical relationship between the size of a camp, as retrieved by satellite imagery, and its population using ground reference data. All of his studies stressed the need for commercially available real-color images with spatial resolutions at the meter scale. Today, Einar Bjørgo is the manager of the UNOSAT program at the United Nations Institute for Training and Research which provides imagery analysis and satellite solutions to relief and development organizations (UNITAR 2013).

Giada et al. (2003) used IKONOS imagery at a spatial resolution of 1 meter for the visual interpretation and classification of tents in the Lukole refugee camp in Tanzania. Their work served as a base for the estimation of the number of hosted refugees and further maps of the camp.

The first ones to mention spaceborne radar imagery in a humanitarian context were Johannessen et al. (2001) in their report on camp monitoring and landcover mapping by remote sensing. Their case studies were the border region between Albania and Macedonia (Kosovo war), southeastern Nepal (around 90,000 Bhutanese refugees) and northeastern Kenya (Dadaab region). While most of their work is based on Landsat, SPOT and IKONOS imagery, they mention ERS, the first radar satellite of the European Space Agency (ESA, see chapter 2.4), underlining its independence from cloud cover and need for daylight, as well as its comparably low price. They name the identification of camps and settlements, the mapping of forests, and the generation of digital elevation models by radar interferometry (section 3.2.4), but only few examples based on radar images are given. Further reported constraints at this time were image interpretation and copyright restrictions.

Not explicitly referring to humanitarian action, but providing an automated approach using radar imagery, Haack & Slonecker (1994) used a combination of images from Landsat and Shuttle Imaging Radar-B (SIR-B), to locate villages along the Blue Nile in Sudan. Their aim was to supplement outdated maps which were only available at a scale of 1:250,000. The high backscatter of man-made structures was stated as a large advantage, especially because it also revealed features which were smaller than the spatial resolution of the sensor (12.5 meters). Related to this idea is the study of Prins (2008) who used Landsat data to identify burnt villages between 2003 and 2004 during the Darfur conflict in Sudan. As major benefits, he names low image acquisition costs and a safe and reliable overview, but a validation has not been carried out because of the poor security situation.

Recent developments in the use of satellites to gain an understanding of situations include the object-based processing of VHR images of refugee camps based on developed rule-sets (Füreder et al. 2012; Spröhnle et al. 2017), machine learning (Ghorbanzadeh et al. 2018; Quinn et al. 2018; Sulik & Edwards 2010), and template matching (Laneve et al. 2007; Tiede et al. 2017).

To increase the level of objectivity and replicability, a shift can currently be observed away from visual inspection, such as manual counting of refugee dwellings (Checchi et al. 2013), to more transferable and automatable ways of processing which can be integrated in operational services (Tiede et al. 2013; Tiede et al. 2010). However, operational services are still rare, and the field of radar remote sensing is widely neglected for camp mapping.

A completely different aspect worth mentioning here is explored by Marx & Goward (2013) who analyze how satellite images can be used to detect international humanitarian law violations. Nearly 15 years after Bjørge's (1999) request for quicker delivery of ready-to-use image products, they confirm that it is still one of the major limitations.

### 1.3.2 Mapping and monitoring environments around refugee camps

The role of satellite remote sensing for the observation of natural landcover is most common applications and widely investigated (Colwell 1968; Melesse et al. 2007; Xie et al. 2008). However, there are only a few studies which demonstrate its potential in a humanitarian context.

Kariuki et al. (2008) provide a detailed study on the allocation of woodland and other natural resources around the camp Kakuma in South Sudan. They used Landsat images between 1985 and 2005 to investigate the presence and health of vegetation, including its distance from the camp to aid in the determination of its potential utilization.

Addressing one of the most basic needs, Wendt et al. (2015; 2014) give explicit recommendations on the allocation of groundwater resources in humanitarian settings, by systematically investigating the local topography, geology, and regional water flows in satellite images. They mention the role of radar images for the identification of soil moisture variations and the derivations of digital elevation models, but no examples are given.

A popular research topic is the investigation of environmental impacts of migration: Lodhi et al. (1998) quantify changes in landcover in Siran Valley, Pakistan, where over 100,000 refugees were settled in the 1980s. They used optical imagery of Landsat and a digital elevation model for a classification of landcover, which proved a decline of forests by 40 % between 1979 and 1993.

Similar studies based on optical imagery were presented for other areas affected by the presence of refugees by Beaudou & Cambrézy (1999; Dadaab region, Kenya), Ndyeshumba (2000; Ngara district, Tanzania), Tachiiri & Ohta (2004; camp Kakuma, Kenya), Hagenlocher et al. (2012; Darfur region, Sudan), and Rossi et al. (2018; Dadaab region, Kenya).

A wider view is given by Stängel et al. (2014) and Langer et al. (2015) who use multi-temporal imagery to describe the state of the environment before and during the presence of the refugee camp Lukole in Tanzania, but also its regeneration after the closing and dismantling of the camp.

The only studies on analyzing environmental impacts of refugee camps based on radar imagery are provided by the author of this thesis (Braun et al. 2016b; Dadaab region, Kenya, and Braun & Hochschild 2017a; camp Djabal, Chad; presented in chapter 3.3.3).

Studies focused on changes to water resources are presented by Al-Adamat et al. (2003) and Müller et al. (2016) who use satellite imagery to demonstrate the decline of groundwater resources in Jordan as a consequence of over-exploitation, mainly related to the displacement of persons resulting from the prolonged conflicts in the Middle East.

### 1.3.3 The role of radar remote sensing

As shown in the two previous sections of this chapter, radar remote sensing has not been commonly associated with humanitarian relief so far. There are studies which use the technique to derive information which are of relevance in this domain, but they mostly address a different audience. In the following, the few studies with a humanitarian focus are chronologically mentioned to narrow down the reason for the underrepresentation of spaceborne radar in this field. However, again, it has to be noted that a detailed presentation of the use of radar images in different fields of study is given at the beginning of each chapter within part 3 of this work.

Wegmüller et al. (2002) provided the first comprehensive view on radar remote sensing as an alternative to optical data in humanitarian relief. They name independence from cloud cover, costs and additional information content as main advantages compared to multispectral sensors. Also, the capability of steering the antenna helps to acquire larger areas within shorter time frames which can be important for time-critical tasks. Similar to the various application fields given in Table 1, they distinguish between rapid mapping, hazard mapping and thematic mapping, as well as comparing the capabilities of different SAR sensors available at this time (mainly ERS and ENVISAT, see section 2.4). They recognize the under-representation of radar in this domain and conclude that “steps to improve the awareness and acceptance of SAR based information are to present the products in a better accessible form and to train the users in the interpretation of the specific products, as well as the understanding of the potential and limitations”.

Amitrano et al. (2013) also directly discuss opportunities brought by imaging radar for humanitarian purposes. Their focus lies on the potential of multi-temporal analyses which were facilitated by freely available data from the upcoming Sentinel-1 mission (launched in 2014, see chapter 2.4) and increasing open access to archived data. They present short case studies on land cover mapping, crop monitoring, seasonal water body mapping and the extraction of a digital elevation model for the Tougou Basin, Burkina Faso. With data being available at no cost, they see one major obstacle removed for their application by humanitarian organizations which allows more funds to remain available “for the formation of local expertise” (Amitrano et al. 2013).

Other studies name radar imagery as a tool for applications related to humanitarian emergencies, such as the disaster and crisis management support related to landslides (Voigt et al. 2007), lava flows, floods, or earthquake-induced deformation (Vassileva et al. 2017), but also humanitarian demining (Sato et al. 2008) and the protection and monitoring of archaeological sites and cultural heritage (Cigna & Tapete 2018; Tapete & Cigna 2017; Tapete et al. 2013).

### 1.3.4 Gap analysis and research deficits

As shown in the previous section, only a few case studies exist which highlight the use of SAR images in a concrete humanitarian setting. The reasons, although often of practical nature, are closely connected to the design, objective, and communication of current research. The following list gives an overview of the main gaps between scientific practice and in-house application by humanitarian relief organization and names the general research deficits identified behind these gaps. A more detailed discussion on research deficits in different application domains will follow in chapter 2.4.

**Complexity:** *Differing from optical data, radar images are based on microwave backscatter and therefore are “somewhat less intuitive to be interpreted by nonexperts” (Voigt et al. 2007).*

- ➔ The interpretation of radar images and scattering mechanisms is not sufficiently covered in current scientific discourse.
- ➔ Their additional information value needs to be demonstrated in tangible studies which directly address the practical relevance for humanitarian settings. This includes the identification of dwellings for population estimates, the identification of natural hazards and risks, the quantification of land degradation, and the monitoring of resources which are relevant to the camps.
- ➔ Beyond radar backscatter, the use of interferometric and polarimetric information present in the data is widely neglected for the assistance of humanitarian operations.

**Processing:** *Conducting analyses of large amounts of radar data requires financial and computational resources, as well as staff which is trained to work with this kind of data.*

- Only a few studies focus on new developments, such as cloud computing, open-source software and big data solutions which provide a cost-effective and easy access to large datasets (Sudmanns et al. 2018b).
- Many published studies are based on extensive scientific research which is, by definition, rather singularly aimed at results of high quality than at an immediate delivery of information, as needed for time-critical decisions in cases of emergency.

**Scale:** *The spatial resolution of radar images is still lower than that of optical imagery. The presence of additional noise-like patterns (speckle, see chapter 2.2) reduce the degree of detail in the images, thus lowering their attractiveness for the humanitarian community.*

- No solutions are provided to deal with comparably low spatial resolution of radar images or speckle effects in images of refugee camps or their surroundings.
- In turn, studies using very high-resolution (VHR) radar imagery are mostly focused on technical aspects and fail to demonstrate the results in comprehensive maps.
- Generally related to remote sensing analyses, a mismatch can often be observed between the spatial resolution of the used imagery and the required level of detail of the resulting output maps (both too high and too low, Lang et al. 2015).

**Communication:** *Although studies exist in various fields of applications, the potential of SAR data for humanitarian purposes is still not fully acknowledged and it is more commonly perceived as an “all weather” replacement for optical data than an independent source with its own advantages (Verjee 2005, indicated by answers of the survey in Appendix 1).*

- The potential of information present in radar images (polarimetric and interferometric information, and image texture, see chapter 2.2) is not sufficiently communicated in studies within the humanitarian domain.
- Not enough case studies exist which are tailored for humanitarian settings and mention the potential and limitations. Existing studies are often additionally hindered by technical language.
- Many studies focus on the derivation of information and fail to discuss their value for possible application. Furthermore, the aspect of putting the results into a geographic perspective is often neglected.

**Procedure:** *Even if the technical expertise is available within organizations, many studies report hurdles related to data collection, data management and data sharing (Bjørge 1999; Cowan 2011; Verjee 2005). The transfer of case studies to be integrated in humanitarian work is slow. Prins (2008) reports that “three years after this pilot study was initiated, no large scale remote sensing monitoring of villages or a comprehensive map of burnt villages in Darfur is available”*

- An operational framework of data acquisition, preparation and delivery within an acceptable period of time is required for the methods to be effective.
- Image provision is not only a technical challenge, but also involves questions regarding licensing and internal organization. No holistic research has yet been conducted encompassing the whole chain between the sensor and the final information available to the user.

Based on these first conclusions, the aims of this thesis are defined in the next chapter.

## 1.4 Questions, aims and structure of this thesis

As demonstrated in the previous chapter, current scientific approaches fail to sufficiently provide suitable solutions for the application of radar imagery in a humanitarian context. The gap identified between scientific expertise in this domain and their exploitation within relief operations results from the fact that most of the published studies cannot directly be transferred into humanitarian practice. To close, or at least reduce, this gap this work intends to...

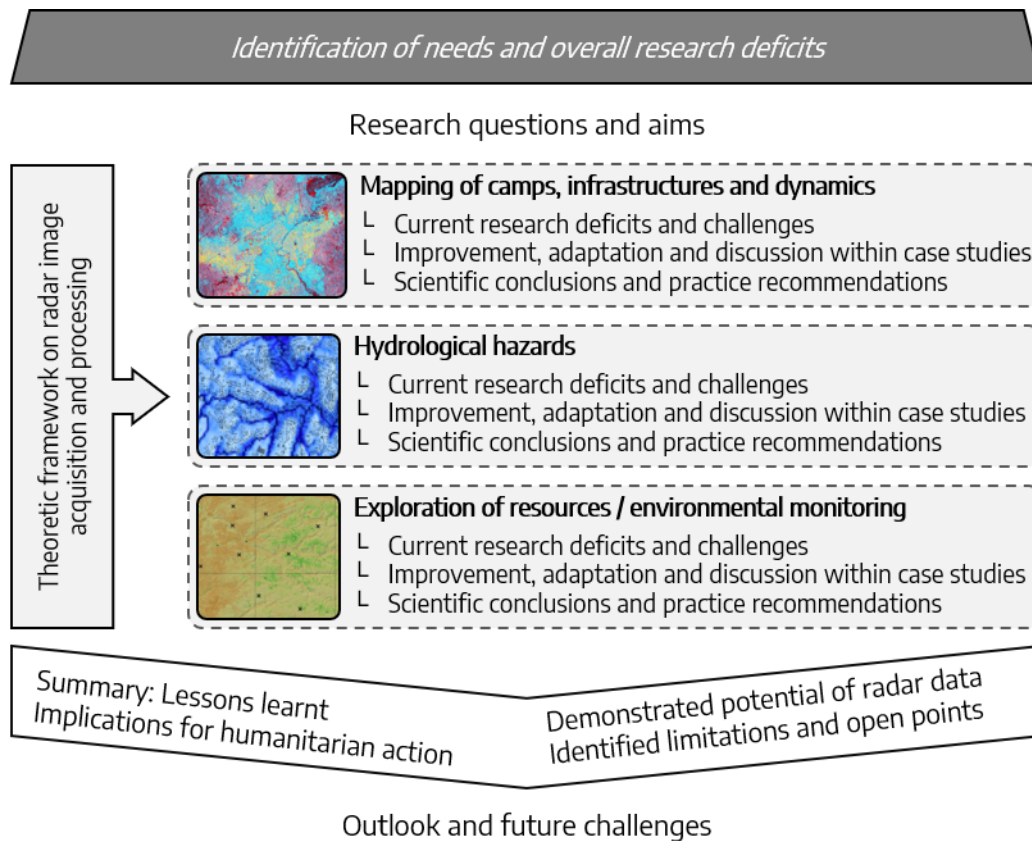
- ... **identify** the current state of research for a clearer understanding of currently existing gaps between science and application,
- ... **reduce** technical and terminological barriers by laying a solid and understandable foundation of theoretical background on radar remote sensing,
- ... **develop** novel and innovative methods within case studies of different complexity and spatial scale for the most important applications field of humanitarian relief operations,
- ... **continue, adjust and improve** current scientific expertise, by integrating challenges arising within of humanitarian settings,
- ... **demonstrate** both the potential and limitations of SAR for the humanitarian domain enabling a better communication of possibilities and expectations,
- ... **initiate** the development of operational routines which can be integrated into humanitarian practice, based on the findings from the case studies, and
- ... **conclude** with an evaluation of the current situation, including future perspectives, unsolved challenges and upcoming developments.

In other words, the research questions of this work ask why the well-investigated field of radar remote sensing is widely neglected in humanitarian relief operations to date. Despite the fact that there are numerous studies on their general application in all types of fields, their contribution to humanitarian aid is still distinctively smaller than the one of optical imagery which is already an elemental part of operational services. Continuing the indications from chapter 1.3, this question is raised again in part 3 of this thesis, where research gaps in different application domains are inspected more concretely.

By the use of cases studies which deal with the identified gaps, this work furthermore asks about the potentials and limitations of radar remote sensing. While the information content of microwave images can be of decisive advantage (clearly beyond the factor of independence from cloud cover), it also brings new hurdles and problems. Both will be carefully addressed for different application fields within this work, while considering their potential for integration into operational procedures. The final question addresses the remaining gaps which were not closed within this thesis, why they were not yet closed, and what is needed in the future to address them in a technical or organizational perspective. It is furthermore to be answered how future developments, which are beyond the scope of this work, can contribute to an improved integration of radar remote sensing for the provision of relevant information for humanitarian relief operations.

Accordingly, this work has three main outcomes:

1. The initiation of a **scientific discourse** on the integration of radar remote sensing in humanitarian operations.
2. The development of innovative, adapted, and technically improved **solutions**, according to the gaps identified in currently available studies (locations shown in Figure 9).
3. The provision of an **entry point** for actors in the humanitarian domain to actively take part in the use of radar imagery, thus stimulating the **interdisciplinary discussion** between scientists and users to improve the help for people in need.



defined. Based on this, case studies are presented which provide solutions to these gaps and challenges. These studies either present new methods or take up related approaches and refine or extend them to address the identified challenges. They are uniformly structured in sections ('background and aims', 'data sources and processing', 'results and discussion' and 'conclusions'). The approaches and results are discussed regarding their scientific quality and applicability in emergency situations. At the end of each case study, the most important aspects are summarized, followed by recommendations and practical implications.

**Part 4** summarizes the findings and evaluates the overall findings of the study and comparatively reviews the presented studies regarding the potential and limitations of SAR data in different application domains. Taking into account the results from the survey, currently identified barriers, expectations and future challenges are discussed. These considerations are summed up with an outlook on future developments to define open tasks to be tackled by both scientists and users of radar imagery.

Figure 8 is an alternate illustration of the structure of this thesis and how it is embedded in a larger framework. Parts 0 and 2 mainly analyze the current situation and investigate why radar remote sensing is not yet integrated into humanitarian action very much. Applications in part 3 provide solutions for the identified challenges and draws initial conclusions on potentials and limitations.

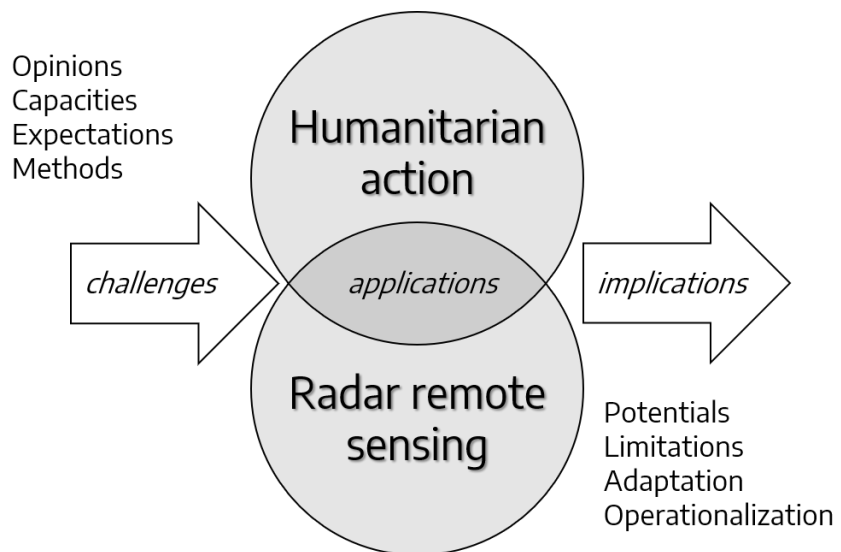


Figure 8: Conceptual representation of this thesis

These are then summarized in Part 4 which discusses the implications of the findings for the future use of radar imagery in the humanitarian domain.

Figure 9 shows the spatial distribution of the case studies selected for this thesis. Although concentrated on the African continent, they provide a variety of humanitarian settings within different landscapes and cultural backgrounds.

Different types of data are used in this thesis which are shortly attributed in the following.

- **TerraSAR-X** and **TanDEM-X** data were provided by the German Aerospace Center (DLR) within PI proposals LAN0625, LAN2391 and DEM\_OTHER1346.
- **Sentinel-1** and **Sentinel-2** data were provided by the European Space Agency (ESA) within the Copernicus program.
- **ERS-1/2** and **ENVISAT ASAR** data were provided by the European Space Agency (ESA) within proposal 29831.
- **ALOS PALSAR** and **ALOS-2** data were provided by the Japan Aerospace Exploration Agency (JAXA) for the PI proposal PI3059 within RA-6.
- **Landsat** and **SRTM** data were provided by the Earth Resources Observation and Science (EROS) Center of the US Geological Survey (USGS).

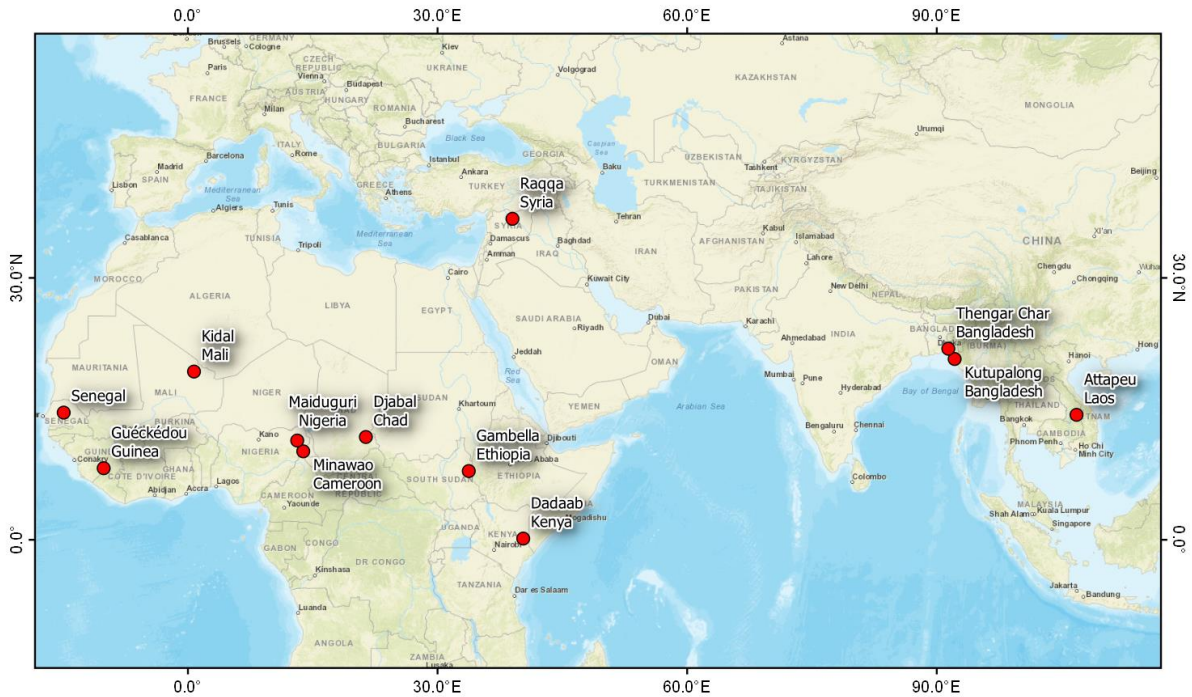


Figure 9: Study areas used in this thesis

*Disclaimer: Base maps throughout this thesis were created with World Topo Map by ESRI. ArcGIS® and ArcMap™ which are the intellectual property of ESRI and are used herein under license. Copyright © ESRI. All rights reserved. Sources: ESRI, DeLorme, HERE, TomTom, Intermap, increment P Corp., GEBCO, USGS, FAO, NPS, NRCAN, GeoBase, IGN, Kadaster NL, Ordnance Survey, Esri Japan, METI, ESRI China, swisstopo, MapmyIndia, and the GIS User Community.*

As some of the work in this thesis is based on jointly published documents, the contribution of each author for the respective chapters is shortly mentioned in the following:

- Groundwater exploration in Mali (section 3.3.2): Based on an internal project document by Geraint Burrows [GB], Andreas Braun [AB] and Lorenz Wendt [LW] (2017): **Briefing Note – water supply in Kidal, Mali. EO4HumEn+ report from 20.05.2017.** GB collected and provided the field reference data and gave the final recommendations for new groundwater extraction sites based on his hydrogeological expertise. LW processed and analyzed all optical data, AB processed and analyzed all SAR data. All authors jointly collaborated in writing the report.
- Environmental impact assessment in Chad (section 3.3.3): Based on a research article by Andreas Braun [AB] and Volker Hochschild [VH] (2017a): **A SAR-Based Index for Landscape Changes in African Savannas, published in Remote Sensing 9 (4), 359-382.** AB and VH designed the study. AB processed and analyzed the data and wrote the article.
- Estimation of biomass (section 3.3.4): Based on a research article by Andreas Braun [AB], Julia Wagner [JW] and Volker Hochschild [VH] (2018): **Above-ground biomass estimates based on active and passive microwave sensor imagery in low-biomass savanna ecosystems., published in Journal of Applied Remote Sensing 12 (4), 46027.** All authors designed the study. AB processed, analyzed and interpreted the data and wrote the article. JW prepared the raster and biomass data, conducted the regressions and assisted the writing process.

## 2 Radar imagery

### 2.1 Basic principles

Within the domain of spaceborne earth observation, satellites capturing radar imagery hold a unique position. Not only do they operate at wavelengths on the order of 1 to 100 cm, which are approximately 100,000 times larger than those of optical measurements (chapter 2.2), but also do they provide an active signal which is emitted by the sensors. The portion of this signal returning from a surface to the radar antenna is measured in order to form an image (Ulaby et al. 1981). This fundamental difference brings numerous consequences and implications for the formation, processing, and analysis of the acquired images. These are presented and largely discussed within the scope of this work, but in this chapter some basic concepts are introduced to help accommodate that.

#### 2.1.1 Physical background

The acronym ‘radar’ stands for ‘radio detection and ranging’ which implies that microwaves (also ‘radio waves’) are used to measure the distance between a sensor and an object by emitting an electromagnetic signal and receiving its reflection (Olshen 2016). Given that radar waves propagate at the speed of light, the time required by the signal to return can be used to calculate the distance  $R$  as described in equation 1:

$$R = \frac{1}{2} ct \quad (1)$$

where  $R$  is the range,  $c$  is the speed of light, and  $t$  is the time of propagation (Skolnik 1980). The factor  $\frac{1}{2}$  is determined by the fact that the signal travels this distance twice, once to reach the object and once to return to the sensor.

The measurements of active radar satellites are based on the principle that an antenna systematically transmits pulses of radio waves to the earth’s surface and records their returned signal. While the satellite moves, its relative position to a location of interest changes, thus inducing a variation in frequency, also known as the Doppler shift (Andrade 1959). Successively recording and processing radar echoes of single targets from multiple antenna positions allows the formation of a two-dimensional image via the returned signals (Richards 2009). However, this has strong implications regarding the acquisition geometry of the operating system: If a spaceborne sensor were to send a microwave beam to earth from the nadir angle, all signals would return at the same time, thus hindering the exploitation of the Doppler shift. Active radar systems therefore must operate in a side-looking geometry such as demonstrated in Figure 10. The flight direction is called azimuth and the look direction is called range. The look angle of this side-looking aperture largely varies between 20 and 45 degrees, but can also lie outside this range in special configurations

The main unit of radar images is the intensity of the signal returning to the sensor. Based on the nature of electromagnetic radiation, large parts of the signal can be absorbed by surfaces, reflected in other directions or scattered away from the sensor (Moghaddam & Saatchi 1995). All signals which are returning towards the sensor are called the backscatter or radar cross section (RCS), as a measure of the reflective strength of a target on the ground. It is often normalized against the area illuminated by the signal to retrieve the backscatter coefficient  $\Sigma$  (also  $\Sigma_0$  or  $\sigma^0$ ).

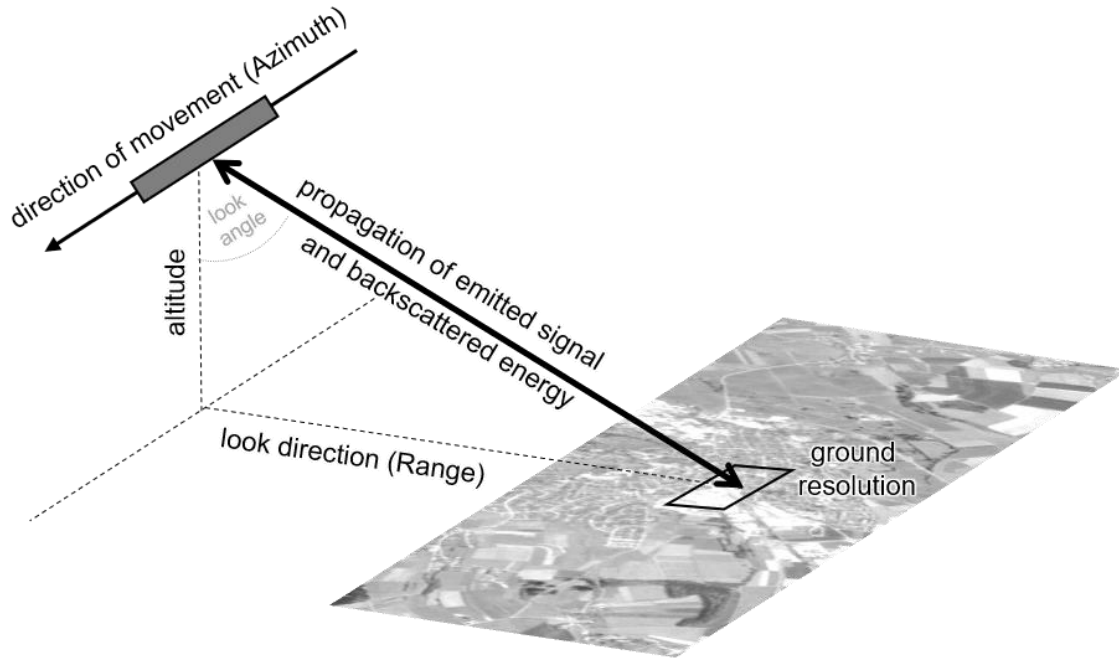


Figure 10: Side-looking geometry of a synthetic aperture radar (SAR) system

The radar range equation (equation 2) (Ulaby et al. 1981) defines the power received at the sensor  $P_r$  as follows:

$$P_r = \frac{P_t G_t A_e \sigma}{(4\pi)^2 R_t^2 R_r^2} \quad (2)$$

where

$P_t$  is the transmitted power,

$G_t$  is the gain of the transmitting antenna (IEEE 1993),

$G_r$  is the gain of the receiving antenna (IEEE 1993),

$A_e$  is the effective aperture (the area of the antenna,  $\frac{G_r \lambda^2}{4\pi}$ ),

$\lambda$  is the transmitted wavelength,

$\sigma$  is the backscatter coefficient (Sigma0),

$R_t$  is the distance between the transmitting antenna and the target (equation 1), and

$R_r$  is the distance between the target and the receiving antenna (equation 1).

The different elements are visualized in Figure 11. In the case of monostatic configurations where the transmitting and receiving antennas are identical ( $R_t = R_r$  and  $G_t = G_r$ ) they can be reduced to  $R^4$  and  $G^2$  respectively. To express the radar backscatter coefficient of a single pixel as a function of transmitted and received energy, equation 2 can be rewritten as follows:

$$\sigma^0 = \frac{(4\pi)^3 R^2 [m]}{A P_t G^2 \lambda^2 [m]} \quad (3)$$

It is dimensionless and ranges between 0 (no returned signal) and 1 (fully isotropic scatterer) for most surfaces but can be extensively larger in cases of double-bounce or volume scattering (section 2.2.1). That is why it is often transformed into log-scale, also leading to optimized contrasts in the image (demonstrated in Figure 29) by the following equation:

$$\sigma^0 [dB] = 10 \log_{10} \sigma^0 [m^2/m^2] \quad (4)$$

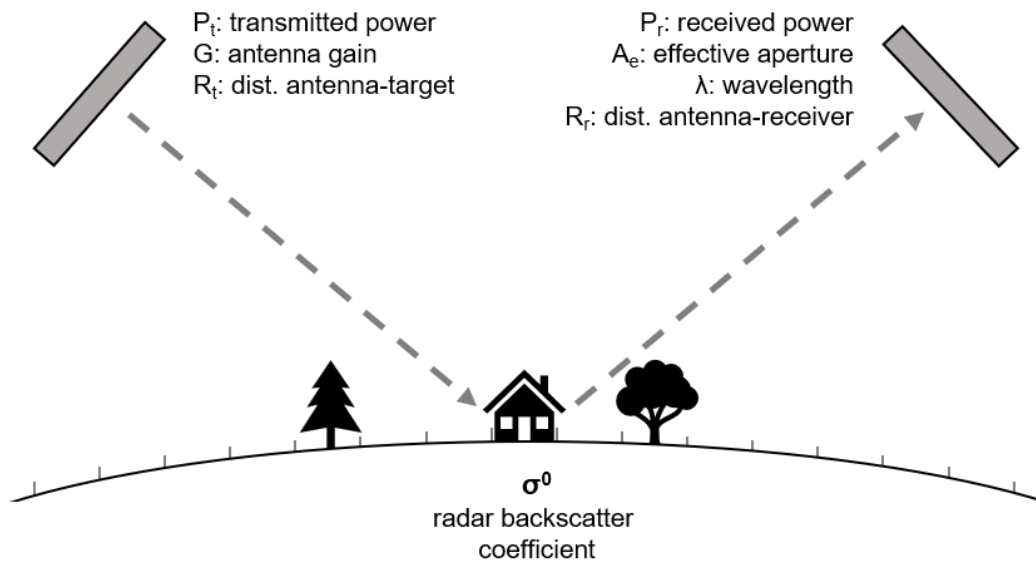


Figure 11: Relationship between radar backscatter and the configuration of the satellite

The spatial resolution at which a sensor can detect different objects on the ground is dependent upon the intervals at which the different signals return. If the spatial distance between two targets is too small their echoes overlap, and they cannot be separated in the received signal. To overcome this technical limitation, the so-called chirp waveform is used, a linear modulation of the frequency within one pulse which allows the sensor to correlate the returning signals against replicas of the emitted ones and to allocate them very precisely in time (Richards 2009). This chirp technique provided a breakthrough for radar measurements because it significantly increased the resolution in range direction, which is determined by the wavelength and the incidence angle. The resolution in azimuth direction is additionally limited by the altitude of the satellite the length of the antenna. As the altitude of a spaceborne radar satellite cannot be decreased significantly, active radar imaging systems are physically constrained to a very low azimuth resolution. To overcome this limitation, the concept of the synthetic aperture radar (SAR) was introduced (Brown 1967): As the satellite moves forward, targets are detected multiple times by the radar beam (Figure 12). Hereby, backscattered signals undergo an azimuth Doppler shift which is constant along the range towards higher frequencies as a target is approached and towards lower frequencies when a target is gradually left behind (Skolnik 1980). The antenna of the satellite is therefore used at multiple locations along the azimuth track and therefore synthetically extended to a multiple of its actual length, allowing the system to measure objects at azimuth and range resolutions at the meter scale. In modern SAR systems, steering mechanisms of the antenna were developed to furthermore reduce this resolution to the sub-meter scale (Mittermayer et al. 2014). In order to derive a common pixel from range and azimuth resolution, multi-looking is applied (section 2.3.2).

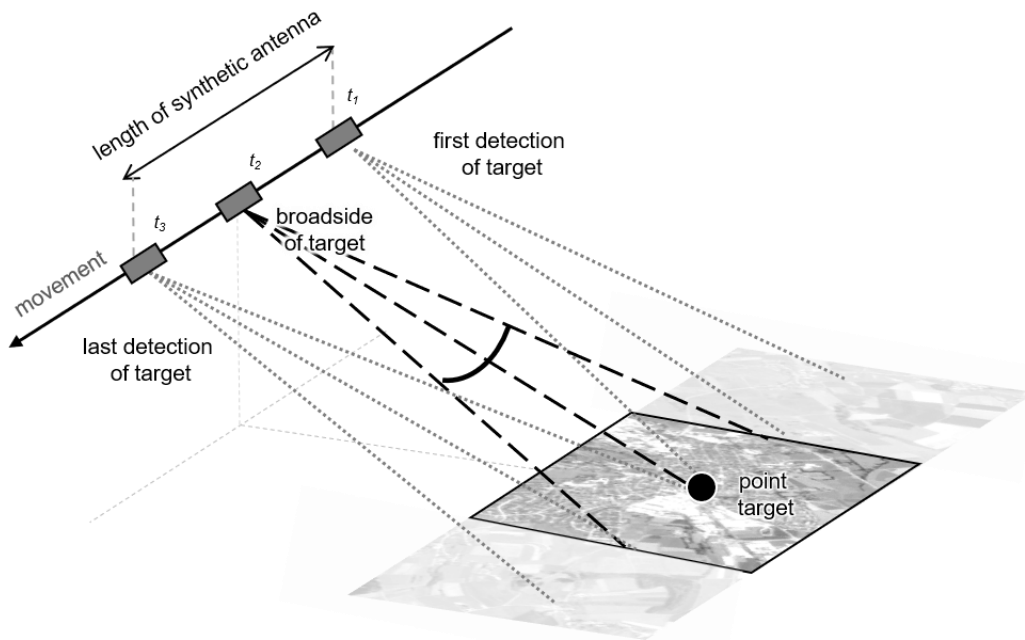


Figure 12: Principle of the synthetic aperture radar (SAR)

### 2.1.2 Imaging geometry

As presented in the previous chapter, the active nature of the radar sensor is the reason for the side-looking geometry of the imaging system. The angle at which a signal reaches the earth's surface varies according to the altitude of the satellite and its configuration, but also to the local topography. As demonstrated in Figure 13, the incidence angle is defined as the angle between the incoming radar signal and the normal of a surface (Lusch 1999). Consequently, a large incidence angle means a more pronounced side-looking aperture and thus, more extreme geometric distortions. Generally, the term incidence angle is typically used for referring to the angle between the sensor and the normal of the earth's ellipsoid, while the local incidence angle refers to the actual topography of a surface (Skolnik 1980). In cases where a slope directly faces the incoming radar beam, the local incidence angle is zero and the signal reaches the surface at 90 degrees.

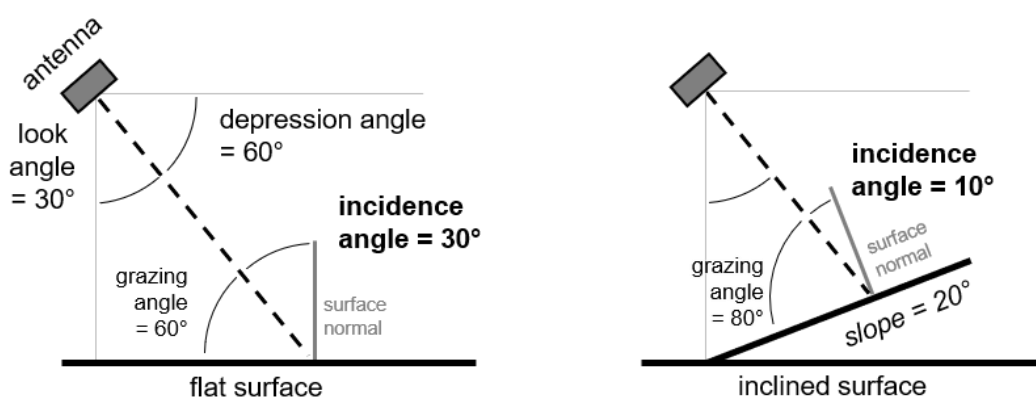


Figure 13: Angular naming conventions in the radar imaging system

Because of the large footprint of a radar image, which can reach up to 400 km (ENVISAT ASAR WS mode, see chapter 2.4), surfaces closer to the sensor (the near range) have a smaller incidence angle than more distant ones (in the far range). As the intensity of radar backscatter is directly influenced

by the incidence angle (Gauthier et al. 1998, Figure 14), a proper calibration of the images is to be performed before any analysis (section 2.3.1).

In addition to the backscatter variations in range direction along a plain, local topography directly influences the backscatter of a surface, regardless of its coverage or physical nature (for the dependency of backscatter from surface characteristics see section 2.2.1). As demonstrated in Figure 14, areas with a large local incidence angle appear generally darker than areas directly facing towards the sensor.

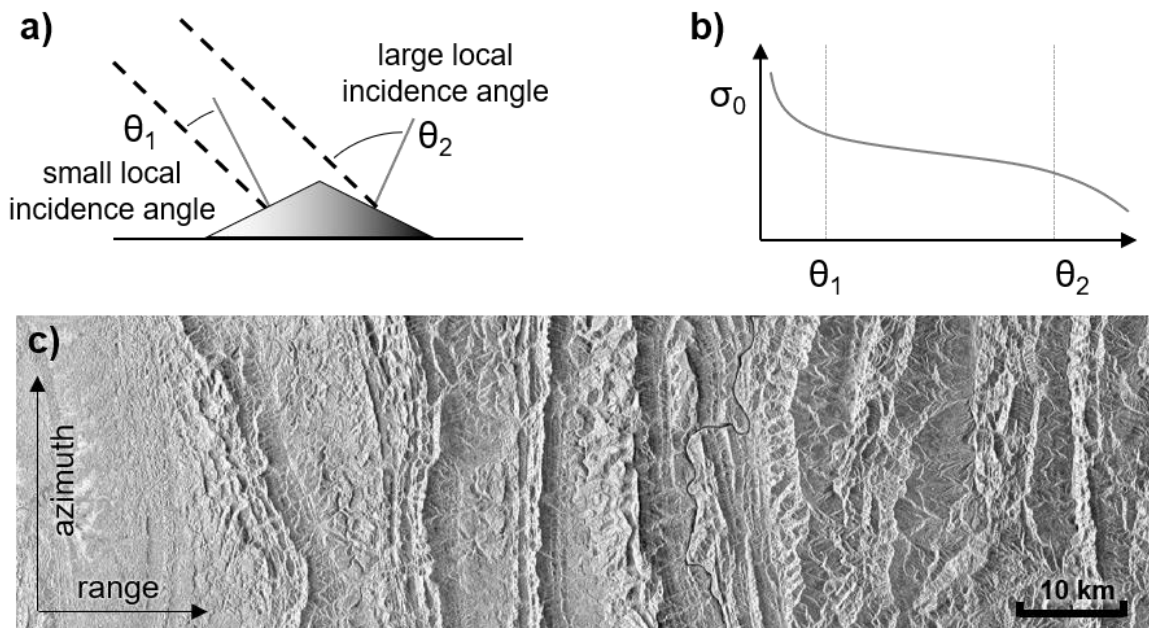


Figure 14: Angular dependence of the radar backscatter coefficient

a) and b) Schematic effects of local incidence angle. c) Uncalibrated TerraSAR-X scene (ScanSAR mode, subset) in the area of the Kutupalong refugee camp, Chittagong Division, Bangladesh. Note the overall decrease of backscatter in range direction (incidence angle) and the radiometric distortions caused by topographic features.

## 2.2 Characteristics of radar images

Both optical and radar remote sensing share the common principle of measuring the reflection or scattering of incident energy from features at the earth's surface. However, because of the active image acquisition principle of radar satellites, there are also substantial differences. In addition to the comparably flat looking angle which causes radiometric and geometric distortions as presented in the previous section, radar images are usually acquired at one single wavelength, thus consist of only one band, namely a grey-tone image of backscatter intensity (Figure 15). While this may seem to be a limitation at first, the advantages of radar imagery become evident in frequently cloud-covered regions, which are, on average, about 52% of the land surfaces according to the US Department of Energy (Warren et al. 1986). Because of the high wavelength of the electromagnetic radiation, clouds can be penetrated by the signal to a very large degree (Ulaby et al. 1981). Additionally, as the sensor brings its own energy, images can be acquired independently from sunlight, which brings more flexibility regarding daytime and seasonal variations of provided solar illumination (Skolnik 1980). These facts are to be considered when selecting suitable imaging systems, especially for urgent or time-critical observations.

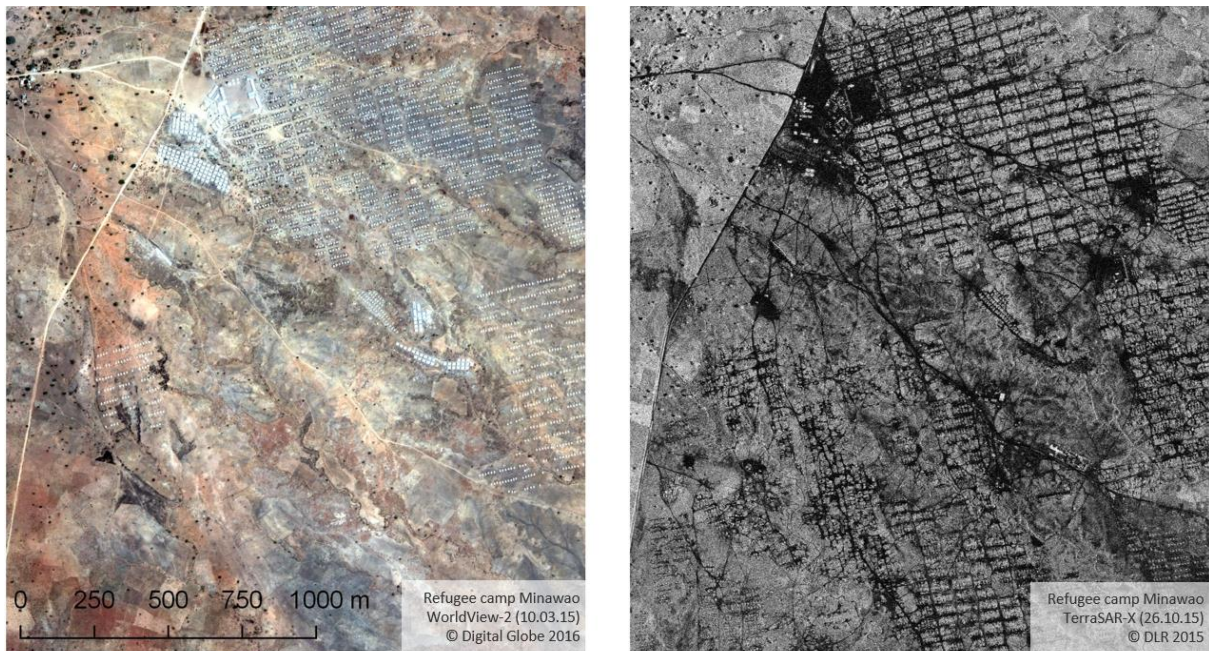


Figure 15: Comparison of very high resolution optical and radar imagery WorldView-3 (left) and TerraSAR-X (right) images of Minawao refugee camp, northern Cameroon

## 2.2.1 Geometric effects

Besides the radiometric distortions of a radar image caused by the incidence angle as described in section 2.1.2, surface topography has strong effects on the location of targets in the initial image (van Zyl et al. 1993). Because the propagation of the transmitted signals and their registration at the sensor occur at a temporal scale, the formation of the images is initially measured in the so-called slant range. It is defined as the diagonal along which the signals propagate between the sensor and the target (Skolnik 1980). Figure 16 demonstrates the three main types of geometric distortions which are caused by variations in topography: If the signal reaches the top of an elevated surface before it reaches its foot slope, it returns to the sensor earlier, thus leading to a shift towards the sensor which is called ‘foreshortening’. The distance between the top and the foot of the hill is then reduced in the radar image. In the case of even more extreme landforms and given incidence angles, the signal returning from the top can be registered at the sensor before the signal of the foot slope which leads to an inversion of the slope facing towards the sensor (‘overlay’). If the inclination of the backslope of a landform exceeds the angle of the incoming radar wave, there can be areas which are not reached by the signal at all. Areas where no measurement is possible are called radar ‘shadow’.

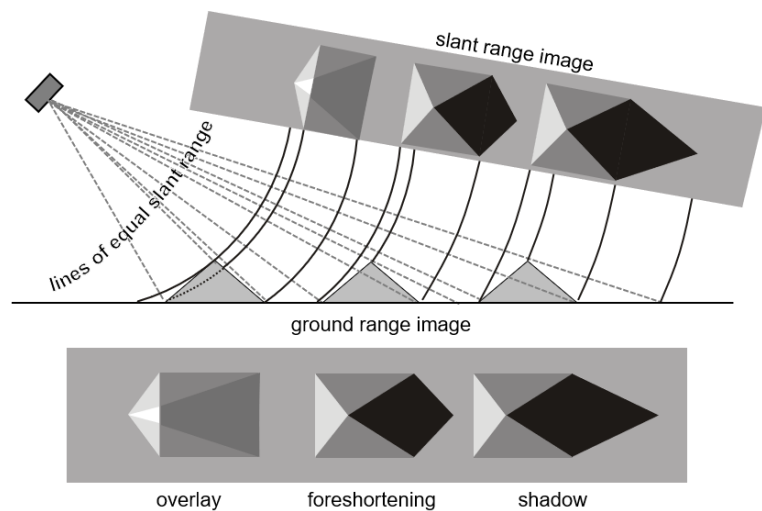


Figure 16: Geometric distortions in radar images  
Adapted from Lillesand et al. (2008)

While the effect of foreshortening can be partly corrected during the preprocessing by converting the slant range image into ground range geometry (section 2.3.2), information in areas of overlay and shadow are considered lost.

Both radiometric and geometric distortions must be considered when processing and interpreting radar data. One main prerequisite for their correction is the availability of a digital elevation model (DEM) of high quality and spatial resolution (sections 2.3.1 and 2.3.3).

## 2.2.2 Scattering mechanisms

Scattering of electromagnetic radiation is defined as any change of the characteristics of propagation as a cause of physical interaction with other media (Long 1983). As a property of the high wavelength of active imaging radars, the transmitted energy is partly able to penetrate materials. Accordingly, the two main interactions between radar signals and surfaces are either absorption or reflectance. Both are dependent from a variety of

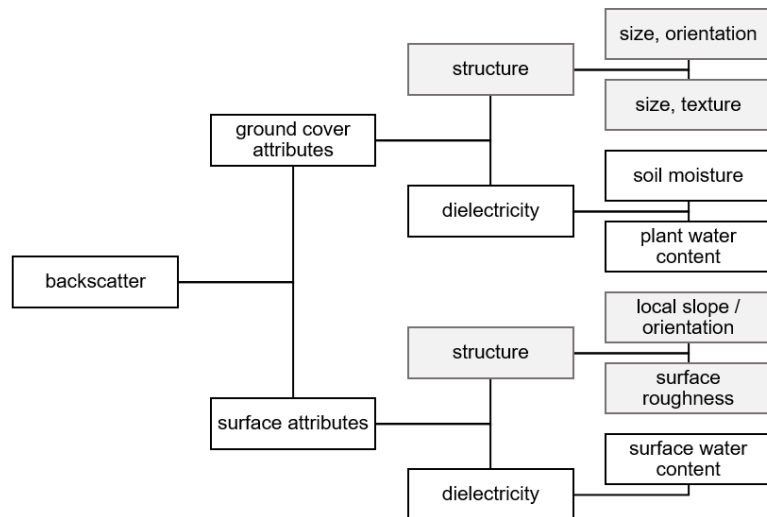


Figure 17: Factors influencing backscatter intensity of a pixel

determining factors which can be summarized in two groups, structure and dielectricity. As shown in Figure 17, the backscatter intensity which is retrieved from a pixel is not explicitly explained by a single variable but rather expressed as the sum of different contributing factors.

As wet materials have higher conductivity and dielectricity, their interaction with the radar signal is more intense which leads to proportionally higher backscatter. This applies to both surfaces with comparably higher soil moisture as well as plants with higher volumetric water content (Ulaby et al. 1986). The influence of moisture on SAR backscatter is hard to measure and makes visual interpretation of SAR images very hard. This influence has been investigated in numerous studies (Danklmayer et al. 2009; Engman & Chauhan 1995; Wang & Qu 2009).

The structural part of backscatter variation is even more diverse and can be divided into three main categories: surface, volume, and dihedral or hard target scattering (Richards 2009, Figure 18).

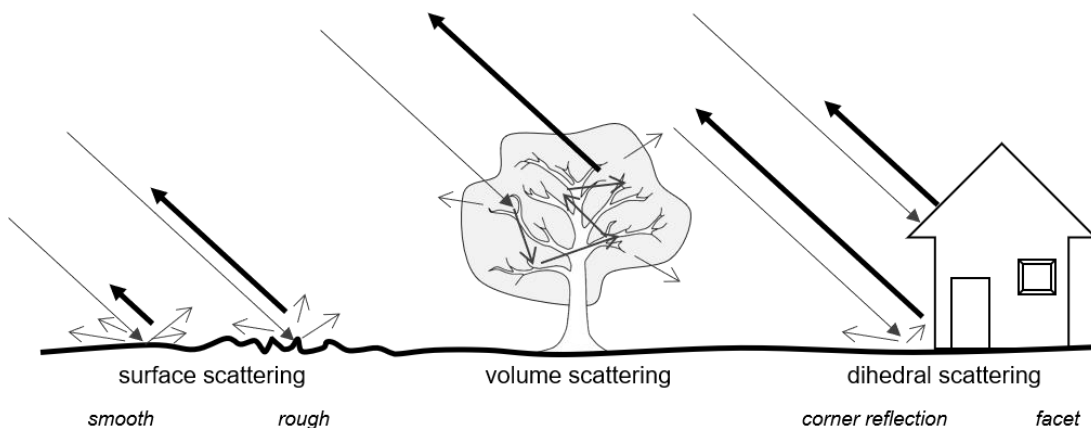


Figure 18: Different types of scattering mechanisms

The most common form of surface scattering is the simple reflection of a smooth surface. As a larger proportion of the signal is mirrored in other directions, backscatter of smooth surfaces is comparably low, and these areas appear dark in the SAR image. In contrast, slightly rough surfaces produce higher backscatter because they contain specular components which reflect larger parts of the signal back to the sensor (Ulaby et al. 1978). Very high roughness, for example formed by coarse gravel or tilled cropland, will produce highly diffuse scattering where the proportion of signals in the direction of the sensor is even higher (Derooin et al. 1997).

Besides dielectricity, the roughness of a surface is the main contributing factor of the backscatter of a plain surface (Benallegue et al. 1995). A special form of high backscatter is volume scattering, which is mostly caused by complex structures of vegetation, such as tree canopies or dense branches, but also by sea ice or dry soils. Volume scattering occurs when backscattered energy is collectively contributed by many individual scatterers of a medium (Daida et al. 1996). Because of this, the backscattered signal of such surfaces often clearly exceeds that which was originally transmitted by the sensor, thus leading to  $\sigma_0$  values larger than 1. This is also the case for hard target scattering where the orientation of mostly man-made objects, such as buildings or electric pylons, but also large trees, causes extraordinarily high return rates. This happens either because of a so-called corner reflection with vertical structures (e.g. walls) where the incoming signal undergoes a double-bounce and fully returns to the sensor or when the orientation of an artificial structure substantially reduces the local incidence angle (e.g. roofs of houses, see section 2.1.2). This becomes especially evident in urban environments (Dong et al. 1997).

As indicated by Figure 17, these various factors which are increasing or decreasing backscatter intensity can coincide, especially for vegetated areas or dry surfaces where the radar signal slightly penetrates dry soil and interacts with embedded dielectric discontinuities (Richards 2009).

### 2.2.3 Speckle and image texture

As a result of the coherent nature (the narrow spectral width) of the emitted radar signal, most surfaces in a SAR image show granular brightness variations, even over homogenous areas (Goodman 1976). This so-called speckle effect is often falsely described as noise but is actually highly systematic (Xia & Sheng 1996). It originates from the fact that many different scattering mechanisms exist within the area of a sensor's spatial resolution (section 2.1.1). If an area is illuminated by microwaves, the contributions of these mechanisms can be both constructive and destructive in relation to the total signal of that area (leading to the term 'multiplicative noise' as designated by Frost et al. 1982). This leads to patterns in the image which can reduce the information content and make visual inspections as well as automated analyses difficult (Raney & Wessels 1988). As demonstrated in Figure 19 (left side), even though agricultural areas around the camp (yellow) are composed of similar surface characteristics, they show variations at the pixel level. The figure additionally shows that the intensity of the speckle effect is varying between different types of land-use or land cover.

For this reason, filtering techniques (section 2.3.2) were developed specifically for SAR images in slant geometry for many different types of applications (Gagnon & Jouan 1997; Lee et al. 1994; Mansourpour et al. 2006). On the other hand, the texture of different parts of the image, as well as the relationship between surface characteristics and their degree of speckle has been used to identify and discriminate forest biomass (Kuplich et al. 2003; Oliver 2000), sea ice (Soh & Tsatoulis 1999), and urban structures (Dekker 2003). As shown in Figure 19 (right side), a SAR image can also be described by its texture which is calculated based on a moving window technique of adjustable size (Woodcock & Strahler 1987). In the given example, image contrast was calculated with a

window size of 9x9 pixels, as one of many measures published under the concept of Gray-Level Co-Occurrence Matrices (GLCM) (Clausi 2014; Haralick 1979; Haralick et al. 1973). It shows low values in areas where speckle is low and high values in areas of high backscatter variations.

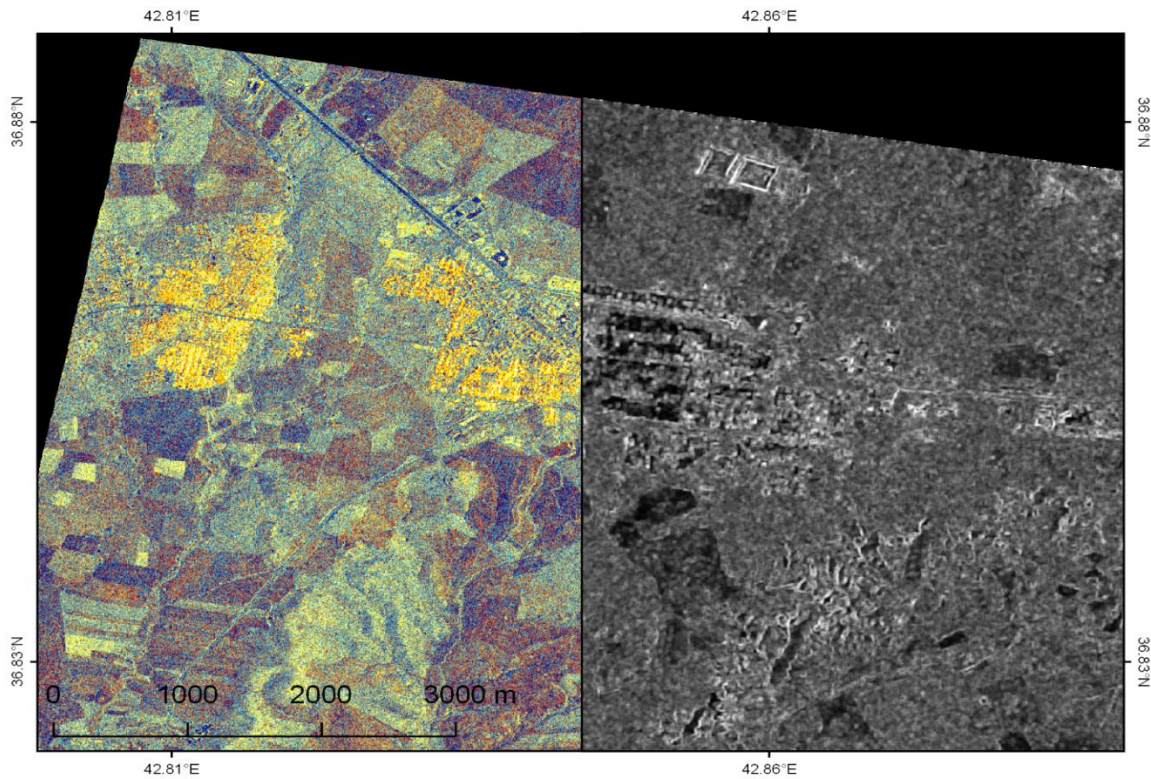


Figure 19: Speckle and texture in radar images

Dual-polarized TerraSAR-X image, Domeez refugee camp in northern Iraq (left, red=HH, green=VV blue=HH/VV) and corresponding image texture (right, contrast of HH band)

## 2.2.4 Polarization of radar waves

Polarimetric radar (PolSAR) makes use of the capability of specific sensors to transmit and receive electromagnetic waves in different directions. They propagate within the coupled field of electric and magnetic force which are at right angles to each other, leading to an elliptic or circular movement of the wave (Pierce 1974). Originally based on the Maxwell equations (Maxwell 1865), this behavior is used by polarimetric SAR satellites which split their signal into a horizontal and vertical component, where horizontal polarization is defined as the state in which the electric vector propagates parallel to the earth's surface and vertical polarization is the propagation orthogonal to the direction of propagation, as demonstrated by Figure 20 (Lee & Pottier 2009).

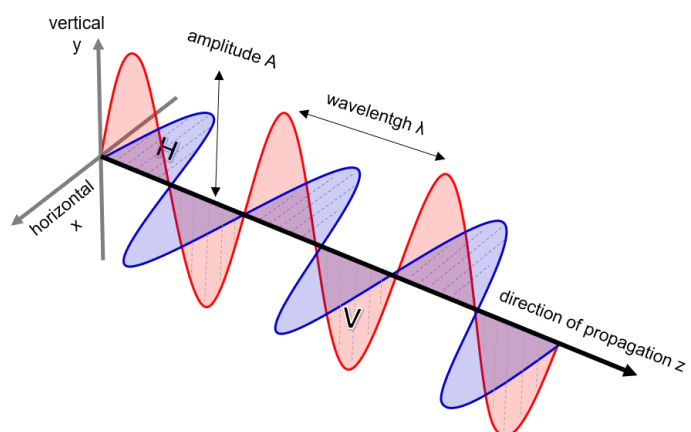


Figure 20: Horizontal and vertical polarization of an electromagnetic wave

The result is an image product consisting of horizontally backscattered waves reflected by horizontally transmitted waves (HH) and the vertical backscatter of vertically transmitted waves (VV). As shown in Figure 19 (left), these two images can be used to form an RGB color composite image by creating a third layer consisting of the ratio of HH and VV information. SAR polarimetry investigates the interrelations of surface characteristics and polarimetric components in order to describe the backscatter characteristics of an area (van Zyl & Kim 2011). As properties of the polarized waves can change when interacting with certain surfaces, fully-polarimetric SAR sensors are able to also capture the portion of the signal which was transmitted horizontally and backscattered vertically (HV) and vice versa (VH), leading to four image products representing one acquired scene (also called quad-pol SAR, Lee & Pottier 2009).

Their information can be expressed as a scattering matrix:

$$S = \begin{bmatrix} S_{HH} & S_{HV} \\ S_{VH} & S_{VV} \end{bmatrix} \quad (5)$$

where  $S_{xy}$  represents the scattering coefficients of the different transmitting and receiving polarizations.

The use of this information brought wide-ranging opportunities (Schmullius & Evans 1997). Useful applications include land cover classification (Khosravi et al. 2017; Pottier & Ferro-Famil 2009), estimations of soil moisture (Hajnsek et al. 2009a), biophysical parameters (Ballester-Berman et al. 2005), identification of ice types (Scheuchl et al. 2001; Soh & Tsatoulis 1999), and characterizations of topography or geomorphologic forms (Blumberg 1998; Schuler et al. 1996).

The largest advantage of spaceborne PolSAR configurations is the capability to identify the main backscatter mechanisms (section 2.2.2) which are dominating an area, most commonly achieved by polarimetric decompositions (Cloude & Pottier 1996; Krogager 1990; van Zyl 1992). Based on the assumptions of Freeman & Durden (1998) a linear combination of the four matrix elements from equation 5 can be used to discriminate different scattering mechanisms. For monostatic systems, the information of HV and VH is considered equal according to the law of reciprocity (Tragl 1990). After transformation of the scattering matrix into a vector, it can be rewritten as follows:

$$S = \alpha[S_a] + \beta[S_b] + \gamma[S_c] \quad (6)$$

where

$$\alpha = \frac{S_{HH} + S_{VV}}{\sqrt{2}}, \quad \beta = \frac{S_{HH} - S_{VV}}{\sqrt{2}}, \quad \gamma = \sqrt{2} S_{HV} \quad (7)$$

These represent the three components of the Pauli decomposition which divides the polarimetric signal into three scattering mechanisms (Freeman & Durden 1998): Surface scattering from even grounds ( $\alpha$ , blue), dihedral scattering caused by double bounce from vertically oriented objects ( $\beta$ , red) and volume scattering from randomly oriented objects, such as the branches of a tree ( $\gamma$ , green, see also Figure 18).

Figure 21 demonstrates how the Pauli decomposition can be useful in an urban context (for the application of the data, see section 3.1.3). Despite the spatial resolution of 6 m, densely built-up parts of the city can be identified in red hues. In contrast, areas with higher vegetation cover (open

architecture, parks, trees, and yards) are clearly identifiable in green. Plain surfaces with higher roughness are visible in the northeast portion of the image where the braided river system reaches the outskirts of the city before it channels through the center as seen here being visible in blue. Areas with few or no backscatter are black. It should also be mentioned that different types of landcover outside the city are exhibited by the radar image while they are uniformly tan in the optical image.

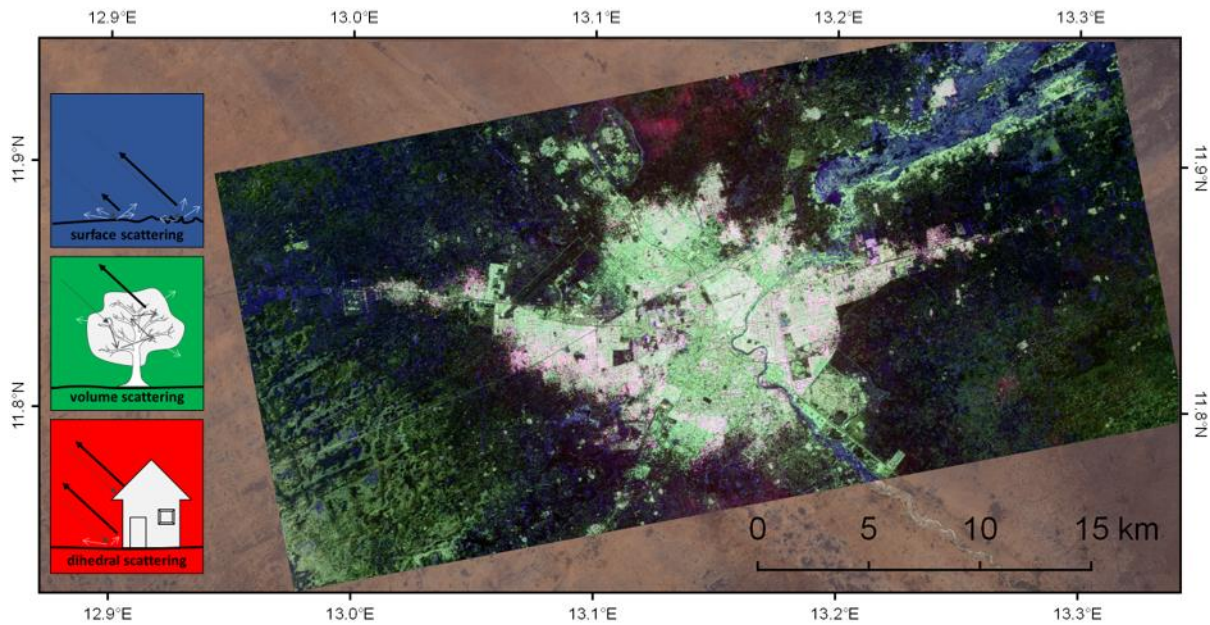


Figure 21: Polarimetric ALOS-2 image of the city of Maiduguri, Nigeria  
 RGB composite: red=dihedral, green=volume blue=surface scattering; background: Sentinel-2 image

## 2.2.5 Interferometric information

As a result of the coherent measurement principle, each signal received by the sensor consists of information of both the amplitude and the phase of the backscattered wave (Cindrich et al. 1977; Wu 1976). The amplitude (sometimes also called ‘magnitude’) describes the height of this wave as a direct measure of the strength of the signal. The phase is a periodic measure which describes the oscillation of the wave with respect to its origin and can be expressed in degrees. As demonstrated by Figure 22, one phase cycle corresponds to 360 degrees or  $2\pi$  respectively.

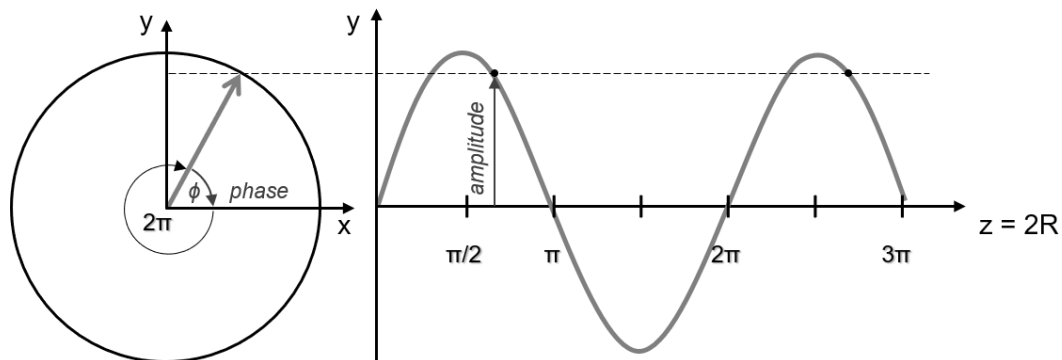


Figure 22: Amplitude and phase of a microwave  
 and their translation in a cartesian coordinate system ( $x$  and  $y$  values)

The radiation transmitted by the sensor travels to the earth and back to the sensor (equals two times the range distance =  $2R$ , see equation 1). The signal returning from objects at the earth's surface underlies different delays according to their slant range distance (section 2.1.2). This delay corresponds to a change in the phase  $\phi$  between the transmitted and returned signal which can be expressed as a function of the Range distance  $R$  and the wavelength  $\lambda$  as described in equation 8 (Ferretti et al. 2007a):

$$\phi = \frac{2\pi}{\lambda} 2R = \frac{4\pi}{\lambda} R \quad (8)$$

As radar images have spatial resolutions at the meter scale and the wavelength is of only several centimeters, the phase of a single image is no greater value. As shown in Figure 23, both amplitude and phase images contain information, but the phase seems random.

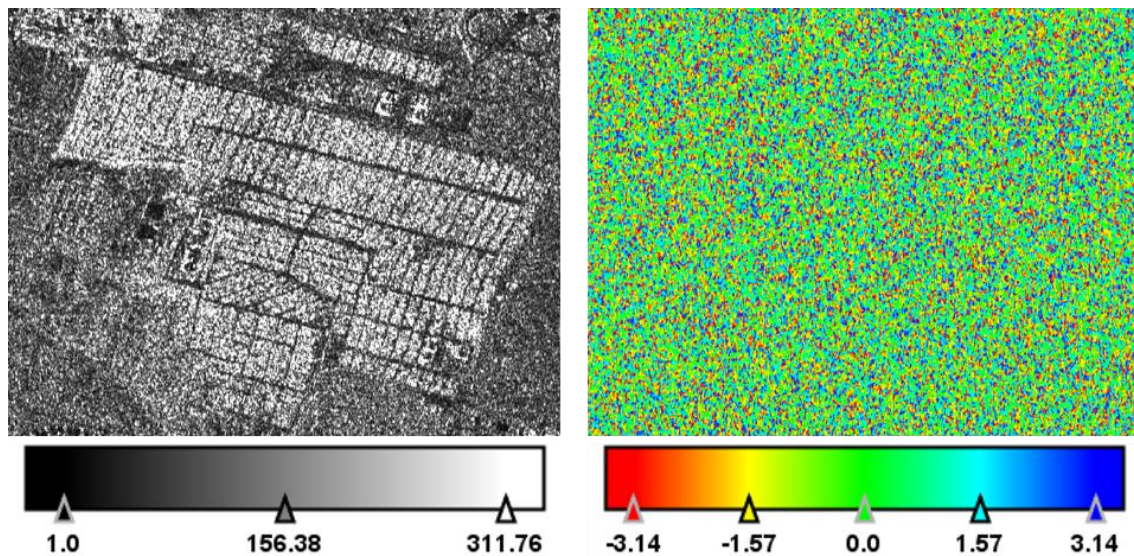


Figure 23: Amplitude (left) and phase (right) information of a radar image  
TerraSAR-X image of the refugee camp Domeez, Iraq

The principle of interferometric SAR (InSAR) analyses is to measure the phase difference of two radar images from slightly different angles in order to get information about the elevation of a surface (Bamler & Hartl 1998; Hanssen 2001; Massonnet & Feigl 1998). This can be achieved with exact knowledge about the imaging geometry, especially the orbital positions of both satellites at the time of acquisitions. Their lateral distance is called the perpendicular baseline, a main determining factor of the quality of InSAR analyses (Figure 24a, Gens & van Genderen 1996). If it is too small, the effect of topography on the phase difference is too small and the impact of noise and atmospheric effects increases (Ferretti et al. 2007b). If it is too large, the waves of both acquisitions oscillate out of phase which causes low coherence (Gatelli et al. 1994). Coherence is the fixed relationship between two electromagnetic waves which is needed for the comparison of phase information of both images (Figure 24b). If characteristics of a surface change between the first time ( $t_1$ ) and the second time of acquisition ( $t_2$ ), for example through growth of vegetation or the appearance of new objects within a pixel, the two waves are no longer in-phase and coherence decreases (temporal decorrelation, Zebker & Villasenor 1992).

Coherence is therefore used as a quality measure for interferometric analysis because it grants that the phase of the received signal is preserved (Polidori 1995). One way to overcome temporal decorrelation is a bistatic radar system, a configuration of two independent sensors, in which one transmits and the other receives within a very short time. Examples are the Shuttle Radar Topography Mission (SRTM, Farr et al. 2007; van Zyl 2001), the ERS-1/2 tandem constellation mission (Schwabisch et al. 1995), ERS/ENVISAT combinations (Hong & Won 2006; Wegmüller et al. 2009) or the TanDEM-X mission (single-pass interferometry Moreira et al. 2004; Zink et al. 2014).

Differential radar interferometry (DInSAR) is a repeat-pass technique which exploits the phase difference to measure the elevation change between two image acquisitions (Figure 24c, Ferretti et al. 2007c; Gabriel et al. 1989). It is mostly used for the measurement of land subsidence of urban areas (Chatterjee et al. 2006; Tesauro et al. 2000; Tomás et al. 2014), geomorphologic phenomena (Liu et al. 2015; Lundgren et al. 2004; Tarchi et al. 2003) or mining areas (Castañeda et al. 2009; Herrera et al. 2007; Perski 1998). As described above, so-called non-coherent changes are not detectable by traditional InSAR methods because the received signal is no longer in-phase of the transmitted one.

A special form of DInSAR is persistent scatterer interferometry (PSI) which uses statistical measures on large time-series of radar images to derive precise deformation trends (Ferretti et al. 2001; Hooper et al. 2007; Prati et al. 2010). It overcomes the problem of decorrelation by identifying echoes from pixels that are dominated by a single scattering object throughout several subsequent images (Hooper et al. 2007). Instead of analyzing the whole image, only information at these points (persistent scatterers) is used along a time-series to retrieve insights about the temporal progress and spatial distribution of deformation.

Other applications use the coherence between two image acquisitions for the classification of surfaces (Dutra 1999; Nizalapur et al. 2011; Vicente-Guijalba et al. 2017) or the detection of changes (Jung et al. 2016; Liao et al. 2008; Preiss & Stacy 2006) by taking into account the different degrees of decorrelation.

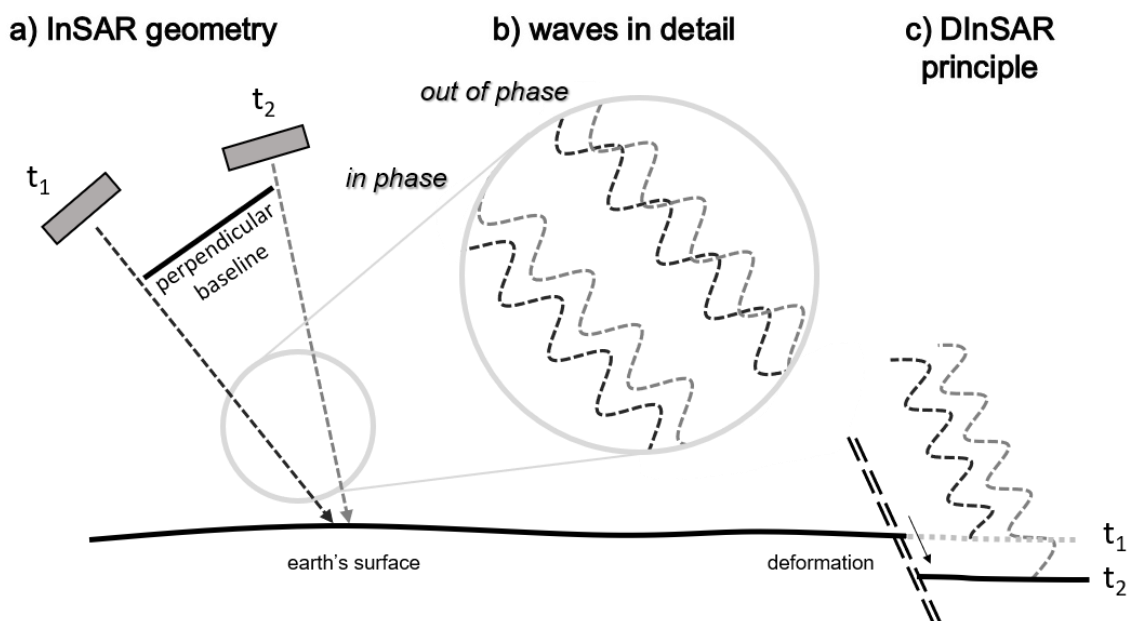


Figure 24: Principles of spaceborne radar interferometry  
 a) radar interferometry, b) coherence, c) DInSAR principle

## 2.3 Data processing

As demonstrated in the last two sections, radar data are very sensitive to imaging geometry and surface characteristics. Good preparation of the images before any analysis is therefore of high importance. The following section shortly describes the steps required to generate usable raster products from imagery acquired in slant geometry using the example of a dual-polarized (HH+VV) TerraSAR-X scene from 29.03.2014. It shows the town of Goz Beida and the refugee camp of Djabal which was opened to Sudanese refugees in 2004 who were fleeing from the violence of the Darfur crisis (Clark & Tan 2004).

It may be noted that any steps required to form the actual SAR image from raw data, including azimuth and range compression, motion compensation or image focusing are not presented in this work and the reader is referred to corresponding external sources (Burns & Cordaro 1994; Cumming & Wong 2005). Additionally, the following steps are the most commonly used, but special sensor configurations (section 2.4) could require additional steps, such as de-bursting of ENVISAT WS or Sentinel-1 IW (Geudtner et al. 2017) or deskewing of ALOS PALSAR data (Song & Kwag 2011).

### 2.3.1 Detection and radiometric calibration

Each radar image consists of amplitude and phase information, which are described by a vector of a given length and an angle respectively (section 2.2.5). To be able to store both measures in a raster grid, they are expressed as a complex number, consisting of the real in-phase component (i) and the imaginary quadrature component (q) (Ferretti et al. 2007a). They refer to the x and y values in the cartesian notation in Figure 22 and unambiguously describe the length and angle of the vector of the measured signal (Figure 25). Equation 9 shows the process of detection, which converts this complex information that is present in every pixel into a so-called digital number (DN) by taking the sum of the squares of the real and imaginary parts (Small & Schubert 2008). This measure describes the amount of backscatter and is often converted to scalar intensity I.

$$I = DN^2 = i^2 + q^2 \quad (9)$$



Figure 25: Real and imaginary part of the complex radar information and resulting intensity

The need for radiometric calibration of the intensity image becomes evident in Figure 14a, where pixels in the near range ( $\theta_i = 39.6$ ) show slightly higher backscatter intensities than pixels in the far range ( $\theta_i = 40.3$ ). Along with this effect, the incidence angle of an acquisition can vary strongly between images of different dates, sensor configurations or satellite missions. Therefore, any use of radar imagery which goes beyond visual interpretation needs radiometric calibration (Freeman 1992; Gray et al. 1990). It ensures that the pixel information can be directly related to the backscatter of an area which is expressed as a ratio between transmitted power and reflected backscatter in relation to a given reference area. Consequently, calibrated images of different dates or sensors can quantitatively be compared.

The most basic form is beta naught ( $\beta^0$ ), also called 'radar brightness', which is referring to a reference area in the slant range domain (section 2.1.2). It can be derived using a calibration constant which is applied on the measured intensity. It transforms radar values into a comparable range. However, it does not compensate for variations of the incidence angle (Figure 14).

In most cases, information of the incidence angle of an image is known (stored in the image's metadata) and the signal can be calibrated to sigma naught ( $\sigma^0$ ), also named 'backscatter coefficient' (equation 10, Figure 27b). This measure refers to a reference area in ground range geometry, usually an ellipsoidal model of the earth's flat surface (Curlander 1982). These Sigma0 values predominantly range between 0 and 1 (where 1 equals fully isotropic scattering) and can be readily used for visual interpretation. Radiometric distortions caused by the local incidence angle additionally give the images a slightly three-dimensional look.

If the reference area lays perpendicular to the line of sight between the sensor and the ellipsoid, gamma naught ( $\gamma^0$ , see equation 11) is the result (Small 2011). These measures directly represent the area of a pixel on the ground.

$$\sigma^0 = \beta^0 * \sin(\theta_i) \quad (10)$$

$$\gamma^0 = \beta^0 * \tan(\theta_i) \quad (11)$$

where  $\theta_i$  is the incidence angle between sensor and the ellipsoidal model of the earth (Figure 13).

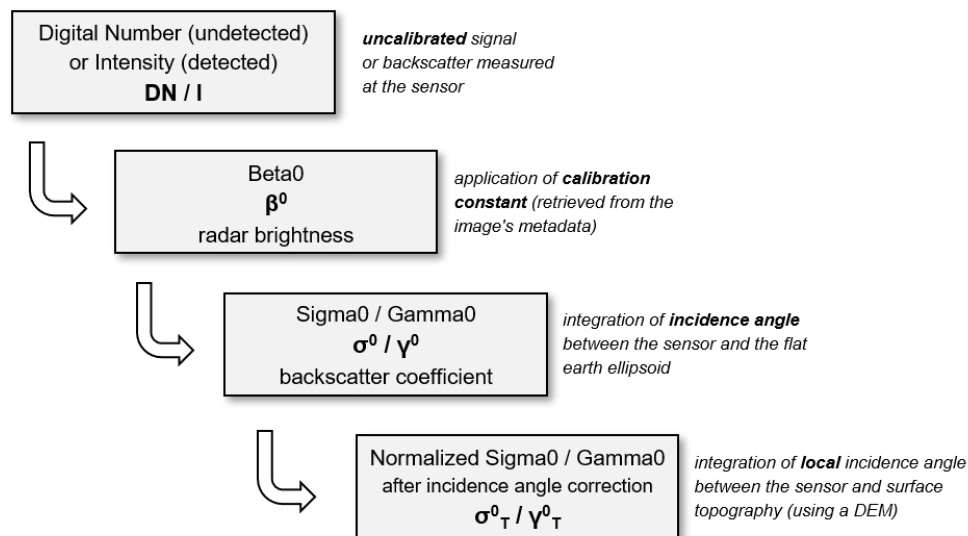


Figure 26: Schematic steps of radiometric calibration of SAR images

However, with increasing spatial resolutions of SAR sensors and advances in geolocation accuracy, calibration measures accounting for local terrain variations were needed (Bayer et al. 1991; Small et al. 2009a). As demonstrated in Figure 14 and Figure 27b, slopes facing the wave incoming from the sensor have systematically higher backscatter values because of their smaller local incidence angles. Because these radiometric variations distort the actual backscatter of land surfaces (Figure 17), the demand for incidence angle normalization becomes evident.

A digital elevation model (DEM) of sufficient spatial resolution and quality can be used to derive the local incidence angle of the signal for each pixel for a slope-based normalization of SAR backscatter ( $\sigma^0_T$ , Figure 26) as demonstrated in equation 12 (Goering et al. 1995; Hinse et al. 1988):

$$\sigma_T^0 = \sigma^0 * \frac{\sin \theta_{LIM}}{\sin \theta_i} \quad (12)$$

where  $\theta_{LIM}$  is the local incidence angle mask derived from the digital elevation model, indicating the angle between the incoming signal and the surface normal of the local slope of a pixel.

However, this normalization was found to be insufficient for many applications in areas of pronounced topography (Small et al. 2009b) and the calibrated measure of ‘terrain flattened gamma’ ( $\gamma_T^0$ ) was proposed by Small (2011). Instead of using the local slope angle, it integrates the area which is illuminated by the radar signal as described in equation 13:

$$\gamma_T^0 = \beta^0 * \frac{A_\beta}{\int_{DEM} A_\gamma} \quad (13)$$

where  $A_\beta$  is the reference area of a pixel in slant geometry,  $A_\gamma$  is the ground surface perpendicular to the line of sight, and DEM is the digital elevation model of the illuminated area.

Figure 27c shows a simulated SAR image of the same area where a DEM is used to predict the variability of backscatter intensity in the image according to the local incidence angle of the pixels, regardless of their roughness or dielectricity (Franceschetti et al. 1995). It demonstrates how topography influences the backscatter, especially at the mountainous ranges facing towards the sensor. If these effects are removed by incidence angle normalization (Mladenova et al. 2013) or radiometric terrain flattening (Small 2011), as described above, the actual backscatter caused by surface characteristics remains (Figure 27d). These images can then also be used for automated image analysis, such as classification of land-use or land cover (section 3.3.3) or the application of mathematical models (section 3.3.4).

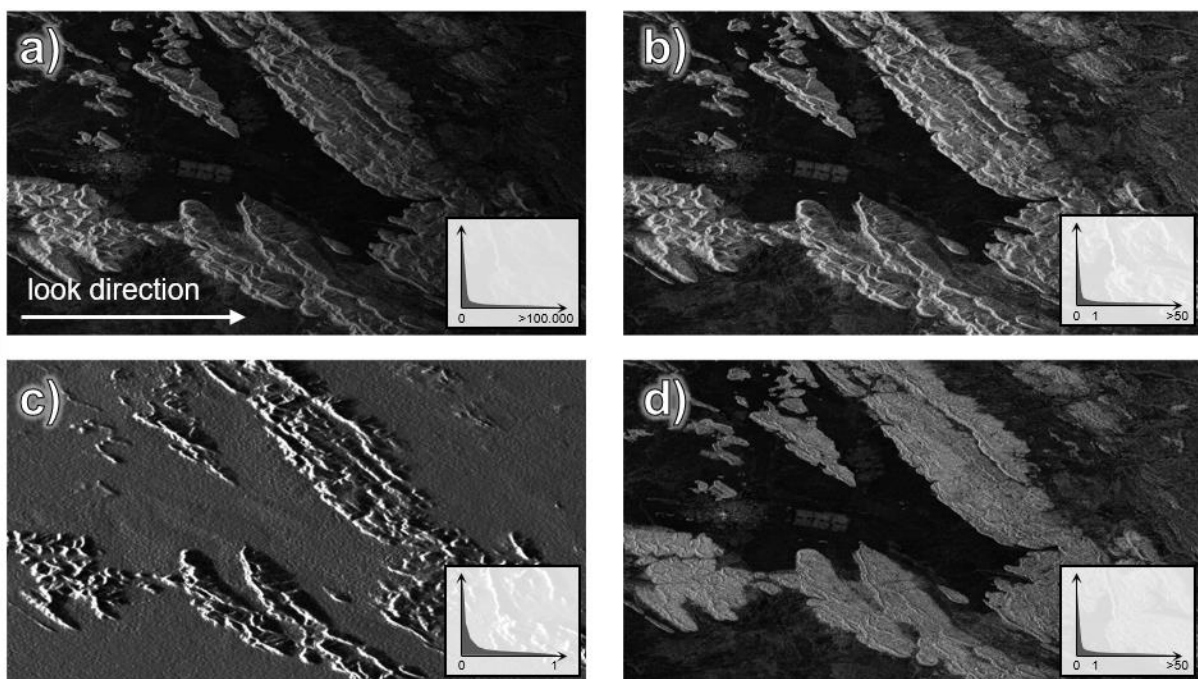


Figure 27: Steps and value ranges of radiometric calibration of SAR images

a) raw intensity image, b) calibrated Sigma0, c) simulated backscatter image based on local incidence angle, d) incidence normalized Gamma0. Note that the image is still in slant geometry and not oriented northwards.

### 2.3.2 Multi-looking, speckle filtering, and image enhancement

Because of the side-looking geometry of SAR, the resolution in range and azimuth direction can strongly differ. Additionally, pixels within a scene have different distances to the sensor and therefore represent different areas at the ground (Richards 2009). Equally-spaced pixels can be retrieved by multi-looking the calibrated image. It reduces the spatial resolution of the image to a calculable degree but improves the quality of the image by producing geometrically consistent pixels and decreasing the effect of speckle. During this process, multiple lines of pixels in range direction are combined with lines of pixels in azimuth direction by convolution within a defined moving window. As a result, an image with square pixels and local smoothing is retrieved (Schwarz et al. 2008). The effects of multi-looking of TerraSAR-X (range: 1.18 m; azimuth: 6.62 m [dual-pol], 3.33 m [single-pol]; Airbus 2015) are demonstrated in Table 2 and Figure 35 (section 3.1.2). Multi-looking is not mandatory because square pixels are retrieved after resampling during the geocoding (section 2.3.3), but many applications benefit from its trade-off between a reduced degree of speckle and lower spatial resolution (Dong et al. 2000). Frequency-domain averaging as proposed by de Vries (1998) is not applied within in this work.

*Table 2: Number of looks for TerraSAR-X StripMap products and resulting spatial resolution*

<b>Range looks</b>	2	3	4	5	6	7
<b>Azimuth looks</b>	1	2	2	3	4	4
<b>Resulting resolution [m]</b>	2.62	4.54	5.25	7.17	9.08	9.79

As described in section 2.2.3, the degree of speckle of an area depends on its surface characteristics and the spatial resolution of the SAR sensor (Goodman 1976). To reduce this effect, speckle filtering techniques have been developed since the beginning of aerial and spaceborne SAR remote sensing. In comparison to standard image enhancement filters, speckle filters were initially designed for images in slant geometry (Huang & van Genderen 1996). While filters exist for many applications and surfaces, the pioneering work of Jong-Sen Lee is mentionable at this point. He developed one of the first radar image filter techniques and revised it according to different applications and along with technological and scientific advancements (Lee 1980, 1981, 1983, 1986; Lee et al. 2006). The main idea is to apply a moving window of given size which uses local statistics to discriminate speckle from actual changes as a result of altered surface characteristics, thus smoothing the unwanted granular effect while conserving sharp edges along the transitions between two areas of differing backscatter. Frost et al. (1982) developed an adaptive filter which focuses on minimizing the mean square error in homogeneous areas of an image. The Gamma Map filter (Lopes et al. 1993) is a technique to address speckle in areas with structural features, such as edges or lines, adapting the shape of the moving window. Other widely-known filters are the intensity-driven adaptive-neighborhood (IDAN) technique (Vasile et al. 2006) or Boxcar averaging (Bouchemakh et al. 2008). As found in many studies, there is no ideal speckle filter configuration to apply in all SAR applications (Lee et al. 1994; Sheng & Xia 1996; Touzi 2002). The selection of a filter type and size depends from the degree of speckle and the spatial scale of the information to be retrieved from the image. As demonstrated in Figure 28, a simple mean filter makes the image blurry and increases speckle at pixels with high values. Adaptive filters such as the Lee Sigma or IDAN filter generate more homogenous areas while maintaining sharp borders, such as the paths within the urban area. It can be observed that the Lee Sigma filter tends to produce patches of equal sizes. In contrast, the IDAN filter is based on a region growing algorithm and results in a generally darker image while smoothing especially low values where most of the speckle occurs.

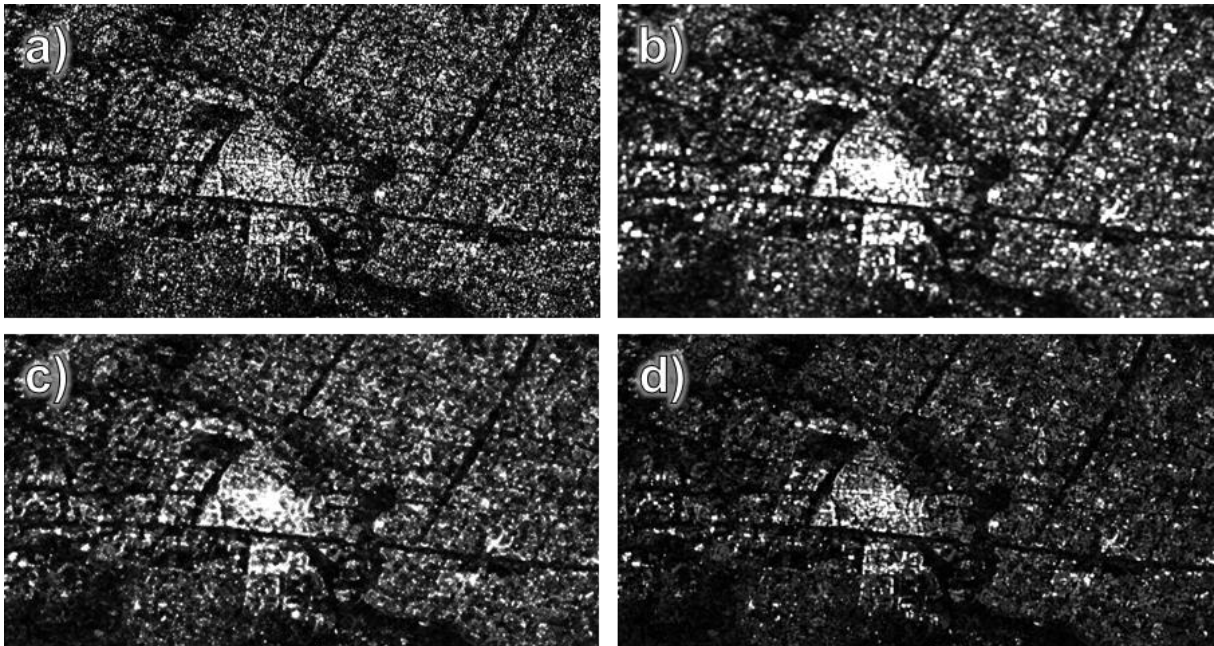


Figure 28: Comparison of different filter techniques

TerraSAR-X image of Goz Beïda: a) original calibrated image, b) mean filter c) Lee Sigma filter, d) IDAN filter

Another way of image enhancement is the conversion of backscatter intensity to a logarithmic scale. By applying equation 14 to a calibrated image, the data is scaled to a value range between roughly -45 and +10 and receives the unit decibel [dB]. Thereby low values are stretched while high values are shifted towards the mean, thus leading to a Gaussian distribution of grey values (see histograms in Figure 29). It often reduces the overall contrast of the image, but normally distributed values are easier to handle for quantitative analyses and outliers caused by dihedral or volume scattering mechanisms are not considered 'outliers' (Deng et al. 1995). As demonstrated in Figure 29, the urban areas become darker, but subtle structures in the low contrast areas are more clearly visible.

$$\sigma_{db}^0 = 10 \cdot \log_{10}(\sigma^0) [dB] \quad (14)$$

Like multi-looking, converting an image to log scale is optional and should only be performed if it is beneficial for later analysis steps. It has, however, to be noted that the value of 0 dB now corresponds to a perfectly isotropic scatterer (as it was 1 in the non-logarithmic scale).

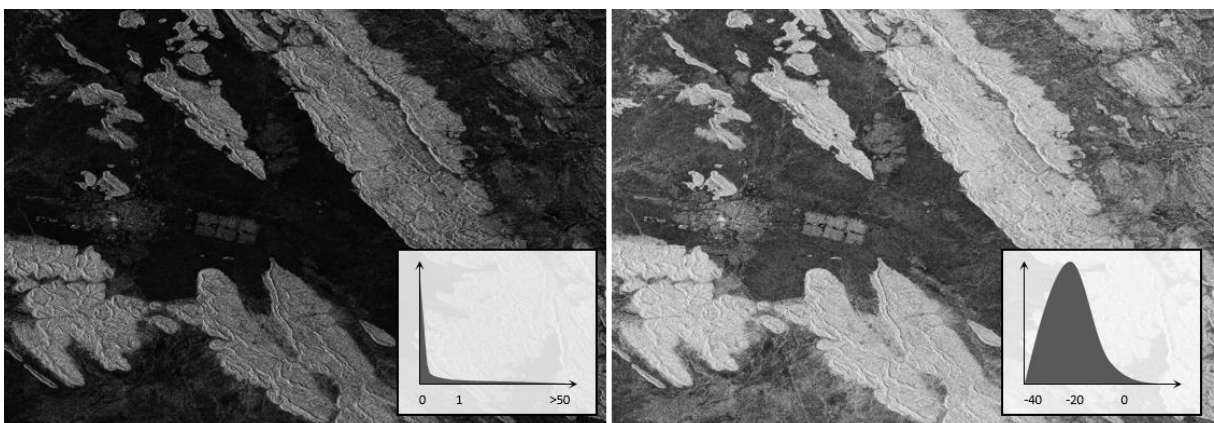


Figure 29: Calibrated image in linear representation (left) and log scale (right)

### 2.3.3 Geometric correction and geocoding

Geocoding projects the pixels into a coordinate reference system and allows the joint use of radar images with other geodata, such as vectors or optical imagery. It should be performed as a last step, because it involves resampling of the pixels. Additionally, calibration and filtering are best performed on data in slant geometry, thus before the geocoding (Meier et al. 1993).

Since image generation is primarily based on temporal measurements (section 2.1.1), the geolocation of the received signal needs to be calculated based on so-called Range Doppler geocoding. During this operation, information from the image's metadata regarding the position of the satellite (orbit state vectors), radar timing annotations, and parameters on the slant geometry of the system are used to calculate the actual position of a pixel within a cartesian coordinate system on the earth's surface (Small & Schubert 2008). This surface is either represented by a flat-earth model (ellipsoid correction) or a digital terrain model including topographic variation (terrain correction or orthorectification). While ellipsoid correction is sufficient to geocode a SAR image on even surfaces, the effects of foreshortening and layover as demonstrated in section 2.2.1 need to be corrected by the use of a digital elevation model (Pierce et al. 1996).

Figure 30 shows the differences between ellipsoid correction and terrain correction for small mountain ridges in the south of the Djabal refugee camp. While the red outlines of the ridges are similarly well located in both methods, the ridges indicated in blue are clearly distorted towards the look direction of the sensor in the ellipsoid correction (middle image). Orthorectification corrects for this shift (right image) but backscatter information within the foreshortening area is only stretched geometrically and is mostly unusable for quantitative analysis (Loew & Mauser 2007).

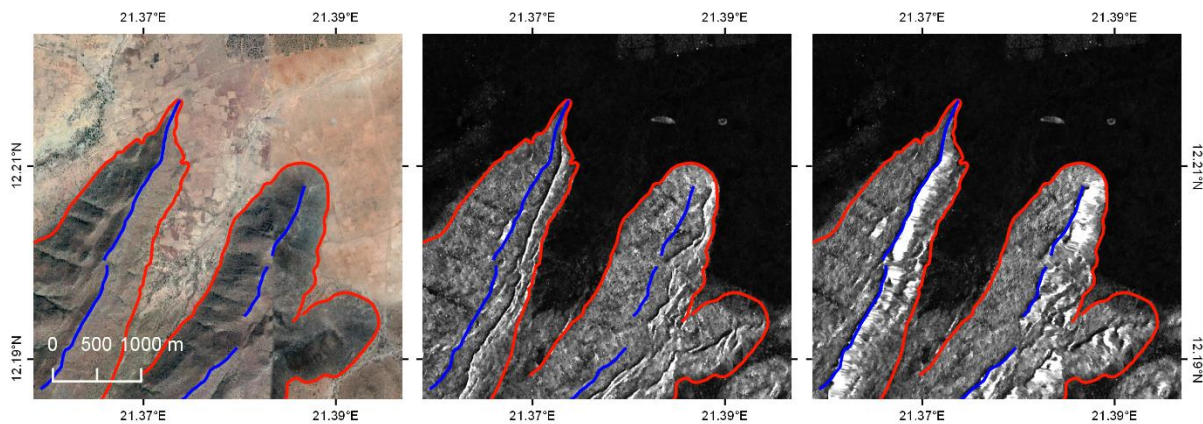


*Figure 30: Effect of geometric terrain correction on areas with pronounced topography  
Optical image (left), ellipsoid correction (middle), terrain correction based on SRTM (right)*

Figure 31 shows that, even on flat areas, shifts can occur in ellipsoid corrected images. While the paths in the town of Goz Beïda are well aligned with the yellow reference lines in the DEM-assisted terrain corrected image (right), they are about 35 meters off in the ellipsoid corrected image (left), probably because the whole region is slightly inclined. Consequently, whenever a digital elevation model is available, orthorectification should be preferred to ensure best possible geocoding.

Other terrain correction techniques use DEMs to create a simulated SAR image (Figure 27) to estimate the radiometric distortions in order to achieve best co-registration with the underlying elevation information (Liu et al. 2004; Wegmüller 1999). In this work, Range Doppler terrain correction is used unless otherwise specified. A fully pre-processed image of TerraSAR-X is shown in Figure 102 (Appendix 4).

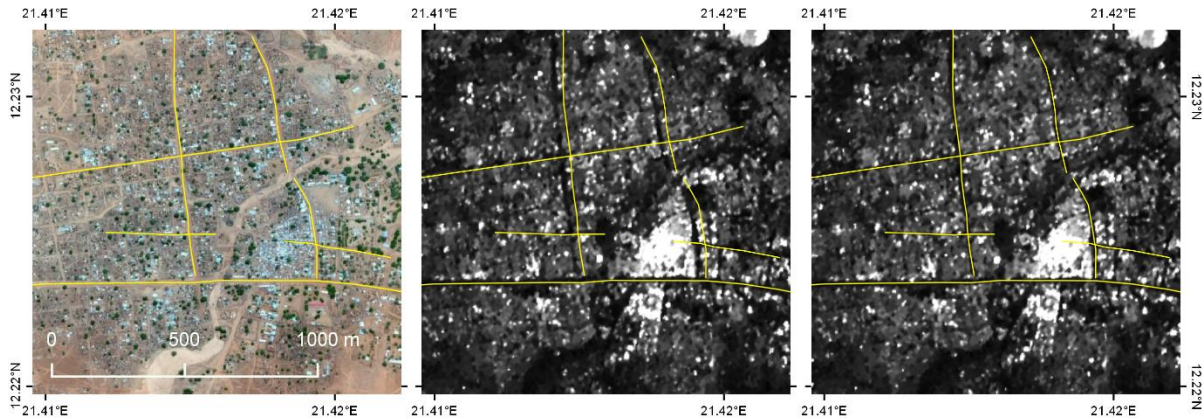


Figure 31: Effect of geometric terrain correction on flat areas  
Optical image (left), ellipsoid correction (middle), terrain correction based on SRTM (right)

## 2.4 Sensors, modes, and products

One reason why the many non-academic organizations and institutions hesitate to use SAR data is the variety of different sensors (and different wavelengths), acquisition modes, and delivered products. Unlike optical data which come with a clear description of multi-spectral band composition and a standardized degree of calibration (from top-of-atmosphere radiance to bottom-of-atmosphere reflectance; extensive reviews are given by Dingirard & Slater (1999) or Chander et al. (2009), the different configurations of SAR satellites seem confusing at first sight. This section tries to clarify the most important aspects in terms of applications in the humanitarian domain, although not claiming to be exhaustive in any technical manner.

Figure 101 (Appendix 3) lists the lifespans of selected SAR missions. They become relevant for monitoring of areas over a long time. Seasat was a very early mission in 1978 which provides one of the oldest SAR images usable (Born et al. 1979). Most of the non-military satellites were launched in the last decade of the 20<sup>th</sup> century, with the missions ERS and ENVISAT ASAR by the European Space Agency (ESA) being the most important program for a systematic and global monitoring of land surfaces (Louet & Bruzzi 1999). They were followed by Sentinel-1 in 2014, which also operates at C-Band (4-8 GHz and wavelengths of 3.7-7.5 cm) and similar spatial resolution, providing optimal continuity conditions. Of similar importance are the missions of RADARSAT-1 and RADARSAT-2 (CSA) because of its long-term coverage and interferometric applications (Gray et al. 1998; Morena et al. 2004).

Most of the Asian sensors, namely JERS-1 (NASDA/MITI/STA), ALOS PALSAR and ALOS-2 (both JAXA), operate at L-band (1-2 GHz and wavelengths of 15-13 cm), providing wavelengths with higher penetration capabilities in terms of atmospheric vapor, canopies, and dry sediments (Kimura & Ito 2000; Nishidai 1993). The shortest wavelength is provided by X-band sensors (8-12.5 GHz and wavelengths of 3.75-2.4 cm) since the middle of the 1990s, starting with TerraSAR-X, a German satellite with high spatial resolution which was launched in 2007, followed by its twin, TanDEM-X in 2010, providing excellent preconditions for radar interferometry (Moreira et al. 2004; Werninghaus & Buckreuss 2010). This mission achieved the computation of a digital surface model of nearly global coverage at a spatial resolution of 12.5 meters (Zink et al. 2017). It was shortly followed by COSMO SkyMed mission, consisting of four satellites which were launched successively beginning in 2007 to assure a long and consistent acquisition of images (Covello et al. 2010).

National SAR programs of lesser international attention are Kompsat-5 (KARI, Lee 2010) or RISAT-1 (ISRO, Misra et al. 2013). The most recently launched satellite PAZ (Hisdesat) is supposed to complement the TerraSAR-X mission in the future (Bach et al. 2018).

Besides the temporal availability, the most important aspect for the selection of a suitable radar satellite image is the spatial resolution. Secondly, the spatial extent of the image, wavelength, or polarization can favor a successful application, depending on its scope. In this context, it has to be noted that many SAR satellite missions operate at multiple modes. While the most common way of acquiring an image is to capture an area along the flight path as the satellite traverses (StripMap), there are also ways to alter the signal's angle in azimuth and range direction to increase or decrease the time of illumination of an area to achieve a higher or lower spatial resolution. Because the time of the satellite over an area is limited, high resolutions allow the coverage of only small areas while the coverage of large areas can only be achieved by lowering the spatial resolution. Figure 32 demonstrates the three main types of image formation: While the antenna is electronically steered backwards in the Spotlight mode in order to increase the illumination time of an area, the ScanSAR mode which is used to capture large areas at lower resolution. During the last three decades, smaller refinements which are based on the same principles have been developed for new imaging modes, such as TOPS of Sentinel-1 (Bai et al. 2010; Geudtner et al. 2017), PingPong mode of COSMOSkyMed (Nunziata & Migliaccio 2013), or Staring Spotlight of TerraSAR-X (Mittermayer et al. 2014).

Table 32 (Appendix 2) lists all acquisition modes of the presented SAR satellites. It shows how both spatial resolution and covered extent evolved during the last three decades. For their application in a humanitarian context, a trade-off between these two determinants can usually be found. However, it has also to be mentioned that it is technically impossible to capture an image with both high spatial resolution (or many polarizations) and a large footprint.

When ordering archived or new satellite imagery, users are able to select the type of product level. These mostly range from raw format to ready-for-use, depending on the requirements and abilities of the user. Like the inhomogeneous naming conventions of the acquisition modes, product levels are often variably named by the providers.

Table 33 (Appendix 5) lists the overall categories of product levels. The most commonly used level is Slant Range Complex (SLC) because it is usable in most image processing software while still providing the user the highest amount of flexibility in terms of processing, e.g. the number of looks or the DEM used for the terrain correction (sections 2.3.2 and 2.3.3). Multi-looking or geocoding cannot be reversed without loss of image quality.

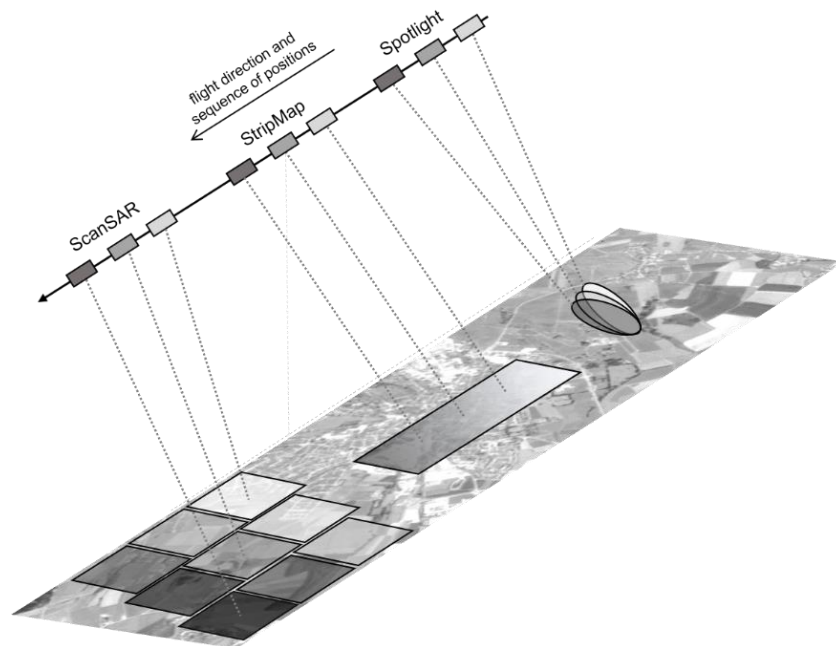


Figure 32: SAR imaging modes: ScanSAR, StripMap and Spotlight  
The grey shades indicate the sequential sensing of the area.

## 3 Applications

### 3.1 Mapping of refugee camps, infrastructures and their dynamics

As defined in chapter 1.2, one of the most evident needs of humanitarian operations is the allocation of people in need, in its both spatial and temporal dimension. Knowledge about population numbers or their developments helps to coordinate relief operations, especially for the provision of food and other basic services, such as access to sanitation or medicine (Cozzolino 2012). This chapter demonstrates in a systematic way how SAR radar information can be employed for the mapping of refugee camps, urban and rural areas, the monitoring of changes and the assessment of damages resulting from disasters or armed conflicts.

The large benefit of radar imagery is their independency from cloud cover. This makes them a valuable source for multi-temporal analyses since early times, especially for the identification of changes (Dekker 2005; Polidori et al. 1995; White 1991). In contrast to multispectral optical imagery, the information content of SAR images is comparably simple to analyze: If the backscatter mechanisms of the study area are well understood (section 2.2.2), the detection of changes can be based on the intensity information alone (Lu et al. 2004).

#### 3.1.1 Current state of research and challenges

Besides monitoring of the environment, urban areas have been a main object of research of earth observation techniques since the beginning, but especially urban remote sensing gained importance with the development of high resolution (HR) and very high resolution (VHR) imagery (Balling & Brazel 1988; Du et al. 2014; Forster 1985; Heldens et al. 2011; Jensen & Cowen 1999; Kadhim et al. 2016; Longley 2002; Weng et al. 2018; Xian 2010). Mentionable in this context is the work of Taubenböck and his research group which is intensively analyzing the characterization of informal settlements from space based on size, internal structure, polarimetric signatures or image texture (Friesen et al. 2018; Jain et al. 2015; Taubenböck & Kraff 2014; Wurm & Taubenböck 2018). An example for structural effects on backscatter is given in Figure 33, where informal settlements in Mumbai are emphasized in pink color by simple band combinations.

In contrast to regular urban structures, refugee camps or informal settlements represent special forms of agglomerations, because of mostly light and low-cost building materials, such as tents, corrugated shacks or huts from clay or wood (Figure 5, Gustavsson 2003; Wells et al. 1998), irregular and usually very densely built-up structures (Alnsour & Meaton 2014; Hailey 2009; Taubenböck & Kraff 2015) and high spatial and social dynamics (Turner 2016). In contrast to these observations, it is increasingly discussed that the differences between urban areas and refugee camps become more and more blurred and that the best way of providing sustainable livelihoods to people on the run is to integrate them into existing cities (Agier 2002; Bowles 1998; Herz 2013; Montclos & Kagwanja 2000). In any case, these settings bring additional challenges for remote sensing applications.

As one of the first in this field, Bjørgo (1999) mentioned the value of radar imagery for humanitarian purposes, including the mapping of road infrastructures and camps. First published applications use combinations of optical and radar remote sensing, making use of the complementary information provided by different sensors: Pohl et al. (1997) presented a joint analysis of SPOT and RADARSAT-1 images of the town of Goma, Zaire, which hosted a large number of Hutu refugees as a consequence of the Rwandan civil war, and report that fusion of both sensors brought an increased reliability and quality of the results. Haack et al. (2000) combined RADARSAT-1 and Landsat TM for the delineation of land-use and the urban extent of the refugee camps in the Dadaab region, Kenya,

but struggle with a 'spectral confusion' between camp areas and bare soil signatures in the radar images. Kuffer (2003) presented a method to derive and monitor urban density in informal settlements of Dar es Salaam, Tanzania, based on ERS-2 and SPOT images and report high accuracies ( $r = 0.89$  for ERS and  $r = 0.95$  for joint method), but also overestimations because of double-bounce effects (Figure 18) and underestimations in sparsely built-up areas.

Increased spatial resolutions of SAR images (Table 32, also ASTRIUM 2011) brought improvements regarding the detection of urban areas and dwellings (Brenner & Roessing 2008; Colin-Koeniguer & Trouvé 2011; Perissin & Ferretti 2007; Zhu & Bamler 2010), but only few studies used them in the context of displaced persons: Stasolla & Gamba (2009) demonstrated the use of ALOS PALSAR for high-resolution camp mapping in Darfur while also playing emphasis on the complementary information content of optical and microwave information. Another application of camp monitoring is presented by Oddone et al. (2015) who demonstrate the use of COSMO SkyMed imagery to track the expansion of the Al-Mafraq refugee camp in Jordan between 2012 and 2013 with RGB color composites.

Another domain relevant to humanitarian organizations is the identification of rural settlements because there are still many areas on this earth which are not sufficiently mapped, for example for the planning emergency operations or vaccination campaigns (Dittus et al. 2017). Radar-based approaches are provided by Pesaresi & Gerhardinger (2011), who use textural measures for the identification of urban areas, or the concept of the 'global urban footprint' which uses the TanDEM-X mission for the global delineation of settlement patterns (Esch et al. 2018; Esch et al. 2013).

Current developments include dwelling estimations in refugee camps based on very high-resolution data, as presented by Bitelli et al. (2015), Spröhnle et al. (2017) or Aravena Pelizari et al. (2018), the integration of machine learning in camp mapping (Quinn et al. 2018), polarimetric approaches for the distinction of different types of materials (Schmitt et al. 2018; Weigand 2017; Wurm et al. 2017) and SAR-based big data applications for camp monitoring (Argyriou et al. 2018; Dumitru et al. 2016; Schwarz et al. 2018).

As refugee camps and urban areas are no static objects but rather underlie massive dynamics, methods identifying changes are required. For this reason, manifold approaches have been presented to extract the information related to changes from SAR images, including object-based methods (Gamba et al. 2006; Ma et al. 2016; Yousif & Ban 2017), statistical models (Gong et al. 2016; Moser & Serpico 2009; Xiong et al. 2012) speckle or texture measures (Gong et al. 2014; Inglada 2003) as well as polarimetric (Ratha et al. 2017; Skriver et al. 2017) and interferometric concepts (Liao et al. 2008; Liu et al. 2001; Werner et al. 1993).

The potential of radar interferometry for displacement mapping caused by earthquakes was already recognized in the early 90s (Massonnet et al. 1993). Its application for measuring ground movement at the centimeter scale has been widely demonstrated in numerous cases (Funning et al. 2005; Lindsey et al. 2015; Peltzer et al. 2001; Reale et al. 2011; Sandwell et al. 2008; Vajedian & Motagh 2018; Yague-Martinez et al. 2012). These displacements, however, mostly occur at the regional level and are of only small relevance to humanitarian response.

In terms of damage assessment in urban areas, many studies exist based in backscatter change (Bovolo & Bruzzone 2007), differential interferometry (Arciniegas et al. 2007; Infante et al. 2016; Moser & Serpico 2006; Peduto et al. 2017; Tomás et al. 2012) or combinations with optical imagery (Brunner et al. 2010; Havivi et al. 2018; Wang & Jin 2012). While amplitude or coherence-based approaches require at least three images (two pre-event and one post-event acquisition), differential interferometry is challenging for urban change detection because it cannot capture non-coherent processes (Figure 24b), such as the collapsing buildings (Preiss & Stacy 2006).

Special importance can be attached to persistent scatterer interferometry (PSI, see section 2.2.5). As the temporal resolution of large image time-series partially compensates lower spatial resolutions of the pixels, these techniques are especially usable in urban contexts, for example for damage assessment (Ardizzone et al. 2012; Gernhardt & Bamler 2012; Perissin & Ferretti 2007).

But SAR-based change detection is also subject to limitations: Most studies listed above use images acquired in StripMap or Spotlight mode (Figure 32) which are mostly not taken at regular intervals. This means that, if archived data is not available, especially before the event, there is no chance to react on emergencies (Plank 2014). Additionally, successful applications rely on the availability of reference data and additional GIS layers, e.g. parcel data or infrastructures (Hoffmann 2007).

Based on literature review on the characterization of both static and dynamic infrastructures, the following challenges are identified in the context of displaced persons with SAR data:

- Very **small dwellings** composed of **light construction materials** are no ideal targets for microwaves (Wurm et al. 2017). The fact that SAR data alone is often not sufficient in urban areas is opposed to its potential as a **flexible** information source for emergencies. The integration of optical data again creates unwished independencies (Boccardo & Tonolo 2015).
- Double-bounce effects caused by the slant incidence angle and vertical structures hinder the proper and analysis of building footprints. In case of **very high-resolution data**, small incidence angles are needed to be able to discriminate buildings in densely-built areas.
- In very dense agglomerations other measures must be found to **harmonize** the spatial resolution of the input data and the scale of the expected output maps.
- The effect of **speckle** must be considered in an urban context, or at best, exploited to discriminate different surface types (Esch et al. 2010; Zhai et al. 2016).
- While the static description of urban bodies can be automatized, methods for the identification of **abrupt changes** in cases of emergencies are a challenge.
- Only few studies exist which use SAR data for the **continuation** or updating already existing data but especially in humanitarian context it might not be required to reinvent the wheel.
- While the delineation of urban bodies has become comparably well-explored, identifying small and scattered settlements in **sparsely-populated areas** is still a challenge.
- Images of **operational radar missions** need to be integrated in analyses to make best use of available-time series.

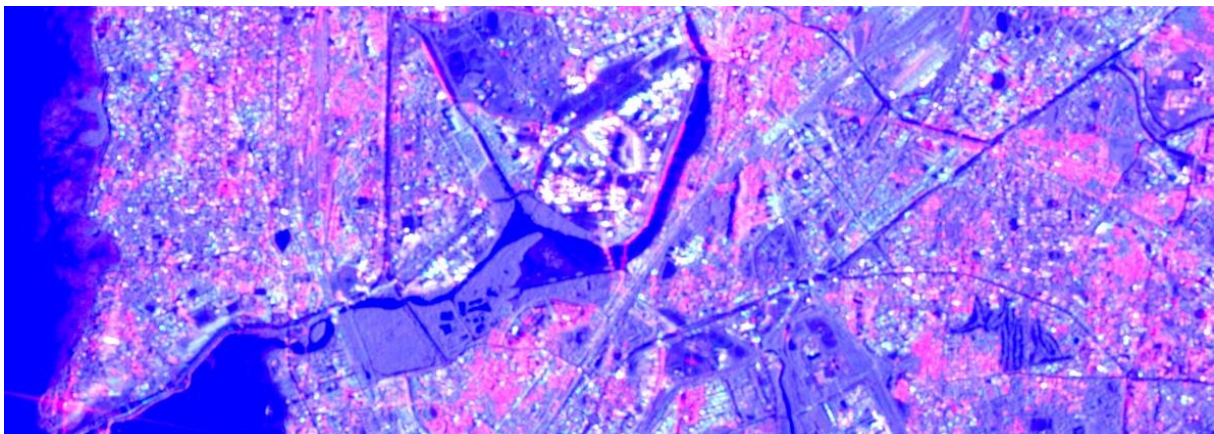


*Figure 33: Sentinel-1 image of Mumbai, India, revealing different urban structures  
Temporal average of VV (red), VH (green) and VV/VH polarization (blue)*

### 3.1.2 High-resolution mapping of camps (Dadaab, Kenya)

#### 3.1.2.1 Background and aims

Dadaab is an collective of originally five refugee camps in Garissa county (Dagahaley, Hagadera, Ifo, Ifo2 and Kambioos [closed in March 2017], UNHCR 2018d), which formed since the early 1990s when people fled from violence in the civil war of Somalia and crossed the border to Western Kenya (Montclos & Kagwanja 2000). Because of its location and continual influx, the region became a permanent settlement with over 350,000 inhabitants at peak times in 2014, making it the largest refugee camp in the world until 2017 when Kutupalong in Bangladesh reached even higher numbers (Cook & Ne 2018, described in sections 3.1.4 and 3.2.4).

The climate in this area is hot and arid with two rainy seasons (March to April and September to January) which reach up to five rainy days per month. With temperatures of constantly around 30 degrees and a total annual rainfall of 370 mm, surface water bodies and rivers are only of seasonal nature. The flat terrain has sandy and nutrient-poor soils which are predominantly covered by shrubland and thicket and sparse patches of grassland and seasonal swamps (Beaudou & Cambrézy 1999).

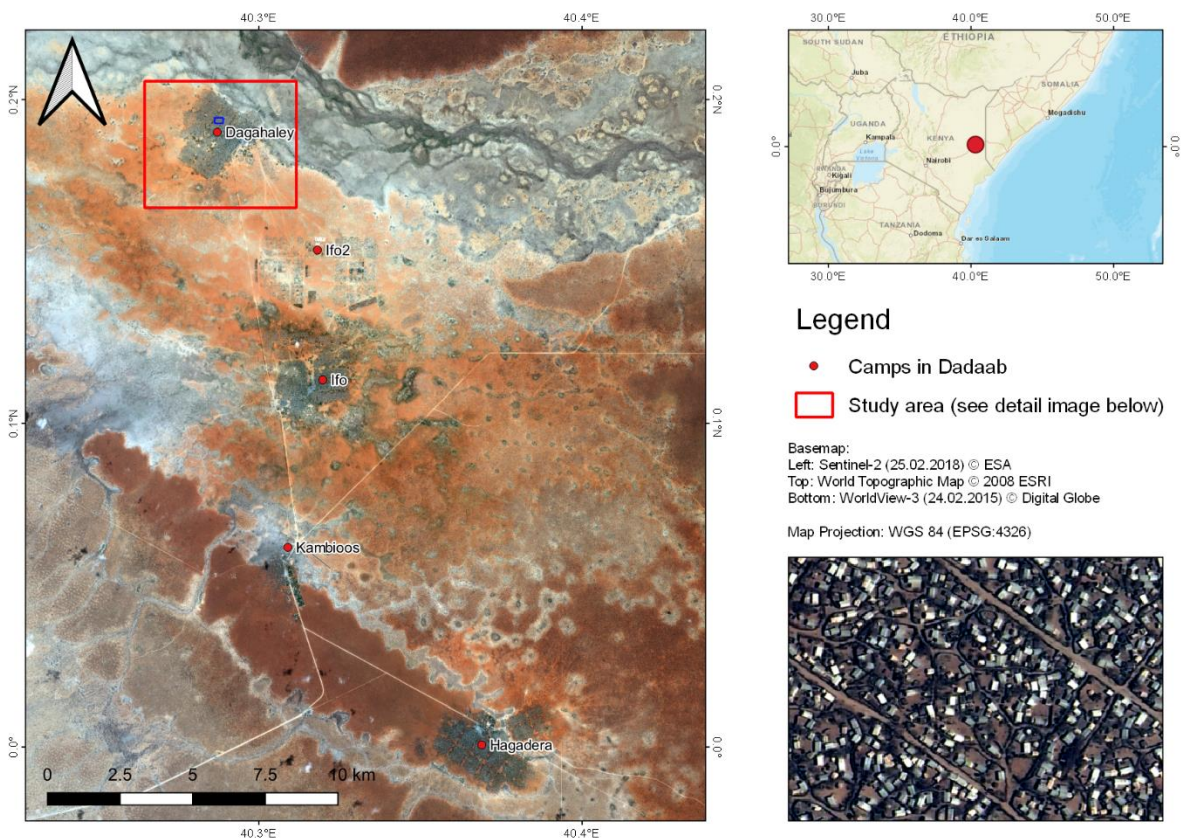


Figure 34: Study area for dwelling estimates in Dadaab region, Kenya

Camp Dagahaley is the second largest of the settlements and hosts 90.000 people in total (UNHCR 2018d). As shown in Figure 34 (detail at the bottom right), the dwellings are scattered within a regular network of roads and single households are separated by planted bushes. Although the overall structure of the camp is well-organized and its spatial extent was kept comparably constant due to management efforts, the need for reliable information on population and dwellings is still

high for the relief workers in the area (Chkam 2016). While maps of highest accuracy and information content are derived from object-based analysis of VHR imagery (Hagenlocher et al. 2012; Tiede et al. 2013; Tiede et al. 2017), the problem of cloud cover persists. This approach presents a novel approach using TerraSAR-X imagery for the detection of dwelling densities and the continuation of existing information on camp structures. It demonstrates how radar data can be used for an automated and operational monitoring of camps.

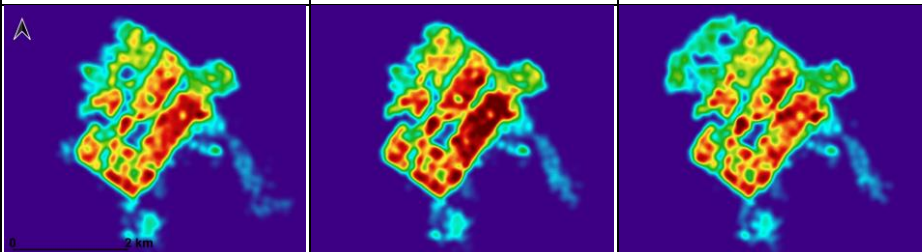
The basic idea is to exploit the increased backscatter intensity caused by corner reflection of the dwellings and volume scattering of the bushes (Figure 18) and relate it to the density of dwellings in different parts of the image. The information retrieved from two dates of 2011 and 2015 is then extrapolated to predict the density for 2018. Finally, an accuracy assessment shows the potential and limitations of this approach and the most important findings are summarized in the conclusions.

### 3.1.2.2 Data sources and processing

Three TerraSAR-X StripMap (SM) products were used in this study, acquired in 2011, 2015 and 2018 in single-polarization (HH, Table 3). They have an initial spatial resolution of 1.7 meters and cover all five camps. Due to insufficient reference data for the other camps, the study is limited to camp Dagahaley, but the presented approach is technically transferable to any area as long as the houses are not completely hidden under a tree canopy, such as camp Yida in South Sudan.

As a baseline information, single dwellings were extracted by Lang et al. (2018) based on object-based analysis of WorldView-3 data at a spatial resolution of 30 centimeters, acquired at similar dates as the TerraSAR-X images. The results were provided to MSF to assist their work in the camp. As shown in Table 3, image pairs of radar and optical reference from 2015 and 2018 were acquired within three weeks. Only the observations from 2011/2012 were 500 days apart, which is a potential error source for analyzing dwelling numbers with backscatter intensities within the radar image. However, according to the UNHCR statistical yearbooks, the population in camp Dagahaley remained stable during that time with 122,214 inhabitants in 2011 and 121,127 in 2012 (UNHCR 2013).

Table 3: Data sources for dwelling estimation in Dadaab region, Kenya

Acquisition date of <b>TerraSAR-X</b>	07.08.2011	25.02.2015	06.05.2018
Acquisition date of <b>VHR reference data</b>	19.12.2012	14.02.2015	24.05.2018
Difference [days]	500	-11	18
Number of dwellings in camp	28,622	32,480	31,822
Dwelling density [dwellings per 100 m radius]			
	<p>0 30 60 90 120 150</p>		

As demonstrated in Table 3, the number of dwellings increased from 28,622 in 2012 and reached a peak in 2015 (32,480), but with the establishment of camp Ifo2, dwelling numbers slightly decreased until 2018 (31,822). Dwelling densities were assessed at a spatial radius of 100 meters for all three reference times. As shown in the images in Table 3, the dwelling density clearly increased between 2012 and 2015, especially in the east of the camp. After systematic demolitions, this densely built-

up areas were reduced at the cost of an expansion of the camp area in the northwest. The other parts of the camp remained comparably stable during the investigated period.

Radar images were radiometrically calibrated to Sigma0 as described in section 2.3.1. As only one polarization is present in the image, a multi-scale approach has been designed by applying multi-looking (section 2.3.2) on each SAR image as shown in Table 4. Four examples are given in Figure 35 and demonstrate the principle behind this idea: While the original resolution of 1.7 meters (top left) and low number of looks (4/4, top right) describe fine differences in within the camp which originate from different dwelling sizes, materials or densities, images with higher number of looks (bottom) are more suitable to discriminate the actual built-up area from the surrounding landscapes. These low-resolution representations are required because rough surfaces and vegetation cause high backscatter outside the camp as well which is strongly reduced in images of higher number of looks.

Table 4: Parameters for multi-looking the TerraSAR-X images for dwelling estimation

Number of range / azimuth looks	2 / 2	4 / 4	8 / 7	16 / 14	32 / 29	64 / 57
Resulting spatial resolution [m]	3.51	7.02	13.12	26.24	53.41	105.89

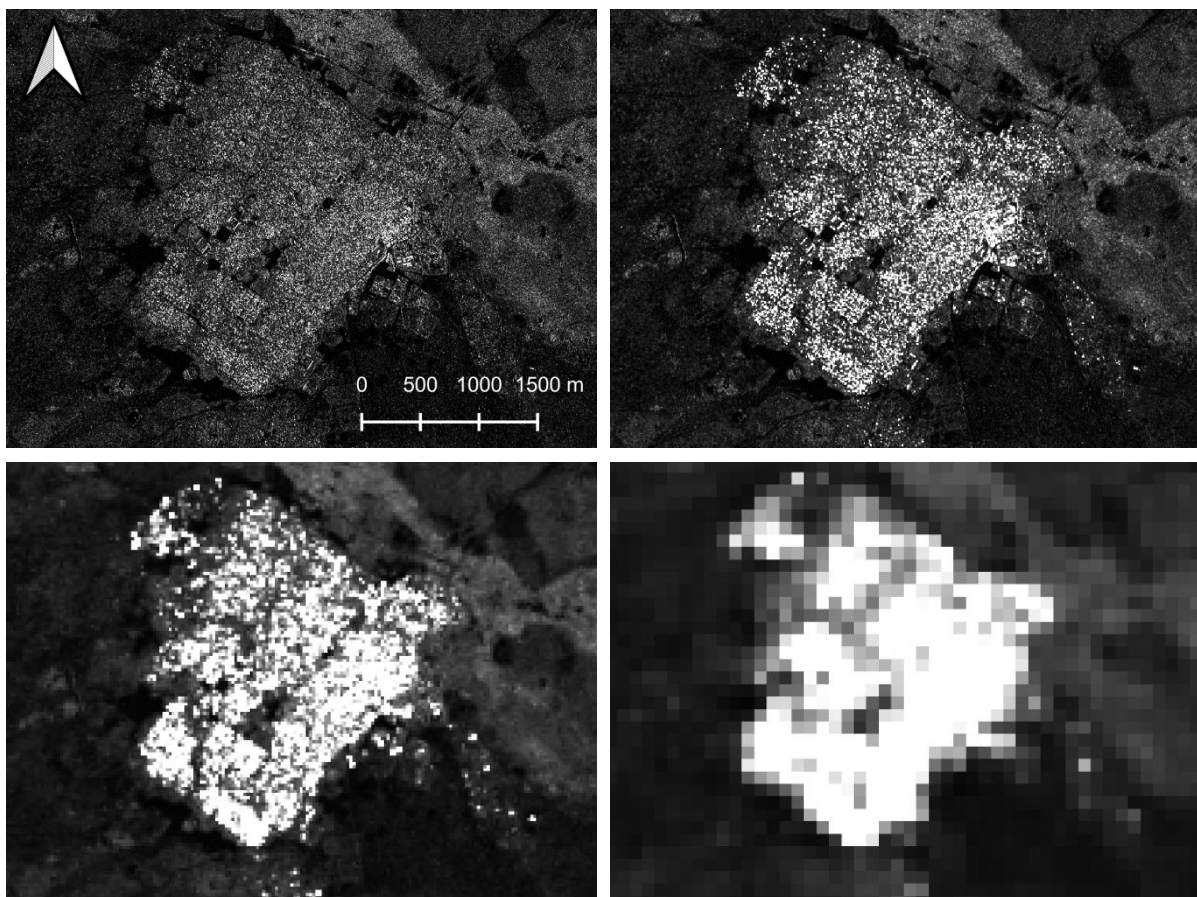


Figure 35: Realizations of multi-looking of TerraSAR-X images for dwelling estimation.

Top left: original resolution, top right: 4/4 looks, bottom left: 16/14 looks, bottom right: 64/57 looks.

All images are scaled between 0 (black) and 0.7 (white).

In a second step, a minimum and maximum filter with a kernel size of 7 pixels was applied to the multi-looked image at 7 meters of spatial resolution to retrieve two additional rasters of each investigated year. In summary, a sum of nine rasters was generated as main feature space for the

explanation of building densities, consisting of one original product, six multi-looked rasters and two filtered images.

To create a model which predicts the number of dwellings in the image based on SAR data alone, a squared grid with a spacing of 20 meters was created and the dwelling densities derived from the VHR data were extracted as an average of each grid cell. This average density is the dependent variable of the spatial modelling, while the SAR rasters described above form the independent variables which are used to explain the spatial patterns of built-up areas of the corresponding years. They were also extracted to each grid cell as statistical descriptions: *Mean, median, minimum, maximum, range, standard deviation* and *sum* of all radar pixels within each cell.

Figure 36 shows the workflow used to estimate dwelling densities for camp Dagahaley: Features were extracted from SAR products of 2011 and 2015 and related to the observed dwelling densities of retrieved from VHR images of 2012 and 2015. Multivariate relations between both data sources were then analyzed by methods of machine learning to create a model which explains the observed dwelling densities based on SAR variables from the images. In this case, a random forest (RF) was used, which randomly permutes the training data to systematically search for thresholds in the independent variables (SAR rasters) to create a set of rules (model) which explain the variance of the dwelling density as the dependent target variable (Breiman 2001). This model is then applied to the SAR rasters from 2018 to get a spatial prediction for this year based on the relationships gained from the years 2012 and 2015.

As in this case the dwelling density of 2018 is also known, a complete accuracy assessment could be performed which gives detailed insights into the capabilities of this approach.

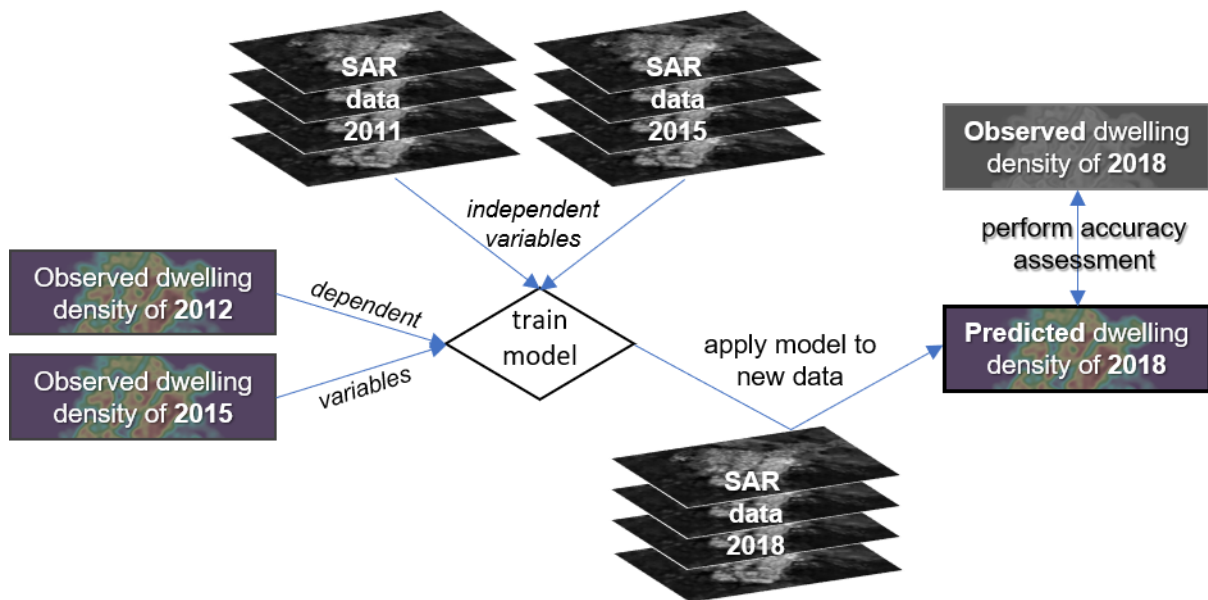
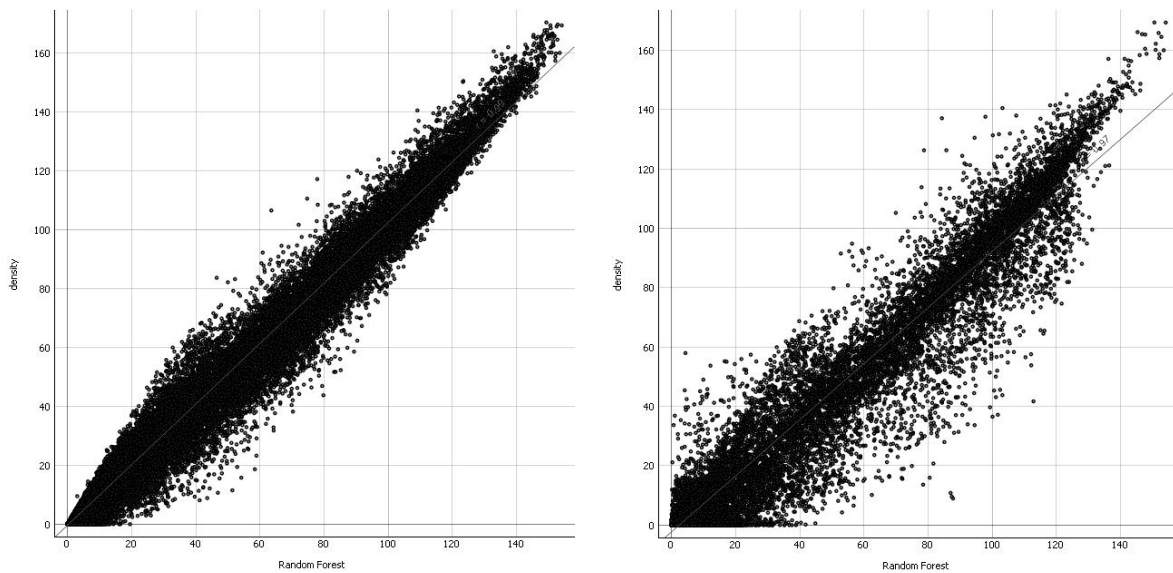


Figure 36: Workflow for dwelling estimation for camp Dagahaley, Kenya

### 3.1.2.3 Results and discussion

Figure 37 shows the dwelling density against the modelled density as learned from the data of 2012 and 2015 plotted (left) and the predicted values for 2018 plotted against the reference data (right). The coefficients of determination are  $R^2=0.99$  (training) and  $R^2=0.97$  respectively. This means, that

radar data was able to describe 99% of the variations in dwelling density for the years 2012 and 2015 and the rule set created based on these findings was able to predict 97 % of the variations in dwelling density of the year 2018 without any training data from this year. As shown in the scatter plots, the training accuracy is high throughout the whole range of values (0 to 170 dwellings within a 100-meter radius). The prediction also shows a high agreement with moderate inaccuracies in very low ranges (0 to 30) and slight underestimations for ranges above 120 dwellings. Yet, the overall performance of the model is very good.



*Figure 37: Training (left) and prediction (right) of dwelling density of camp Dagahaley*

A visual representation of the prediction is given in Figure 38: Image A shows the dwelling density for the year 2018 as observed with the VHR optical data (Table 3), while Image B shows the prediction for this year based on the model trained on data from 2012 and 2015. It is notable that especially the unbuilt area was almost completely mapped correctly (as shown by the dashed line). Only at the margins between the camp and its surroundings, smaller errors occurred. These could have been caused by volume scattering of smaller bushes around the dwellings along the edges of the camp. The documented overestimations in the north, south and east of the camp are also shown in the scatterplot of Figure 37 (right) where the dwelling density should actually be zero but was falsely predicted between 21 and 60. If exact outlines of the camp are already known, unbuilt areas could be as well masked during the training process to reduce the feature space on the built-up area.

Regarding the patterns within the camp, both the very high-density regions in the center and the east of the camp, and the lesser built-up areas along the roads and around the open space in the middle of the camp were accurately predicted. One limitation of the random forest classifier is the fact that it is rarely able to predict extreme values (here: the highest observed density), especially when they make up only a small proportion of the training areas. The randomized use of training subsets therefore disadvantages statistically underrepresented values. This is why the highest values of over 150 were not predicted by the model. The difference image clearly shows the underestimation of very high values in the center of the camp while the open areas were slightly overestimated. Although the newly constructed areas in the northwest of the camp were included in the result, the model was not able to predict the full range. At these locations, the largest differences occurred which is a clear downside of the approach. Only when camp expansion and

dismantling can be correctly predicted, the approach reaches its full potential. This can however be achieved by two strategies: The more input data is used for training (here: two years), the more stable and reliable is the result that can be expected by the trained classifier, because smaller radiometric differences between the years are levelled out. The second option is to include small fractions of training data of the year which is to be analyzed. For example, if only a small transect is included in the training data, ranging from the lowest to the highest expected value of the dataset on which the model is to be applied is sampled, the classifier is able to statistically integrate these values in the model which makes it more stable and accurate (Ren et al. 2015).

Both the accuracy assessment and the visual inspection of the results proof the concept of the presented approach and underline its potential for a long-term monitoring of refugee camps which is solely based on SAR data.

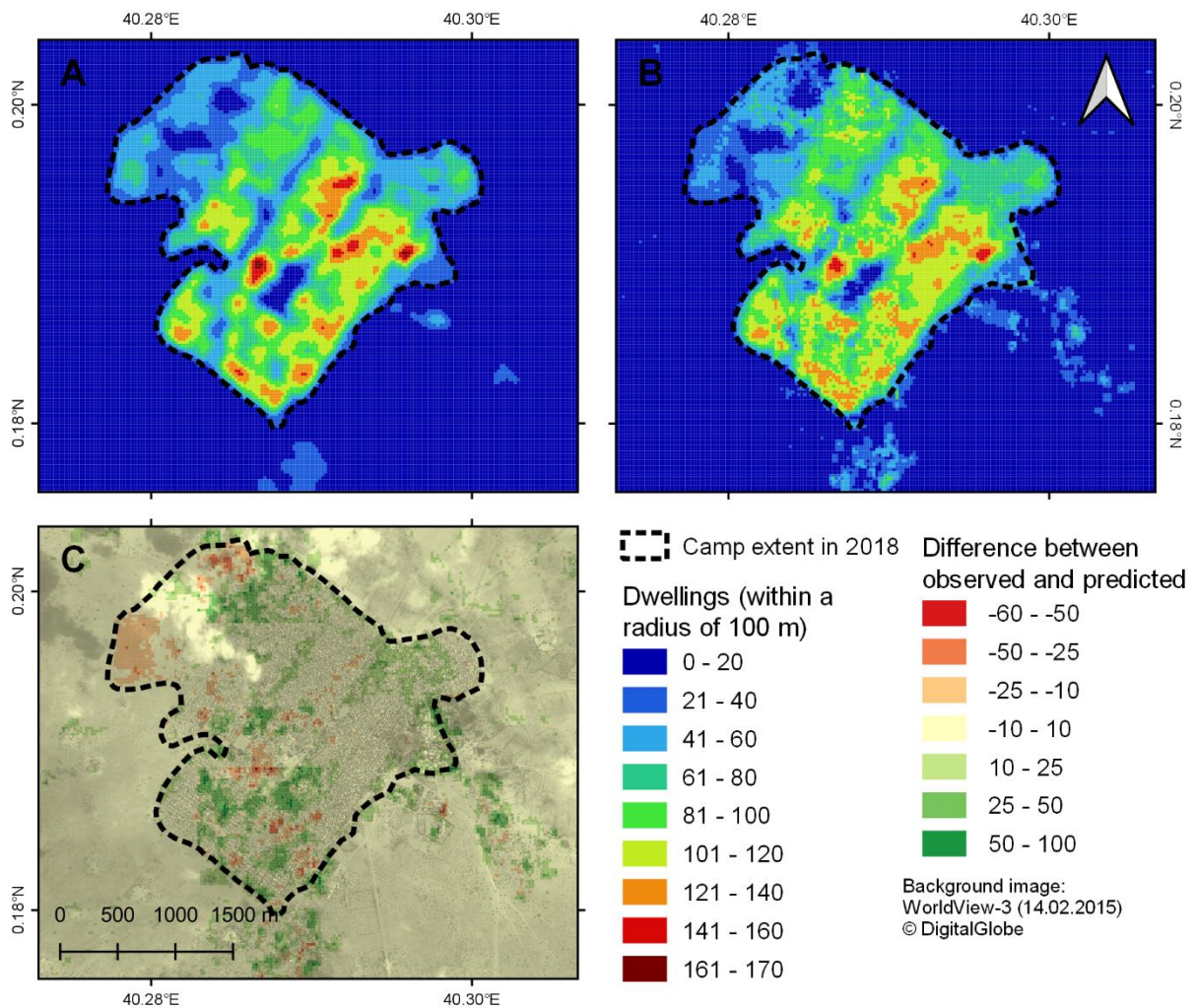


Figure 38: Results for dwelling density estimates in Dagahaley, Kenya  
 A: observed by VHR imagery, B: predicted with TerraSAR-X data, C: absolute difference

### 3.1.2.4 Scientific conclusions and practice recommendations

The following points can be concluded regarding the monitoring of camp densities with radar data:

- The detection of **single houses** is still challenging, especially when the backscatter of light construction materials is superimposed by volume scattering of vegetation present in the camp. Empirical tests by Kempf et al. (2007) report lower backscatter rates for wooden construction materials, which make them nearly invisible in urban environments.
- **Dwelling density** is a suitable proxy which can be predicted by radar imagery by using backscatter intensity at various spatial scales. These can be derived by simple multi-looking or the application of minimum and maximum filters. 0
- It has to be defined by the user, if the observed **uncertainties** (differences of  $\pm 60$  buildings) are within a tolerable range. As these could make a difference when it comes to the precise monitoring of camp changes, the following suggestions on the improvement of the accuracy should be considered.
- Once a model is trained based on a **sufficient number of input reference samples**, it can be applied to newly acquired images without new training input. As this study showed, two training inputs are sufficient to cover the variation present in a third image. Certainly, a **higher number of baseline years** used for training leads to more stable and accurate results.
- The presented approach is applicable to any camp or area. However, **transferring** a trained model to a completely different camp is critical because slight differences in the composition of built-up areas can have drastic effects on the **backscatter signature of the camp**. Regression models based on SAR data should therefore only be applied to the same area.
- **Over-fitting** of the models can be a problem and should be avoided by pruning the random forest model (Kulkarni & Sinha 2012). If the backscatter variations between the images are extreme, a simple classification and regression tree (CART, Breiman et al. 1984 ) or simple linear regressions could be more favorable.
- One further application of this approach is the **completion of missing information** within one scene, for example because of cloud cover or incomplete training data. This will be demonstrated in section 3.1.3.
- Another way to substantially improve the prediction is the integration of training data collected together with the newly acquired SAR image. A small fraction of the training data is sufficient to represent the variations in the image to be predicted and **reduce uncertainties** caused by radiometric variations between the images, for example by seasonal variations.
- Once such a method is established, one radar image acquired at the same time every year is sufficient for a **regular and precise monitoring** of a camp. Given that more and more training input is generated, the prediction accuracy is expected to increase with time.

### 3.1.3 High-resolution mapping of urban areas (Maiduguri, Nigeria)

#### 3.1.3.1 Background and aims

Maiduguri is the capital and largest city of the Borno state in northeastern Nigeria (Figure 39). The last official number on population is from 2006 which estimated 618,687 inhabitants and 103,346 households (NPC 2006). As the whole North of Nigeria faces intense population dynamics caused by dysfunctional social structures, unemployment of the youth and religious extremism, the real numbers are expected to be higher (Ordu 2017). Especially the city of Maiduguri suffers from these dynamics which is reported to have both the highest numbers of internally displaced people (Nuhu & Kwenin 2016) and the strongest population dynamics (Nuhu & Kwenin 2017). To cope with these dynamics, local administration require dense monitoring measures to keep track of changes in urban built-up areas (Porter 2002). While in many western countries, volunteered geographic information, such as OpenStreetMap (OSM) reaches quality levels which can compete with administrative data bases, the coverage in developing countries is comparably low (Sui et al. 2013). As shown in Figure 39, only buildings in the southern part of Maiduguri are currently mapped.

This case study demonstrates the potential of high-resolution SAR imagery for the estimation of building density to generate maps for population monitoring. Based on the findings in section 3.1.2, the approach focuses on the continuation of incomplete or outdated spatial information (buildings from OSM in this case) and the question, if elevation information retrieved from radar data can increase prediction quality of these approaches. Furthermore, the role of spatial resolution and polarization of radar images is analyzed by comparing predictions resulting from different datasets.

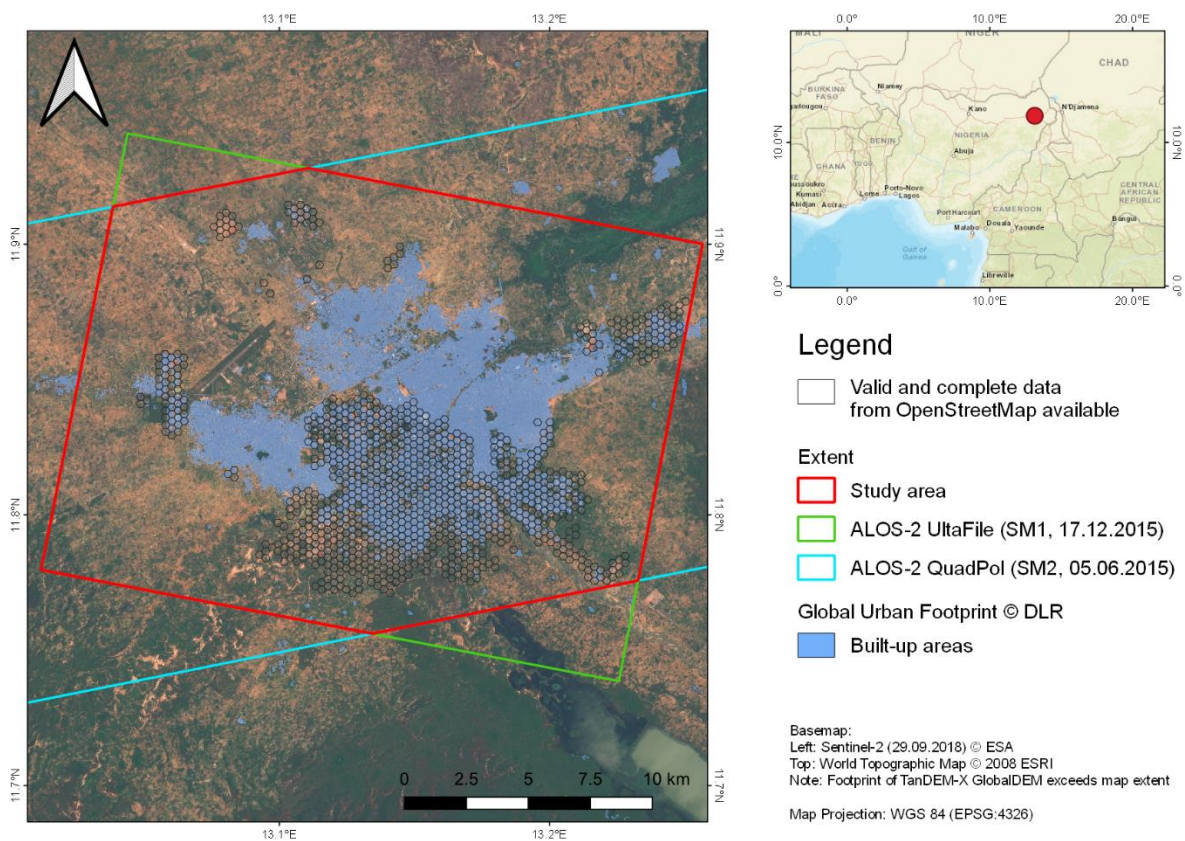


Figure 39: Study area for dwelling density estimations in Nigeria

### 3.1.3.2 Data sources and processing

Table 5 lists the satellite data used in this case study. Two images of ALOS-2 were selected, one with high spatial resolution (17.12.2015) and one with four polarizations and a slightly lower resolution (05.05.2016). This allows to identify the effect of both characteristics on the quality of population density estimates. Furthermore, a digital surface model of the TanDEM-X mission was used at a spatial resolution of 12.5 meters to test if the height information inherent in this product influences the result. Finally, a binary thematic mask of built-up areas from the Global Urban Footprint (GUF, Esch et al. 2018) was included to select unbiased sample areas for the training process.

Table 5: Satellite data used for population monitoring in Maiduguri, Nigeria

Sensor	Mode (abbreviation), polarization	Acquisition date	Spatial resolution
ALOS-2	UltraFine Mode (SM1), HH	17.12.2015	3 m
ALOS-2	QuadPol Mode (SM2), HH+HV+VH+VV	05.05.2016	6 m
TanDEM-X	Digital Elevation Model	12/2010-10/2015	12.5 m
TerraSAR-X	Global Urban Footprint (GUF)	2013-2014	12.25 m

In a first step, a hexagon grid with a spacing of 250 meters was generated over the study area and intersected with the existing building data from OpenStreetMap. Hereby, the study area outlined in Figure 39 (red line) was divided into 5,326 hexagons. The share of built-up areas within the single hexagons was subsequently calculated for all hexagons with complete building coverage (mean=8.9 %, minimum=0.01 %, maximum=46.1 %, standard deviation=7.82 %, n= 1,063). These were then used for training and validation of the building density. To also include areas with no buildings in the training process, 530 randomly selected hexagons were used which are located outside the area which is defined as urban by the Global Urban Footprint. Consequently, a total number of 1,593 hexagons was available for training (66 %) and validation (34%) of built-up areas.

ALOS-2 data were radiometrically calibrated as described in section 2.3.1 and topographically corrected using the TanDEM-X DEM. To generate a feature space of independent variables for the modeling of the building density (dependent variable), image textures (Haralick 1979) were computed from the ALOS-2 SM1 data, including *Angular Second Moment*, *Contrast*, *Correlation*, *Dissimilarity*, *Energy*, *Entropy*, *Homogeneity*, *Maximum Probability*, *Mean* and *Variance*, at kernels of 5 and 11 pixels, leading to a total of 21 features.

For the ALOS-2 SM2 data, the following polarimetric decompositions (section 2.2.4) were computed: Pauli decomposition (into *volume*, *surface* and *dihedral* scattering, shown in Figure 21), Yamaguchi (into *surface*, *double-bounce*, *volume* and *helix* scattering, Yamaguchi et al. 2005) and Entropy Alpha (into *Entropy*, *Anisotropy*, *Alpha*, *Beta*, *Delta*, *Gamma*, *Lambda*, as well as their Eigenvalues *Lambda1*, *Lambda2* and *Lambda3* and the eigenvectors *Alpha1*, *Alpha2* and *Alpha3*, Cloude & Pottier 1997). Together with the four original polarizations, 21 features are created here as well.

The digital surface model of TanDEM-X (Figure 40 a and b) was used to extract coarse building heights by repeatedly applying a morphological opening filter with a kernel size of 7 pixels to the image (Serra & Soille 2012). It removes small objects from the image which are present as small local elevation peaks in the area of the city. After 5 iterations, the elevation caused by built-up structures is almost completely removed from the image, leaving the elevations of the ground (Figure 40 c). After subtraction of the ground elevation from the surface model, the normalized surface heights of the buildings within the city remain (Figure 40 d), ranging from 0 to 10 meters in total. These heights are additionally used for the derivation of dwelling densities in the city.

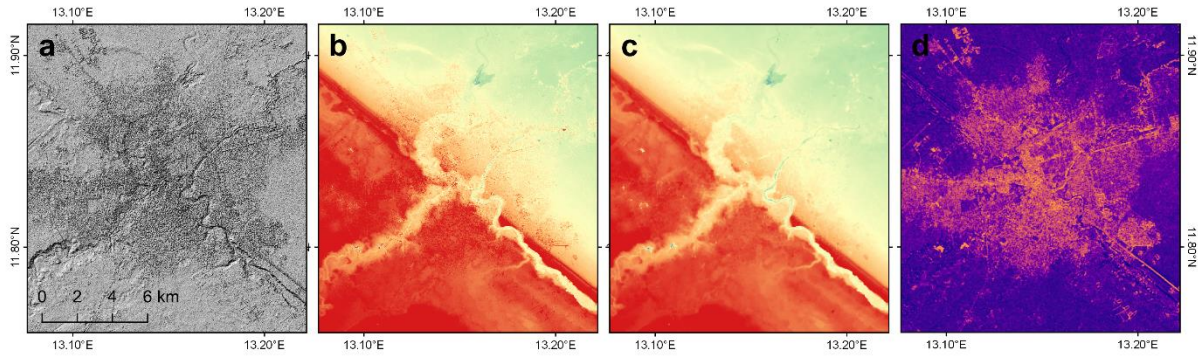


Figure 40: Generation of a digital surface model from TanDEM-X data in Maiduguri, Nigeria  
 a) hillshade, b) elevation [315-350 meters], c) filtered image [same scale], d) surface model [0-10 meters]

Zonal statistics (*mean, median, minimum, maximum, standard deviation and range*) of all features were calculated for each hexagon. This led to 126 features for both ALOS-2 datasets and 6 additional features derived from the normalized surface model, as shown in Table 6. These serve as input data for a systematic analysis of their contribution to the explanation of building density measures.

Table 6: Feature space used for building density estimation in Maiduguri, Nigeria

Name	Layers (total number)	Number of zonal statistics	Sum of features	Sum of features per dataset
SM1	HH polarization (1)	6	6	ALOS-2 Ultra Fine Mode (SM1) <b>126</b>
T5	Textures at kernel size of 5 pixels (10)	6	60	
T11	Textures at kernel size of 11 pixels (10)	6	60	
SM2	HH, HV, VH, VV polarization (4)	6	24	ALOS-2 Full Polarization Mode (SM2) <b>126</b>
P	Pauli decompositions (3)	6	18	
Y	Yamaguchi decompositions (4)	6	24	
H	Entropy-Alpha decompositions (10)	6	60	
TDX	Normalized surface height (1)	6	6	<b>6</b>

A random forest (RF) classifier was then applied to the 1,593 hexagons to create a model based on the different sets of independent variables shown in Table 6. It takes subsets of the training input data and searches for patterns in these variables to successively identify thresholds which can predict the variation of the dependent variable. This process is repeated with randomized subsets of the training inputs to create an ensemble model with those variables which are most suitable to explain the observed building density (Breiman 2001). Table 7 lists different combinations of input data and their corresponding Root Mean Square Error (RMSE) and coefficient of determination ( $R^2$ ).

Table 7: Accuracy assessment for building density estimations with different input data

	SM1	TDX	SM2	SM1+T5	SM1+T5+T11	SM1+T5+T11+TDX	SM2+P	SM2+P+Y+H	SM2+P+Y+H+TDX
<i>n</i>	6	6	24	66	126	132	42	126	132
RMSE	0.042	0.050	0.036	0.036	0.038	0.038	0.036	0.035	0.033
$R^2$	0.698	0.556	0.773	0.724	0.726	0.750	0.793	0.838	0.841

### 3.1.3.3 Results and discussion

Figure 41 plots the measured building density against the predictions based on single (SM1+T5+T11+TDX, red) and full-polarization (SM2+P+Y+H+TDX, blue) ALOS-2 data as listed in Table 6. This plot demonstrates how well the random forest classifier can reproduce the observed patterns. It is notable that the texture-based approach (red) overestimates values smaller 10 % while the polarization-based approach (blue) underestimates them.

As shown in Table 7, the  $R^2$  ranges between 0.69 and 0.84, which means that up to 84 % of the variation of the building density can be explained by the radar-related variables. The RMSE lies between 0.033 and 0.05 denotes that the mean error of prediction is 3.3 to 5 % (in the unit of building density).

Comparing the two ALOS-2 products of single polarization (SM1, 3 m) and full polarization (SM2, 6 m), it is shown that the number polarimetric information outperforms spatial resolution. As the building density is calculated at the hexagon level, spatial resolution plays a minor role in this study. As shown in Table 7, the four channels of the quad-polarized product already reach an  $R^2$  of 0.773, but the integration of polarimetric decompositions increases it up to 0.79 and 0.83 respectively.

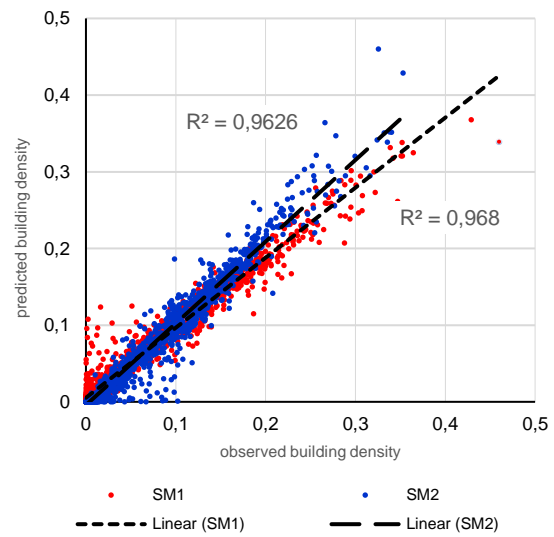


Figure 41: Observed vs. predicted building density based on ALOS-2 single polarization (SM1, red) and full polarization (SM2, blue) data

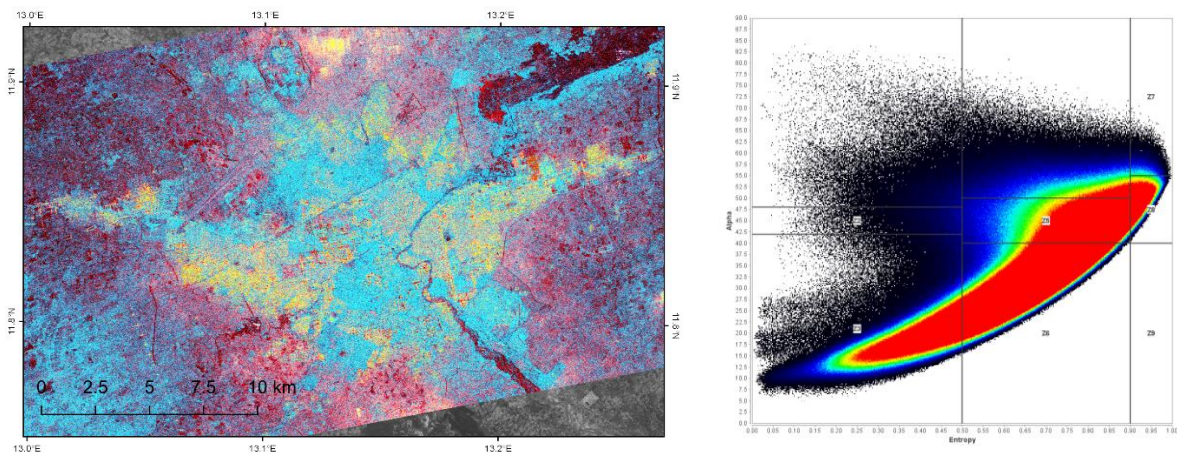


Figure 42: Anisotropy (red), Alpha angle (green) and Entropy (blue) derived from ALOS-2 data for the city of Maiduguri (left), Entropy-Alpha plane (right)

While Pauli decompositions already include the contribution of double bounce, which is a main scattering mechanism caused by buildings (Figure 18 and section 2.2.4), the integration of helix scattering of the Yamaguchi is beneficial in complex urban environments as well, because it takes into account the co-polarization and cross-polarization correlations (Yamaguchi et al. 2005). Also, Entropy and the Alpha Angle ( $\alpha$ ) are suitable indicators for the presence of built-up areas (Colin-Koeniguer & Trouvé 2011; Hariharan et al. 2016). As shown in Figure 42 (left), the city shows high Entropy (blue) and Alpha values (green), resulting in cyan and yellow signatures. Parts with

different building densities area already visible in the RGB image. They correspond to zones 4 and 7 in the Entropy-Alpha plane Figure 42 (right), which represent double bounce and complex scattering (Cloude & Pottier 1997). The table also shows that once fully polarimetric data is integrated, the normalized surface heights do no longer bring a benefit in terms of prediction accuracy ( $R^2=0.838$  and  $0.841$ ). This means that, at a spatial resolution of 6 meters, the decomposed measures already sufficiently represent the built-up structure of the city, especially by double-bounce and helix scattering.

A final map based on the result with the highest accuracy (SM2+P+Y+H+TDX) is shown in Figure 43. It has a training accuracy of  $R^2=0.96$  (Figure 41) and a coefficient of determination of  $R^2=0.84$  (Table 7). The hexagons clearly delineate the city's extent and agree with the ones covering built-up areas according to the Global Urban Footprint (white line). It is also notable that the city's building density was correctly predicted throughout the whole image and almost no area outside the urban footprint was predicted higher than 1%. And despite the comparable low representation of high density areas (> 30%) in the training data (black hexagons), the random forest classifier was able to detect the historic center around the districts Shehuri and Limanti at  $11.85^\circ\text{N} / 13.15^\circ\text{E}$  (REACH 2017). The algorithm was also able to detect changes at the edges of the city, for example the refugee camps of Afra Shagari in the northwest or Bakasi in the southwest of the city, as well as the expansion of the Dusuma district in the northeast, containing Muna Garage El Badawe, a temporary shelter for currently 17,000 displaced people (CCCM 2016).

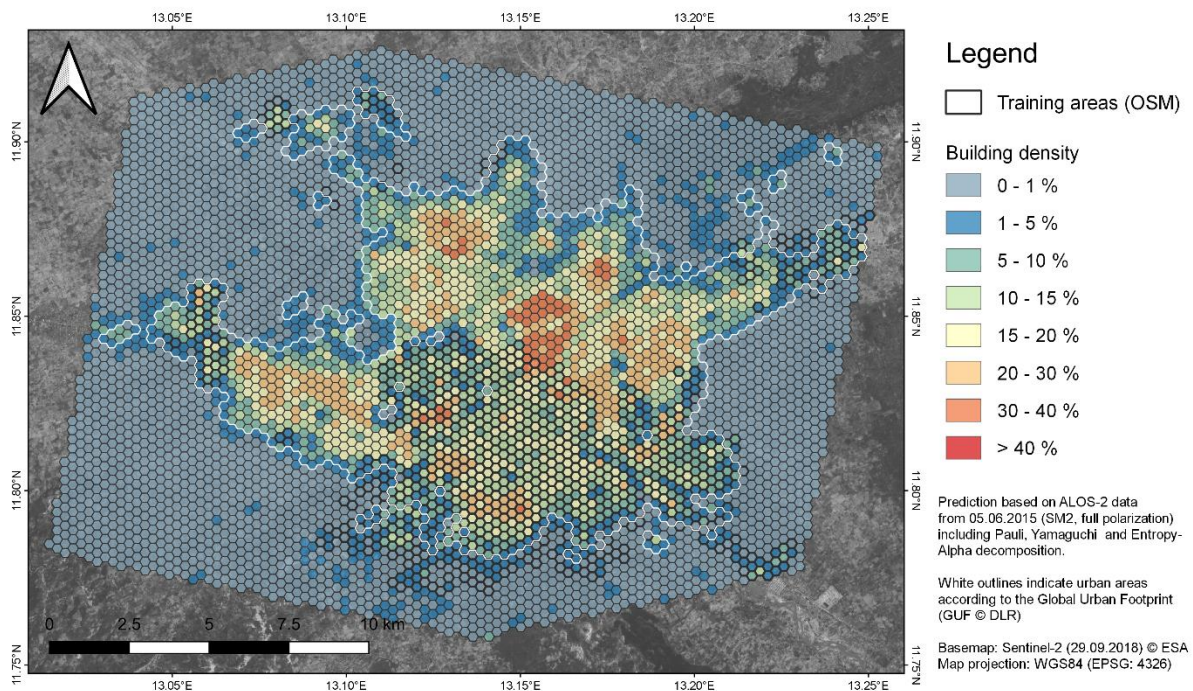


Figure 43: Building density for Maiduguri, Nigeria

Despite the demonstration of the value of SAR products for building density mapping, there are some points to discuss: At first, the used data of ALOS-2 were not acquired within the same time but with approximately 5 months apart. Especially comparisons of both approaches (SM1 vs. SM2) could therefore underlie smaller temporal changes within the city's structure. Another uncertainty is introduced by using the OpenStreetMap data for training purposes because there is no information on their quality. However, the visual comparison with VHR optical imagery show a

very high degree of completeness in the edited part of the city and most of them were digitized in November 2016 according to the metadata (Figure 103). This means, that there is also a potential mismatch between the radar imagery and the density measure derived from OSM which could result in higher or lower densities than actually captured by the SAR products, especially in the emergency camps constructed since 2016. Lastly, the dates of acquisition of the images underlying the ancillary data in this study (GUF, 2014-2015 and TDX 2010-2015, see Table 33) are not consistently from the same period and might also introduce smaller discrepancies.

Finally, as in every remote sensing analysis, the built-up environment can only serve as an indicator for population density (Wu et al. 2005). Especially as the average number of inhabitants per dwelling is higher in camps and emergency shelters, additional information is required on the dwelling types in different parts of the city as well as their occupancy rates (Hailey 2009). Still the proposed method proves that SAR data is a suitable input for building density and a potential input for long-term monitoring.

#### 3.1.3.4 Scientific conclusions and practice recommendations

The following concluding remarks can be made regarding the estimation of building densities in urban environments:

- A minimum amount of **training data** must be available, either from surveys, maps or crowd-sourced platforms, as in this case. Calculating spatial statistics at an aggregated level (here: hexagons of 250 meters) substantially increases the feature space and the prediction accuracy.
- **Incomplete data** can be extrapolated to a larger area if it contains a representative sample of the whole city, e.g. including buildings of different types and sizes at a statistically sufficient number.
- **Machine learning techniques**, such as the random forest classifier used in this case, are suitable for the prediction of a dependent variable, because they allow the integration of a large number of input data (independent variables), even if they are or of different units redundant regarding their information content, as it is the case for texture-related SAR analyses.
- High resolution SAR data of **single polarization** can be enriched by calculating image textures (mostly sufficient at one scale) while **fully polarimetric data** can be decomposed into more complex measures.
- In this case, data with full polarization (SM1) was more efficient than data with higher spatial resolution (SM2) and should be preferred in case of **tasking new images** for urban analyses, whenever the sensor supports it (Table 32, Appendix 2). If these data are not available, prediction accuracies can be increased by the integration of **ancillary data**, in our case surface heights. Here, any data can serve as ancillary data if they are available for the whole investigated area, for example optical imagery.
- Whenever possible, all data used for training (OSM) and prediction (SAR images, surface heights, GUF) should be from a **similar date of acquisition** to reduce errors caused by temporal changes within the investigated areas.
- Dealing with **uncertainties** is important in any spatial prediction because possible error sources should be communicated to the user. This includes a proper accuracy assessment naming the overall standard error of the model, as well as the spatial distribution of the prediction quality, for example by the standard deviation of all random forest realizations (Ließ et al. 2012). This helps the user to evaluate the given values in a context and increases the general usability of the results.

### 3.1.4 Mapping camp growth at different spatial and temporal scales (Kutupalong, Bangladesh)

#### 3.1.4.1 Background and aims

Kutupalong is a refugee camp in southeastern Bangladesh, close to the border to Myanmar (Figure 44, top left) which was opened, together with camp Nayapara, in the year 1991 to host refugees fleeing from oppression by the government and expulsion by the Burmese military force. The refugees are mainly of the Muslim Rohingya minority which suffer from ethnic conflicts accompanied by deprivation of many of their human rights, including their citizenship, since the outbreak of violent conflicts in the 1960s (Martin et al. 2017). The population gradually increased since the opening of the camps, but at a decent rate (de Vries et al. 2017). However, the numbers dramatically increased when 6,700 Rohingyas were killed in military clearance operations in August 2017, leading to over 900,000 people on the run (Gee 2017). Within a few weeks, the number of people hosted in Kutupalong and Nayapara doubled from 34,000 to 70,000 until the end of September 2017 (ISCG 2018). After several expansions, Kutupalong became the officially largest refugee camp with a population of over 600,000 inhabitants in February 2018 (OCHA 2018).

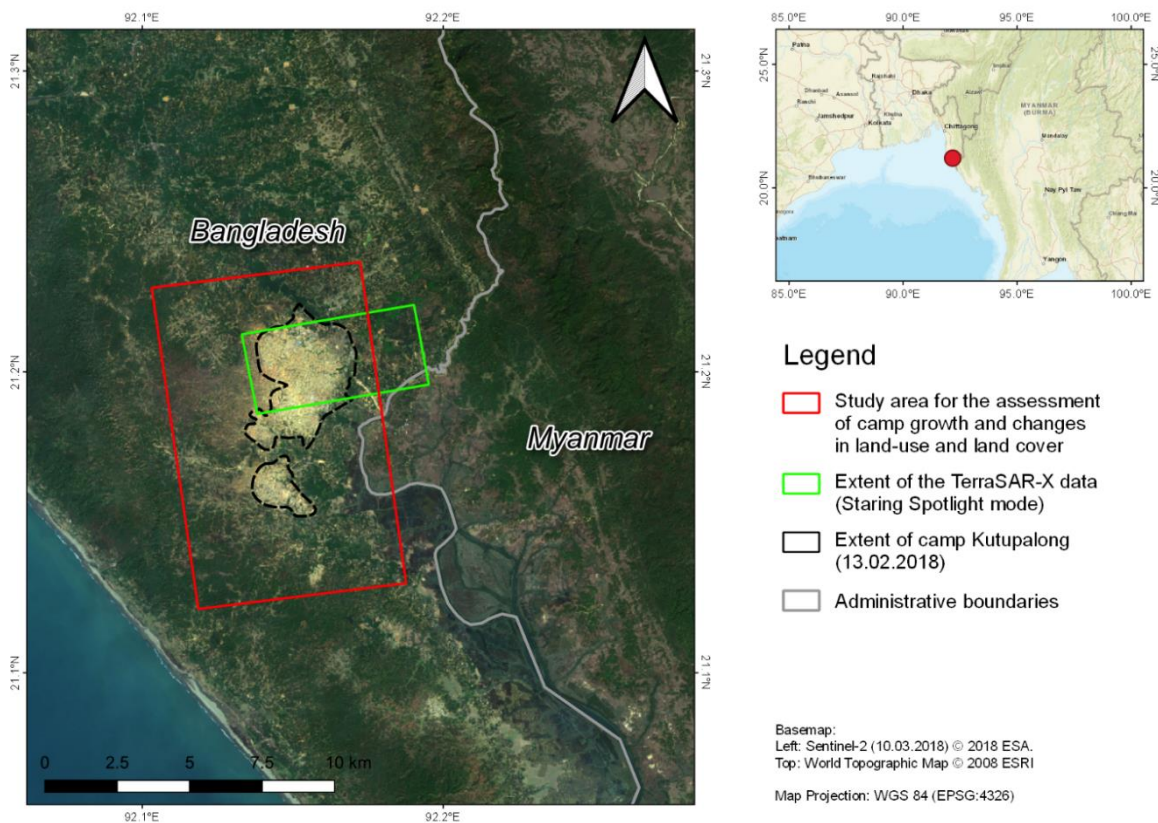


Figure 44: Study area for the monitoring of camp growth, Bangladesh

Although the camp is supported by various international organizations and governments, the rapid growth of the camp led to miserable living conditions, malnutrition, diseases and vulnerability towards natural disasters (Leidman et al. 2018). Although the site planning taskforce of the Refugee Relief and Rehabilitation Commission (RRRC) put efforts in the management of camp expansion, the uncontrolled sprawl of the camp is one of the main challenges of humanitarian response (Cook & Ne 2018). Besides that, massive deforestation leads to a loss of environmental resources, clashes with local wildlife populations and an increased risk of flooding (Labib et al. 2018; Rahman 2018).

Two studies have already investigated the growth of Kutupalong based on optical imagery, but both report obstacles with insufficient spatial resolution and data quality (Landsat ETM+, Labib et al. 2018) and limited data availability because of cloud cover during the rainy season (Sentinel-2, Hassan 2018). This study shows how SAR imagery can be employed for the monitoring of camp growth by using the retreat of forests as a proxy. It furthermore demonstrates the capabilities and limitations of very high-resolution (VHR) radar images to identify changes within the camps.

### 3.1.4.2 Data sources and processing

Three different approaches are presented in this section: a) Rapid visualization of deforestation caused by camp growth, b) quantification of deforestation caused by camp growth by supervised classification and c) detection of changes within the camp based on VHR imagery. All approaches deal with the challenge of monitoring camp expansion but use different data and methods.

#### *a) Rapid visualization of camp growth*

SAR images are suitable to get a quick impression of temporal developments by combining information of different dates in one image. The most straightforward method is to create an RGB composite which combines SAR backscatter of two or three different acquisitions based on the additive color mixture model (Stabel & Löffler 2003). The result is a color image where each pixel's tone represents the contribution of backscatter at each date compared to the other dates. More advanced techniques use RGB composites based on principal component analyses (PCA, PCA Siegert & Ruecker 2000) or interferometric coherence based on different image pairs (Liu et al. 2001). For the camp of Kutupalong, three periods related to the displacement of the Rohingya were compared:

- Red: 01.06.2017 – 25.08.2017 (before the immigration)
- Green: 26.08.2017 – 30.11.2017 (during the immigration)
- Blue: 01.12.2017 – 28.02.2018 (mostly after the immigration)

For each period, a temporal average of the VH polarization channel was calculated using the Google Earth Engine (Gorelick et al. 2017), as described in section 3.1.5.2. The RGB composite is shown in Figure 45 (left) as well as a visual interpretation (right). It shows different stages of the growth of camp Kutupalong and its effects on the forest areas. While pixels in white, grey and black represent stable backscatter intensity during all three periods, the colors give indications on the change of surface characteristics. Before the immigration started on 25<sup>th</sup> of August 2017, the inhabited sites, visible as bright white clusters of pixels, had core areas of 74, 38 and 77 hectares (Figure 45 left, area #1). They were surrounded by areas of mixed land use. The first retreat of forests caused by expansion of the camps is shown as bright red areas (#2). Originally, these areas showed high backscatter because of volume scattering of the forest canopies. Once these forests were cleared, backscatter intensity decreased for the second (green) and third (blue) period, thus leaving the red component dominant in the RGB mixture. The further deforestation is shown in yellow, because backscatter decreased after 01.12.2017, reducing the blue component of the RGB mixture (#3). Bright yellow patterns indicate first partial loss of forests in the westernmost areas (#4). A densification in the areas around the camps which did not have any forests cover is shown as indifferent colored textures.

This kind of image combination allows a quick identification of temporal dynamics but basic knowledge on the study area and the scattering mechanisms is required. For example, the valleys in the northwest and the wetlands in the southeast also show strong color variation because of

different water levels which cause alternating rough and smooth surfaces. They could be mistaken as changes caused by deforestation or camp growth by users who are unexperienced in this area.

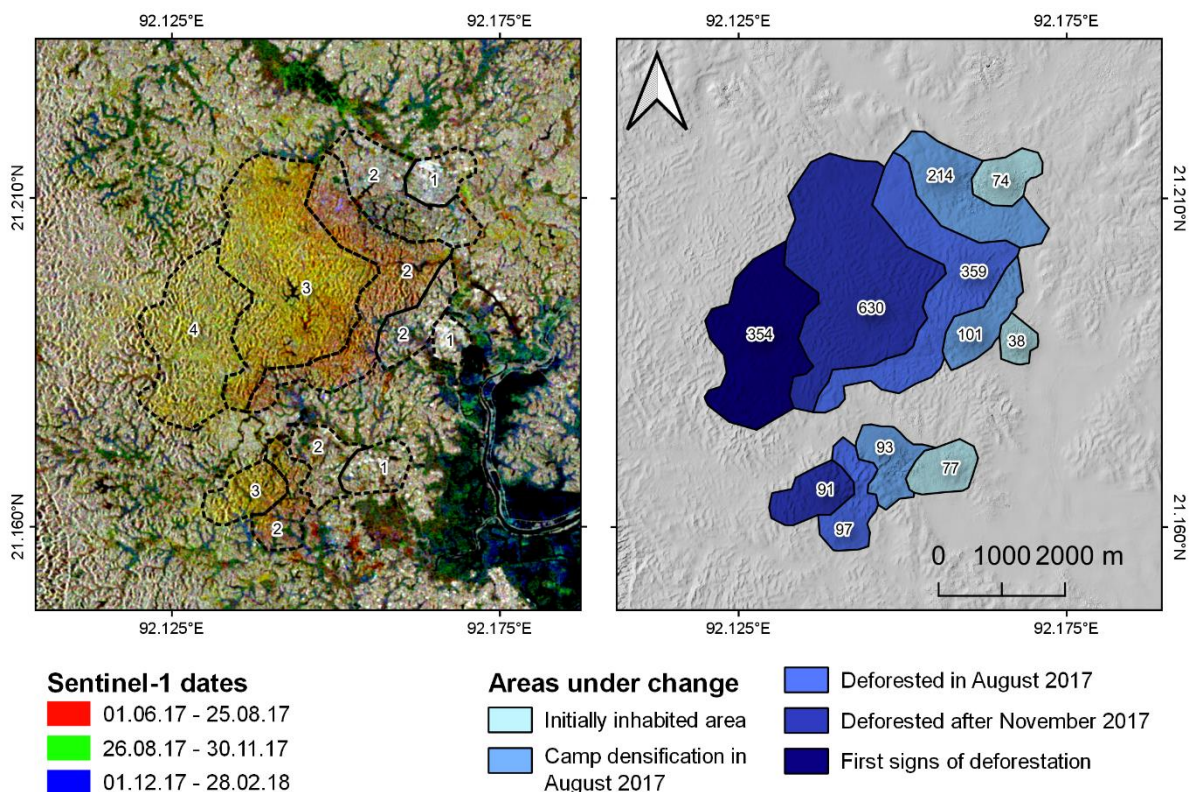


Figure 45: RGB composite of Sentinel-1 images (left) and corresponding interpretation (right)

The overall increase of the camp area was digitized based on visual inspections (Figure 45, right), leading to a total increase of the camp area from 190 ha before 25<sup>th</sup> of August 2017, to 1000 ha until the end of November and a total size of 1800 ha at the end of February 2018. Including the areas which were already being deforested (#4), a total area of 2500 ha was affected by the camp.

#### b) Quantification of deforestation by supervised classification

While the manual digitization of images is a quick method, it might deliver different results according to the interpretation of the corresponding user. A more objective approach is the automated forest classification based on radar imagery which is presented in the following. As a reference, two forest classifications based on Landsat imagery from December 2016 and December 2017 were used as provided by Hassan et al. (2018). They represent the spatial distribution of forest areas before and after the influx of the Rohingya people in August 2017. Six Sentinel-1 images acquired between October and February of the respective years were used for the classification (Table 8).

The images were radiometrically calibrated to Sigma0, converted to dB scale and geometrically corrected using the SRTM digital elevation model as described in sections 2.3.1 and 2.3.3. All scenes were acquired as dual-polarization products (VV and VH). A temporal average was calculated for each polarization of all pre-influx and post-influx images as described in equation 15 in section 3.1.5.2. A ratio was then calculated for both periods by dividing means of VV by VH. This ratio

describes the tendency of areas for changes in polarization, which is often caused by tree canopies and other vegetation structures (Chen et al. 2009; Omar et al. 2017; Ranson & Sun 1994).

Table 8: SAR images used for forest classification in Kutupalong, Bangladesh

Sensor	Mode	Dates	Remarks
Sentinel-1	Interferometric Wide Swath (IW)	23.10.2016, 16.11.2016, 10.12.2016, 03.01.2017, 27.01.2017, 20.02.2017	pre-influx
Sentinel-1	Interferometric Wide Swath (IW)	23.11.2017, 05.12.2017, 29.12.2017, 10.01.2018, 22.01.2018, 03.02.2018	post-influx

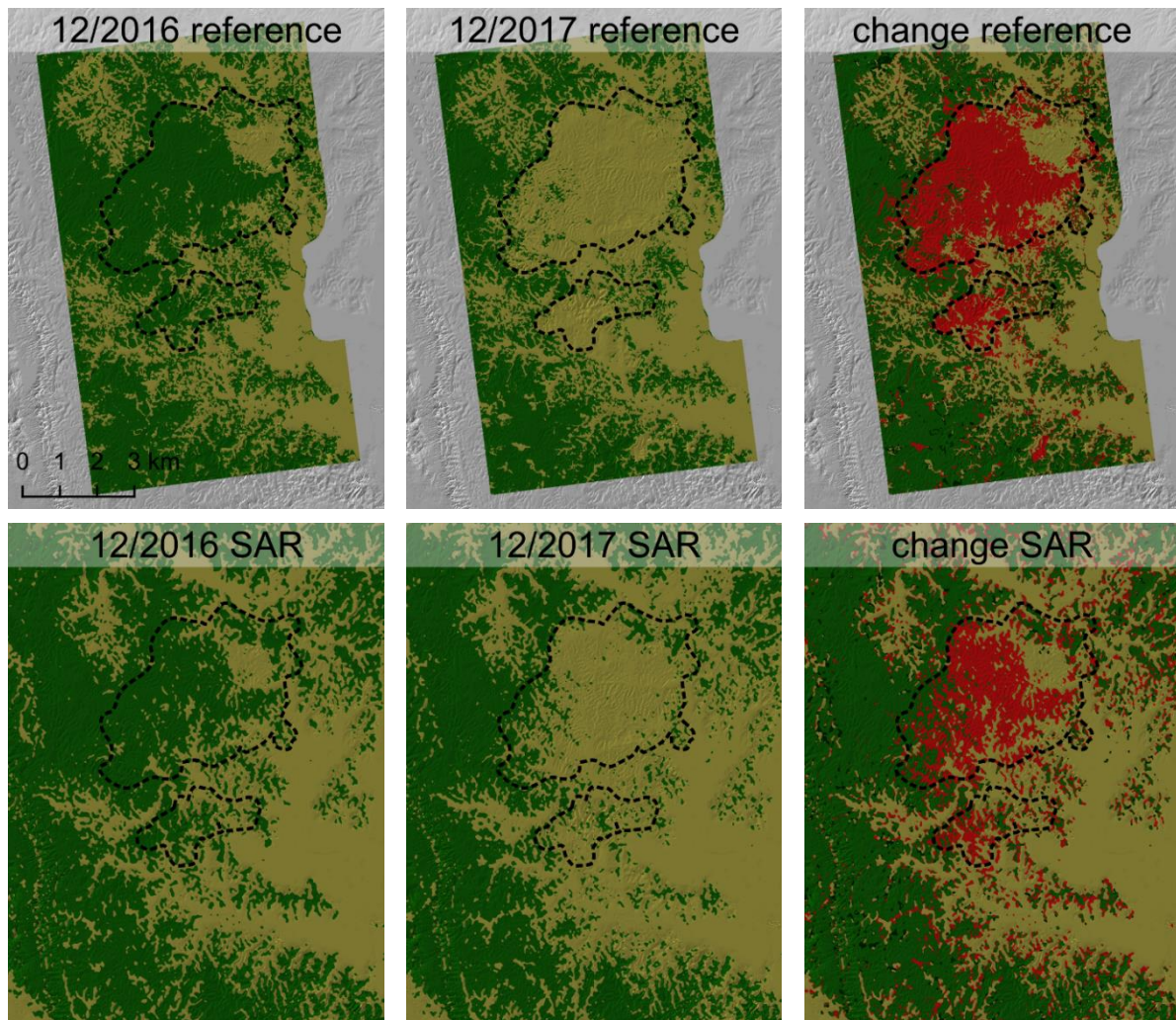


Figure 46: Forest change around Kutupalong between December 2016 and December 2017  
 Top: reference (Hassan 2018), bottom: SAR-based classification

All computed raster data served as input layers for the supervised classification which was conducted by randomly selecting 5000 sampling points for the two classes “forest” and “non-forest” based on the classification by Hassan et al. (2018). A random forest (RF) classifier was used which systematically analyzes patterns in the training data to create a set of rules to describe the presence of forest for the whole study area based on the available SAR information (Breiman 2001). A more sophisticated use of a RF classifier is demonstrated in section 3.3.3. The result are two forest maps for December 2016 and 2017 (Figure 46, left and middle). As shown, the overall pattern of forested areas is classified well by the radar data. A change map was computed on both the

reference images and the SAR-based classification (Figure 46, right). The results are discussed in the next section.

*c) Detection of changes within the camp based on VHR imagery*

To demonstrate the potential of very high-resolution (VHR) SAR imagery for the mapping of camp dynamics, six TerraSAR-X images acquired in Staring Spotlight (ST) mode were used. It achieves an azimuth resolution of up to 25 centimeters by widening the azimuth beam steering angle range, thereby extending the synthetic aperture (Figure 12, Mittermayer et al. 2014). However, this imagery is not captured systematically, but only after tasking by the user. Consequently, the first available image of camp Kutupalong was acquired on 30.09.2017 when the camp has already grown considerably. The further scenes were acquired at the following dates: 11.10.2017, 27.12.2017, 07.01.2018, 18.01.2018 and 04.08.2018. Their extent is shown in Figure 44 (green area). Prior to the analysis, all images were radiometrically calibrated to Sigma0 and geocoded using the DEM generated in section 3.2.4.

To highlight changes during this period, temporal RGB composites were created for all consecutive image triplets. Areas of no change are displayed in black, grey or white while colors indicate changes in backscatter intensity. As the core area of the camp is only sparsely vegetated, most of the changes result from the construction of dwellings or their demolition. Examples are shown in Figure 47 and a full map of Kutupalong is shown in Figure 106 (Appendix 8). The RGB is composed of images from September 2017 (red), December 2017 (green) and August 2018 (blue) so that changes within the camps can be related to the different periods. The image on the left shows changes in the core area of the camp which has been densified since September at various locations (cyan and blue), but also some buildings were demolished (red and yellow), while the image in the middle shows the growth of the camp in westward direction after September 2017 (cyan objects). The image on the right demonstrates how new buildings were constructed in the floodplain but have been removed before August 2018 because of safety concerns. The RGB images serve as a valuable input for the visual identification of changes between three selected dates. Based on this information, building-related changes were manually mapped which is demonstrated in the following.

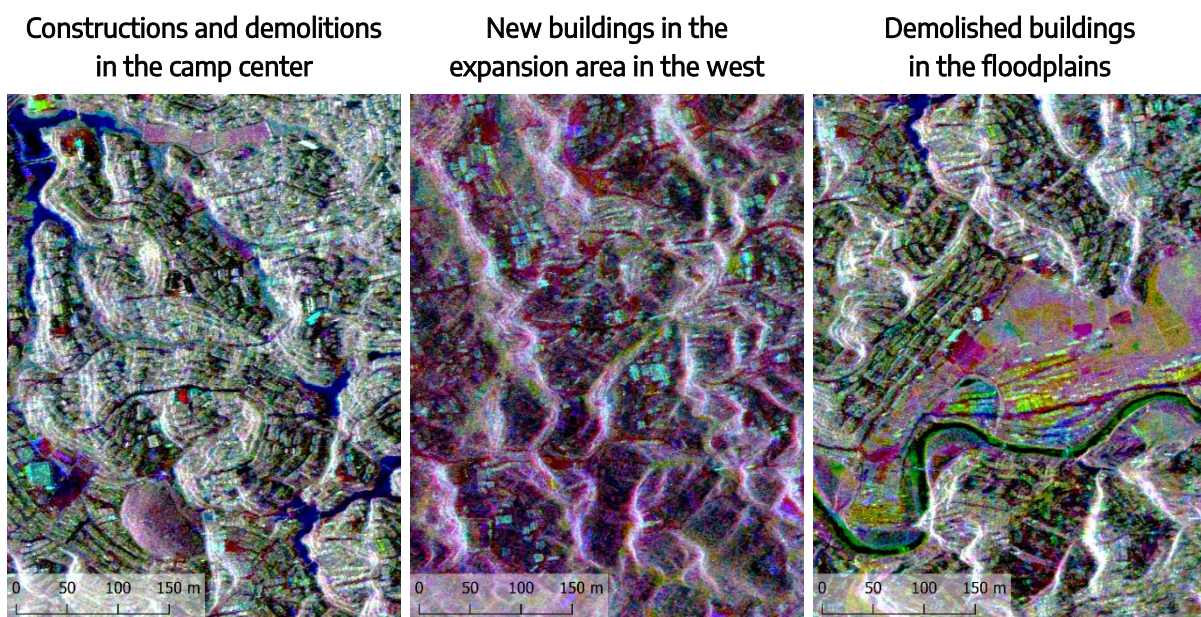
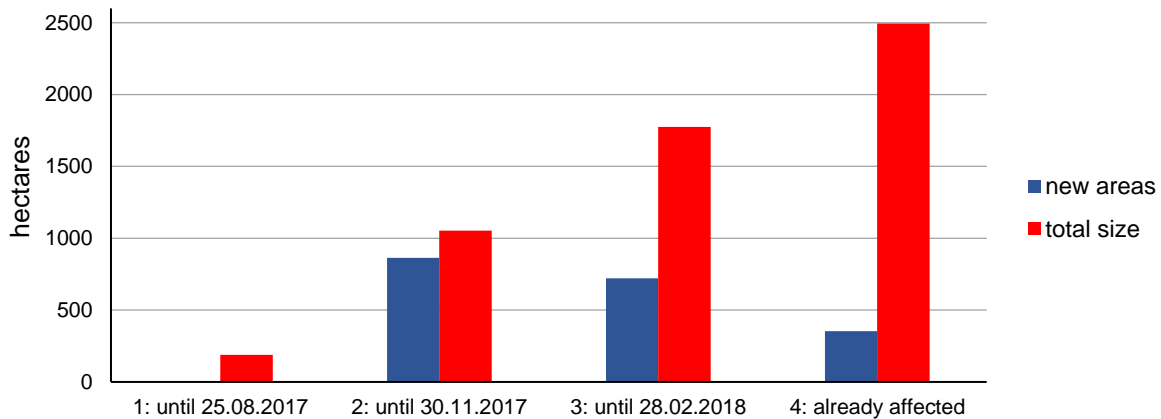


Figure 47: Temporal changes within camp Kutupalong as identified by VHR SAR color composites

*Red: 30.09.2017, green: 27.12.2017, blue: 04.08.2018*

### 3.1.4.3 Results and discussion

Figure 48 shows the growth of the camp between August 2017 and February 2018, as identified in the RGB composite of the Sentinel-1 imagery. Upon the massive influx of refugees from Myanmar, the original area of 190 hectares increased by the factor of 13 to a final area of around 2500 hectares within only half a year. At the same time, the population increased by a factor of 18, leading to overcrowding, tumult and scarcity of foods and medical care in the camp.



*Figure 48: Size of camp Kutupalong as identified in the Sentinel-1 RGB image  
Numbers in the x-axis correspond to the stages of camp growth as shown in Figure 45.*

As already stated, visual inspection of temporal composites requires skilled users which are able to interpret the changes in backscatter characteristics of surfaces in order to prevent false deductions. This is especially critical regarding loss of vegetation because it can cause both decrease (loss of volume scattering) and increase (replacement by other surfaces with higher roughness) of backscatter intensity. It is advisable to map changes by multiple users to reduce the risk of misinterpretation and lacking objectivity of individuals.

Changes of built-up structures, as shown for the TerraSAR-X images, are easier to interpret because most of the buildings cause very high backscatter and any change is clearly identifiable. Major challenges in Kutupalong, and probably also in many other refugee camps, are the density of buildings and their light construction materials. Despite the very high spatial resolution of 0.5 meters, individual buildings were not distinguishable in some parts of the camp because they were too close together or covered by natural materials (palm leaves, wood) which hardly interact with the incoming microwave signal, leading to low backscatter intensity. Furthermore, the signature of single buildings can be obscured or distorted by the surrounding vegetation. This was also reported by Checchi et al. 2013 who performed manual counting of buildings in Kutupalong based on VHR optical imagery and struggled with similar spectral characteristics of huts and adjacent trees. The SAR-based derivation of absolute of buildings in a refugee camp based on SAR data is therefore still a challenge and requires either assumptions on the size and orientation of the buildings (Jin & Davis 2005) or detailed a-priori knowledge of the study area and the employed scene (Franceschetti et al. 2007). More advanced approaches suggest fusion with optical data (Spröhnle et al. 2017) but this again increases dependency from up-to-date and cloud-free acquisitions.

To assess the quality of the classification-based approach, a pixel-based accuracy assessment was carried out. The share of correctly classified forest areas was 78.1 % (2016) and 67.9 % (2017) and

the share of correctly classified non-forest areas was 82.4 % (2016) and 85.8 % (2017). Accordingly, the investigated periods score an overall accuracy of 79,9 % (2016) and 78.5 % (2017). The spatial extent of decreased forest areas was correctly classified, but underestimated forest areas in the period of 12/2016 led to a slightly lower area of deforestation (Figure 46, right, red areas). This underestimation led to considerably lower accuracies of the resulting change map because it adds classification errors from both dates together (Table 9). A complete map of correctly classified changes is shown in Figure 107 (Appendix 9) which shows that the overall change was correctly assessed but smaller misclassifications occur mainly along the edges between both classes.

Table 9: Accuracy of the SAR-based classification of forest changes between 2016 and 2018

		Reference				User's accuracy
		forest to forest	forest to non-forest	non-forest to forest	non-forest to non-forest	
Classification	forest to forest	<b>207,174</b>	39,785	12,954	21,717	73.6 %
	forest to non-forest	39,532	<b>97,262</b>	4,350	21,715	59.7 %
	non-forest to forest	6,525	1,761	<b>2,629</b>	7,693	14.1 %
	non-forest to non-forest	50,753	48,512	13,888	<b>259,791</b>	69.7 %
Producer's accuracy		68.2 %	51.9 %	7.8 %	83.6 %	<b>67.8 %</b>

For the analysis of changes at the building levels three periods were defined (Table 10). The visual inspection revealed that the numbers of newly constructed buildings decreased from 14 per day during the first period (October 2017) to about 5 buildings per day for the third period (January to August 2018). However, looking at the ratio between newly constructed and demolished buildings, the images show that the number of demolitions strongly increased in the third period. While every fourth change was caused by the removal or dismantling in 2017, the ratio dropped to 1.7. This can be explained by the fact that the TerraSAR-X images were acquired over the center of the camp which experienced strong densification during the early stage of influx. At later stages, when the total camp area excessively grew to a larger size (Figure 48), pressure was released in these core areas by removing some of the buildings, possibly to reduce the risk of flooding in the wetland areas (Figure 47, right) or to prevent communicable diseases.

Table 10: Number of building changes in Kutupalong refugee camp between 10/2017 and 08/2018

#	Period of investigation	New buildings (per day)	Demolished buildings (per day)	Ratio
1	30.09.2017 - 11.10.2017	156 (14.2)	39 (3.5)	4.0
2	11.10.2018 - 27.12.2017	613 (8.0)	140 (2.8)	4.4
3	27.12.2017 - 04.08.2018	1079 (4.9)	644 (1.9)	1.7

These indications are underlined by the spatial distribution of changes, which were visualized by calculating the number of changes within a radius of 500 meters at spatial intervals of 15 meters. This was done for both new and demolished buildings, as shown in Figure 49. It shows that there was nearly no change in the center area of the camp during the first period of highest growth while most of the densification happened in the areas west of it. A second area of increased building density was south of the wetlands. Between October and December 2017, these areas remained the

center of camp growth, but first removal was observed at various locations. Since January 2018, the camp excessively grew in westward direction, carving into the previously forested areas, which was also found by the analysis of Sentinel-1 images (Figure 45).

Based on these observations, the selection of the satellite footprint turned out as slightly unfortunate (Figure 44), because most of the growth occurred west of the camp. And as already stated, an image acquired before 26<sup>th</sup> of August 2017 would have provided a valuable baseline for the size of the camp before the massive influx of the Rohingya refugees. However, a map of Kutupalong from 07.06.2017 provided by UNITAR (2017a) shows that the initial camp extent was limited to the core area as identified by the Sentinel-1 analysis in Figure 45.

This study showed how SAR imagery of different resolutions can be integrated into humanitarian work in a quick and easy way for an assessment of changes within and around of refugee camps, even if single dwellings cannot yet be exactly outlined in such images.

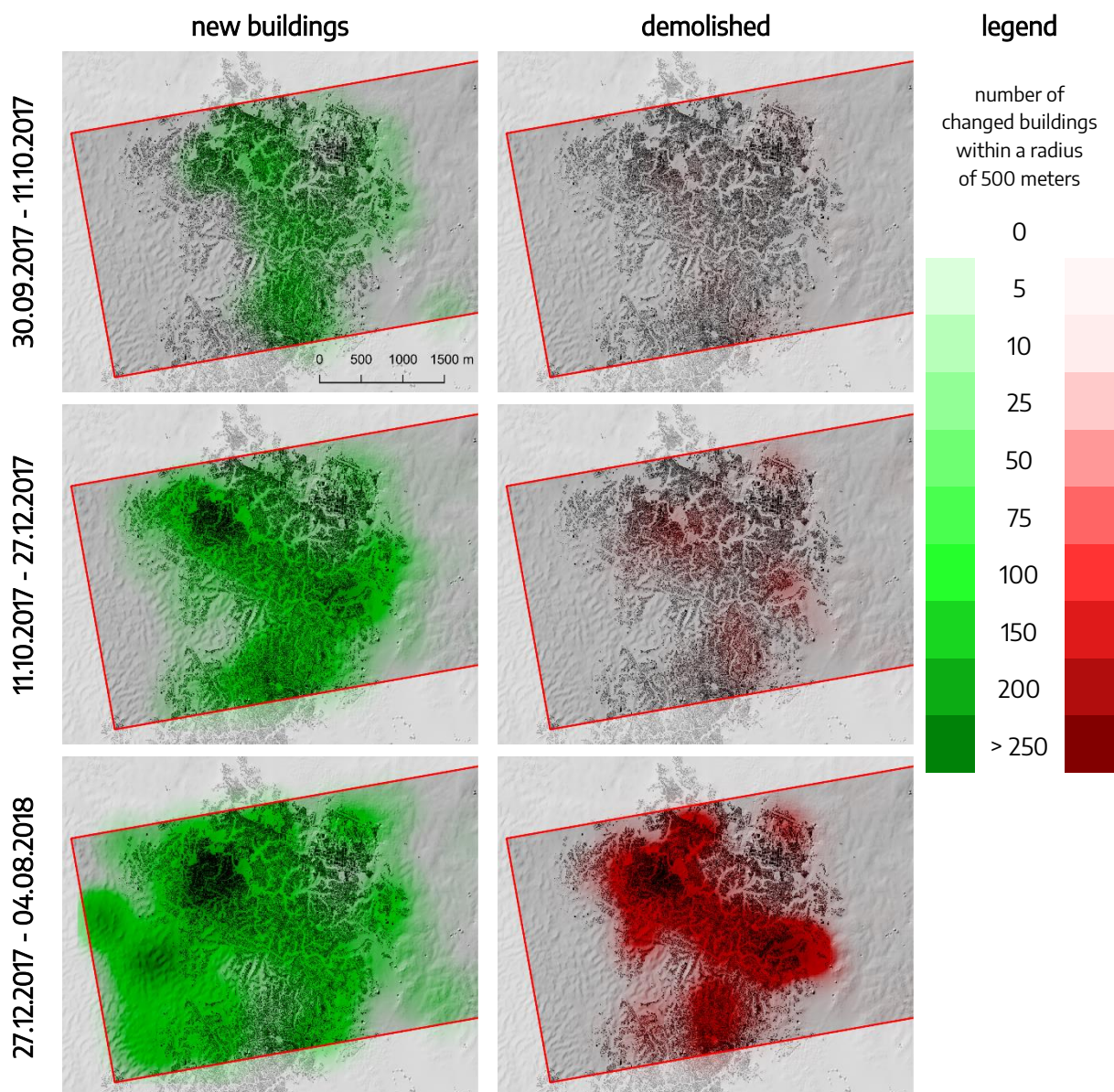


Figure 49: Spatial distribution of building changes in Kutupalong refugee camp

Background: Hillshading from elevation model as demonstrated in section 3.2.4.

Red outline shows the footprint of TerraSAR-X data; black areas show dwellings on 24.12.2017 (provided by MSF).

### 3.1.4.4 Scientific conclusions and practice recommendations

The following things can be summarized from the different approaches presented in this section regarding the mapping of changes in refugee camps with SAR data:

- Temporal **RGB composites** provide an excellent method for the quick visualization of changes (Figure 50 and Figure 100). It is important to compare radiometrically calibrated images from representative dates or periods (Freeman 1992).
- Sentinel-1 data provide excellent conditions regarding **spatial and temporal resolution** for the observation of camp extents and the surrounding landscapes along a defined period. This has been already demonstrated outside the field of humanitarian action in several studies (Heldens et al. 2017; Lehner et al. 2017; Lisini et al. 2018)
- Using **cloud-based techniques** to process large amounts of data allows the quick generation of multi-temporal image averages which contain less speckle and are easier to interpret.
- Images of **ascending and descending passes** should not be merged for any kind of SAR-based change detection because of the impact of looking direction on SAR backscatter and the topographically induced radiometric and geometric distortions (Figure 50, Derrode et al. 2004). Nor should images of different polarizations be quantitatively compared without considering their different interaction with surfaces.
- Although spatial resolutions of some SAR missions reach the sub-meter level (Table 32, Appendix 2), the identification of single buildings is constrained in refugee camps because of the densely built and scattered dwellings. Furthermore, layover effects hinder the proper identification of buildings at this spatial resolution (Zhang et al. 2016). In the **case of emergency**, visual interpretation is currently both faster and more reliable.
- Whenever visual interpretation is conducted, it is advisable to collect, compare and combine **information digitized by multiple users**. Otherwise, the individual's perception of the image has a large impact on the result and can lead to considerable bias. The assurance of sufficient data quality has to be addressed, for example with the preparation of detailed manuals for interpretation and digitization, and the definition of quality standards and indicators (Antoniou 2018).
- To increase the utility of VHR SAR data, it is decisive to have a **reference image** which was acquired before an incident (e.g. sudden growth or damages because of natural hazards). It is therefore advisable to collect one image per year of each site of interest to be able to respond to emergencies. Having a TSX ST image of Kutupalong before 25.08.2017 would have surely increased the possibilities regarding change monitoring within the camp. The Smallsat concept which deals with the launch of satellites lighter than 200 kg could increase the operational acquisition of SAR images to a substantial degree (Freeman 2018)

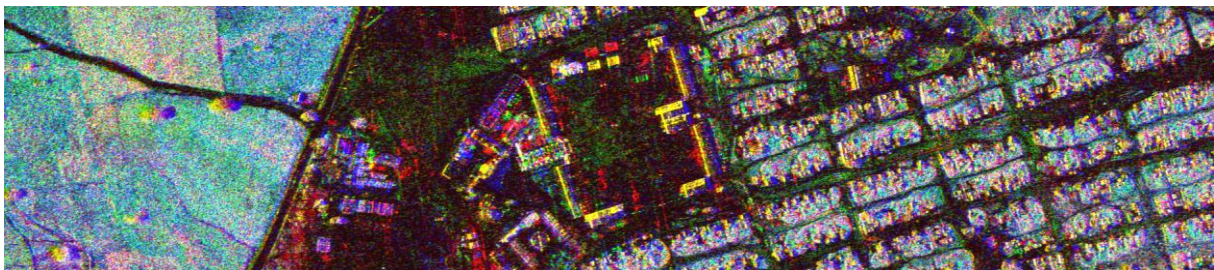


*Figure 50: RGB composite of three TerraSAR-X images of the refugee camp Minawao, Cameroon. They were acquired in ascending (red & green) and descending (blue) pass. Note the backscatter of walls of the administrative buildings (center). Combining these images gives an indication on the true width of the building.*

### 3.1.5 Mapping rural settlements and infrastructures, (Guéckédou, Guinea & Gambella, South Sudan)

#### 3.1.5.1 Background and aims

Besides knowledge about camps and cities, the success and efficiency of humanitarian relief operations strongly relies on information on larger regions, especially when it comes to the provision of food supplies and medical care (Kovács & Spens 2009). However, especially countries of the global south are lacking a comprehensive spatial data infrastructure for the production and administration of up-to-date maps, which foster sustainable development and allow precise response to natural disasters or humanitarian emergency situations (Williamson et al. 2010).

This chapter shortly demonstrates the use of radar imagery for the quick mapping of structures as a base for effective and humanitarian relief work, exemplified by two cases. Both study areas are located between 8°N and 9°N latitude where average cloud cover of Sentinel-2 is estimated between 40 and 60 % (Sudmanns et al. 2018a). The development of approaches which are independent from atmospheric conditions and based on regularly acquired images is therefore the main interest of this chapter.

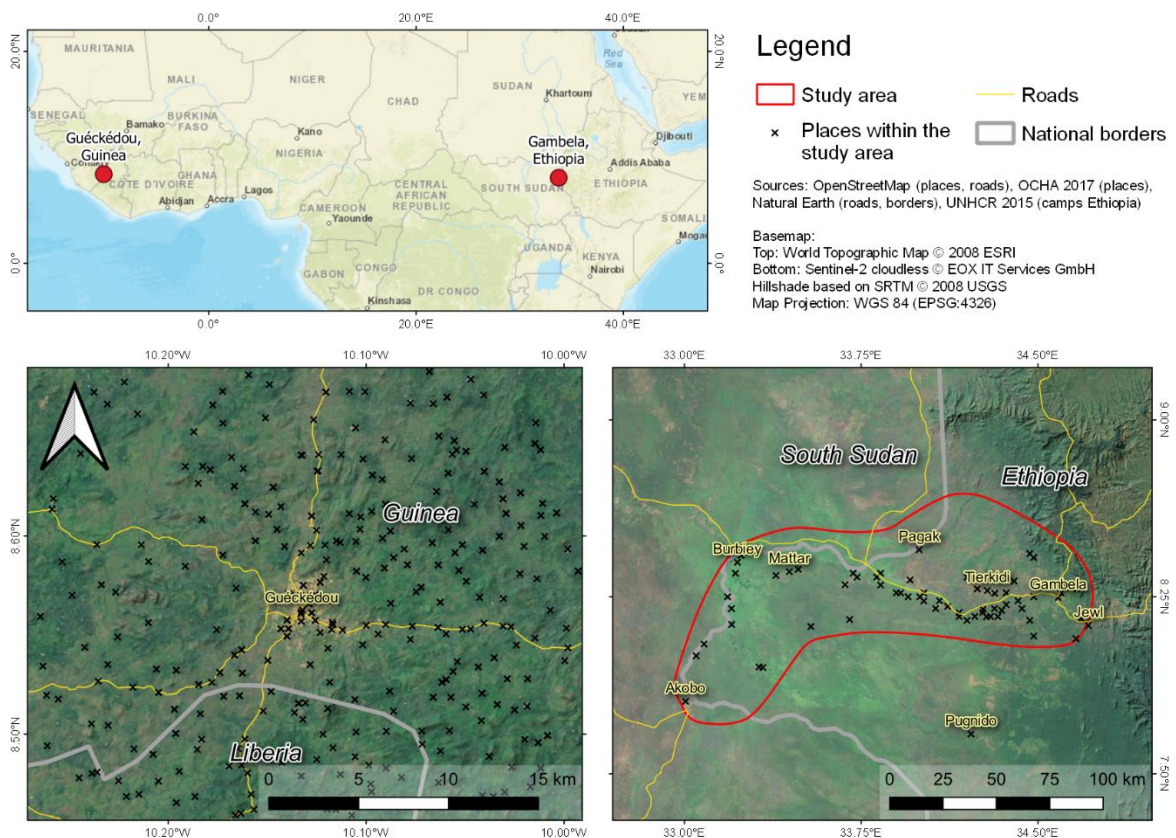


Figure 51: Study areas for the mapping of rural areas and infrastructures

The first case is the area around the city of Guéckédou, located in the south of Guinea in West Africa (Figure 51). It has a population of 71.000 inhabitants, according to the 2016 census, and is the capital of the prefecture of the same name with a total of 310,000 inhabitants (INS 2017). In March 2014, the World Health Organization (WHO) was notified of an outbreak of the Ebola virus disease which is associated with a case fatality rate of 30 to 90% (Baize et al. 2014). When three of the eight

patients hospitalized in Guéckédou died, epidemiologic investigations were initiated, and vaccination campaigns prepared. Southeastern Guinea turned out as the epicenter of the first Ebola outbreak in West Africa which in the end caused over 11,000 fatalities, mainly in Liberia, Sierra Leone and Guinea. One of the reasons for the rapid geographic expansion of the disease was the high degree of interconnectivity between the populations of these three countries and the cross-border traffic along the dense road network cities and their rural hinterland (Aylward et al. 2014).

One of the main challenges for MSF, who mainly conducted vaccination campaigns, was the dispersal of small settlements in the center of the epidemic. Hundreds of small villages around Guéckédou had to be supplied, but official maps were incomplete and outdated (Lüge et al. 2014). For this reason, crowd-sourced mappings were organized to complete the existing but highly incomplete OpenStreetMap data based on visual interpretation of very high-resolution satellite imagery (Lessard-Fontaine et al. 2015, Figure 51, bottom left, black marks). These helped to depict a complete and reliable image of the area and improved the planning and logistics of the vaccinations (Dittus et al. 2017). This chapter analyzes how radar data can assist such mappings in the case of new emergencies in poorly mapped areas.

The second case is Gambella region in Western Ethiopia (Figure 51, top), which hosts large numbers of Sudanese refugees who fled across the border. Since the outbreak of violent conflicts in December 2013, these movements reached up to 800 newly arrived refugees per day (MSF 2014). Figure 51 (bottom right, yellow labels) shows the region and the most important refugee settlements in the area. The natural circumstances are challenging for humanitarian logistics, the transport of supplies and relocation of refugees, the road network is sparse and only few roads are paved (IOM 2017). Furthermore, environmental conditions are a constraint, because the area is regularly flooded, making the roads impassable (Wakuma Abaya et al. 2009). Especially during the rainy season, lasting from May to December, the region's function as an important road corridor between West Ethiopia and the interior of the country is severely constricted (WFP 2012). And it was also demonstrated by Wolde (2016) that the performance of humanitarian logistics in this area is strongly linked to environmental situational factors. But like the case in Guinea, official data and maps are rare. While settlements and camps were already mapped by UNHCR (2015) and OCHA (2017), information on roads is scarce. This chapter proposes a method to improve their visibility in SAR images for visual interpretation and gives a quick estimate on their reliability during the rainy season.

### 3.1.5.2 Data sources and processing

Besides the SAR data itself, no additional sources were used in this study case, because it aims to demonstrate the potential of radar imagery for mapping or digitizing structures, especially when no other information is present. One exception are the places of Guinea which were digitized by contributors of OpenStreetMap to react on the demand for maps during the Ebola outbreak (OSM 2018). They serve as a reference for the later accuracy assessment.

To ensure quick response in cases of emergencies, a simple method based on visual interpretation of was chosen. The basic assumption is that rural settlements cause distinct signatures in SAR images because double-bounce and corner reflection cause increased backscatter intensity (Figure 18). These signatures would enhance their visibility compared to optical imagery because dwellings in rural areas are of small sizes and often of similar color as their surroundings because of natural construction materials (Figure 52). The same principles apply the study case of Ethiopia where the gravel paths and dirt roads are hardly visible in optical imagery.

Images of Sentinel-1 are selected for analysis because they are acquired at regular intervals and provided at a spatial resolution of 10 meters. However, as explained in section 2.3.2, the presence of speckle in radar images hinders visual interpretation, especially in areas where signals from multiple elementary scatterers interfere, as it is the case in tropical environments with various different layers of vegetation (Lee et al. 1994). While speckle filtering techniques or multi-looking can reduce this effect to a considerable degree, especially small and fine structures are often disadvantaged in favor of generally smoothed homogenous areas (Sheng & Xia 1996). Another way is therefore the temporal averaging of multiple scenes, where the output image is the result of the backscatter of a large number of input files (Engdahl & Hyyppa 2000), as demonstrated in equation 15:

$$b_{xy} = \frac{1}{n} \sum_{i=1}^n a_{i xy} \quad (15)$$

where

$b_{xy}$  is the new pixel value at column  $x$  and row  $y$ ,  $n$  is the number of images, and  $a_{i xy}$  is the backscatter of a pixel of image  $i$  at column  $x$  and row  $y$ .

Averaging images is constrained by two factors: The availability of archived images and technical capabilities to download and process these large amounts of images. In Terms of Sentinel-1 imagery, the first limitation is not a problem in most regions of the world where over 200 acquisitions have been collected since the launch of the satellite in late 2014 (EODC 2018, Figure 105, Appendix 7). However, one GRD product has the size of approximately 800 MB and its pre-processing for temporal averaging requires at least radiometric calibration and Range Doppler terrain correction (chapter 2.3). Both downloading and processing large amounts of images takes a considerable time or might even exceed the capacities of common desktop processors. Therefore, three types of products were compared for both study areas:

- A. One single Sentinel-1 image from July 2018.
- B. A temporal average of 10 Sentinel-1 images acquired between June and August 2018, representing the approximate maximum number of products to be practicably downloaded and processed on ordinary computers.
- C. A temporal average of all available Sentinel-1 images processed in the cloud system of the Google Earth Engine (Gorelick et al. 2017).
- D. Very high-resolution satellite imagery available within Google Earth, as suggested by the “Field Guide To Humanitarian Mapping” (MapAction 2011)

Products of type A and B were manually downloaded, radiometrically calibrated to Sigma0, converted to dB scale and geometrically corrected using the SRTM digital elevation model as described in sections 2.3.1 and 2.3.3. No speckle filtering was applied, but products of type B were then averaged to one temporal mean as described in equation 15.

Products of type C were computed in the Google Earth Engine (code provided in Appendix 10), for both study areas where 190 images were available in ascending orbit for Guinea and 247 images in descending orbit for Ethiopia. Google Earth Engine features the full archive of Sentinel-1 images and creates calibrated GRD products in dB scale which were also terrain corrected using the SRTM digital elevation model with a spatial resolution of 30 meters. Accordingly, pre-processing of products A/B and C are comparable and the only difference is the number of images used for the temporal averaging as demonstrated in Figure 52. A comparison is shown in Figure 52.

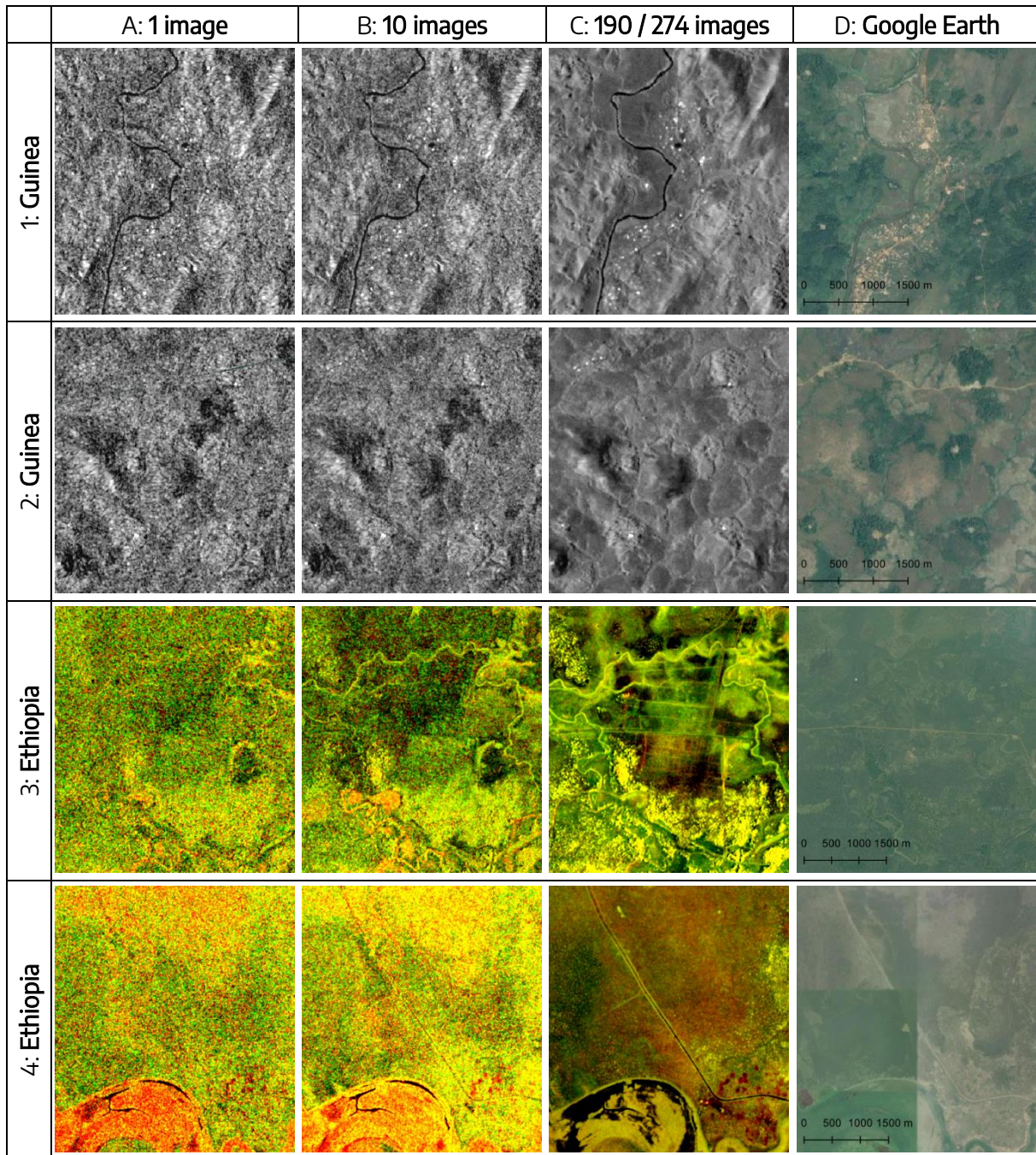


Figure 52: Image enhancement by temporal averaging

### 3.1.5.3 Results and discussion

As demonstrated in Figure 52 (1 and 2) rural dwellings are present as small bright areas in the Sentinel-1 image. Although they do not necessarily represent the full extent of the settlements, backscatter characteristics indicate man-made structures at these locations. While they are hardly visible in the single image (A) and the ten-image composite (B), their pattern becomes much more distinct in the overall average image (C) based on 190 products. This is because signal interference and seasonal variations are attenuated while the persistent backscatter of the dwellings persists throughout all images. Compared to the optical imagery, this temporal average has decisive advantages: Firstly, very high-resolution images are not available for free and those available to OpenStreetMap are composites of different sensors and dates (especially visible in 4D). Radar

average products might no longer give information on temporal dynamics but, as they are openly available, their time frame and corresponding numbers can be precisely selected by the user. Secondly, while settlements in optical images can be composed different colors and patterns, their signature in the SAR image is always the same and comparably easy to find. Thirdly, temporal changes during an investigated period are of minor significance because the extraordinary high backscatter of artificial structures dominates the calculation of a mean value. That means, even dwellings were constructed during the investigated period, their contribution to the temporal average is sufficient to be present in the final product.

To illustrate a possible benefit of radar images over optical imagery for the mapping of rural settlements, an experiment was conducted with 18 participants who were asked to identify the rural settlements within the study area based on the products B, C and D, as defined above. The experiment was set-up in a computer lab with a short introduction on the mapping procedure, so that all participants had the same knowledge and technical background. Three groups were created, so each product was mapped by 6 participants by placing a point at each identified settlement. All points were collected in the end and analyzed regarding a) the number of identified settlements during the experiment time of 20 minutes, and b) the degree of correctly identified settlements after a comparison with the OSM data available for the study area. Unsurprisingly, most settlements were found in the Google Earth image (between 45 and 162, median 131.5), as illustrated in Figure 53 (left). But as described above, the dates of these base maps are not always known, nor is the base map up to date in all parts of the earth. As the experiment showed, temporally averaged SAR images are a suitable alternative because they reach slightly lower detected settlements in the given time (between 66 and 137, median 108). However, the temporal average consisting of only 10 Sentinel-1 products achieved significantly lower scores, probably because of the granular pattern of the backscatter resulting from the landscape in the study area (Figure 52, B1 and B2). If all speckle is eliminated in the temporal average over the full period, the settlements remain as bright spots (Figure 52, C1 and C2). These numbers indicate that this way of image enhancement substantially increases the visibility of settlements for quick mapping in emergencies. However, more importantly are the correctly identified settlements (Figure 53, right). Here, Google Earth and the long-term average achieve similar true positive rates of larger than 90% while many false positives were detected in the average from ten images, where only 65 % were correct at average.



Figure 53: Results of the mapping of rural settlements based on SAR images versus optical imagery

These findings support the hypothesis that averaging Sentinel-1 images over a large temporal span makes them a suitable basemap for the quick and accurate mapping of small settlements. They should be considered as a free and reliable source of information in the case of emergencies, when the spatial distribution of local population is of interest to humanitarian organizations, for example, for vaccinations, evacuations or the provision of medical supplies.

As for the case of road infrastructure in Ethiopia, all identified roads could have been mapped based on visual identification of the multi-image average. It was generated from 274 images and both polarizations were used to highlight the linear structures which are mostly characterized by constantly low backscatter intensities. Linear structures, as identified in Figure 52 (C3 and C4) were manually digitized to get a complete map of the existing road infrastructures in the study area.

To include the vulnerability towards flooding in the rainy season, two additional pieces of information were included in the resulting map (Figure 108, Appendix 11):

1. All roads crossing river systems or areas of larger surface discharge were marked with a caution sign to highlight that these areas might be the first to be affected by high river levels. These were identified by generating an RGB composite image consisting of the temporal average as described above, as well as the maximum and standard deviation of each pixel in the stack. Examples are given in Figure 54.
2. Flooded areas were mapped for two flood events reported during the rainy seasons in May 2016 and September 2017 (OCHA 2016; UNICEF 2017). They were automatically derived from images acquired before and during the flood event by a hierarchical thresholding which is described at more detail in section 3.2.3.

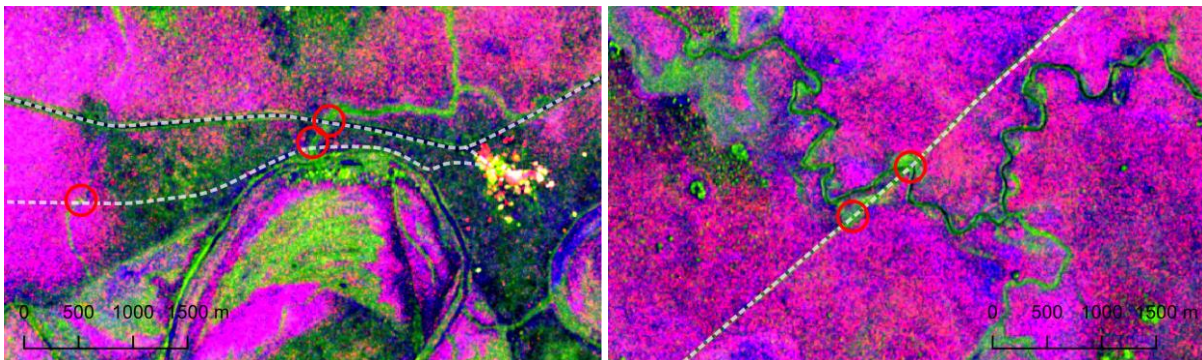


Figure 54: Areas prone to flooding as identified by the SAR RGB composite

*Temporal product of maximum (red), average (green) and standard deviation (blue) of all Sentinel-1 images acquired in descending orbit between 10/2014 and 10/2018; the dashed lines indicate roads; scale 1:50,000*

Concludingly, it has to be stated that the use of SAR facilitates the mapping of rural settlements and infrastructures, such as roads, in parts of the world which lack digital and updated maps for humanitarian relief efforts. As shown for the study in Guinea, the corner reflection of the SAR signal can be effectively exploited to locate artificial structures in rural areas. These can only be identified in VHR optical imagery which outperformed the SAR images in terms of number of identified dwellings and accuracy, but their use is limited by licensing, acquisition costs or timeliness.

As for the study in Ethiopia, information of SAR images can be combined to map both transportation networks and flood prone sections of these roads. While the roads show a constantly high or low signature, depending on their roughness, the surrounding landscapes and their surroundings show distinct variation, expressed in distinct temporal minima or maxima and standard deviations.

### 3.1.5.4 Scientific conclusions and practice recommendations

The following points can be concluded regarding the use of SAR images for the visual interpretation of settlements and infrastructures:

- While single radar images show a considerable amount of speckle, the readability can be largely increased by **combining multiple images** of several dates. Our study showed that a temporal composite of 10 images already reduces speckle, but is not yet sufficient for the identification of point-like or linear patterns at the scale of the pixel resolution.
- Temporal averaging of radar images is especially applicable for images of **operational missions** which are openly accessible, such as Sentinel-1, in combination with cloud-based infrastructures for their processing.
- By the end of the year 2018, some regions of the earth were imaged over 800 times (Figure 105, Appendix 7) by the Sentinel-1 constellation, while other regions are rather neglected by the observation plans (Potin et al. 2018). But any **temporal average based 25 images** or more provides an advantage over single scenes regarding the degree of speckle and the emergence of fine structures.
- More images can be used when combining acquisitions of **ascending and descending orbits**. However, this is not advised in mountainous areas and for the investigation of very fine structures (at the size of 10 meters) because both are very **sensitive to the look direction** of the sensor (Derrode et al. 2004; van Zyl et al. 1993).
- If available, information of **different polarizations** should be combined, as demonstrated in Figure 53, to distinguish scattering mechanisms at the earth's surface. Especially cross-polarization channels (HV and VH) are sensitive to volume scattering and therefore often used to analyze vegetation patterns (Mitchard et al. 2009; Ranson & Sun 1994; Robinson et al. 2013).
- Additional to the temporal average, standard deviations or minima/maxima can be derived from a series of radar images because they give further information on the **temporal dynamics** of surfaces. These dynamics can be caused by seasonal variations as well as irregular disturbances, such as flooding (Martinis et al. 2015; Santoro & Wegmüller 2014). Combining them, as demonstrated in Figure 54 helps to create multi-information composites for the distinct extraction of information.
- Although it creates smooth images, the averaging of SAR images pre-processed to dB scale does not reflect their true mean because they underlie the **laws of logarithms** (Carlson 1966). For the analysis of radar signatures, the logarithmic mean should be used instead.
- Methods for the **automated** delineation of image features, such as rural settlements or roads, are widely discussed but mainly limited to VHR optical imagery (McKeown 1990; Poullis & You 2010; Trinder & Wang 1998). Automated approaches based on radar imagery are currently focused on coastlines with a distinct border between water and land (Mason & Davenport 1996; Yu & Acton 2004).
- Large potential lies in **fully-polarimetric sensors** (e.g. ALOS PALSAR, RADARSAT-2) which can highlight double bounce effects from vertical structures within pixels, such as small houses, based on target decomposition techniques (Cloude & Pottier 1996). Their big advantage is that only one image is required to determine these scattering effects. An example for the area of Guéckédou is given in Figure 109 (Appendix 12).
- **Operational solutions** for the regional and SAR-based mapping of areas of conflict or emergency are still to be developed. Most promising in this context are methods of machine learning (Quinn et al. 2018), deep learning (Gong et al. 2016), and big-data approaches (Ali et al. 2017).

### 3.1.6 Damage assessment in urban areas (Raqqa, Syria)

Note: Some figures of this section are taken from Braun (2018a) which was published as an open access article distributed under the Creative Commons Attribution License which permits unrestricted use, distribution, and reproduction in any medium, provided the original work is properly cited and the content is not altered (CC BY-ND 4.0). Agreement of the publishing company (VÖAW) was explicitly given. The reader is advised to consult this publication for a more detailed description of the study.

#### 3.1.6.1 Background and aims

Raqqa is a city in the north of Syria (Figure 55, top left) and has a population of around 220,000 according to the census in 2004. It is located north of the Euphrates river and surrounded by intensive agriculture of wheat and cotton. Because of its geostrategic importance, Raqqa was the first provincial capital of Syria which was captured by rebels in the Syrian civil war in March 2013 (Aljazeera 2013). Until its liberation in October 2017, the city and its population were subject to various occupations and heavy combats. During this time, numerous deaths of civilians were reported and nearly 90 percent of the city's infrastructure was found to be damaged (Malsin 2017).

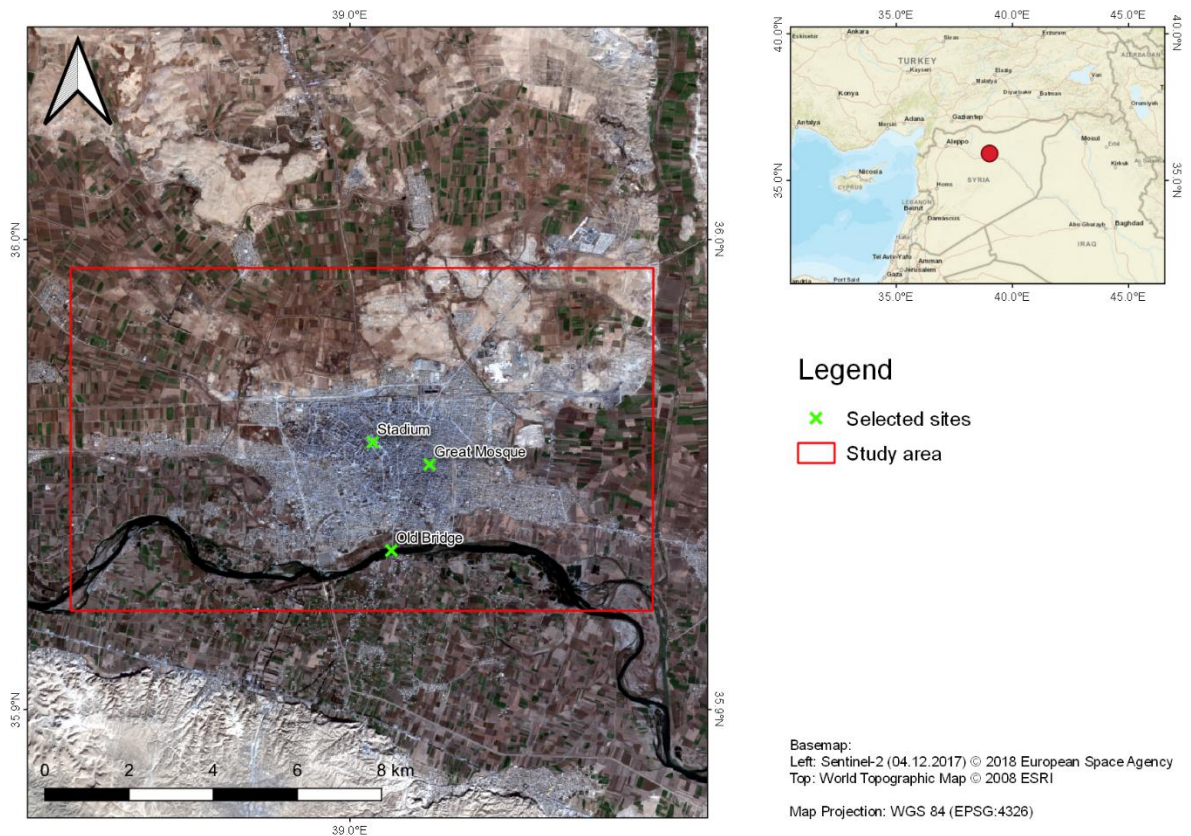


Figure 55: Study area for damage assessment in Syria

Mapping damages in areas of conflict or natural disasters fulfills tasks at different temporal scales:

- **Short-term needs:** Information on damages can assist to evacuate people in need, to estimate the vulnerability of different parts of the affected areas and to organize cleanup efforts after the incident (Nisha de Silva 2001; van Zandt et al. 2012)
- **Medium-term needs:** Information on the spatial distribution of destructions is important for the estimation of social and financial damage. It allows to draw implications for the national economy and public health sectors regarding reconstruction and disaster prevention (Atmanand 2003; Mathew 2005).

- **Long-term needs:** Being able to determine the amount of damage in a retrospective is important in terms of prevention of misuse of financial and medical aid (Hildreth 2009; Zarocostas 2010) and advocacy or accountability in cases of civil or non-governmental institutional victims of military action (Geis & Schlag 2017; Rubenstein & Bittle 2010).

This study aims to demonstrate how radar data can be used by humanitarian organizations for a quick assessment of damages in cases of disasters or military combats. It shows the potential and limitations of freely available data for the case of the city of Raqqa and selected sites and gives information on the reliability of the results.

The basic assumption is that built-up structures show high backscatter caused by solid materials (Figure 17) and corner reflection (Figure 18) and are therefore suitable targets for long-term investigations. If then a building is damaged (loss of roofs or walls) or destroyed, the amplitude decreases significantly. This allows to identify both the location and date of damages in the city and overcomes the limitations of DInSAR to measure non-coherent processes, such as abrupt changes in the height of urban structures (section 2.2.5).

### 3.1.6.2 Data sources and pre-processing

A total number of 55 Sentinel-1 images between 10/2014 and 12/2017 were used in this study. They were acquired in time intervals between 12 and 48 days, as shown in Figure 56. This high amount of data is required for two reasons: The first is to be able to identify the exact date of damage of each structure. The second is related to the method of persistent scatterer analysis (section 2.2.5) which uses statistical measures on long time-series of backscatter intensity to extract reliable information on stable radar targets and their behavior over time (Perissin & Ferretti 2007). Although the combats for Raqqa started already before the first Sentinel-1 acquisition, no image was available before October 2014. Figure 56 also shows selected dates, such as occupations and military offensives.

All Sentinel-1 data was acquired as SLC products (Table 33) and co-registered to a stack with an accuracy of 0.132 meters RMSE with SARPROZ software (Perissin 2018).

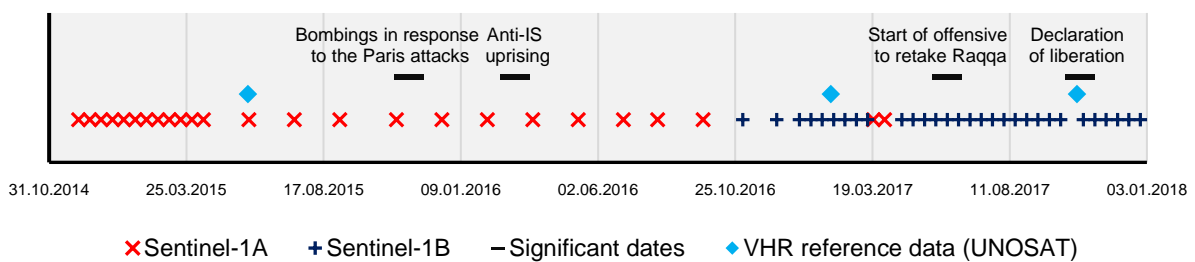


Figure 56: Data sources for building damage assessment in Syria

For validation purposes, a dataset provided by the UNOSAT program was used which consists of a total of 13,160 points of manually identified damages based on visual interpretation of five VHR satellite images (UNITAR 2017b). Three of them lie in the investigated period (Figure 56, light blue diamonds), while most of the damages (11,342 ± 85 %) were determined between the last image pair (03.02.2017 to 21.10.2017). This fact highlights the severity of damages in the final phase of the fight for the city. Each point represents one identified location damage and contains information on both the severity and the degree of confidence (Table 11). For example, a sum of 2,537 buildings were found to be destroyed at a very high confidence which makes about 20 % of the dataset. But as the table also shows, a number about the half of the data were only detected with medium confidence or less because the visual interpretation was not always clear, and the data was never

validated in the field. This means that the dataset should not be taken as ultimately correct, yet it serves as a suitable reference to assess the quality and plausibility of the SAR-based findings.

Table 11: Damage confidence and severity in the reference dataset for damage assessment in Syria

		Damage confidence			
		uncertain	medium	very high	sum
Damage severity	no change	14	102	1	117
	impact crater	0	27	235	262
	moderate damage	353	5,117	23	5,493
	severe damage	0	293	3,669	3,962
	destroyed	0	750	2,576	3,326
sum		367	6,289	6,504	13,160

### 3.1.6.3 Identification of damages

Depending on the spatial resolution of a radar image, a varying number of surfaces contribute to the backscatter of a single pixel. Accordingly, the backscatter information of this pixel tends to change over time (Zebker & Villasenor 1992). However, if the pixel is dominated by a single scattering mechanism, for example by man-made structures or point-like targets, their backscatter intensity is comparably stable in the long-term. These targets are called persistent (or permanent) scatterers (PS) and their location can be determined at sub-pixel accuracy (Ferretti et al. 2001). Having this high backscatter as a proxy for the presence (or absence) of a building, the temporal profile of a pixel and its underlying objects can be investigated. Of peculiar interest are the changepoints in these profiles which are identified by applying Gaussian functions on these amplitude time-series (Chambers et al. 1996).

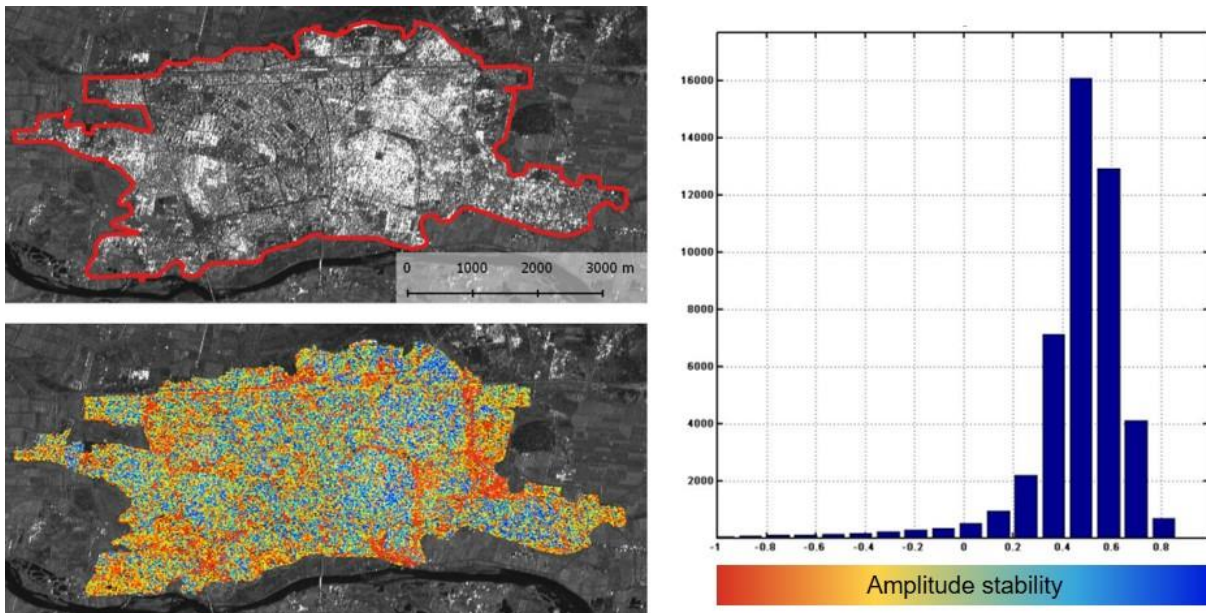


Figure 57: Mean backscatter intensity, identified permanent scatterers and histogram of amplitude stability of the selected PS

In a first step, the number of potentially usable PS was reduced by applying a mask on the urban area of Raqqa (Figure 57, top left, red line), so only objects within the city were considered for

processing. The remaining 46,472 PS are shown in Figure 57 (bottom left), color-coded by their stability which was derived based on the mean and standard deviation of all backscatter values under each pixel during the investigated period (Lei et al. 2013). As indicated by the histogram on the right-hand side, most of them are of very high stability with values larger 0.5 which means that these pixels contain stable targets which did not undergo significant changes. In turn, the pixels with lower values in yellow and red colors were subject to dynamics. PS with a limited life-time were identified as those pixels which show a significant backscatter decrease which persists until the end of the investigated period (Perissin et al. 2006). These 3,334 remaining pixels were supposed to contain damaged buildings, which are analyzed in the following.

### 3.1.6.4 Results and discussion

Figure 58 shows the overall changes detected in the Sentinel-1 time-series analysis compared to the findings by UNOSAT in the given time-periods. While moderate damages (light blue) are highly underestimated, there is a good correlation with the amount of severe damages (dark blue). Later analyses show that they are not necessarily at the same location, but this agreement proves that radar data at a resolution of 10 meters can be a good indicator for heavy damages urban areas. The difference of nearly 10,000 damages which were not assessed by Sentinel-1 are discussed later in this section.

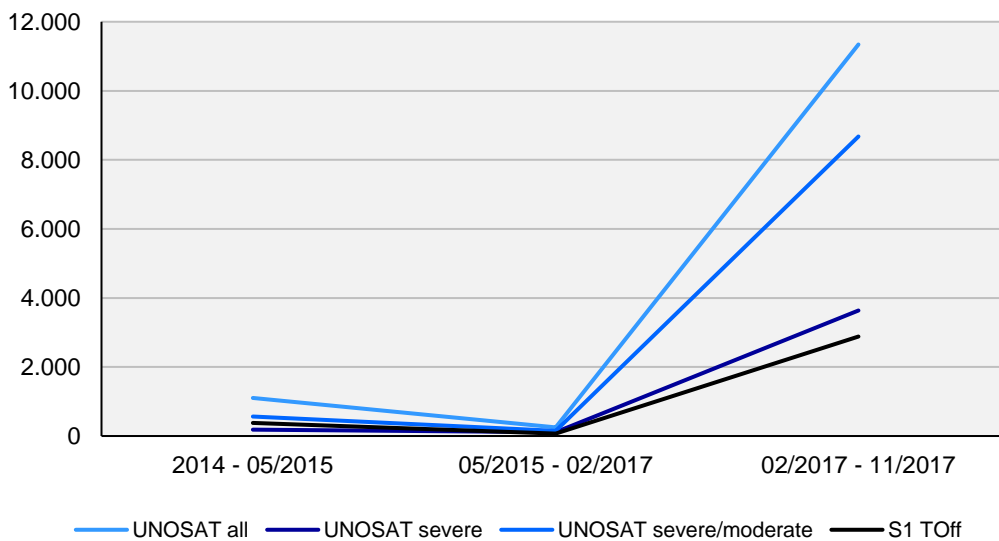


Figure 58: Number of changes identified by UNOSAT (blue) and in this study (black)

The spatial distribution of changes is shown in Figure 59. As the spatial resolution of the Sentinel-1 data was not directly relatable to the point-wise mappings based on VHR optical imagery by UNOSAT, destructions of medium or very high confidence (according to Table 11) were aggregated by a kernel density analysis with a radius of 150 meters for visual comparison. A considerable agreement between both maps can be observed, especially in the eastern part of the city. Yet, there are areas in the city where both approaches show different patterns.

To illustrate the information content of Sentinel-1 time-series analyses, three sites were selected for a more detailed inspection. Their locations within the city are given in Figure 55 (main map, green markers). The first example shows the Great Mosque in the east of the city (Figure 60, top). The

large points indicate the 3,334 PS which showed a permanent decrease of backscatter at some defined point. All other points in blue are identified radar targets of different amplitude stability. The PS marked red shows a significant decrease on in July 2017, according to the amplitude time-series shown on the right-hand side. It is an example for a plausible change at the building, probably caused by collapsing parts at the southeastern corner of the wall. This time coincides with the second battle for Raqqa (May to October 2017), when the Great Mosque was recaptured by US troops in September 2017 (Weinstein 2017). This location was also labelled as damaged in the UNOSAT dataset, but already in May 2015. One explanation would be that the structure was damaged at an earlier stage but finally collapsed in summer 2017.

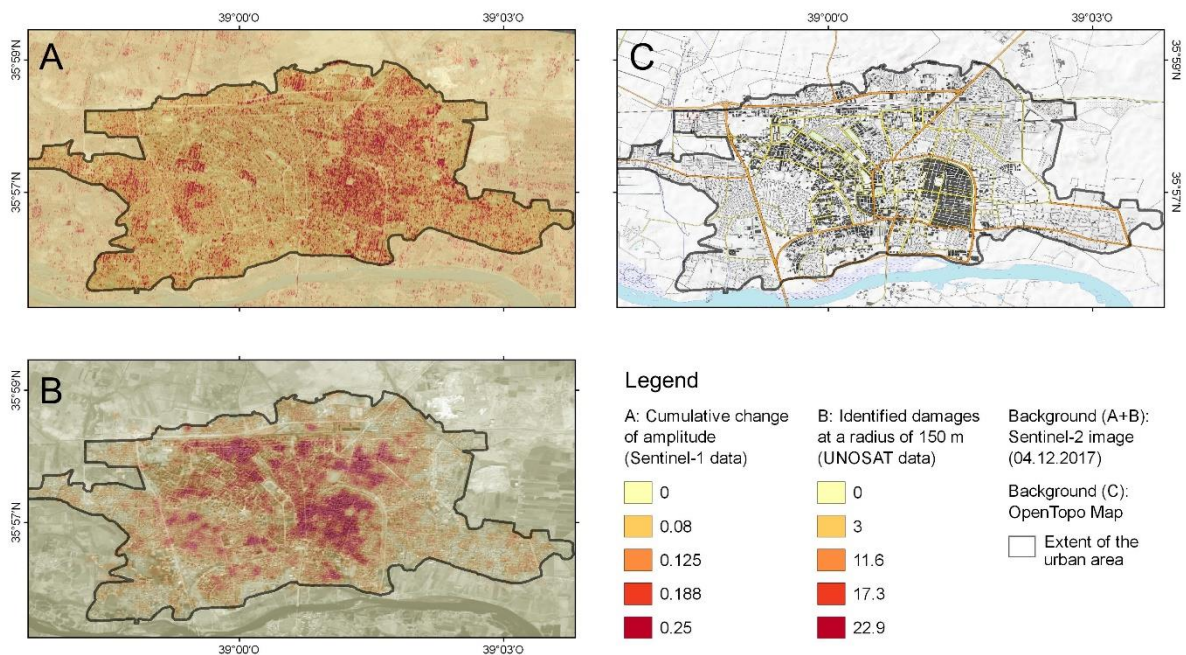


Figure 59: Locations of changes identified by UNOSAT (A) and this study (B)

The second example shows changes around the stadium of Raqqa (Figure 60, middle), which was used as a headquarter and prison by the IS during their occupation (Walsh 2017). A clear concentration of damages was identified along the ceiling of the grandstand. The colors indicate the date of the changes, which are distributed between November 2015 and May 2016. During that time, the city was heavily under attack as a consequence of the Paris attacks and an uprising against the IS occupation (Abou Fadel 2016). The drone footage on the right-hand side confirm the damages identified by our study, as marked with the red ellipse (note that the image is flipped). Notably, the damages to the stadium were not detected by UNOSAT.

The third example shows the Old Bridge crossing the Euphrates river in the south of the town (Figure 60, bottom). Many of the stable points (dark blue) can be excluded as processing artefacts over the water area, but there are four points in the northern part of the bridge which indicate clear decrease of backscatter between May and August 2017.

The amplitude series of the two points marked in red are shown on the right-hand side. For comparison, the PS marked yellow in the southern part of the bridge shows stable backscatter over the whole investigated period. Because of its location outside the city, there is no UNOSAT data available for comparison, but its destruction was later confirmed by aerial imagery (Walsh et al. 2017).

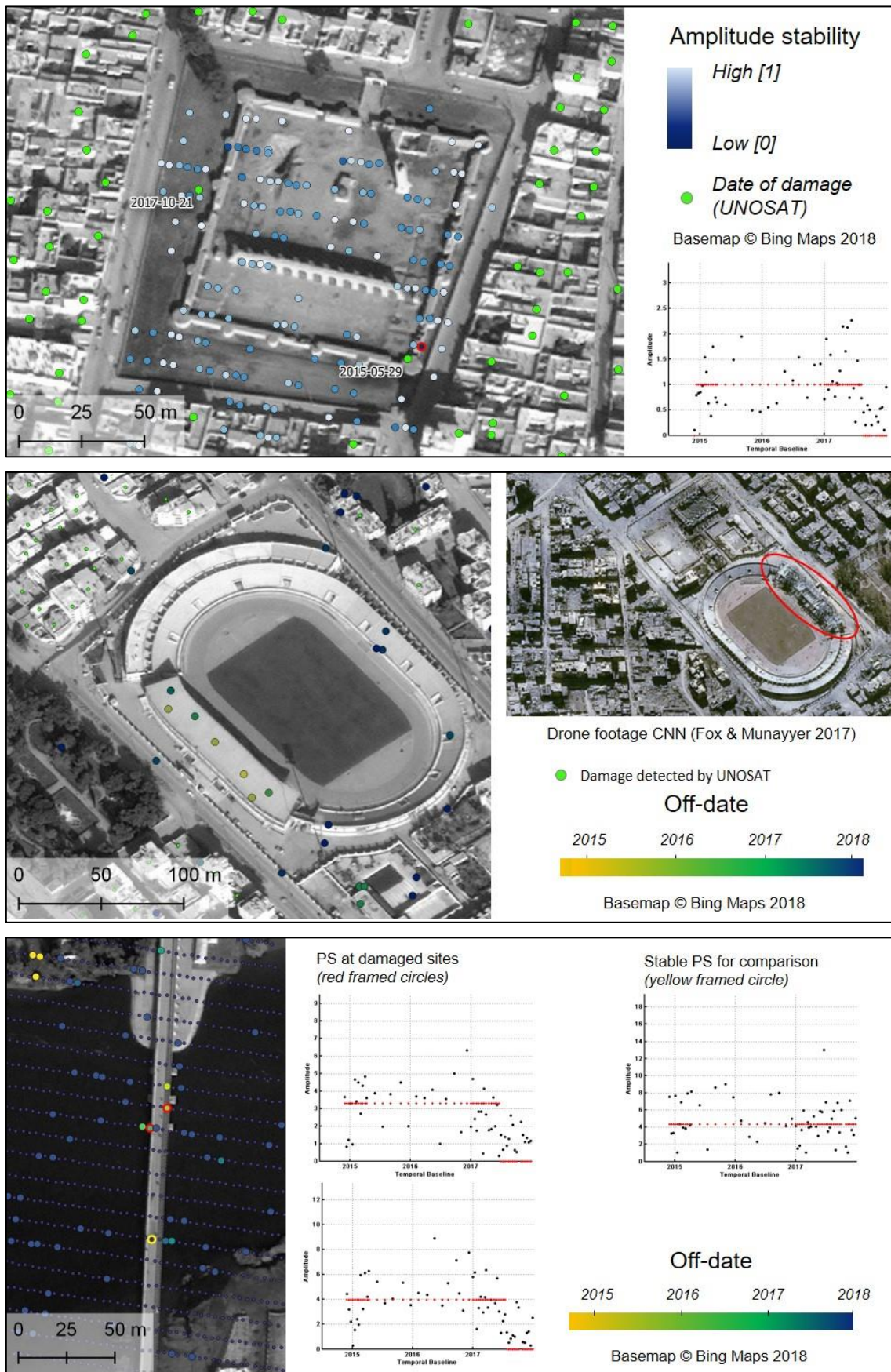


Figure 60: Change analysis for the Great Mosque, the Raqqa stadium, and the Old Bridge

These examples demonstrate the necessity for large time-series of data: As the radar signal underlies variations caused by incidence angle and atmospheric effects, a large population of values is required to statistically discriminate between actual changes and random fluctuations.

This study showed that the high temporal resolution was partly able to compensate the lower spatial accuracy for damage assessments in urban areas. As shown in Figure 58, SAR data is not as exact as visual inspection of VHR optical imagery. The reason for this is that the proposed method is not able to detect subtle damages, such as cracked walls or partly collapsed roofs, because the backscatter is not changed accordingly (Karimzadeh et al. 2017; Matsuoka & Yamazaki 2004). Additionally, changes identified based on altered colors, for example caused by fires or dust, are not detectable by microwaves.

However, SAR data bring the advantage that large archives are available and ready to use in case of emergencies. In contrast, actual optical imagery of the pre-disaster situation is often not available or the tasking of a post-disaster image is hindered by cloud cover or smoke (Towler et al. 2012). A further point is that visual identification is always prone to lack of objectivity (Yamazaki et al. 2005). This study, however, also showed that at least a number of post-disaster acquisitions are needed for the reliable detection of significant changes. The proposed method therefore primarily addresses the middle- or long-term needs described in section 3.1.6.1. One way to make it more efficient in terms of detectability of moderate changes would be the integration of other sources of information, such as optical imagery (Brunner et al. 2010) or UAV data (Fernandez Galarreta et al. 2015). This, in turn, increases the complexity of analyses and reduces its potential for operationalization.

### 3.1.6.5 Scientific conclusions and practice recommendations

The following points can be concluded regarding damage assessments based on SAR data:

- The proposed method is suitable for the detection of **intensity changes** as an indicator for destructions of heavy infrastructure. As only persistent scatterers are used, many other radar targets are excluded from the analysis in advance. This can be advantageous for studies on buildings, but also brings the risk that some changes are missed. It is still a sound method to get a general understanding of the spatial distribution and damages over a longer time, given that large time-series are already available.
- For **time-critical assessments** of changes, coherence-based methods deliver more promising and accurate results about the location of changes (Plank 2014). These, however, require high-resolution SAR data (spatial resolution < 5 meter), precisely speaking two images shortly before the event and one shortly after. Again, Smallsat SAR satellites could lead to a temporal coverage which allows preparedness for sudden disasters and unforeseeable emergencies (Freeman 2018). Other studies use combinations with optical satellites for the provision of pre-disaster information (Jung et al. 2018)
- **Medium-term needs**, such as the steady monitoring of changes, or the reconstruction of their temporal occurrence, are now technically covered by freely available Sentinel-1 data which are acquired at regular intervals. Their enormous potential for operational methods is now identified (Vicente-Guijalba et al. 2017), but it depends on the exact question if Sentinel-1 imagery at this resolution can be used or not.
- The detection of **slight damages** remains challenging for SAR data, given that no change in backscatter intensity or a coherent change of the buildings' elevation is involved. To estimate the level of damage, the integration of polarimetric information is advised (Chen et al. 2018).

## 3.2 Hydrological hazards

Despite the fact that one of the reasons for the migration of people is environmental risk itself, displaced people are in many cases vulnerable to natural hazards and disasters in their new habitations as well (Wisner 2007). Reasons are poor housing conditions (Al-Khatib et al. 2003; Bonner et al. 2007), unsuitable camp sites and unstable building grounds (Cimy 1977; Corsellis 2001) as well as limited resilience towards incoming threats (Jerneck & Olsson 2008; Methmann & Oels 2015).

In many countries, water-related risks are the main challenge of climate change, especially in countries of the Global South (Afifi & Jäger 2010; Alfieri et al. 2012; Birkmann et al. 2012; Romero Lankao 2010). This chapter deals with the role of radar remote sensing in the context of water mapping, flood modelling and ground subsidence in areas of refugee camps or displaced people.

### 3.2.1 Current state of research and challenges

Because of the usually smooth surface of standing water, radar images are predestined for the detection flooded areas (Biggin 1996; Henry et al. 2006; Pierdicca et al. 2013; Schumann & Di Baldassarre 2010). However, mapping of water bodies becomes increasingly challenging over turbulent water surfaces roughened by waves and currents (Brakenridge et al. 1998; Holthuijsen 2010). Other limitations occur when the proportions of water and land surfaces are imbalanced within an image and global thresholding methods fail (Martinis et al. 2009; Matgen et al. 2011). And despite the penetration capability of radar waves, the detection of standing water under a vegetation layer can be a problem (Tsyganskaya et al. 2018). For these reasons, specialized approaches were presented for urban areas (Giustarini et al. 2013; Mason et al. 2014; Mason et al. 2010) and flooded forests or wetlands (Henderson & Lewis 2008; Hess et al. 1990; Martinez & Le Toan 2007).

Because of the availability of SAR data in large archives, flood risks can be assessed by analyzing the inundation frequency of an area within several decades (Meier et al. 2010; Ramsey et al. 2011; Sudmanns et al. 2017; Ward et al. 2014). But besides the retrospective characterization of flood extents, approaches are needed which can be integrated in emergency applications, such as the Copernicus Emergency Management Service (Ajmar et al. 2017; Boccardo 2013). Current trends therefore target at the automation and operationalization of methods (Matgen et al. 2011; Pulvirenti et al. 2011; Solbø & Solheim 2005; Twele et al. 2016) and focus on integrated workflows which are stronger oriented at risk management, damage assessment and crisis response (Bell et al. 2017; Chen & Sato 2013; Schultz et al. 2017; Schumann & Di Baldassarre 2010; Schumann et al. 2007; Taubenböck et al. 2011).

Another application domain of SAR remote sensing is the derivation of topographic information or surface changes based on radar interferometry (section 2.2.5). This field is well-understood and implemented in multiple domains, mainly glaciology (Eldhuset et al. 2003; Neckel et al. 2013; Shugar et al. 2010), landslides and mass movements (Bhattacharya & Mukherjee 2017; Catani et al. 2005; Ye et al. 2004), volcanism (Di Traglia et al. 2014; Lu & Dzurisin 2014; Poland 2006), earthquakes (Massonnet et al. 1993; Tolomei et al. 2015; Tronin 2006) or DSM generation (Crosetto 2002; Sanders 2007; Wegmüller et al. 2009; Zink et al. 2017). Yet, in case of earthquakes and volcanism, InSAR is mainly used to describe changes after the incident, thus its contribution to disaster response is still limited (Milillo et al. 2016). Applications related to humanitarian emergency preparedness are therefore mainly targeting the assessment of risks in terms of flooding or alarming trends of surface movement.

Jarihani et al. (2015) showed that the InSAR-based SRTM had a higher accuracy than the optically-derived ASTER DEM (Hirano et al. 2003) in a river catchment in Australia and was therefore of greater use for hydrodynamic flood modelling. These findings are confirmed by other studies as well (Czubski et al. 2013; Forkuor & Maathuis 2012; Musa et al. 2015; Wang et al. 2012). However, the spatial resolution of the freely available SRTM (30 meters) is often not sufficient for detailed hydrologic modelling (Westerhoff et al. 2010). To overcome this limit, DSM of higher resolutions can be computed, as demonstrated by d'Ozouville et al. (2008), for example, who used ENVISAT InSAR information to increase the quality of topographic information for runoff and catchment modelling for water management on Santa Cruz Island, Galapagos. However, DEM generation is constrained by several factors, such as shadow effects resulting from large incidence angles (Eineder 2003), inaccurate baseline information (Nguyen 2012), temporal decorrelation (Zebker & Villasenor 1992) volume scattering (Hajnsek et al. 2009b) or atmospheric disturbance (Ding et al. 2008).

The TanDEM-X DSM released in 2014 has a spatial resolution of 12.5 meters sets new standards for globally available elevation information (Zink et al. 2014) Its use for hydrological modelling was already successfully demonstrated by a few studies (Gutenson et al. 2017; Mason et al. 2016; Rudari et al. 2016).

Water-related risk assessments raise several scientific, technical and methodologic challenges in a humanitarian context:

- While the identification of calm water bodies is widely investigated, problems arise for **uneven water bodies** which are roughed up by waves and currents, as well as for shallow and partly vegetated waters. In both cases, high backscatter hinders the clear delineation of the water extent.
- Common global thresholding approaches fail for inland **flood areas** which take up comparatively small areas in the image because the histogram no longer shows the required bimodality with a distinctive local minimum point (Matgen et al. 2011).
- Because of differences regarding resolution and wavelength, backscatter images of different SAR satellites are not directly comparable. Accordingly, long-term analyses of **time series** require carefully calibrated images acquired at the same frequency. Only few studies use Sentinel-1 data to continue information retrieved by ERS and ENVISAT for water applications (Guimaraes et al. 2017; Santoro & Wegmüller 2014).
- Freely available digital elevation models, such as SRTM, ALOS World 3D and ASTER GDEM provide **spatial resolutions** of 30 meters which is often not sufficient to determine areas at risk within refugee camps (Ajmar et al. 2017; Alganci et al. 2018)
- The generation of digital elevation models by means of **radar interferometry** (section 2.2.5) is well investigated, but especially repeat-pass interferometry is constrained by temporal decorrelation (Zebker & Villasenor 1992). Their use for the hydrologic modelling of flood risks requires phase information of high quality at the catchment scale (Fisher & Tate 2006; Ludwig & Schneider 2006).

## 3.2.2 Analysis of sea level changes (Bhasan Char, Bangladesh)

### 3.2.2.1 Background and aims

This study shows how large image archives can be valuable to monitor processes at the earth's surface over a long period, especially in regions which are regularly obscured by clouds, the Indian Monsoon in this case. Bhasan Char is an island which lies approximately 20 kilometers before the coast of Bangladesh in the Bay of Bengal (Figure 61). It was selected by the government of Bangladesh in early 2017 for the relocation of about 100,000 Rohingya refugees from Myanmar (section 3.1.4) because of overcrowding and upcoming violence in the existing reception camps of Nayapara and Kutupalong (Monju 2017). However, many human rights organizations see massive problems: The uninhabited and mainly featureless island is only accessible by boat, making the people highly dependent from aid shipments in the first place. Besides that, people would be exposed to natural calamities, such as storms, high sea levels, and lack of drinking water (Chowdhury 2017).

The marshy, flat island has an extent of around 8 kilometers in east-west direction and is only a few meters above the sea level, making it vulnerable to flooding during the monsoon season between June and September (Scarr et al. 2017). Despite the governments' efforts to prepare the island save for habitation, experts estimate that it would take around 15 to 20 years until the island would provide basic living conditions including the potential for subsistence agriculture (Sen 2017).

While information on the ground of the island cannot be given without careful field inspection, this study investigates how strong sea level variations influence the extent of the island over nearly three decades to get information about its vulnerability towards flooding. The island of Thengar Char located southwest of it (Figure 61) is additionally analyzed as a reference.

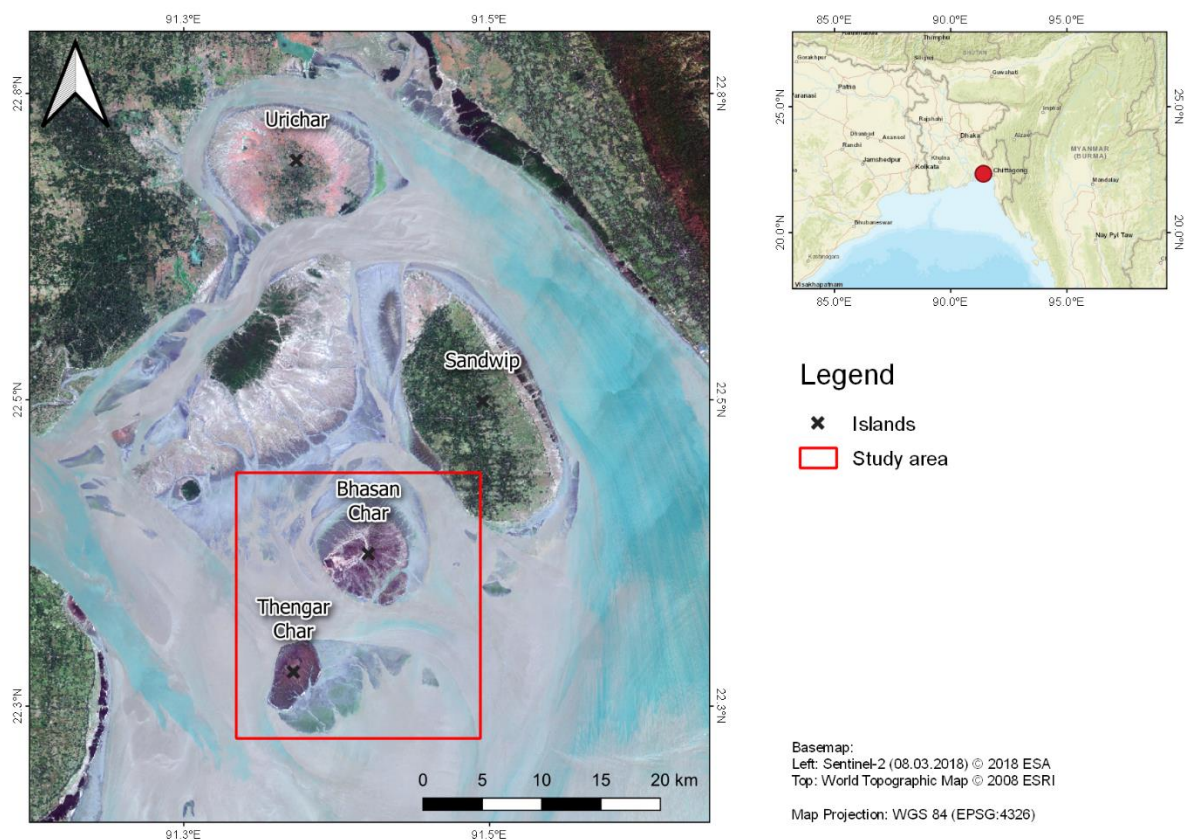


Figure 61: Study area for the analysis of sea level changes in Bangladesh

### 3.2.2.2 Data sources and processing

72 Sentinel-1 images acquired between 10/2014 and 02/2018 were used for the medium-term analysis of sea surface dynamics. Additionally, 74 ERS-1/2 images acquired between 12/1991 and 07/2004 and 48 ENVISAT ASAR images acquired between 05/2003 and 06/2012 were used for the long-term investigations on the presence of the island. In total, 194 C-band radar images served as input to this study. They were acquired as GRD products (Table 33), radiometrically calibrated and geocoded to WGS84 projection. A Lee Sigma filter (Lee et al. 2009) with a window size of 7 pixels and a sigma value of 0.9 was applied to the images to reduce speckle. All images were clipped to the area shown in Figure 61, resampled to a common spatial resolution of 20 meters, converted to log-scale (equation 14) and a co-registered stack of all products was created.

Temporal statistics were calculated for each island based on the Sentinel-1 data as shown in Figure 62 to get a general understanding of the extent. These statistics represent the mean, minimum, maximum and standard deviation of all pixel values during the whole investigated period. They serve as a first indicator of the dynamics of these islands. In order to get an exact extent of each investigated image, the images were converted to a binary classification using the automatic thresholding proposed by Otsu (1979) which searches the minimal turning point in the histogram of each image which is separable in bright pixels representing the island and dark pixels representing the sea surface. An example for the binary image retrieved on 22.01.2018 is also shown in Figure 62.

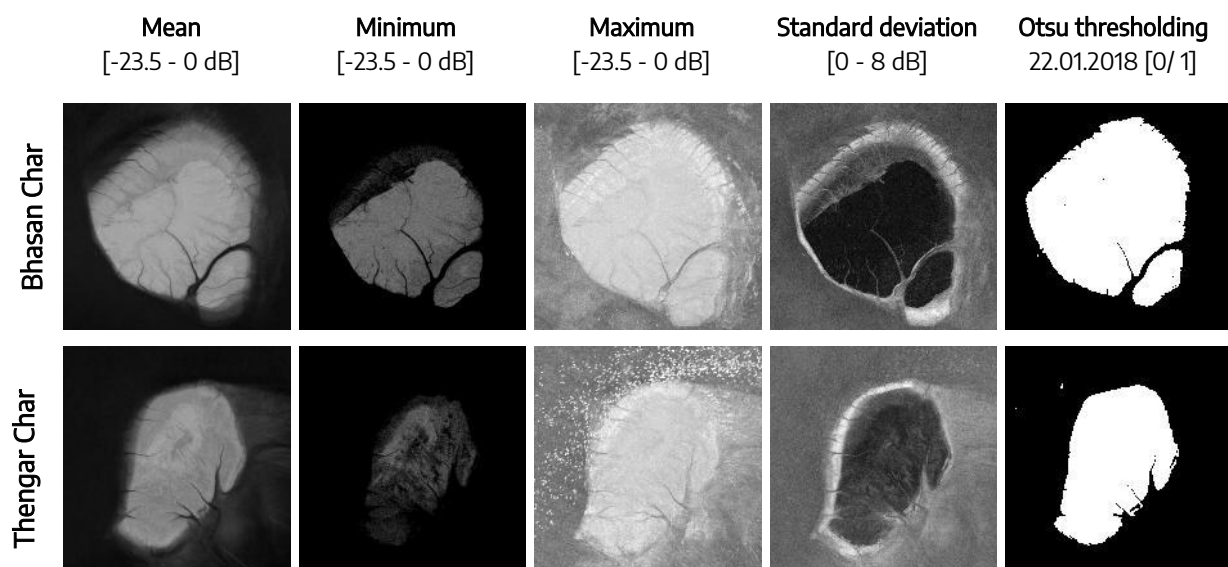


Figure 62: Temporal statistics and thresholding for the SAR images of the two islands

### 3.2.2.3 Results and discussion

To get an idea about the long-term development of Bhasan Char, the number of pixels identified as land by the thresholding was used to calculate the size of the island at the date each image (Figure 63). Two things can be observed here: Firstly, the sizes of both islands correspond very well over most of the time which underlines that sea level changes are the main influencing factor on the sizes of the islands. Secondly, there is no agreement before the year 2008 and the two curves show a rather random variation. The reason for that was found after visual inspection of these images: The islands did not exist until 2009 and the thresholding falsely divided the image of the dark sea surface into bright and dark pixels. It turned out that both islands were formed by silts washed from

the Himalayan mountains which began to accumulate as land surfaces in the delta since late 2008. This was later confirmed by other sources (Scarr et al. 2017; Sen 2017). The results imply that both islands are very recent landforms and subject to large dynamics regarding their size and spatial extent.

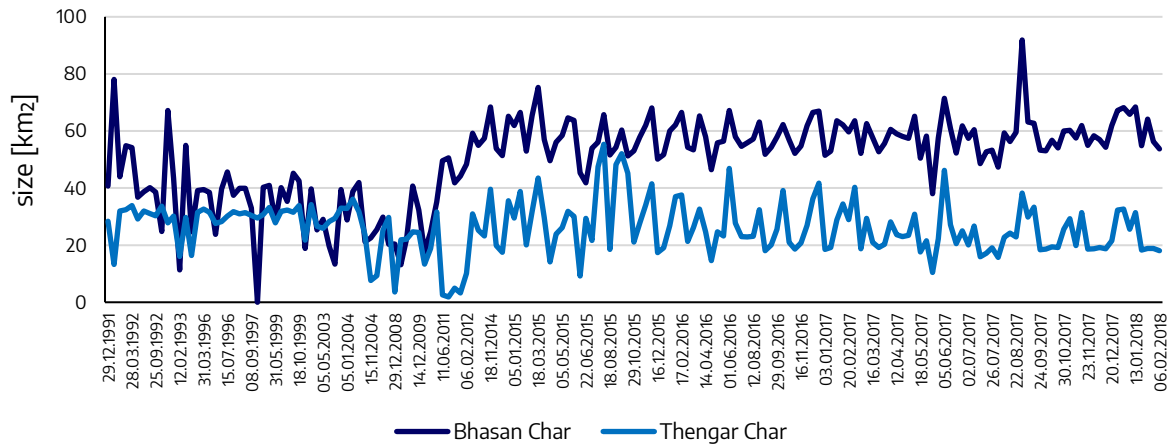


Figure 63: Size of the islands because of sea level changes since 1991  
 Note the non-linear scale of the x-axis as it was adjusted to the available data.

To quantify these dynamics, image statistics of the 72 Sentinel-1 images were compared. At average, an area of around 60 square kilometers is identified as land for Bhasan Char and at maximum this area is 76 square kilometers. This accounts for an increase of 26 %. However, decisive is the smallest area to be identified as land, which is only around 39 square kilometers, which accounts for a decrease of -35 %, compared to the mean. These numbers underline the impact of sea level changes on the islands and are especially notable as they refer to a period of only three years.

Another possible visualization is given in Figure 64. It shows the mean images of the years 2015, 2016 and 2017 in the colors red, green and blue.

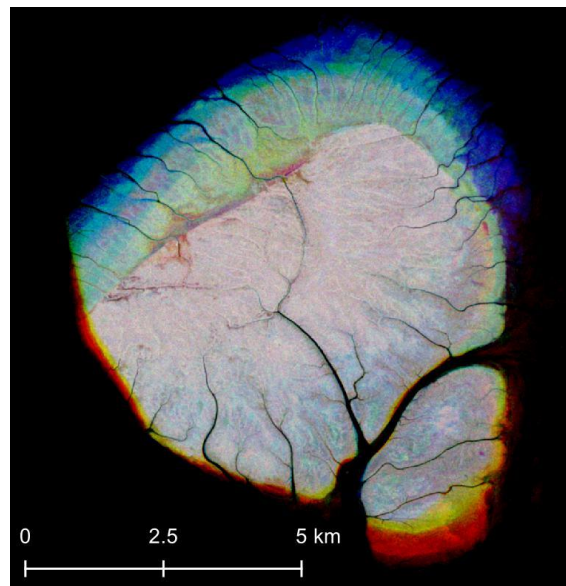


Figure 64: Bhasan Char in 2015 (red), 2016 (green) and 2017 (blue)

The figure emphasizes the overall movement of the island's surface towards the north. This is possibly because silts are continually washed from the inland into the delta while the southern part of the island successively vanishes. Concludingly, there is not only the risk of flooding during the monsoon season, but also points which indicate that the island is being eroded by the tidal moves in the Bay of Bengal and surface wash by runoff processes after heavy rainfall.

To assess the accuracy of the thresholding, 20 of the images were randomly selected and the island's extent was manually digitized and compared to the binary image. The accuracy, as a ratio between correctly classified pixels of land (true positive) and water (true negative) and misclassifications of land (false positive) and water (false negative) is calculated as described in

equation 16 and demonstrated in Figure 65 (right image). A mean accuracy of 88 % for all tested 20 images was calculated. The thresholding failed for images which did not show a clear land-water pattern (Figure 65, top left), resulting in very low accuracies. Waves (Figure 65, top middle) also caused problems for a clear distinction between land and water surfaces. But most cases led to satisfying results, making the time-series analysis a valid measure for dynamics of the island's size.

$$Accuracy = \frac{(true\ positive + true\ negative)}{(true\ positive + true\ negative + false\ positive + false\ negative)} \quad (16)$$

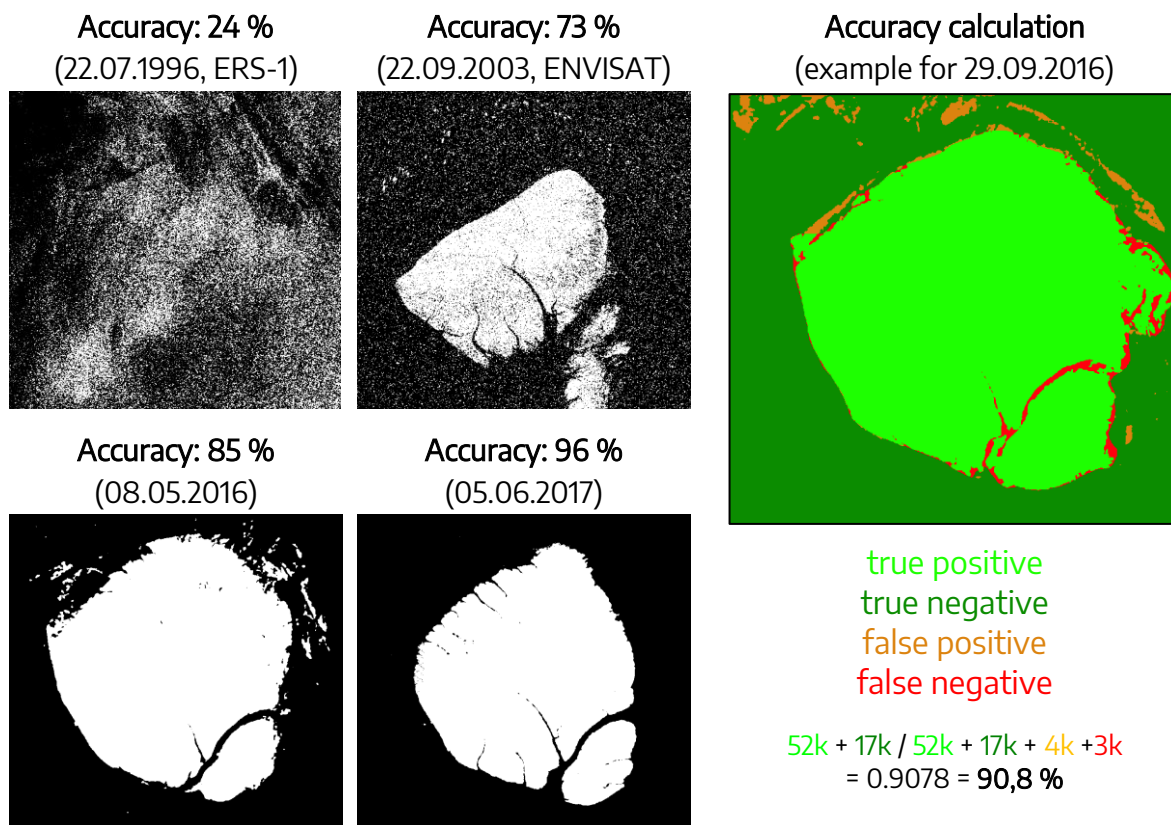


Figure 65: Accuracy of selected binary island classification of Bhasan Char (left) and example of its calculation (right)

As the complexity of this study was limited, there is only little to discuss about the methodological part. Still it demonstrated the value of large time-series for risk assessments in coastal areas.

As it turned out, the histogram-based thresholding only works if there is a clear distinction between water and land. High backscatter caused by ships or rough waves is easily misinterpreted as land. Additionally, the thresholding works best if the proportions of sea and land areas in the image are predominantly equal in the images.

Of course, it can be argued if the presented findings are enough to prove unsafe living conditions on these islands. But it delivers several indications that the island is subject to dramatic dynamics which are a risk that is not calculable. This should be reason enough to refrain from the plans of relocating people on this island. It is furthermore of importance that these findings are not perverted to a counterargument: Just because an area is considered land in most of the images of this study

does not make it a safe place for living in general. Both ways lead to the conclusion that the island is not stable enough to draw final conclusions. Neither data availability nor spatial resolution were limiting factors in this study.

#### 3.2.2.4 Scientific conclusions and practice recommendations

The following points can be concluded for the mapping of sea levels from radar data in humanitarian application cases:

- Because of their similar configuration, missions of ERS-1/2, ENVISAT ASAR and Sentinel-1 by the European Space Agency (ESA) provide an **unprecedented archive** of continuous and systematic data acquisition at a global scale (Guimaraes et al. 2017; Lisini et al. 2018; Torres et al. 2012), allowing for effective exploitation, transfer and adaptation of approaches.
- **Histogram thresholding** is an easy method which can quickly be applied to a large number of images. Its potential for operationalization is large, especially in coastal areas (Matgen et al. 2011; Santoro & Wegmüller 2014; Yu & Acton 2004) or for hydrologic early warning systems (Boni et al. 2016; Ding & Li 2011; Pedersen et al. 1995).
- For automated thresholding using the method proposed by Otsu (1979), a **preselection** of input images has to be conducted. In the presented study, the images without any land mass were falsely binarized by the algorithm. For **operational** work flows, control points have to be integrated to prevent false
- The only requirement is careful **pre-processing** (chapter 2.3), including radiometric calibration, filtering and geocoding. It is furthermore advised to select an area which equally contains water and land, so the maximum bi-modality of the histogram is achieved.
- Very flat coastal areas, such as sand beaches and alluvial fans, are hard to detect because of their high moisture content and low backscatter intensity. In these cases, **the integration of additional sources**, such as optical data (Chini et al. 2013), polarimetric information (Yu & Acton 2004) or image texture (Onana et al. 2001) is advised.
- To establish an **early warning system**, newly acquired images have to be automatically downloaded and processed as suggested in this section. Operational processing pipelines for Sentinel-1 has been successfully demonstrated by Twele et al. (2016), Arko et al. (2016) and Hua et al. (2017). One key task is to observe the sizes over a longer time-span and then to automatically identify unusual patterns (Keogh et al. 2002) or anomalies (Wei et al. 2005) regarding the sizes of the islands and their temporal trends.

### 3.2.3 Flood mapping (Attapeu, Laos)

#### 3.2.3.1 Background and aims

On 23.07.2018 at around 8:00 pm, a saddle dam of the Xe-Namnoy hydropower water reservoir near the city of the city of Paksong collapsed in the southeast of Laos (Figure 66). It is believed that heavy monsoon rains in the weeks before the incident in combination with a faulty construction led to the collapse (Souksavanh 2018). As a consequence, the water masses leaked downstream and increased the discharge of the Xe-Pian rivers, mainly in the Attapeu subdivision of Laos southwest of the reservoir. The floods caused nine fatal casualties, 111 missing persons and 16,000 persons were supposed to be directly affected (Gong 2018). Although many neighboring countries, humanitarian NGOs and companies from the private sector quickly offered their help, the relief workers were facing challenges arising from the terrain and impassable areas. A report on potentially affected villages in the areas was provided by UNOSAT seven days after the incident (UNITAR 2018a). Furthermore, several flood maps based on RADARSAT-2 (UNITAR 2018b), TerraSAR-X (UNITAR 2018c), Kompsat-5 (UNITAR 2018d), Sentinel-1 (Brakenridge & Kettner 2018; UNITAR 2018e) and ALOS-2 (JAXA 2018) were published. However, little is known about the methods and accuracies of these maps because they were either produced fully automated or based on visual interpretation, and the time for validation was not given in this emergency situation.

This study demonstrates the suitability of Sentinel-1 data for the automatic detection of small inland water bodies in emergency situations. It targets the challenge of low contrast of small water bodies with rough surfaces, as it is often the case for inland floods. These low contrasts limit the potential for automation. As Sentinel-1 data is freely available and has short revisit times, it is an extremely valuable source for relief operations. Therefore, this study furthermore gives an estimation on the reliability and limitations of this kind of data.

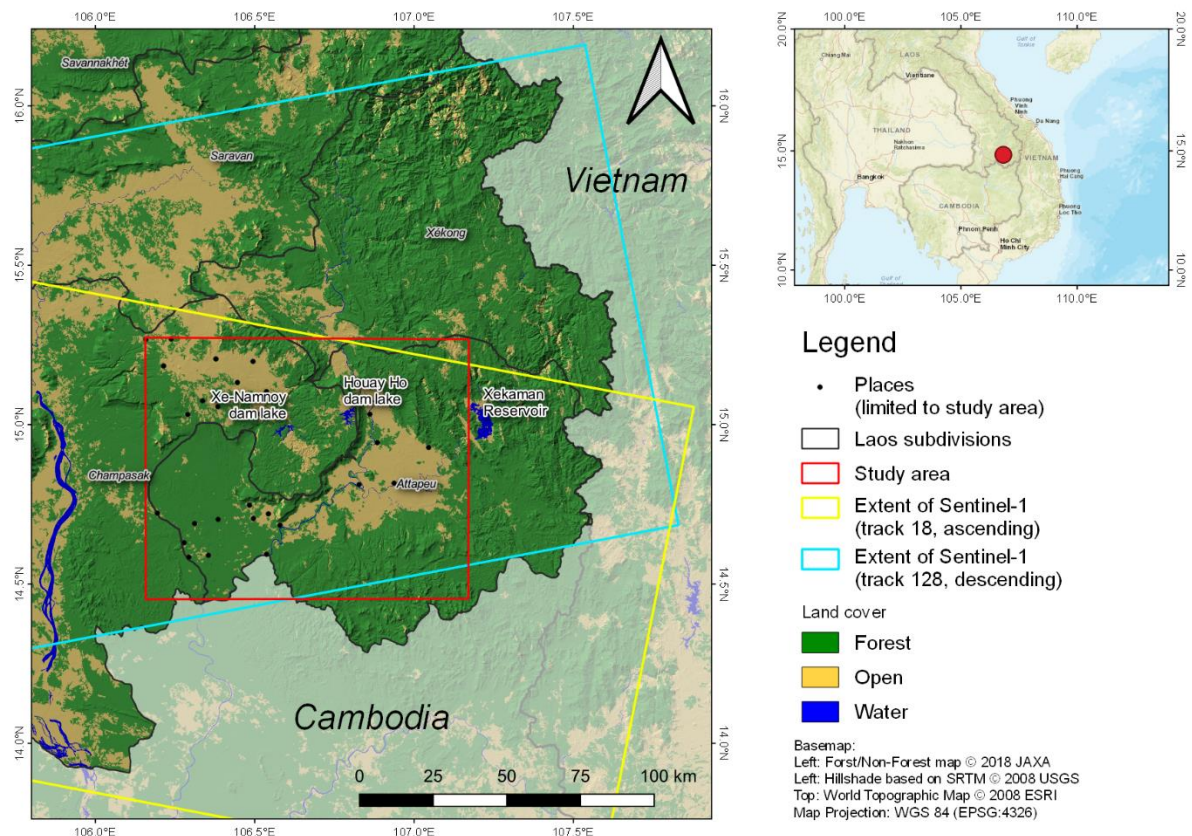


Figure 66: Study area for flood mapping in Laos

### 3.2.3.2 Data sources and processing

Flood maps based on RADARSAT-2 (UNITAR 2018b) were chosen as reference data because they have a spatial resolution four times higher than Sentinel-1 and the underlying acquisitions were temporally closest to the ones of Sentinel-1 (Table 12). This is of special importance because water masses rapidly change within few days this increasingly affects the accuracy assessment.

Table 12: Satellite data used for flood mapping in Laos

Satellite	Date	Spatial resolution	Content	Orbit (S1 track)
RADARSAT-2	10.07.2018	5 m	pre-flood	descending
Sentinel-1	13.07.2018	10 m	pre-flood	ascending (18)
Sentinel-1	17.07.2018	10 m	pre-flood	descending (128)
RADARSAT-2	24.07.2018	5 m	post-flood	descending
Sentinel-1	25.07.2018	10 m	post-flood	ascending (18)
Sentinel-1	29.07.2018	10 m	post-flood	descending (128)

Figure 67 shows the study area before and after the dam break (indicated as the black line) in the Sentinel-1 images as described in Table 12. They are the base information for this study and show two notable things: Firstly, the surface of the Xe-Namnoy reservoir in the center of the image extremely shrank between 17.07.2018, indicating the immense water masses released southwards. These become more visible in the floodplain in the last two images, especially in the southwest. On 29.07.2018 the flooded areas have already retreated to a certain amount. This amount is to be specified in the upcoming analysis. Secondly, the images show the extreme effect of the look direction of the sensor on the image radiometry: The slopes of the plateau look brighter because of the smaller incidence angle (Figure 14), on the west side for the ascending images (13.07. and 25.07) and on the east side for the descending images (17.07. and 29.07.) as a consequence of the different look direction. Although radiometric normalizations for topographic effects exist (section 2.3.1), artefacts can remain which are very likely to be falsely identified as flood areas in a pair-wise image comparison. Therefore, separate analyses were performed for both the ascending and image pair.

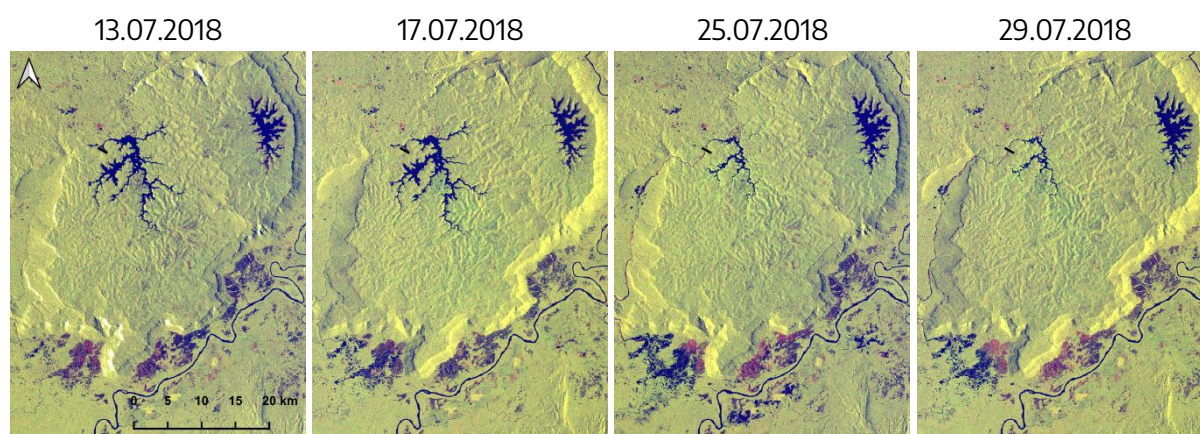


Figure 67: Sentinel-1 images of the study area before and after the dam break on 24.07.2018

Red=VV, green=VH, blue=VV/VH

As described in section 3.2.1, automated thresholding of images for change detection works well if the histogram can be split into two parts (Patra et al. 2011; Rosin & Ioannidis 2003). But whenever the water and land areas are not equally represented within a radar image, pixels of low backscatter

representing water global thresholding methods, such as shown in section 3.2.2, mostly fail. The temporary flooded areas in Figure 67 make up only a small proportion of the study area and are therefore not separable with a single backscatter threshold. Therefore, a hierarchical split method developed by Chini et al. (2017) was employed in this study which gives higher flexibility regarding local minima of smaller flooded areas. It is based on a systematic segmentation tiling which uses the quad-tree technique (Spann & Wilson 1985) to split the original image  $S_1$  into a so-called child  $S_2$  consisting of four squared tiles (Figure 68). This allows to compute separate histograms for different parts of the images at various scales.

Table 13: Criteria for the selection of image tiles for thresholding

#	Criterion	Measure	Value in this study
0	The minimum number of children is reached	<i>manually defined</i>	> 3
1	The histogram shows a clear bimodality	Ashman coefficient (Ashman et al. 1994)	> 2.4
2	Both curves of the bimodal histogram show a normal distribution	Bhattacharyya coefficient (Aherne et al. 1998)	> 0.99
3	The ratio between the frequencies of both classes exceeds a minimum value	Surface ratio (Bazi et al. 2007)	> 0.1
4	Minimum pixel number of a child is not reached	<i>manually defined</i>	> 1000

In a first step, the histogram is coarsely separated into two classes using Otsu's thresholding (Otsu 1979). If certain criteria, defined in Table 13 as adapted from Chini et al. 2017, are fulfilled, the tile is selected for a more precise threshold determination. This leads to a successive refinement of the binarization of the image's tiles into water and land pixels. As still some overlap between water and land pixels exist in the histograms, the thresholds are used for the distribution of seeds which serve as starting points for region growing algorithms presented by Haralick & Shapiro (1985).

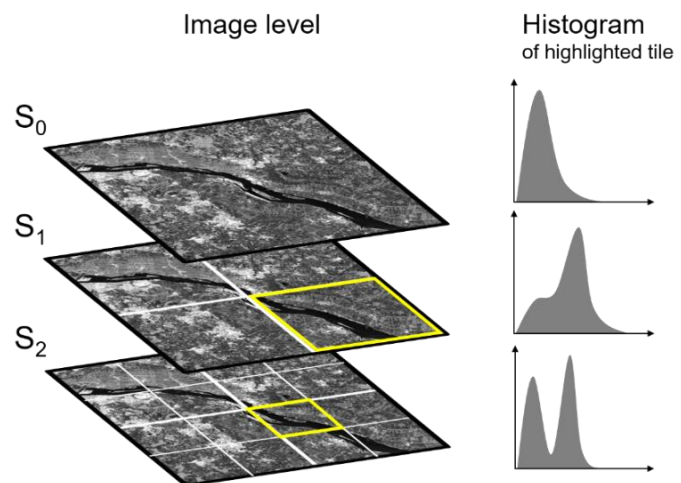


Figure 68: Schema of the hierarchical histogram splitting  
Adapted from Chini et al. (2017)

These spatially extend the detected flood areas based on a tolerance criterion derived from the histogram of the tiles and their statistical evaluation as presented by Giustarini et al. (2013). The result is a binary image of the image's water extent.

As the study area also contains permanent water bodies, this algorithm is also applied to a reference image taken before the flood incident (23.07.2018) which has the same orbit and track as shown in Table 12. A comparison of both flood maps then indicates which areas are only temporally flooded. In a last step, flood areas smaller than a manually defined size (here: 1000 pixels) are deleted from the result because small slivers are often processing artefacts and not related to real backscatter change (Martinis et al. 2015).

### 3.2.3.3 Results and discussion

For an evaluation of the results and an estimation about the accuracy of the products derived from Sentinel-1, four binary classifications were compared:

1. **RS2**: Water body classification based on a RADARSAT-2 image from 24.07.2018 (UNITAR 2018b). It serves as the reference classification for the accuracy assessment.
2. **S1**: Flood classification based on Sentinel-1 data from 25.07.2018 (and 13.07.2018 as non-flooded reference) which was created as described in the previous chapter.
3. **S1m7**: Maximum filter of 7x7 pixels applied to S1. It was additionally computed to slightly enlarge flood areas and to remove smaller gaps.
4. **S1g**: Flood classification based on a global thresholding of the difference layer between the Sentinel-1 images of 13.07.2018 and 25.07.2018. All values < -1 dB (indicating clear decrease of backscatter intensity) were classified as water.

The last dataset (S1g) was taken into account to show the superiority of hierarchical local thresholding over a global threshold which is applied to the whole image at once.

Figure 69 shows a comparison of the results of the different flood products and the reference classification of RADARSAT-2 (RS2). It shows one main challenge for SAR-based flood mapping at first sight: To detect water bodies to a sufficient degree, but without overestimating them.

High agreement is shown in the areas around the villages of Ban Hinlat and Ban Mai south of the plateau where the water masses flooded the plains due to reduced slopes (blue tones). In contrast, areas in orange and yellow near the villages of Ban Nongkè and Ban Phônstaat show water where the flood did not occur at this extent. At least compared to the reference data of RADARSAT-2. Most strikingly, the global threshold produced strong overestimations in all parts of the image (red).

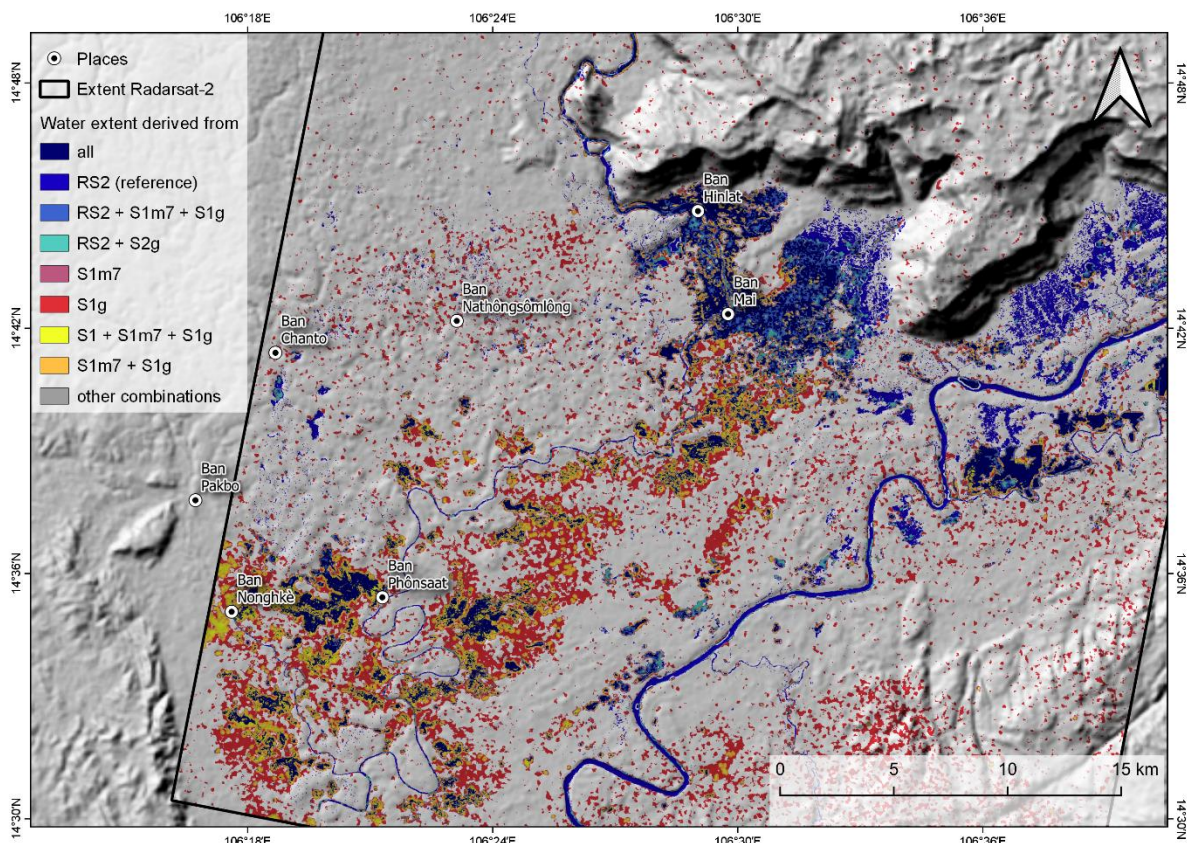


Figure 69: Validation of flood mapping with various approaches for 25.07.2018

To get a quantitative understanding of the quality of the several products, an accuracy assessment has been performed with the binary water mask of the RADARSAT-2 product as a reference. As the measures fulfill different purposes regarding the usability of the results, they are briefly explained in the following:

User's accuracy: Defines the reliability of the classified map from the view of the map user. That is, how often water in the map will actually be present on the ground. For example, a user's accuracy of 80 % indicates that 20 % of the water bodies were missed by the classifier and are not present in the map.

Producer's accuracy: Defines the accuracy of the classified map from the producer's perspective: It indicates how often are the classes present in the study area correctly shown on the map. In other words, it defines the probability that a certain class is classified as such. For example, a producer's accuracy of 65 % indicates that 35 % of the water bodies in the map are wrong (non-water).

Kappa: The Kappa coefficient (Viera & Garrett 2005) is a measure for the accuracy of a map which takes into account that the correctness of a classified map could also be the result of coincidence. It is scaled between -1 and 1, while a number near 1 indicates that the classified map is significantly better than a random distribution of the classes. In turn, a Kappa value around zero means the produced classification is not better than random (e.g. a chessboard map of water and non-water pixels) and negative values respectively worse.

Overall accuracy: The overall accuracy includes the correct identifications of all classes present in a map. In our case, it combines the detection of both water and non-water bodies in the study area.

*Table 14: Accuracy assessment for flood mapping in Laos*

	<b>S1</b>	<b>S1m7</b>	<b>S1g</b>
User's accuracy water	35.0 %	55.4 %	60.9 %
User's accuracy non-water	99.0 %	97.4 %	82.4 %
Producer's accuracy water	78.5 %	51.3 %	30.1 %
Producer's accuracy non-water	93.6 %	95.0 %	96.1 %
<b>Overall accuracy</b>	<b>95.2 %</b>	<b>94.1 %</b>	<b>86.2 %</b>
<b>Kappa</b>	<b>0.903</b>	<b>0.881</b>	<b>0.741</b>

Table 14 lists the different accuracy metrics of the flood mapping for 25.07.2018. At first sight, the overall accuracies between 86 % and 95 % seem very high. However, they result from the large proportion of non-water areas in the map which are correctly classified to a numerically large degree. For this reason, user's and producer's accuracy have been taken into account as well. The table nicely shows the trade-off between correct classifications of water and overestimations by filtering (S1m7) or global thresholding (S1g). In the original result S1, the user's accuracy is comparably low with 35 %, that means, 65 % of the water bodies in the study area were missed. For S1m7 and S1g the completeness of detected water increases up to 61 %. In turn, the producer's accuracy significantly drops, meaning that too many areas were identified as water which were not flooded in reality. So, the producer's accuracy of 79 % is the highest for S1, meaning that only 21 % of the identified flood areas are wrong. For the other two results, producer's accuracy drops up to 30 %, meaning that 70 % of the flood extents were false classifications. The Kappa values also indicate that the unmodified hierarchical thresholding S1 is the one which describes the reference dataset the closest.

These findings highlight that there must be a trade-off between completeness (high producer's accuracy) and reliability (high user's accuracy) when flood is mapped based on SAR data, especially when the water bodies are roughed up by wind or discharge or when the water signature vanishes under vegetation. In case of emergencies in complex landscapes, users have to define if they are willing to accept over-estimations for a higher completeness of the flood extent or if they want more accurate predictions at the cost of a higher errors of omission. Although there might be cases where the identification of floods is easier, being prepared for such decisions is key for quick and effective response analyses.

The numbers in Table 14 seem comparable low for their use in an emergency. However, three points have to be noted which could have falsely decreased the accuracy measures. The main uncertainty of the accuracy assessment is the difference between the reference image's date (24.07.2018) and the used Sentinel-1 acquisition (25.07.2018). A temporal difference of one day can lead to significant changes in the inundated areas. This is especially notable, because many flood areas in the Sentinel-1 result seem to be overestimated, but some of these areas might actually have retreated between the two acquisitions. Consequently, some of the spatial differences might be true (for example the purple areas in Figure 69) and the respective producer's accuracies could be accordingly higher.

A second point addresses the fact that the reference dataset based on RADARSAT-2 mapped water bodies in general. As shown by the blue areas in Figure 69, the rivers and small lakes were not detected as floods by the hierarchical Sentinel-1 thresholding because it involves the analysis of both the reference image and the flood image. This fact lowered the user's accuracies while this is actually not a failure of the thresholding itself but rather an inconsistency between the classified map and the reference data which was available for that date.

Lastly, the difference in spatial resolution between RADARSAT-2 (5 m) and Sentinel-1 (10 m, originally 20 m) does not only reveal different levels of detail, but also can the pixels sizes lead to different backscatter intensities, even if the roughness of the area is the same (Ulaby et al. 1986). Although this difference was part of the research question, namely if Sentinel-1 data can produce results comparable quality at lower spatial resolution, a final answer cannot be given because of the two aforementioned inconsistencies regarding acquisition date and the divergent definitions of water mapping.

Being aware of these uncertainties, a final map was produced based on all Sentinel-1 images available as listed in Table 12. It shows the water extents in the study areas before, during and after the flood event (Figure 70). It furthermore demonstrates how automated mapping of water bodies can be used in the aftermath of flood events. As shown by the color coding, areas in dark red were flooded the longest (until 29.07.2018) while at other locations the water masses already retreated (red). Other areas were inundated with a temporal delay (pale red). Comparing the water extents of different dates, also shows the drastic decrease of the dam's capacity: While permanent water bodies are shown in blue, water extents before the dam break are highlighted in cyan, especially at the Xe-Namnoy reservoir in the center part of the image. Analyzing these changes increases the understanding of hydrologic processes of an area, which is especially required if continuing rainfalls involve the risks of new floods and threaten the provision of aid supplies. Lastly, proper understanding of flood mechanisms is required for strategies of disaster preparedness and the construction for adaptation measures (Eriksen & O'brien 2007; Verburg et al. 2012).

Concludingly, this study showed how SAR can effectively assist flood mapping in emergency situations. The hierarchical thresholding is objective and based on an automated workflow and can therefore be integrated in operational services.

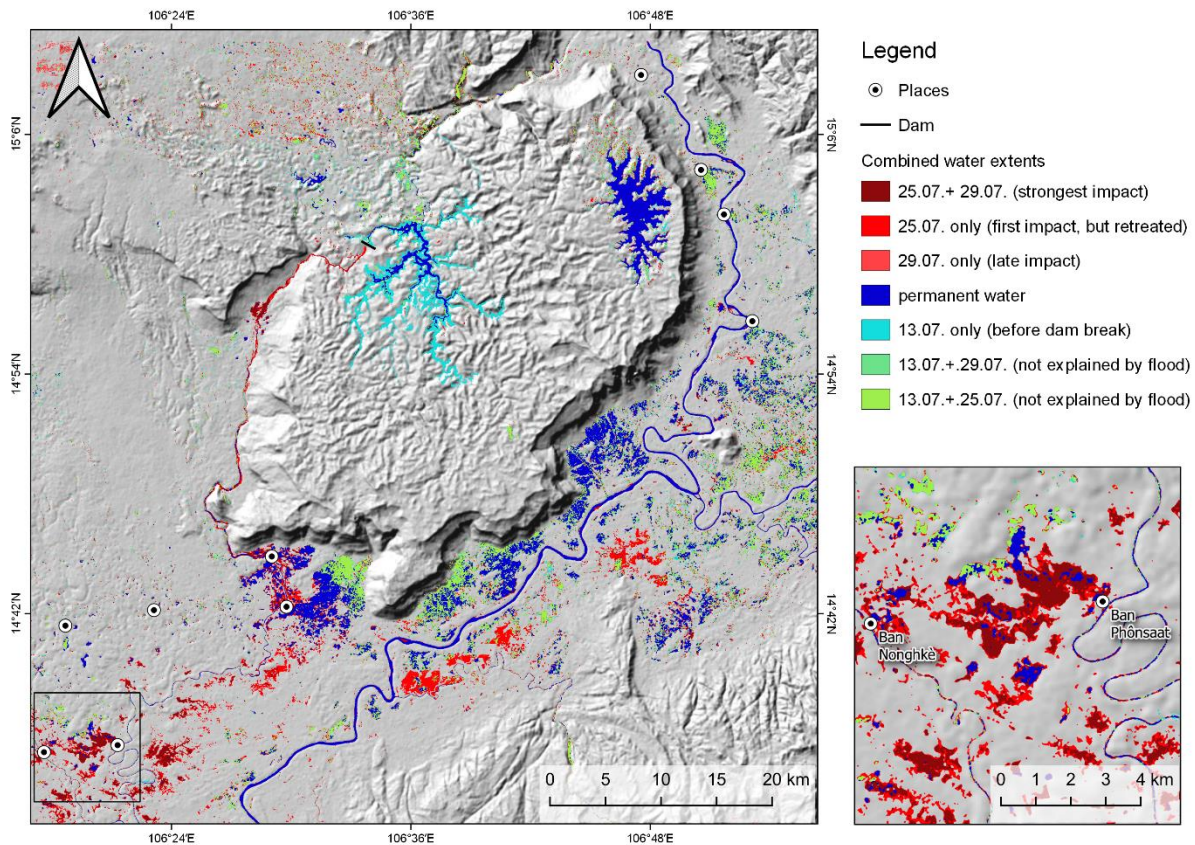


Figure 70: Evolution of water masses during July 2018 in southeast Laos

### 3.2.3.4 Scientific conclusions and practice recommendations

Mapping of water bodies with SAR data is a widely investigated topic. The following remarks can be made with respect to the application in the humanitarian domain:

- If **time** is critical, the quickest way to produce a flood map is manual digitizing of polygons based on a filtered and geocoded SAR image. For small, scattered inundations, point-like signatures might also be sufficient. It, however, needs to be considered that this is not an objective method and dependent on the interpreter's understanding of the study area.
- Regarding the selection of a suitable satellite, attention should be placed on the **temporal availability** of new taskings or archived images. Spatial resolution is only of secondary importance but can provide more detail in case of small flood events or urban environments.
- It is the task of scientists to prepare and provide ready-to-use **workflows** for the case of an emergency (Cian et al. 2018; Martinis et al. 2015; Mason et al. 2012; Solbø & Solheim 2005)
- Approaches based on hierarchical and **locally-adaptive thresholding** are preferable because over global ones because they clearly reduce the overestimation of naturally dark surfaces.
- **Communication** between the map maker and the map user is required to highlight the desired information in the most useful way (Zeil & Lang 2009). Development of standardized mapping procedures is also helpful for a quick and established layout.
- Dealing with **uncertainties** is key for flood mapping (Merwade et al. 2008). As the study showed, many automated approaches are a trade-off between overestimation and incompleteness. The user should make a preference what is more helpful in the case of emergency while the analyst should find a way to identify and communicate the areas which might be overestimated or missed.

### 3.2.4 DEM generation for runoff modeling (Kutupalong, Bangladesh)

#### 3.2.4.1 Background and aims

As described in section 3.1.4, since the influx of Rohingya refugees from Myanmar in late 2017, Kutupalong has become the largest refugee camp in the world (Cook & Ne 2018). Not only do the people suffer massive malnutrition and lack of medical basic services (Chan et al. 2018; Leidman et al. 2018), the area along the west coast of Bangladesh is heavily affected by cyclones at regular intervals. Furthermore, the vulnerability of the whole region towards natural disasters is expected to increase in the coming decades as a consequence of intensified storm surges and the rise of global sea levels (Dasgupta et al. 2014). These circumstances are extremely threatening the wellbeing of the people in the camp, because many of them are living in poor quality dwellings of light construction materials (GSC 2017). Additionally, many of the makeshift dwellings were constructed on muddy slopes and in flood prone areas, and many organizations warn of a humanitarian catastrophe (Baldwin & Marshall 2018; Sengupta & Fountain 2018).

This study shows how SAR data of the TerraSAR-X / TanDEM-X mission (Moreira et al. 2004) can be processed to derive elevation as a base information need for a proper risk and vulnerability assessment. Emphasis is placed on the quality of the elevation information compared to the currently freely available DEMs of the SRTM mission provided by the U.S. Geological Survey (USGS). Furthermore, the limitations of repeat-pass interferometry of the Sentinel-1 mission are demonstrated. A comparison of different data sources is finally tested for the modeling hydrological parameters within the camp area to detect dwellings which are endangered by landslides and flooding.

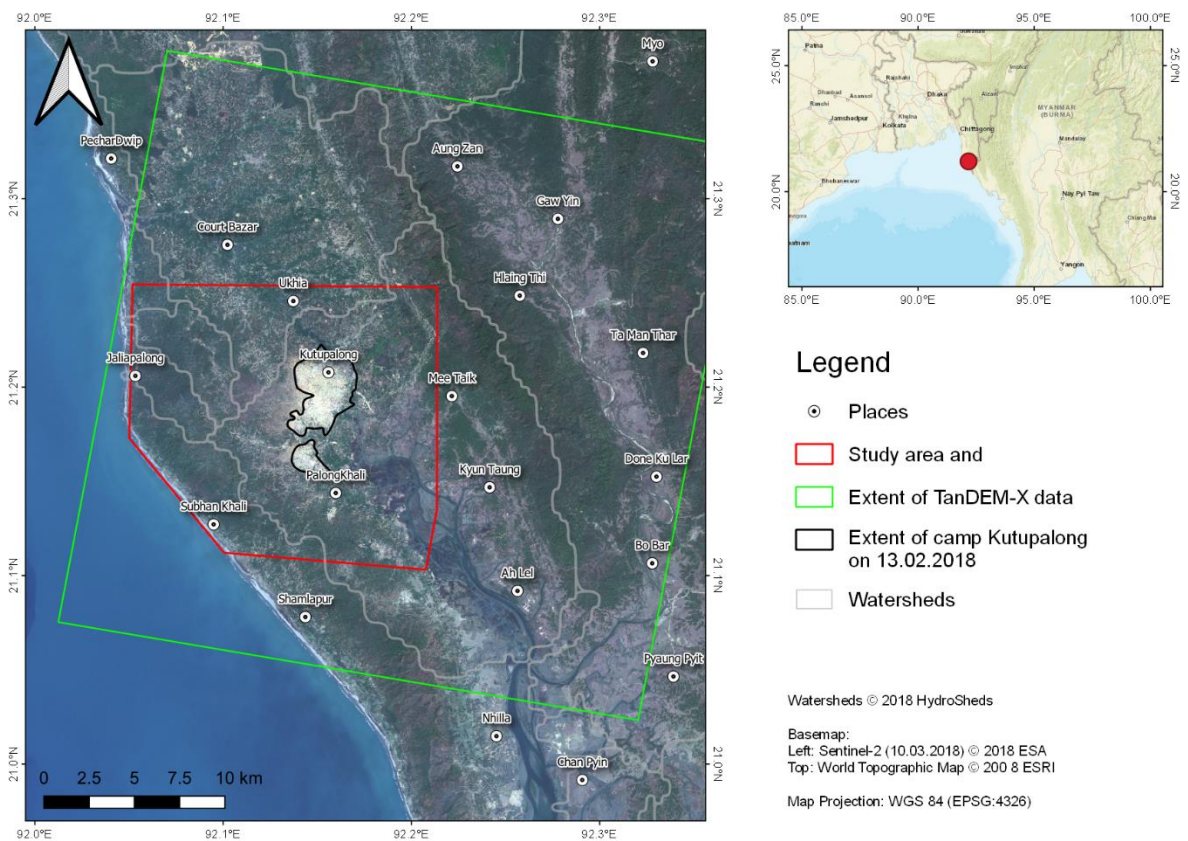


Figure 71: Study area for elevation extraction in Bangladesh  
Footprints of Sentinel-1 data are not shown in the figure as they exceed the map extent.

### 3.2.4.2 Data sources and processing

The study area is located approximately 35 kilometers south of the city of Cox's Bazar, the regional capital of the district of the same name in the Chittagong division in southeast Bangladesh (Figure 71). It includes the refugee camp of Kutupalong which was of a size of nearly 15 square kilometers in early 2018 (black line). To determine an initial extent of the study area, watersheds were investigated which show that the camp lies at the northern edge of a larger catchment which is fed from the southeast (Lehner et al. 2008).

Modeling terrain parameters and hydrologic discharge processes for landslide and flood susceptibility analyses requires digital elevation models (DEMs) at a high spatial resolution (Singh et al. 2005). Currently freely available DEMs, such as ASTER GDEM (Wang et al. 2012), SRTM or AW3D30 have a spatial resolution of around 30 meters which is often not enough to describe the complexity of the earth's surface (Bayburt et al. 2017).

For this reason, a SAR image pair of the bistatic TanDEM-X/TerraSAR-X constellation of the study area (Figure 71) acquired in StripMap mode was used. It consists of two X-band images from 08.10.2013 with a perpendicular baseline (Figure 24a) of 95.7 meters. The spatial resolution is 3.29 meter in azimuth direction and 1.76 meters in range direction. For comparison, an image pair of Sentinel-1 acquired on 28.10.2018 and 09.11.2018 was used. It has a perpendicular baseline of comparable length (95.8 meters) and a spatial resolution of 2.7 meters in azimuth direction and 22 meter in range direction.

As a first step, co-registration of the image pairs was conducted to retrieve a locally adjusted stack of both scenes. A key concept of radar interferometry (InSAR) is that local topography alters the phase of the electromagnetic wave. The interferometric phase  $\phi$  can be expressed based on the acquisition geometry (Figure 24) as demonstrated in equation 17:

$$\phi = \frac{4\pi}{\lambda} \Delta R \quad (17)$$

where  $\lambda$  is the wavelength and  $\Delta R$  is the slant range difference computed by the positions of both satellites  $R_2 - R_1$  and solved as

$$\Delta R = \sqrt{R_1^2 + B^2 - 2R_1B \sin(\theta_i - \beta)} - R_1 \quad (18)$$

where

$B$  is the perpendicular baseline,

$\theta_i$  is the look angle (Figure 13), and

$\beta$  is the angle of the baseline with respect to the horizon.

Based on the satellites relative position towards each other, expressed by the perpendicular baseline, as well as the incidence angle and the wavelength, the phase difference can be calculated which describes the influence of topography on the image. The resulting interferogram is shown in Figure 72 (top). It is clearly visible that the interferogram derived from the single-pass TanDEM-X data shows clearer patterns, so-called 'fringes', while the one based from the repeat-pass Sentinel-1

image pair is noisy and less has less connected patterns. This can be explained by the temporal baseline of the image pairs. While the two images of TanDEM-X and TerraSAR-X were acquired almost simultaneously, 12 days have passed since the first and the second image of Sentinel-1. During this time, natural surfaces, such as forests and water bodies have changed their surface characteristics and the two waves were no longer in-phase (Figure 24b). This so-called temporal decorrelation makes phase information unusable for topographic analyses (Zebker & Villasenor 1992). The reliability of phase information can be described by the interferometric coherence  $\gamma$ , also called the complex correlation coefficient, which denotes the stability of information between two image acquisitions (Ferretti et al. 2007a). It is computed as follows:

$$\gamma = \frac{|E\{S_1 S_2^*\}|}{\sqrt{E\{|S_1|^2\} E\{|S_2|^2\}}} \quad (19)$$

where \* denotes the complex conjugate,  $S_1$  is the master image,  $S_2$  is the slave image and  $E\{x\}$  is an ensemble average, because coherence cannot be calculated for a single pixel but has to be computed over several pixels in azimuth and range direction (6\*20 for Sentinel-1 and 10\*12 for TanDEM-X).

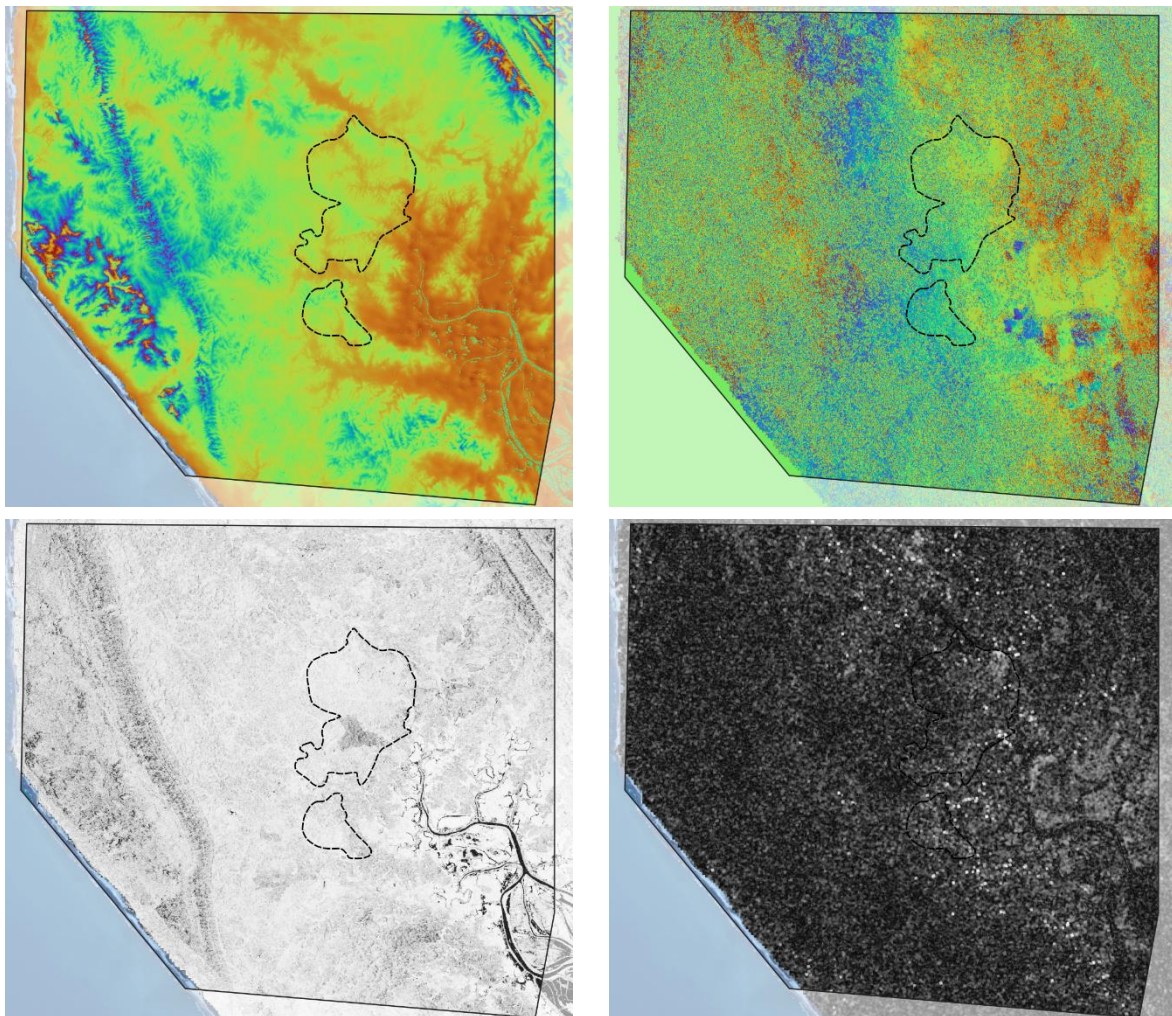


Figure 72: Interferogram (top) and coherence (bottom) of TanDEM-X (left) and Sentinel-1 (right) of the area of Kutupalong (black dashed line). Interferogram values range between -3.14 and 3.14 and coherence is scaled between 0 (black) and 1 (white).

As demonstrated in Figure 72 (bottom), coherence in the Sentinel-1 images is too low for interferometric analyses because of the dense forests. With a mean value of 0.2 and an 80%-percentile of 0.2, the data cannot be used for the derivation of a digital elevation model. In turn, Coherence of TanDEM-X is 0.83 with an 80%-percentile of 0.92. Only areas along the river in the southeast and in the mountainous ridges have lower coherence. This will affect the produced result, as it will be shown later.

Subsequently, only the TanDEM-X data is used for multi-looking was applied to the TanDEM-X interferogram with 3 range looks and 4 azimuth looks to remove smaller noise areas, resulting in a pixel size of 6.94 meters. A Goldstein phase filter was applied with a window size of 3 pixels and a FFT value of 64 (Goldstein & Werner 1998). This adaptive filter was designed specially to enhance the patterns of fringes in interferograms. As demonstrated in Figure 73 (middle), the fringes are pronounced by the filtering and the noisy areas of low coherence along the floodplains were partly filtered out. Resulting from equation 17, an interferogram can only describe the topographic features in a cyclic dimension (between  $-\pi$  and  $+\pi$ ) where one periodic cycle describes the difference at the scale of the wavelength (in the case of TanDEM-X 3.1 cm). This means, the measure is ambiguous, and no certain values can be assigned to it. To resolve these uncertainties, unwrapping has to be applied to the interferogram which translates the patterns of the fringes into an absolute measure (Ferretti et al. 2007c). This is done using the statistical-cost network-flow algorithm by Chen & Zebker (2001). The result of the unwrapping is a steady surface where each value can be assigned a corresponding elevation. To put the values into a reasonable context, a reference DEM can be used (Bamler & Hartl 1998). As shown in the unwrapped interferogram (Figure 73 right), the fringes are no longer present, and the values now describe an absolute change from areas of low (red) to high elevation (purple). The final pixel size is 7.31 meters and therefore 16 times higher than the one of freely available SRTM (30 m). The absolute vertical accuracy was estimated smaller 12 m and the relative vertical accuracy  $< 7$  m. Especially the latter is important for the modeling of surface discharge as shown in the following.

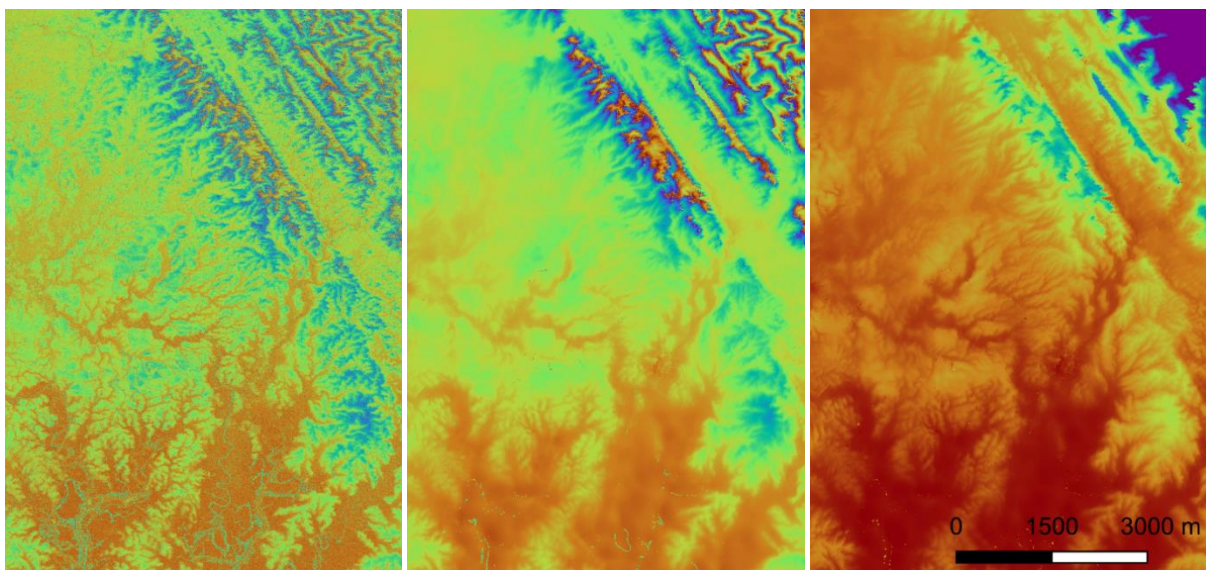


Figure 73: Raw interferogram (left), after multi-looking / filtering (middle), and unwrapping (right)

A topographic map based on this DEM including contour lines, local peaks, the extents of camp Kutupalong, the locations of other known settlements and the main road network was produced, tiled into 6 parts and provided to MSF for their work in the field.

### 3.2.4.3 Results and discussion

Figure 74 shows a hillshading representation of the derived digital elevation model. The overall degree of detail is very good, not only because of the high spatial resolution of 7.31 meters but also the different landscape features are well described: The long mountainous ridges ranging from northwest to southeast, the hilly woodland around the camp and the floodplain in the southeast. The enlarged areas on the right hand side show some limitations of the InSAR technique: 1) processing artefacts in the densely built camp area with phase errors caused by double bounce effects (Li et al. 2004), 2) very low coherence over water areas and flooded land caused by temporal decorrelation and 3) low coherence for steep slopes because of geometric distortions and unwrapping errors (Lachaise et al. 2012). The vertical profile along the red dashed line is shown in Figure 75. It shows the agreement between both DEMs and the increased level of detail of the TanDEM-X data compared to the SRTM data. How this affects hydrologic modelling will be shown in the following.

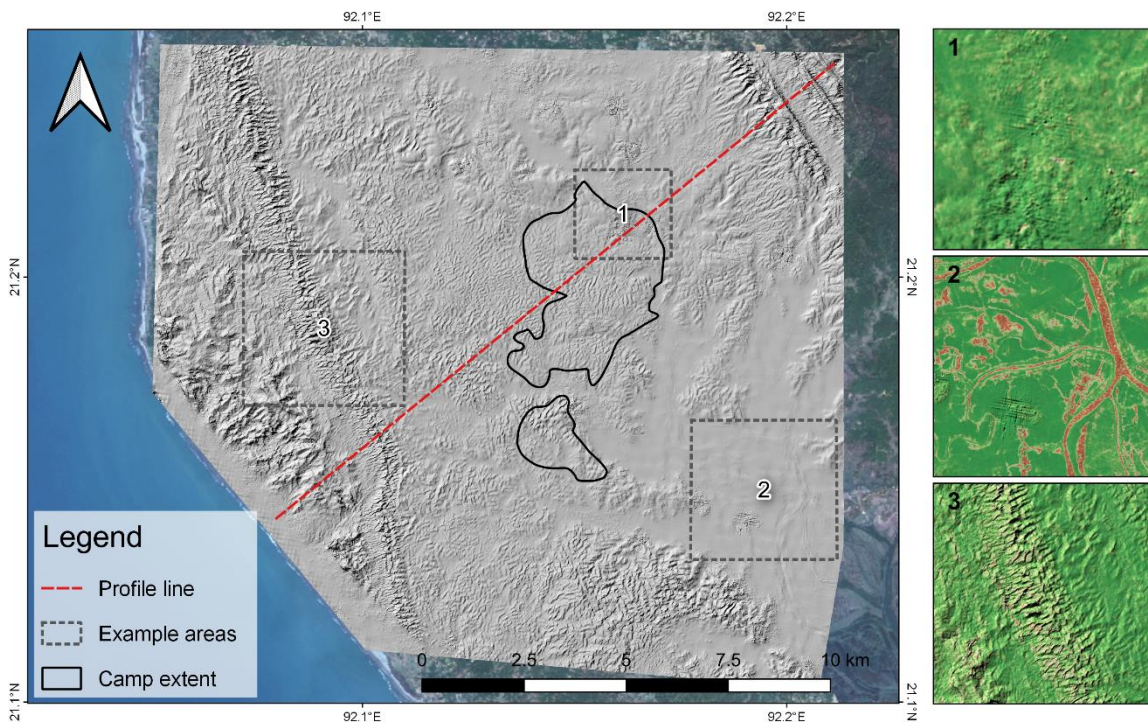


Figure 74: Digital elevation model derived from TanDEM-X interferometry  
 Right side: coherence for selected areas (red=0, green=1)



Figure 75: Terrain profile of DEMs from TanDEM-X (blue) and SRTM (red)

To identify dwellings prone to flooding or landslides, a hydrologic terrain analysis was performed which calculates flow directions, flow accumulations and catchment areas based on the digital elevations on both SRTM and the interferometric DEM produced in this study. (Fairfield & Leymarie 1991). As one main indicator for potentially vulnerable areas, the topographic wetness index (TWI, Beven & Kirkby 1979) was calculated. It takes into account the slope of an area as well as the upstream area contributing to discharge at this location and is a unitless measure. Secondly, the vertical distance to the local drainage network is computed as described by Böhner & Selige (2006) as a measure of a point above the surface drainage.

Figure 76 shows a selected part of the Kutupalong refugee camp. 125,000 dwellings were estimated in February 2018. Figure 77 demonstrates how spatial resolution influences the quality of the calculated TWI. While the wet areas seem comparably equal in the top image, the TanDEM-X derivative reveals that much of the wetness is entering the camp from the north and southeast. Also, the small channels are clearer at this resolution.

Figure 77 depicts a similar image. The scattered hills and ridges are not well represented in the SRTM elevation model while they are better visible in the TanDEM-X data. Both comparisons show how data of insufficient quality can lead to false conclusions about risk and vulnerability. If it comes to construction of new dwellings at topographically safe locations or the evacuation of the camp according to a priority list, reliability of modelled measures is essential.

Calculations based on TanDEM-X and SRTM are made in the following to demonstrate this discrepancy.

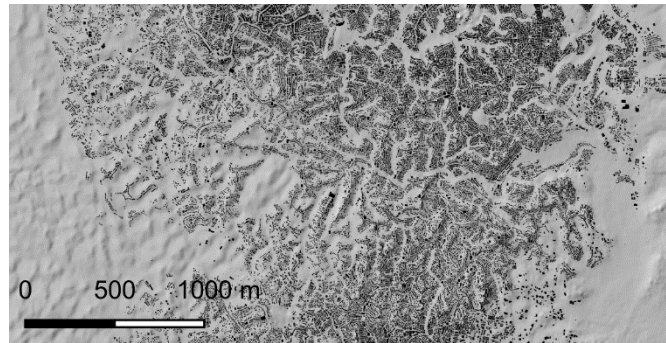


Figure 76: Dwellings in camp Kutupalong (February 2018)

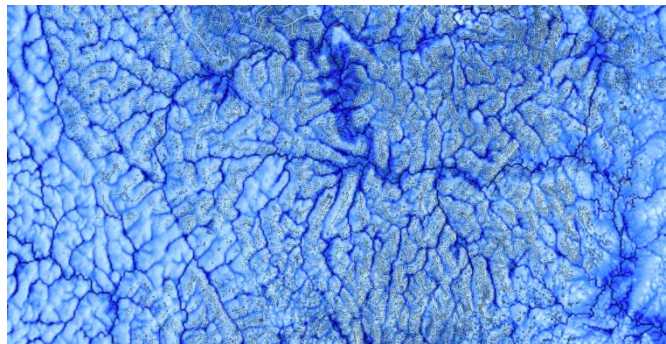
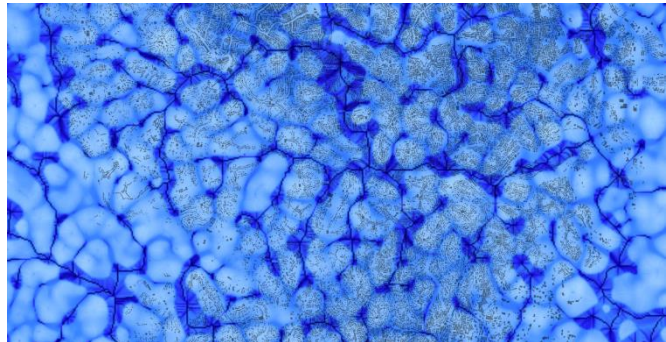


Figure 77: TWI based on SRTM (top) and TanDEM-X (bottom)

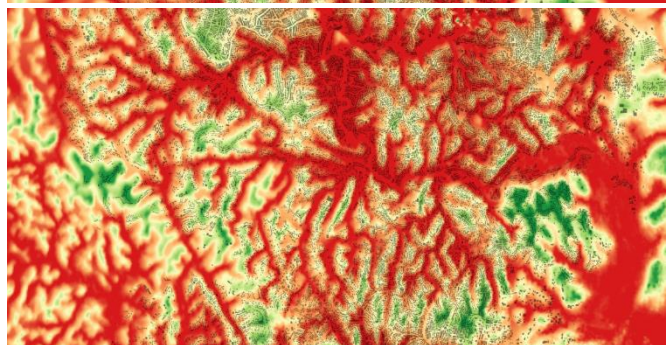
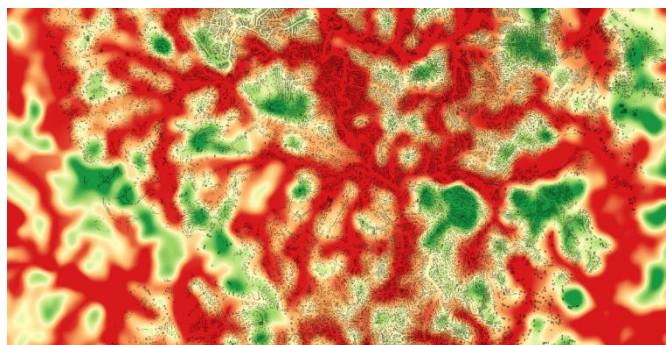


Figure 78: Distance above local drainage based on SRTM (top) and TanDEM-X (bottom) [0-10 m]

Statistical analyses of the 125,411 dwellings show that in 31.3 % of all cases (n=39,196) the  $TWI_{TDX}$  was larger than the  $TWI_{SRTM}$ . Furthermore, for even 57.8 % of all dwellings (n=72,322), the  $VDN_{TDX}$  was smaller than the  $VDN_{SRTM}$ . This means that in both cases the number of dwellings affected by a potentially high wetness and a low distance to the drainage was underestimated by the digital elevation model of SRTM of lower spatial resolution. As the TanDEM-X model has a higher spatial resolution and a better vertical accuracy, these values can be considered as more correct.

These indications are furthermore supported by the numbers given in Table 15. A total number of 46,165 buildings are located within a vertical distance to the local drainage network (VDN) of smaller 2 meters based on the TanDEM-X model, while these numbers are lower based on SRTM area. This means, in case of an emergency, 8.25 of the affected buildings would not have been prepared. The numbers of the Topographic Wetness Index (TPI) are even higher.

Table 15: Dwellings vulnerable to flooding based on TanDEM-X and SRTM elevation models

	TanDEM-X	SRTM	Difference
VDN < 2 m	46,164	42,645	+3,519 (+8.25 %)
VDN < 5 m	92,731	82,024	+10,707 (+13.1 %)
TWI > 5	76,662	116,037	-39,375 (-33.9 %)
TWI > 10	8,148	13,422	-5,274 (-39.2 %)

Figure 79 shows a scatter plot of TWI values of both products. It shows that there is large agreement between both datasets, but SRTM data both over- and underestimates the topographic wetness compared to TanDEM-X. While overestimating risks only leads to insufficiently managed measures of mitigation and prevention, underestimating of risks (blue ellipse) can have severe consequences for human security. In this case, dwellings which were originally considered safe would have unexpectedly been flooded.

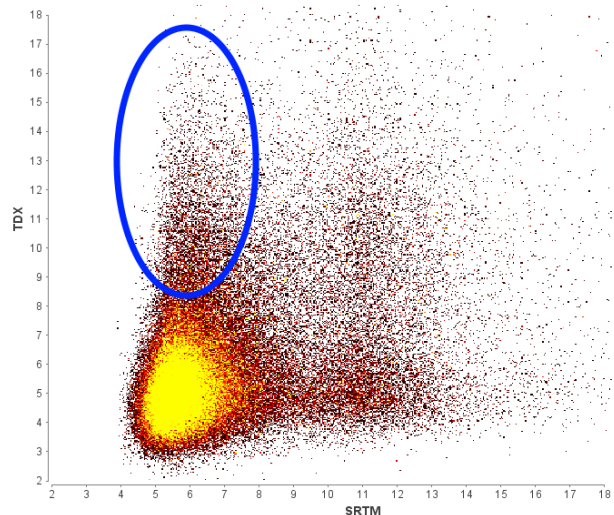


Figure 79: TWI derived from SRTM (x) and TanDEM-X (y)

Figure 80 shows how a risk assessment based on these two parameters could look like.

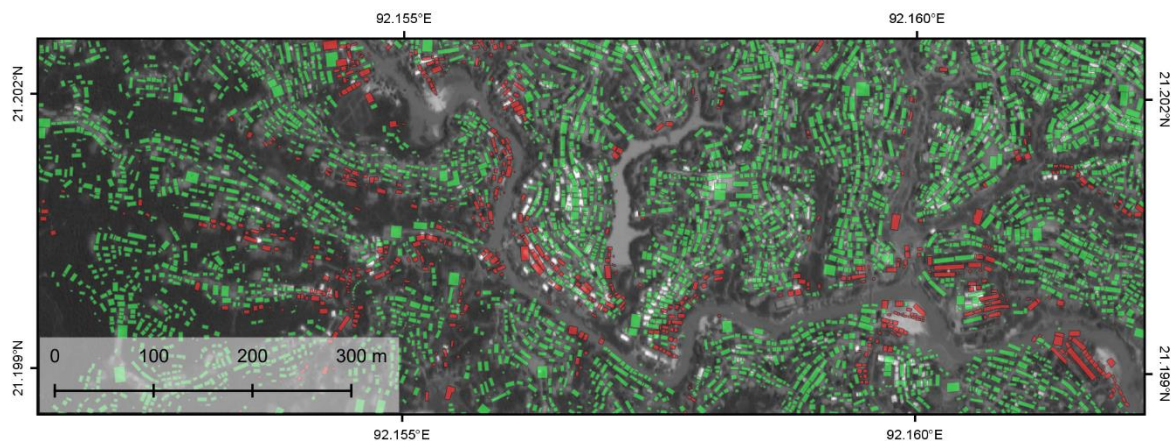
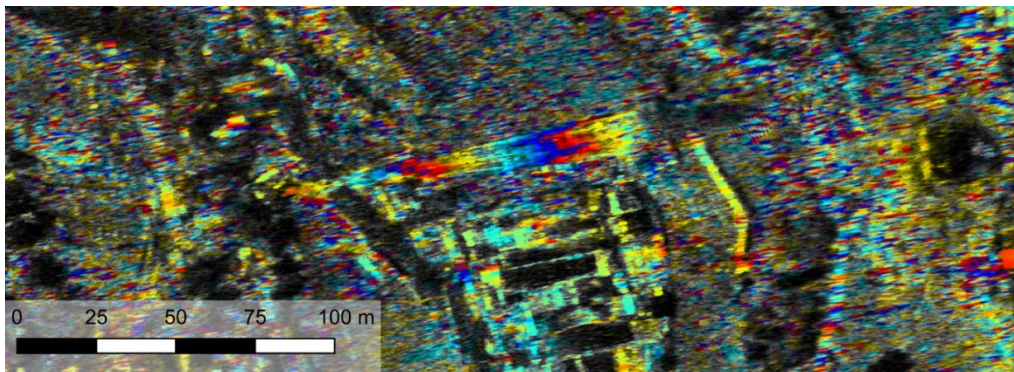


Figure 80: Dwellings potentially vulnerable to flooding based on TanDEM-X InSAR DEM  
Criteria for their selection:  $TWI > 5$  and  $VDN < 2$  m

### 3.2.4.4 Scientific conclusions and practice recommendations

This study showed how SAR interferometry can be used to generate topographic information at high spatial resolution. This information outperforms the freely available DEMs regarding spatial resolution and vertical accuracy for a more accurate flood assessment, if the following conditions are given:

- For **repeat-pass interferometry** (same sensor, different dates), the temporal baseline should be kept as short as possible. The repeat cycle of a sensor is the main limitation in this context. Furthermore, SAR images have to be acquired within the same orbit (flight path). Repeat cycles of currently active sensors which can be used for SAR interferometry are:
  - Sentinel-1 A/B: 6 days
  - TerraSAR-X: 11 days (in future: up to 4 days, with PAZ, see section 4.2.4)
  - ALOS-2: 14 days
  - COSMO SkyMed (+ Second Generation to be launched in late 2019): 16 days
  - RADARSAT-2: 24 days (in future: 12 days, under the RCM, see section 4.2.4)
  - Kompsat-5: 28 days
- As a consequence, the more vegetation present in the study area, the less reliable is the phase information due to **temporal decorrelation** (Figure 24b, Zebker & Villasenor 1992). Therefore, there is often a trade-off between spatial resolution and short repeat cycles.
- **Single-pass interferometry** (two sensors, same date) is less sensitive to temporal decorrelation because one sensor transmits the microwaves while the other receives the echo. However, phase information can still be subject to atmospheric disturbances. Consequently, acquisitions at without rainfall, snow or strong wind are recommended, which are more likely at nighttime (Hanssen 1998)
- For both methods, exact **orbit information** on the positions of the satellites is required to correctly derive the imaging geometry. When ordering SAR data, new taskings including precise orbit information often take a couple of days longer. This should be considered, especially in cases of emergencies.
- When selecting sensors, **perpendicular baselines** (Figure 24a) between 150 and 300 are most suitable for most terrains (Ferretti et al. 2007a).
- For **time-critical decisions**, the availability of already existing DEMs, such as AW3D (spatial resolution of 5 meters, Tadono et al. 2014) or TanDEM-X (12 meters, Zink et al. 2014) has to be checked. Factors to take into consideration are spatial coverage, temporal validity, acquisition costs, as well as horizontal and vertical accuracy.



*Figure 81: Interferogram at an antenna mast in the refugee camp of Kutupalong derived from two TerraSAR-X images at Staring Spotlight (ST) mode (background: backscatter intensity)*

### 3.3 Exploration of resources and environmental monitoring

#### 3.3.1 Current state of research and challenges

The use of SAR information for the observation of abiotic (water, minerals) and biotic (crops, animals, forests) resources is manifold. While groundwater-related applications mostly concentrate on the disclosure and description of geologic settings, the classification or quantification of vegetation and biophysical parameters is more diverse. Both will be briefly introduced in the following.

The potential of SAR imagery for geologic mapping has been demonstrated since the middle of the 1990s. Of vital importance was the SIR-C/X-SAR system on board of the Endeavour space shuttle in April and October 1994 which simultaneously acquired X-band, C-band, and L-band radar images (Jordan et al. 1995). The combination of wavelengths allowed different penetration depths in snow, vegetation, and soils thus enriching the information content of a single image. Equally significant was the discovery of subsurface features in arid environments, such as wadis, paleoclimatic structures, and organic deposits underlining the valuable contribution of this technique to geologic explorations (Abdelsalam & Stern 1996; Dabbagh et al. 1997; Schaber et al. 1997; Stern & Abdelsalam 1996). A large number of SAR-based studies followed, including mapping of geologic and geomorphologic structures (Abdelsalam et al. 2000; Argialas & Mavrantza 2000; Paradella et al. 2017; Saint-Jean et al. 2014), identifications of paleo drainages (Abdelsalam & El-Baz 2015; Paillou et al. 2009; Xinyuan et al. 2004), lineament extraction (Corgne et al. 2010; Filho & Rossetti 2012; Flores-Prieto et al. 2015; Koch & Mather 1997), and exploration of fossil fuels (Ezeoke & Tong 2012; Peña & Abdelsalam 2006; Singhroy et al. 2014).

While groundwater exploration is of general concern in many settings of displaced people, only a few studies directly address the use of radar in a humanitarian context. Bouchardy (2005) reports how images of ERS-1 and JERS-1 were used during the Darfur crisis to provide water to Sudanese refugees. Because of the penetration capabilities of the microwaves, hidden alluvial reservoirs were identified over large areas and locations for new boreholes within paleo-dunes were suggested based on correlation measures with existing drilling rigs. This study was able to assist the UNHCR with the selection of suitable sites for refugee camps which fulfill criteria of a sustainable water supply for both the refugees and the local population.

Wendt et al. (2015) provide a structured workflow for the hydrogeological assessment of groundwater potential for the drinking water supply in refugee camps. They give distinct recommendations for different aquifer systems and climate regimes to assist the generation of groundwater reconnaissance maps for humanitarian purposes.

The most complete overview on remote sensing applications to groundwater was compiled by Meijerink et al. (2007) who systematically demonstrated the use of different observation methods in a wide-ranging field of potential geologic settings. They also include a short chapter on radar remote sensing dealing with the information content of radar waves, lineament mapping, subsurface structures, terrain analysis, radar interferometry, and soil moisture.

As for natural resources, many studies exist which use radar for the identification, classification, and monitoring of vegetation or cropland. Popular approaches are based on polarimetric information, because of its capability to distinguish scattering mechanisms (sections 2.2.2 and 2.2.4) of different types of land cover (Khosravi et al. 2017; Kim et al. 2014; Qi et al. 2012; van Zyl & Kim 2011). In particular, polarimetric decompositions allowed the further refining and quantifying of the specifics of surface and volume scattering for systematic analysis of areas (Cloude & Pottier 1996; Lee et al. 1999; Touzi 2016). Interferometry-based approaches make use of the fact that temporal

decorrelation occurs at different rates in accordance with the surface characteristics of each area ('loss of coherence', Askne & Hagberg 1993, Engdahl et al. 2001, Antonova et al. 2016, Khalil 2017). Another popular application domain of SAR data is the quantitative derivation of vegetation parameters. It was found early that there is a linear relationship between backscatter intensity and above-ground biomass (AGB) generated by increased double-bounce and volume scattering effects (section 2.2.2) caused by stems of solid plants or from the branches in shrubs or the crowns of trees (Dobson et al. 1992; Le Toan et al. 1992). By collecting field measurements and relating them to the information provided in SAR images, manifold studies were published, ranging from boreal regions (Rignot et al. 1994; Suzuki et al. 2013), across temperate climates (Austin et al. 2003; Robinson et al. 2013), and on to tropical ecosystems (Luckman et al. 1997; Saatchi et al. 2011). Most of them agree that large wavelengths are more sensitive towards biomass (Ghasemi et al. 2011; Schmullius & Evans 1997), but also report a 'saturation effect' which leads to a flattening curve of the relationship between backscatter and AGB, often above 100 and 250 tons per hectare (Imhoff 1993; Joshi et al. 2017). This is overcome by the integration of polarimetric interferometric (PolInSAR) information (Lavallo et al. 2008; Neumann et al. 2011), LiDAR measurements (Hyde et al. 2007; Sun et al. 2011) or multi-frequency approaches (Englhart et al. 2011; Omar et al. 2017), as well as combinations of the aforementioned. Especially appropriate to mention is the work of Mitchard and Saatchi who investigated the use of SAR data for biomass estimates for the African continent in numerous studies (Mitchard & Flintrop 2013; Mitchard et al. 2011; Mitchard et al. 2012). They were one of the firsts to calibrate and prove the consistency of the relationship between biomass and backscatter intensity across various differing landscapes (Mitchard et al. 2009). In 2018, an AGB map for the entirety Africa at a spatial resolution of 25 meters was provided by Bouvet et al. (2018).

Information on biomass can substantially contribute to the management of resources and assistance of people in need, especially for the provision of firewood (Rivoal & Haselip 2017). However, while research focuses on the retrieval of biomass in forest ecosystems, arid or semi-arid climates with herbaceous ground layer and generally sparse vegetation cover are mainly neglected (Svoray & Shoshany 2010; Tian et al. 2017). But it is exactly in these climates where resources such as firewood are limited to people seeking help in refugee camps (Barbieri et al. 2017; Caniato et al. 2017) that this challenge has to be addressed in the future.

Throughout all applications, speckle also effects the investigation of landscapes and their dynamics, especially in traditional pixel-based change detection methods (Dekker 1998). This requires more elaborate techniques for the identification and quantification of changes, such as Markov Random Fields, which make use of predefined change probabilities (Hagensieker et al. 2017), Neural Networks (Gong et al. 2017; Gong et al. 2016), or fuzzy membership methods (Bi et al. 2014; Li et al. 2016).

Change detection studies in distinctively humanitarian context are rare:

Lodhi et al. 1998 describe the land cover changes near Afghan refugee camps in Pakistan based on optical Landsat TM images to assess the impact of the camps on forest resources. They found reasonable indications that the arrival of nearly 1.8 million refugees in the early 80s led to the clearance of pine forests for fuel wood and livestock forage, especially in Northern Pakistan. They were thereby able to objectively confirm the observations described by Allan (1987) who was one of the first to address environmental impacts of migration. Impact of the influx of more than 100,000 Rwandan refugees into the Ngora district in northwestern Tanzania was already subject to several studies based on optical sensors, starting from the deforestation at early stages until the dismantling of the camps in 2015 (Langer et al. 2015; Ndyeshumba 2000; Stängel et al. 2014).

Other studies on land-use change in conflict areas were presented by Stephens & Matson (1993) who monitored oil fires during the Persian Gulf war with low resolution AVHRR imagery. As another example, Thu & Populus (2007) investigated the effects of warfare using herbicides on mangrove forests during the Vietnam War based on SPOT imagery and GIS data. Eklund et al. (2017) demonstrated how agricultural land-use in Syria changed in areas occupied by the Islamic State and were able to detect patterns of intensification, abandonment and transition. More examples on war-related impacts on land-use changes based on multispectral imagery are given by Witmer & O'Loughlin (2009), Hagenlocher et al. (2012), Schöpfer et al. (2017), Hanson (2018) and Hassan et al. (2018). However, all mentioned studies use optical data while the benefits of SAR imagery in terms of archived data and information content are widely neglected. The only work currently on impact assessments of refugee camps upon their environment including the benefits of SAR imagery are presented by the author of this thesis (Braun & Hochschild 2015, 2017a; Braun et al. 2016b).

The following challenges regarding the monitoring of groundwater and environmental resources have to be addressed in a humanitarian context:

- Visual Interpretation of SAR images regarding geologic information and natural resources is hard for non-experts because of the **ambiguous information content** of radar backscatter. As multiple factors contribute to spatial and temporal backscatter variations, a-priori knowledge of an area is of advantage (Hess et al. 1990).
- When it comes to **groundwater**, different kinds of information and data sources have to be combined to identify suitable recharge conditions in a structured and integrated procedure.
- No fully automated approaches for the identification of groundwater resources exist, nor do they eliminate the need for geologic surveys in the field (Verjee & Gachet 2007).
- Many landscapes are not composed of isolated vegetation patches but rather of **gradual changes** in vegetation communities. This complicates the distinct classification of landcover classes and their monitoring (Franklin 1995). **Fuzzy methods** based on SAR-data have to be found.
- Instead of filtering **speckle** effects in SAR images, methods exploiting the degree of speckle for vegetation studies are required, instead of concentrating on its elimination (Nezry et al. 1995).
- Many studies exist for the derivation of biomass from radar imagery in forest ecosystems. While they already contribute to the allocation of resources, such as firewood, the application of SAR data in **low productivity areas**, such as grasslands, steppe or savannas where resources are generally scarce, are widely neglected.

### 3.3.2 Groundwater exploration (Kidal, Mali)

Note: Findings of this section are partly based on the project deliverable “Water supply in Kidal, Mali” by Burrows, Braun and Wendt (2017) compiled within the project EO4HumEn+. It is not publicly available but was provided to the International Committee of the Red Cross (ICRC) within the scope of the project. The contribution of all authors is listed in chapter 1.4.

#### 3.3.2.1 Background and aims

Kidal is a town and commune located in the northeast of Mali, as shown in Figure 82 (small map). It has an estimated population of around 15,000 inhabitants which is reported to have increased by 5,000 since 2010 (INSTAT 2013) as a consequence of the northern Mali conflict (Hoogeveen et al. 2017). The local people earn their livelihood from stock farming of sheep, goats and cattle (Cheng et al. 2017), trade and construction (Etang-Ndip et al. 2015). Because of the arid climate, agriculture of crops and vegetables is limited to the wadi areas and only of minor significance in this area (Butt et al. 2006). The region suffers from severe water scarcity as the rainy season lasts from June to September with an annual precipitation of 144 mm and a mean temperature of 36 °C, as reported for the 30-year average by the World Meteorological Organization (WMO, 2018). Evapotranspiration rates are accordingly high.

The groundwater sources in the study area were reported to produce 837 m<sup>3</sup> per day in 2010 (Hydro-R&D International & Proman 2011), and 466 m<sup>3</sup> per day in 2017 (Burrows et al. 2017). This is a decrease from 80 liters per day to 31 liters per day per person, accounting for a reduction of 60 %. As a consequence of the armed conflicts in the north of the country, the government departed from Kidal in May 2014, this administrative action included discontinuation of all technical services (Hoogeveen et al. 2017). Since then, the ICRC provides for the distribution of drinking water and the maintenance of the networks and generators.

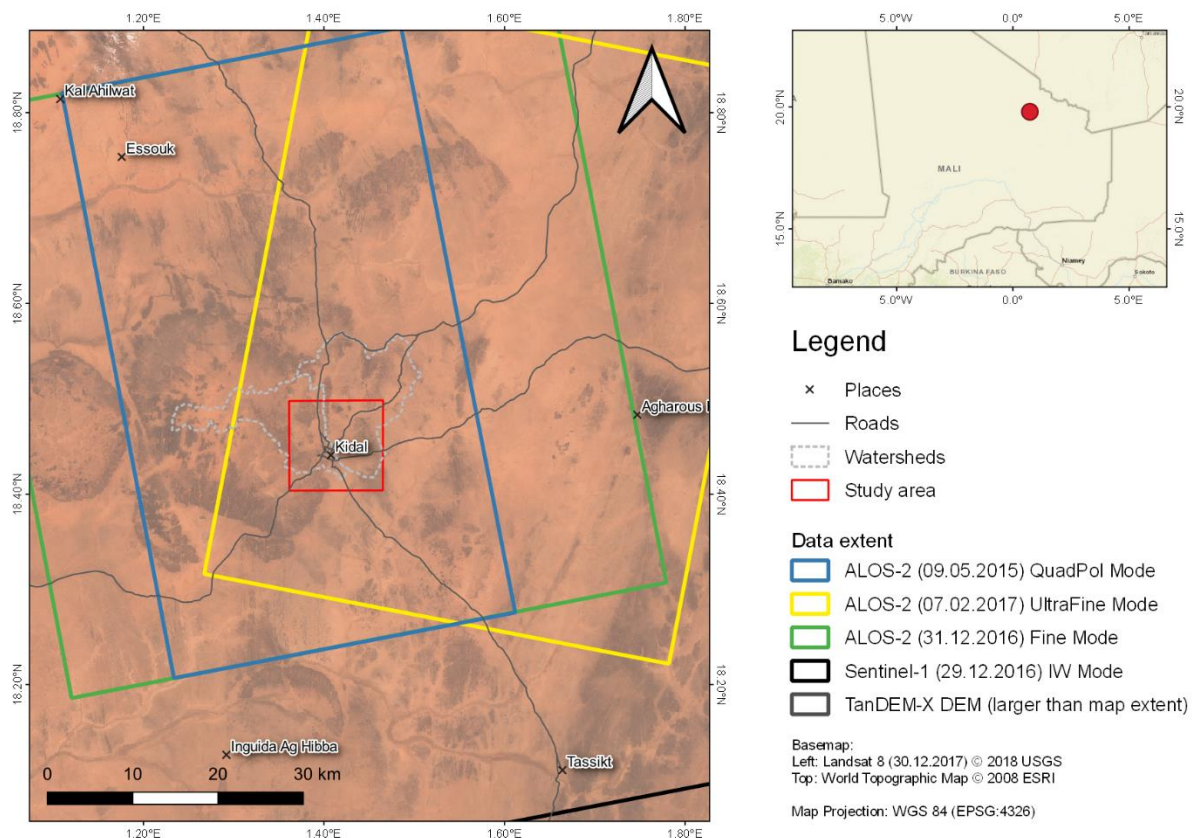


Figure 82: Study area for groundwater assessment in Mali

The decline in water production of the existing wells and boreholes combined with the lack of official water provision threaten the food security of the local population. The aim of this study was to suggest locations for the drilling of new groundwater extraction sites in the vicinity of the city.

This study demonstrates the use of SAR for the mapping of subsurface water. It has a strong practical component, but it follows the scientifically developed structure by Wendt, Braun et al. (2015) for the systematic approach on the exploration of drinking water supplies. An extended version of this approach is provided by Wendt, Braun et al. (2014). Figure 83 summarizes the most important steps for the derivation of information to suggest potential extraction sites for drinking water. If no surface water is present, as is the case in this study, landforms vegetation cover and geologic structures have to be mapped to progressively localize suitable locations for drillings. These lie within zones of water discharge, necessarily upstream of contaminants, outside of flood areas and are preferably near to the people in need. In porous aquifers, most promising locations are in coarsely-grained sediments which have the highest water storing potential. In fractured aquifers water bearing fractures or layer boundaries have to be identified (Wendt et al. 2015).

While some of the steps substantially benefit from the information in SAR imagery, others require expert-based interpretation and knowledge about local conditions. The contribution of radar information is demonstrated in the following.

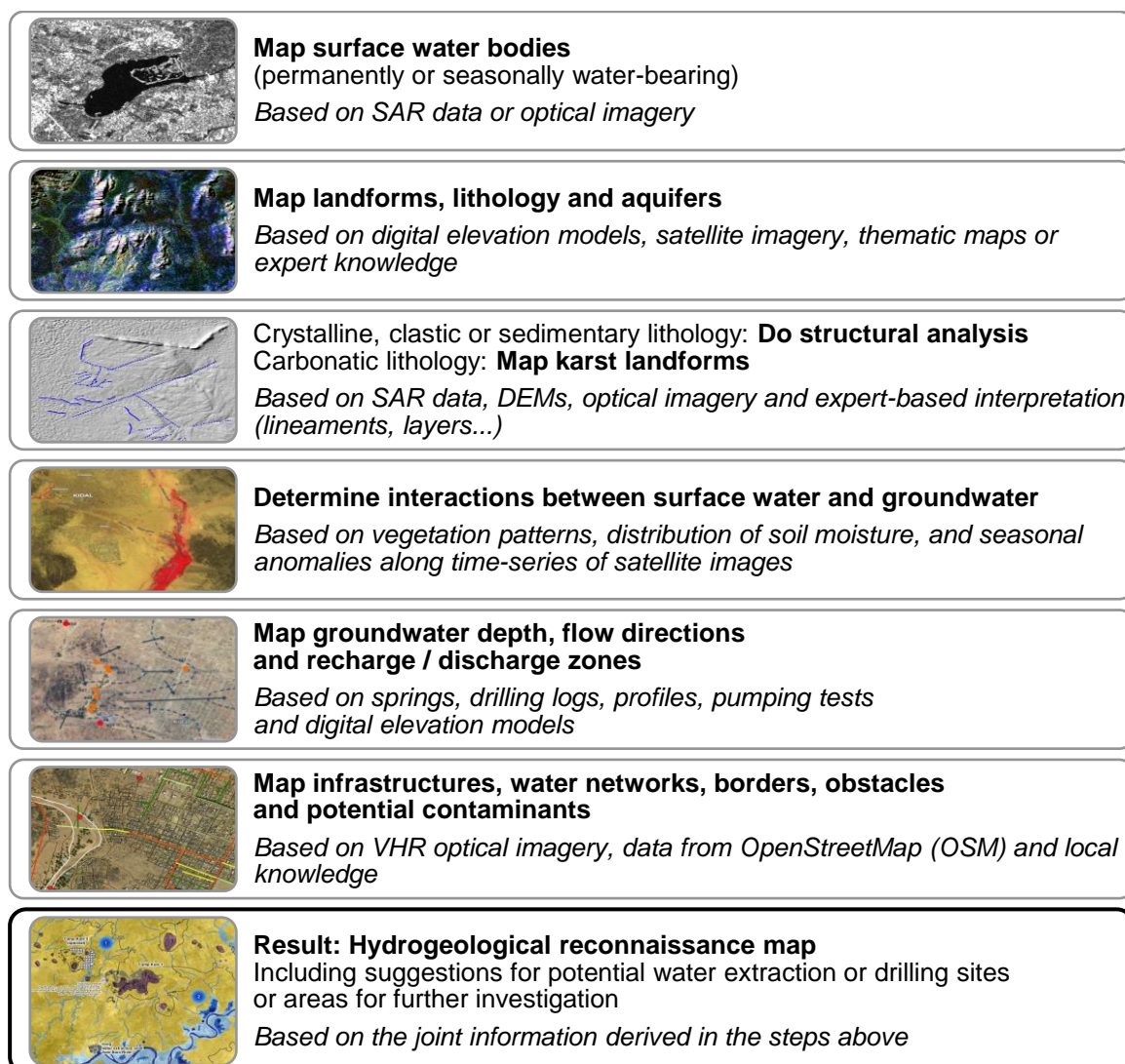


Figure 83: Work flow for the systematic derivation of potential water extraction sites  
Adapted from Wendt et al. (2014)

### 3.3.2.2 Data sources and processing

Kidal is situated in the Adrar des Ifoghas massif, a Precambrian basement rock terrain which is characterized by wide, shallow valleys and mostly granitic hills (Girard et al. 1998). As shown in Figure 84, the city lies at the border between two watersheds, each of them containing a wadi area in the middle. Two main aquifers can be distinguished in the study area: Firstly, metamorphic crystalline rocks of the basement geology which potentially store groundwater along fractures or faults in depths, Secondly, quaternary deposits cover the valleys along the two wadis (Buscaill & Caby 2004). These deposits formed from weathering of basement rock and are of high importance for groundwater exploration because of their permeability and water storage capacity.

Table 16 lists the different radar products used in this study. As they were taken by several sensors in various modes, polarizations and wavelengths (Table 32), they interact with different surface scattering mechanisms and reveal different levels of detail. The acquisition date did not play a significant role because almost no vegetation is present in the study area (Figure 82) and surface conditions are considered stable throughout the year. Besides the layers of the imaging radar systems, a digital elevation model derived from image pairs of TerraSAR-X and TanDEM-X collected between 2010 and 2015 (Wessel 2013) was used for the characterization of the surface landforms.

*Table 16: Radar information used for groundwater assessment in Mali*

Sensor	Mode (abbreviation), polarization	Acquisition date	Spatial resolution
ALOS-2	UltraFine Mode (SM1), HH	07.02.2017	3 m
ALOS-2	QuadPol Mode (SM2), HH+HV+VH+VV	09.05.2015	6 m
ALOS-2	Fine Mode (SM3), HH+HV	31.12.2016	10 m
Sentinel-1	Interferometric Mode (IW), VV+VH	29.12.2016	10 m
TanDEM-X	Digital Elevation Model	12.2010-10.2015	12.5 m

Besides the satellite data, locations of existing wells and boreholes were provided by Hydro-R&D International & Proman (2011) who conducted drillings and pumping tests to estimate depths and flow directions of groundwater and specific capacities of the existing boreholes. Additionally, the locations of micro dams (Forzieri et al. 2008) are known which were constructed across the wadis to use the sediments for water storage and access. The following findings were drawn from the tests, measurements, drillings and the report by Hydro-R&D International & Proman (2011):

- The wadi in the east is of wider extent but shallow, while the wadi in the west was found to be deeper (up to 25 meters). The latter is therefore of higher importance for groundwater storage because of its potential to retain water longer at the surface.
- Porosity in the wadi sediments was initially stated 10 %, but values between 20 and 35 % are more realistic in the study area (Forzieri et al. 2008).
- Discharge accumulates at the wadis' surfaces only after rainfall events as flashfloods which reach levels of up to 1 meter. The water then rapidly percolates, usually within 12 hours.
- Both aquifers are hydraulically interconnected, and the wadis recharge the basement aquifers.
- The groundwater table in the basement aquifer is very reactive to floods with a recharge period of two to three days and a rise of groundwater of 50 to 70 centimeters per flood period. During the year, overall levels naturally fluctuate by four to five meters.
- Based on the groundwater logs and the elevations of the surface retrieved by the DEM, groundwater depth could be approximated and coarsely interpolated (Figure 84). Findings supported the indication that the main direction of groundwater flow is towards the east. Therefore, the wadi running along the western edge of Kidal is the principal recharge area for the basement aquifers underneath.

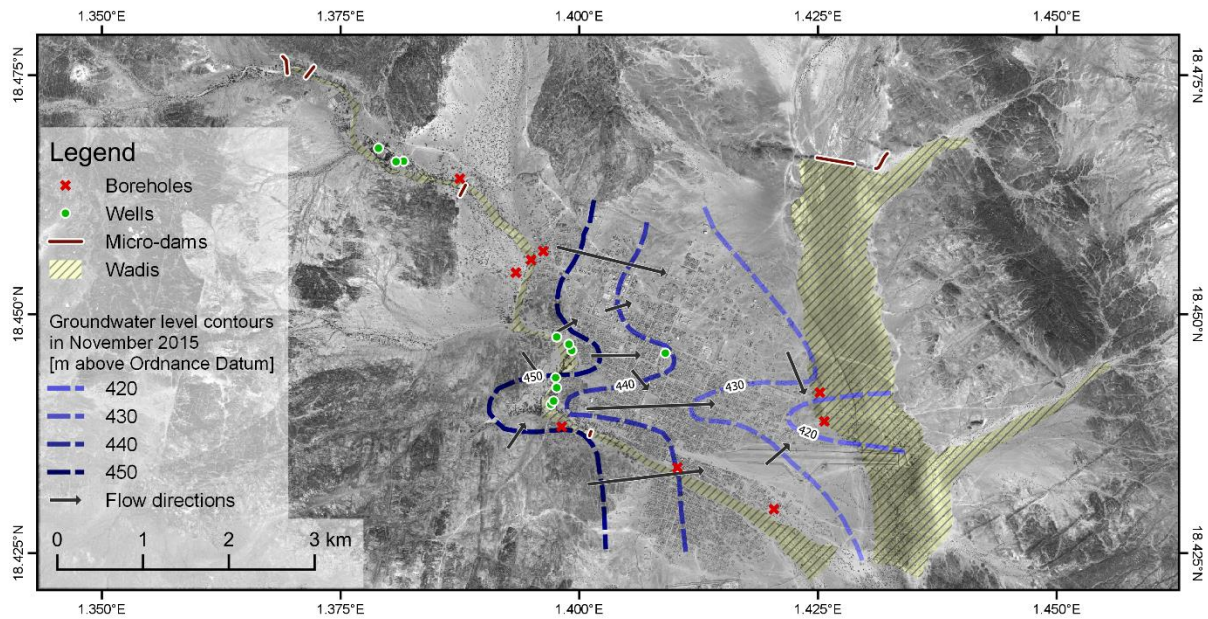


Figure 84: Data to assist groundwater exploration in Mali

As a demonstration of the contribution of radar information for geological mapping, dual-polarized data from ALOS-2 and Sentinel-1 which have the same spatial resolution of 10 meters were combined (L-band with HH+HV and C-band with VH and VV, see Table 16). Because they were not acquired at the same incidence angle and wavelength, they interact with different surfaces and may not be combined in a fully-polarimetric decomposition (van Zyl et al. 2008). But after proper calibration and terrain correction (chapter 2.3), they can still be combined to generate a RGB image, as demonstrated in Figure 85 (bottom). It combines information of Sentinel-1 VV (red), ALOS-2 HV (green) and ALOS-2 HH (blue) which is then compared to the geological map (Buscail & Caby 2004, Figure 85 middle) and an optical image of Landsat 8 (30.12.2017, Figure 85 top). As shown, the study area reveals only few structures in the visible spectrum. The information content of multispectral imagery can be substantially increased by the use of infra-red bands as shown in multiple studies (Grasso 1993; Ninomiya et al. 2005; van der Meer et al. 2012) but limitations regarding cloud cover remain. In turn, the microwave's capability to penetrate dry materials can be exploited best in arid environments with sparse vegetation cover, as is the case for Kidal.

Subsurface channels and vegetation-covered wadi areas are highlighted in blue because of the high penetration depth of ALOS-2 and the volume scattering from the subsurface grains. The granitic formations are displayed in red, purple and cyan as a result of their varying degree of conductivity and varying mineralogical composition. The quaternary deposits (white in the geological map) are mostly dark in the radar image because of their smooth surface and coarsely-grained sands which allow penetration of the L-band signal. The image shows how the fusion of radar information from different sensors can assist the interpretation and mapping of lithological units, the refinement of existing maps and the characterization of surface minerals and subsurface structures. Additionally, because of the large footprints of the dual-polarized modes of the sensors (Figure 82 and Table 32), this can be done for wide areas at a high resolution of 10 meters.

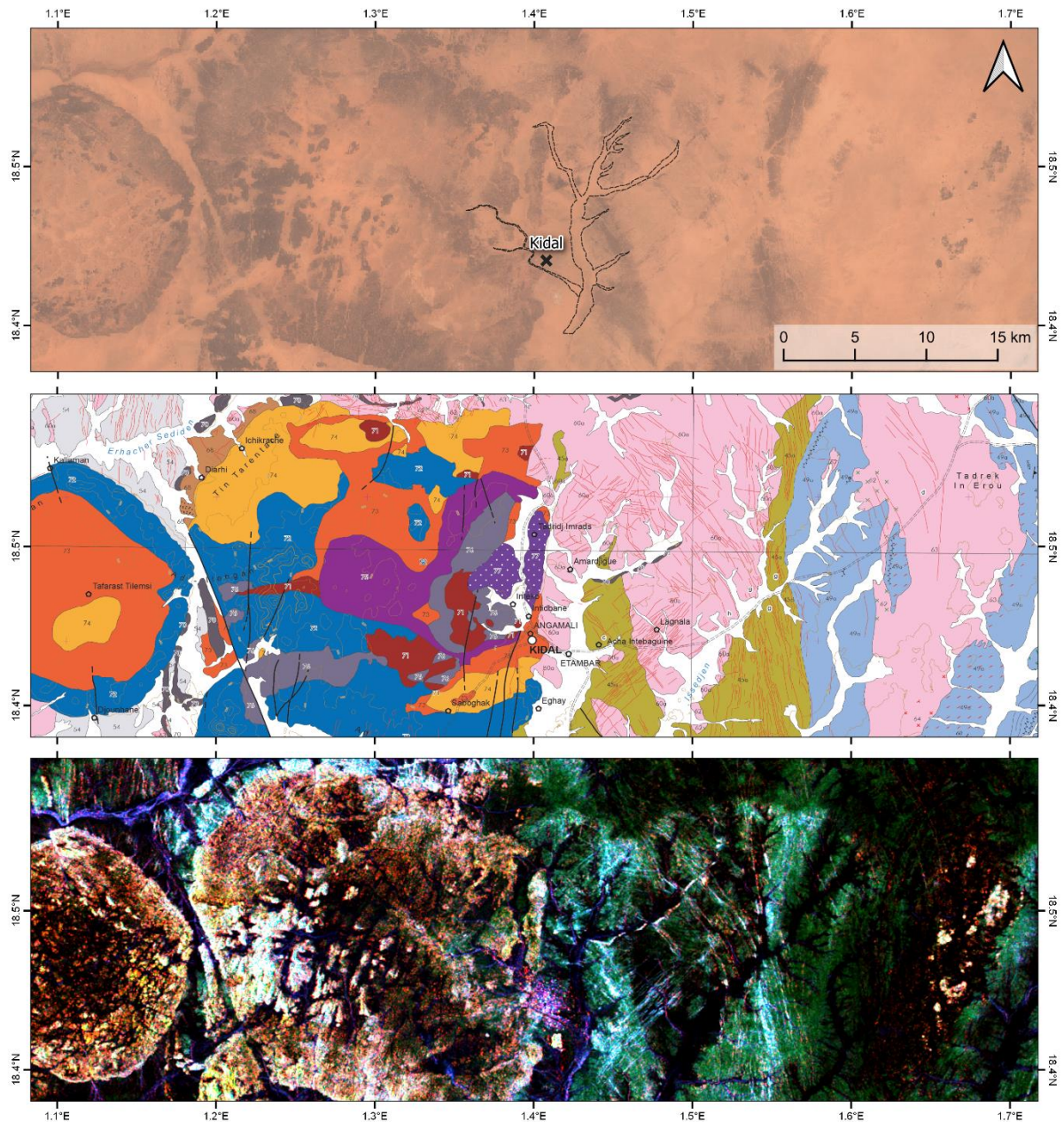


Figure 85: Geology of Kidal in optical image, geological map and SAR image

Top: Landsat 8 (showing city and wadis), middle: geological map, bottom: ALOS-2/Sentinel-1 RGB

While the different geologic units were nicely outlined in the fusion image, the wadis had a rather dark and indifferent signature and their exact outlines were not clearly shown at this spatial resolution. For this reason, fully-polarized ALOS-2 data was additionally used at a spatial resolution of 6 meters. Polarimetric SAR data is needed because many imaged surfaces on the earth's surface are subject to spatial and temporal dynamics. Depending on the pixel size, a single pixel may contain more than one object, making this imaged area a distributed target which partly polarizes the transmitted wave returning to the sensor (Deng et al. 2017). To analyze these distributed targets, second order moments are often used, such as the polarimetric coherency  $T$  (Lüneburg et al. 1991). This allows describing the analysis of different scattering mechanisms within one pixel as well as their contribution to the total signal (Lee & Pottier 2009). Its matrix representation is described in equation 20:

$$[T] = \begin{bmatrix} T_{11} & T_{12} & T_{13} \\ T_{21} & T_{22} & T_{23} \\ T_{31} & T_{32} & T_{33} \end{bmatrix} \quad (20)$$

$$= \frac{1}{2} \begin{bmatrix} |S_{HH} + S_{VV}|^2 & (S_{HH} + S_{VV})(S_{HH} - S_{VV}) * & 2(S_{HH} + S_{VV})S_{XX} * \\ (S_{HH} + S_{VV}) * (S_{HH} - S_{VV}) & |S_{HH} - S_{VV}|^2 & 2(S_{HH} - S_{VV})S_{XX} * \\ 2(S_{HH} + S_{VV})S_{XX} * & 2(S_{HH} - S_{VV})S_{XX} * & |4S_{XX}|^2 \end{bmatrix}$$

where  $S_{HH}$ , and  $S_{VV}$  represent the horizontally and vertically polarized components of the scattering matrix (equation 5) and  $S_{XX}$  represents the cross polarized components HV and VH which are considered symmetrically equal (Tragl 1990). The coherency matrix can be reduced to the diagonal entries of  $T_{11}$ ,  $T_{22}$  and  $T_{33}$  which represent surface scattering, double-bounce and volume scattering (Figure 18). Expressed as a Pauli vector (section 2.2.4), as described in equation 21, they can be used to create a RGB composite (Figure 85, bottom) and describe the various scattering mechanisms present in the image.

$$\underline{k}_{3P} = \frac{1}{\sqrt{2}} (S_{HH} + S_{VV}, S_{HH} - S_{VV}, S_{HV} + S_{VH}) \quad (21)$$

Because of their high importance for the provision of drinking water, the outlines of the wadis have to be known to make estimates on their contribution to groundwater recharge. Figure 86 shows how the coherency matrix image highlights the wadi areas at higher detail and reveals both subsurface structures and vegetation cover. The outlines were extracted by visual comparison. Additionally, the watershed boundaries were derived from the TanDEM-X data as described by Band (1986) and demonstrated by Schillaci, Braun and Kropáček (2012). Both elements are shown in Figure 86 and were used for the calculation of the groundwater storage capacity and potential recharge potential of the wadis, the derived areas of both wadis were 920,180 m<sup>2</sup> and 4,606,640 m<sup>2</sup> respectively.

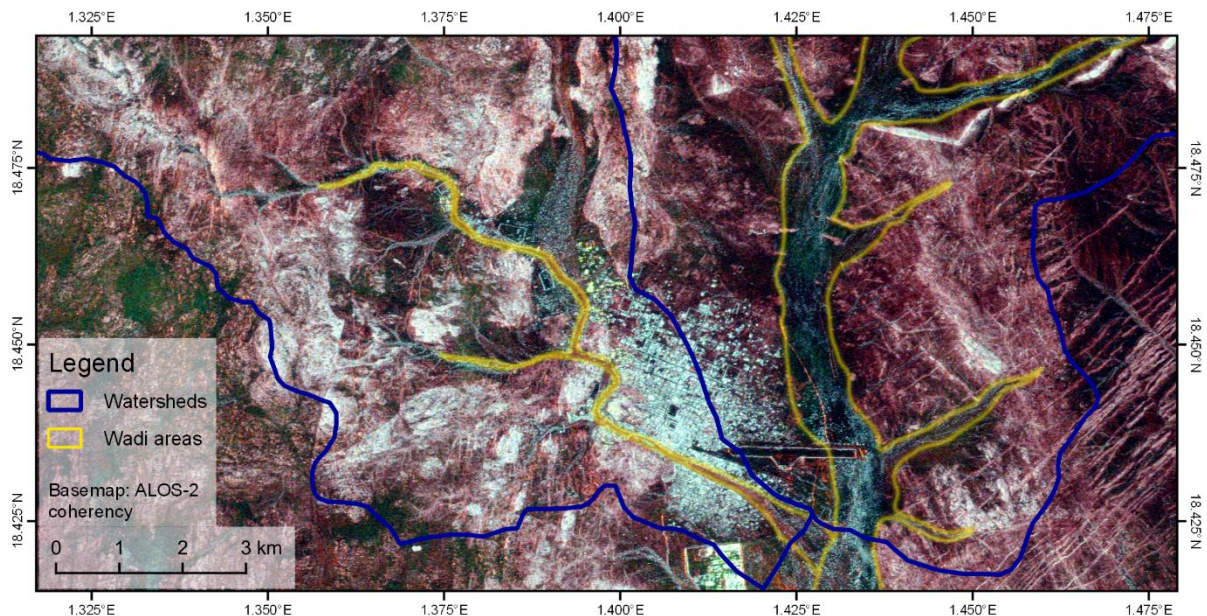


Figure 86: Wadis as shown in the ALOS-2 coherency matrix representation

The potential groundwater storage capacity  $c_{GW}$  of the wadi in the west was calculated as follows:

$$c_{GW} = a_w \cdot n \cdot t_0 \quad (22)$$

where  $a_w$  is the wadi area (920,180 m<sup>2</sup>),  $n$  is the porosity (20-35 %) and  $t_0$  is the thickness of the saturated sediments in the wadi (15-20 m), leading to an overall storage capacity between 2,760,540 m<sup>3</sup> and 6,441,260 m<sup>3</sup>.

The groundwater recharge potential  $r_{GW}$  can be derived from the wadi area  $a_w$ , the porosity  $n$  and the annual piezometric fluctuations  $\Delta_a$  (4 m) as demonstrated in equation 23, resulting in a recharge potential of 736,144 m<sup>3</sup> per year. This is only a crude estimation which does not incorporate further water withdrawal by subsurface flow away from the wadi and evapotranspiration, but this number is four times larger than the production reported for 2017 (466 m<sup>3</sup> per day, or 170,090 m<sup>3</sup> per year). Still, it suggests that the overall amount of water entering the wadi is larger than its withdrawal, although the abstraction rates at some few boreholes (F11 and F13) exceeded the recharge. This explains the decrease of production described in section 3.3.2.1, but also encourages the plans of searching more favorable drilling locations.

$$r_{GW} = a_w \cdot n \cdot \Delta_a \quad (23)$$

Vegetation patterns are often used as an indicator for the presence and accumulation of subsurface water (Bromley et al. 1997; Loheide & Gorelick 2007) and as indications on drillings or subsurface dams within the wadis (Forzieri et al. 2008). However, this would require dense time-series of quad-polarized data for the generation of multiple vegetation maps as shown in Figure 86, especially within one year to describe seasonal dynamics. As these were not available, linear structures were additionally mapped based on the DEM. This is because linear structures often indicate fractures in the crystalline basement and lead to groundwater transportation and storage (Koch & Mather 1997; Sander 2007).

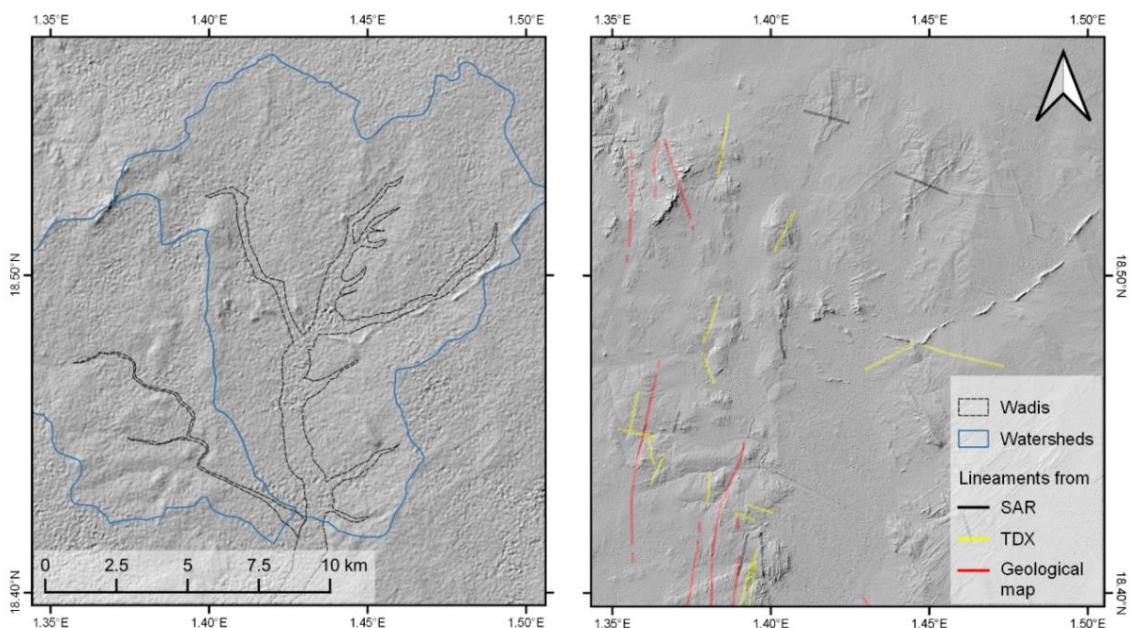


Figure 87: Hillshading of SRTM (30 m, left) and TanDEM-X (12.5 m, right) with detected lineaments

As shown in Figure 87, the freely available SRTM data does not reveal much detail about the study area for two reasons: The spatial resolution of 30 meters is too low to detect fine structures, and secondly, the SRTM data was generated based on a C-band radar mission, which potentially stronger penetrates into dry bodies. This explains the granular pattern of the hillshade generated by SRTM. In turn, the TanDEM-X mission operates at a shorter wavelength which lacks these penetration capabilities and is therefore more suitable to describe the actual surfaces. Additionally, the spatial resolution of 12.5 meters reveals finer structures.

Figure 87 shows the lineaments detected based on the elevation (yellow) and SAR data (black). It is notable that more structures were identified than mentioned in the geological map (red). Besides that, lineaments found in the ALOS-2 quad-polarized data are predominantly oriented in northwest-southeast direction. This can be explained by the look direction of the sensor (Figure 82) which is predominantly sensitive to lineaments along the azimuth direction. In turn, structures which range perpendicular to the look direction of a SAR sensor are often missed (Corgne et al. 2010). Lastly, the combination of elevation data, SAR images and existing maps resulted in an adequate description of structural features in the study area.

### 3.3.2.3 Recommendations and discussion

Based on the spatial extent of the wadis, the distribution and directions of lineaments and the coarse calculations on groundwater storage capacity and recharge, a set of recommendations was formulated by Burrows, Braun and Wendt (2017). Along with suggestions for new drilling sites, the most important aspect was the establishment of a monitoring program which was ceased during the Northern Mali conflict in 2011 (Hydro-R&D International & Proman 2012). Reviving this program requires sustainable conditions, such as defining clear responsibilities of the persons involved, open data storage and access for all involved persons and engagement of the government to guarantee long term success. Monitored resources are groundwater levels, abstraction rates and water quality as well as rainfall measurements. These could substantially improve the knowledge of the hydrogeological conditions in the study area for a sustainable provision of water to the local population.

To cover the short-term need for drinking water, suggestions for two new drilling sites were made under the precondition that they should not be in close proximity to existing wells or boreholes. This is because the new boreholes would simply drill into the same aquifer and existing water resources would be used up more quickly, thus intensifying the current water scarcity. The two selected sites are shown in Figure 88.

Site 1 lies approximately five kilometers upstream of the wadi in the northwest of the city of Kidal (13.653° N, 18.4757° E). At this location, a regional fault structure intersects the wadi which is expected to be deeper than the one in the east. The structure strikes north-northeast and can be clearly identified in the TanDEM-X hillshading (Figure 87) and the radar images because the granitic ridges north and south of the wadi form a clear line which might have been shaped by erosion as a cause of uplift along the fault. Two subsurface dams are constructed downstream of this point which additionally assist the accumulation of water and groundwater recharge at this location.

Site 2 lies approximately four kilometers southeast of Kidal where a large linear structure intersects the wadi in the east (14.29600° N, 18.4043° E). Clearly visible in the elevation data and the radar images, the basaltic intrusions are cut by this structure, confirming its large depth and geologic age. Additionally, a road crosses the wadi at this location which can potentially block or slow down subsurface water movement and lead to increased recharge of the basement aquifer.

It is recommended that a geophysical survey be conducted at both locations before a borehole is drilled to precisely identify the locations where the geological structures intersect the sediment bodies of the wadis and to get a more precise understanding of their thickness. This can be achieved by measuring electrical resistivity along transects perpendicular to the linear structures and perpendicular to the wadis.

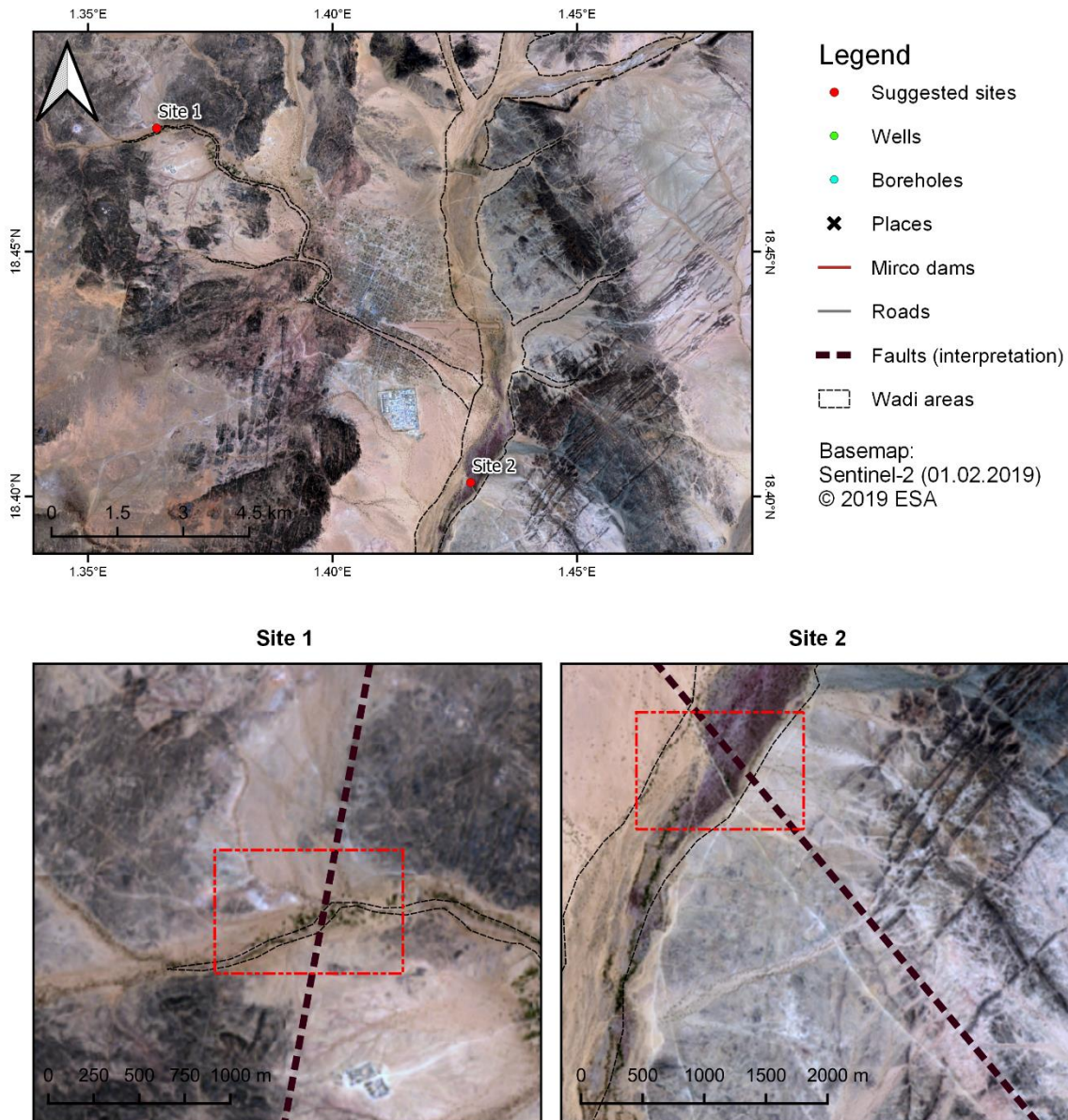


Figure 88: Suggested sites for groundwater drilling

This study showed how information derived from SAR images can contribute to the exploration of groundwater resources. At the time of completion of this thesis, no response was available to confirm if drillings have been realized and if their water production was satisfactory. It can, however, be stated that the selection of the two sites was conducted with highest care and based on the most appropriate data available.

Still, there are some points to discuss: Firstly, the generation of groundwater contours (Figure 84) was subject to various uncertainties, mainly the measurements of groundwater levels. These were

taken at unknown reference points and probably not referring to a common datum. Furthermore, the dates of water level measurements might be different throughout the study area. As no protocol is available for the pumping tests, it is not clear how long after the pumping that the water levels were assessed. As a consequence, the groundwater contours were generated at a comparably coarse interval of 10 meters.

To improve the estimates on groundwater flow, a more regular distribution of boreholes is needed as is a standardized procedure for the pumping tests. Furthermore, the estimates on groundwater storage capacity and potential recharge can be refined by a better knowledge of the wadis' horizontal profiles. These could be estimated using Vertical Electrical Sounding (VES, Smith et al. 1997) as suggested above.

Another crucial point is the availability of geologic maps. Although they are mostly generated for larger areas and therefore not revealing geologic information at the local scale, they still give an important overview of the overall fault and fracture system in areas with crystalline basement rocks. These substantially help to search for finer patterns in the SAR images or digital elevation models. Knowledge about the main direction of faults was important in this study area because one main challenge was to distinguish the many dykes and basaltic intrusions (Figure 86, left to the eastern wadi) from actual fractures because they are not indicators for groundwater flow in the crystalline basement. For this reason, expert knowledge is required to interpret the results from the geologic maps and the digital images.

As for the use of SAR images to detect lineaments, it is important to consider the look direction of the radar system and its incidence angle because structures perpendicular to the flight direction are hardly visible. If little is known about the study area, the integration images of both ascending and descending orbits is advisable (Koch & Mather 1997; Paradella et al. 2014).

#### 3.3.2.4 Scientific conclusions and practice recommendations

Many studies exist which show the benefits of SAR data for groundwater exploration (section 3.3.1). This study showed an example of how this can lead to well-grounded recommendations on drilling. The following remarks can be made for applications in a humanitarian context.

- The **penetration depth** of microwaves is limited to the first 20 centimeters, given that the surfaces are dry and not covered by vegetation. Identification of the groundwater itself from images is impossible, but indications for its presence can be systematically collected.
- SAR data can assist groundwater exploration in various ways (lineaments, vegetation patterns, soil moisture, DEM generation from InSAR image pairs) but **additional data** is always required to put the findings into a context. Generally, a large variety of different data sources compiled and combined within a digital environment is the best base for successful mapping. Whitmeyer et al. (2010) conclude that a working knowledge of GIS and digital field methods is “no longer a luxury, but rather a necessary skill”.
- **Field measurements** substantially increase the chance that correct assumptions are drawn based on the indications retrieved from the data. Detection of groundwater without field expertise is nearly impossible.
- When searching for **lineaments**, scenes of multiple orbits, angles and sensors should be combined to reduce the risk of overlooking structures caused by the imaging geometry.
- The **degree of automation** is comparably low because local geologic settings can be extremely complex and cannot be compared between different study areas. Therefore, data analysts, relief workers and hydrogeologic experts should work together. For a **sustainable retrieval**, involvement of local or regional authorities is favorable.

### 3.3.3 Environmental impact assessment (Djabal, Chad)

Note: Some figures of this section are taken from Braun & Hochschild (2017a) which was published as an open access article distributed under the Creative Commons Attribution License which permits unrestricted use, distribution, and reproduction in any medium, provided the original work is properly cited (CC BY 4.0). The reader is advised to consult this publication for a more detailed description of this study. The contribution of each author is listed in chapter 1.4. A similar study based on ERS data was conducted for the area of Dadaab (Braun et al. 2016b).

#### 3.3.3.1 Background and aims

Djabal is a refugee camp in the center Sila region, eastern Chad (Figure 89, top left). It was selected as a case study for several reasons: It is located at the southern border of the Sahel zone where resources are generally limited and monitoring the impacts of climate change is a major concern (Rishmawi & Prince 2016). The savanna landscapes in this area were observed to respond indifferently towards season creep and also show different degrees of persistence (Southworth et al. 2014). Besides that, camp Djabal has been in existence since 2004, which allows a long-term investigation of impacts on its surroundings. It was opened as one of many camps along the Sudanese border to host refugees seeking shelter from the violent conflicts of the Darfur crisis (Bouchardy 2005).

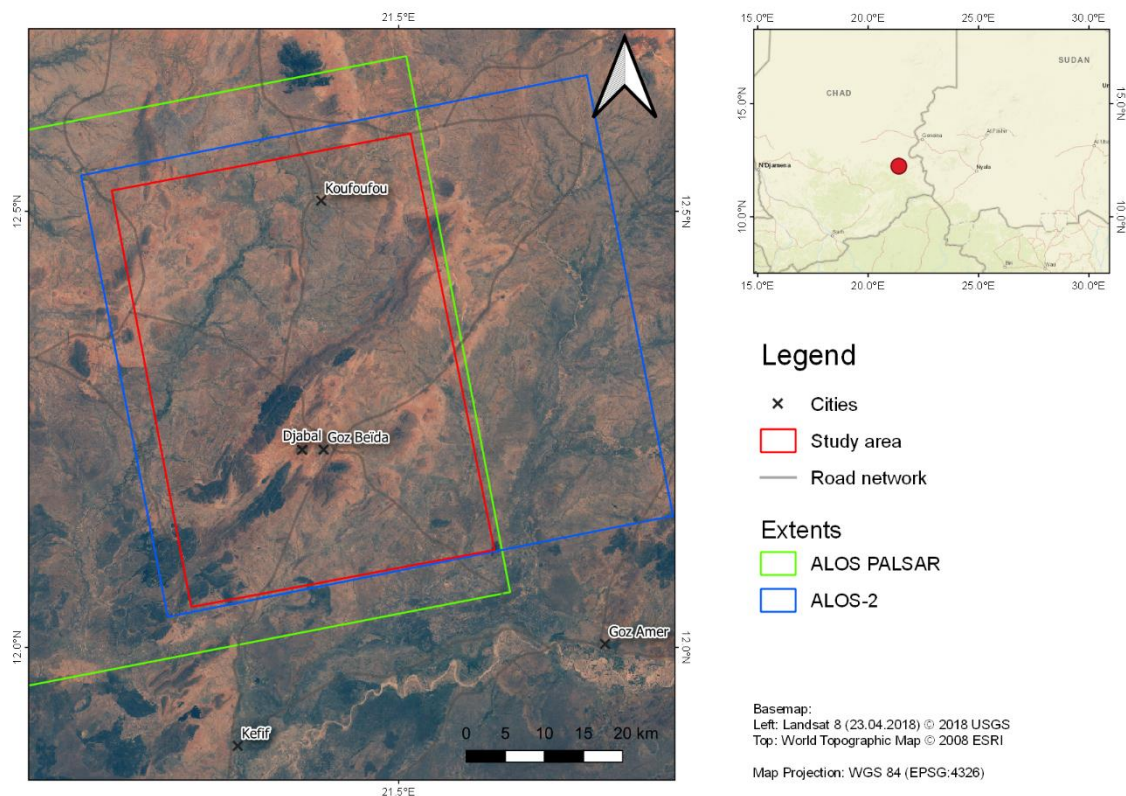


Figure 89: Study area for the environmental impact assessment in Chad

Djabal lies in direct proximity to the town of Goz Beïda and is located along an important transport route of eastern Chad which connects the larger cities in the north (Fada) with those in the south of the country. Both cities are enclosed from the south to the northwest by the Hadjer Arkop massif which is sparsely covered with smaller trees (Figure 89, main map). As a result of climatic constraints, most of the region is covered by edaphic grasslands and small cultivated fields encompassing roughly one third of the area. One exception is Wadi Auada which ranges from west to north in the study area (Figure 89, red line) having smaller semi-deciduous riparian forests.

The climate can be described as hot and semi-arid with a pronounced seasonality. Most of the 600 mm of precipitation are concentrated in the rainy season between June and September, while the rest of the year is highly arid (Harris et al. 2014). Despite the fact that the area is often affected by droughts, semi-permanent agriculture is possible on suitable ground (Middleton & Thomas 1997).

This study presents an innovative approach on the quantification of changes in this semi-arid landscape based on SAR imagery during a ten-year observation period to detect a decrease or increase of resources, both as a general trend and near the human settlements. It furthermore considers the ecological and socio-economic value of different types of land-use and land cover, and proposes a suitable visualization of both the severity and the variability of these changes.

### 3.3.3.2 Data sources and pre-processing

All radar data used in this study was acquired during the dry season (November until March) in order to reduce the effects of soil moisture and phenologic variations on backscatter intensity. Data from the ALOS missions was used as it operates at L-band which is more sensitive to vegetation structures (section 3.3.1). Furthermore, optical imagery of the Landsat mission was used for the collection of reference data. As shown in Table 17, for each radar image an optical image has been selected with a maximum temporal difference ( $\Delta t$ ) of 30 days. Because of the failure of ALOS PALSAR in 2011, there is a gap of three years without usable imagery.

All radar data was radiometrically calibrated and terrain corrected as demonstrated in sections 2.3.1 and 2.3.3. No filtering was applied to the images, as it is recommended by Collins et al. (2000), in order to preserve the texture which present in the images (Figure 19). 25 textures layers were extracted from the radar images based on the concept of grey-level co-occurrence matrix (GLCM, Haralick et al. 1973), including Cluster Prominence, Cluster Shade, Correlation, Difference Of Entropies, Difference Of Variances, Energy, Entropy, Grey-Level Nonuniformity, HT10, Haralick Correlation, High Grey-Level Run Emphasis, IC1, IC2, Inertia, Inverse Difference Moment, Long Run Low Grey-Level Emphasis, Low Grey-Level Run Emphasis, Mean, Run Length Non-uniformity, Run Percentage, Short Run High Grey-Level Emphasis, Short Run Low Grey-Level Emphasis, Sum Entropy, Sum Variance, and Variance. These textures were calculated with kernels of 3, 9, and 15 pixels to emphasize patterns emerging at different spatial scales, leading to a total of 75 SAR texture layers per analyzed year. Landsat images were radiometrically calibrated to top-of-atmosphere reflectance (TOA) as proposed by Chander et al. (2009).

*Table 17: Satellite data used for the environmental impact assessment in Chad*

Year / $\Delta t$	Date	Sensor
2007 / 18 days	24 December 2006	ALOS PALSAR
	11 January 2007	Landsat ETM+
2008 / 2 days	27 December 2007	ALOS PALSAR
	29 December 2007	Landsat ETM+
2009 / 18 days	29 December 2008	ALOS PALSAR
	16 January 2009	Landsat ETM+
2010 / 30 days	2 December 2009	Landsat ETM+
	1 January 2010	ALOS PALSAR
2011 / 20 days	19 February 2011	ALOS PALSAR
	11 March 2011	Landsat ETM+
2015 / 0 days	23 January 2015	ALOS-2
	23 January 2015	Landsat OLI/TIRS
2016 / 6 days	22 January 2016	ALOS-2
	28 January 2016	Landsat OLI/TIRS
2017 / 15 days	2 March 2017	ALOS-2
	15 February 2017	Landsat OLI/TIRS

### 3.3.3.3 Image classification

The 75 SAR layers served as a feature space for a supervised classification of land-use and land cover (LULC) based on the random forest classifier (Breiman 2001). This method has its origins in machine learning and repeatedly takes random subsets of the input datasets (here: 22 of the 75 image textures) and sample areas (Figure 90) and uses them for multiple training cycles (here: 500 iterations) where thresholds in the training data are identified which describe the target classes (Table 18) best. The result of these iterations is a classifier which makes use of the most suitable and robust thresholds. It is furthermore able to process training data of different units and value ranges, which makes it suitable for the processing of textural features.

To reduce the degree of subjectivity and to increase the potential for operationalization, the sample areas used for training the classifier were automatically detected based on literature values. Only areas which fulfilled the criteria defined in Table 18 throughout all eight Landsat images were taken. This grants that only areas which represent the corresponding class are used for training. Only the samples for urban areas were manually digitized.

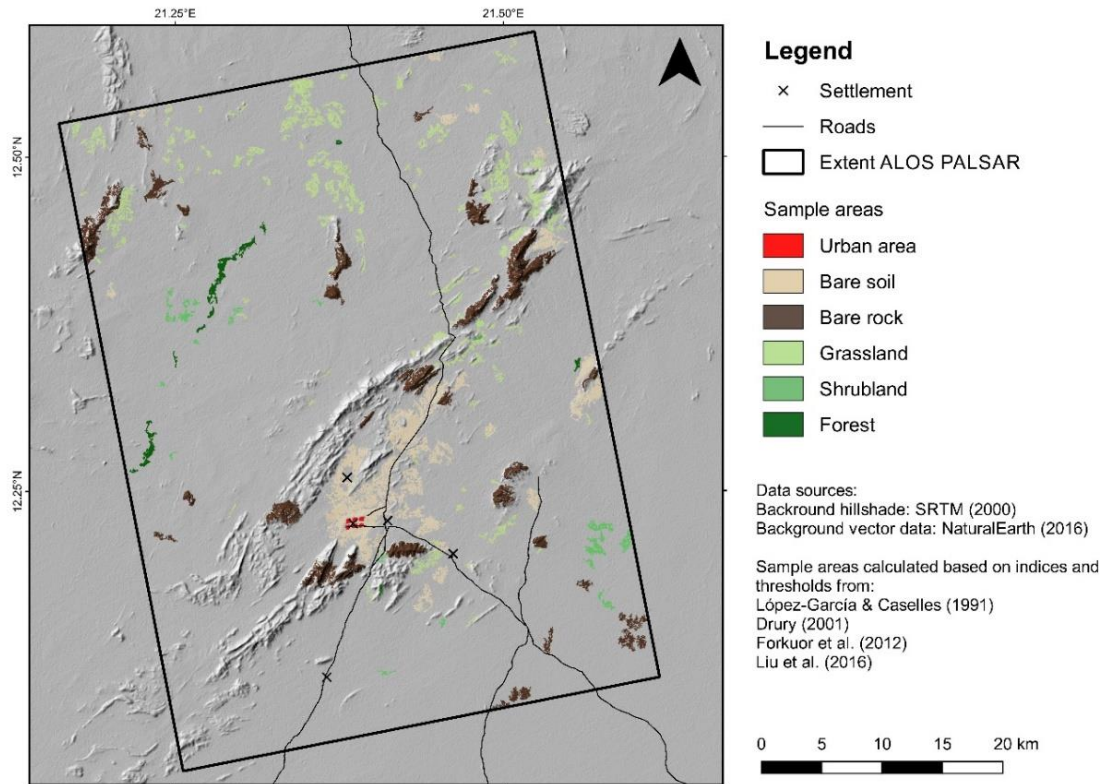


Figure 90: Automatically selected training areas for the environmental impact assessment in Chad

Table 18: Target classes and criteria of training areas for impact assessment in Chad

Class	Samples	Criterion	Source
Urban area	161 (7.2 %)	Area of the camp in 2007	-
Bare soil	390 (17.6 %)	Red < 0.25 & SWIR1 > 0.35	Drury (2001)
Bare rock	352 (15.9 %)	SWIR1/SWIR2 > 1.5	Drury (2001)
Grassland	374 (15.6 %)	NDVI > 0.15 & NDVI < 0.25	Forkuor et al. (2012)
Shrubland	126 (5.6 %)	Red < 0.2 & NIR > 0.3 & SWIR < 0.3	Liu et al. (2016)
Forest	172 (7.8 %)	NDVI > 0.2	Forkuor et al. (2012)
Burnt areas	0 (0 %)	NBR > 0.15	López-García & Caselles (1991)

To test the classification accuracy, 150 validation points per class were manually collected based on the Landsat imagery. Table 19 shows the user's accuracy (reliability) of the different target classes, as well as the overall accuracy (quality of the land-use and land cover map) and the Kappa coefficient (Viera & Garrett 2005). It shows that forests and shrubland have generally lower accuracies than urban areas or non-vegetated areas, for example. These errors, however result from the granular pattern of the classified maps (indicated in Figure 92, left side) which is typical for pixel-based classifications of SAR images (Dekker 2003). For this reason, an index had to be found which aggregates the LULC classifications at a larger spatial scale for a well-grounded detection and evaluation of changes.

Table 19: Accuracy Assessment for the environmental impact assessment in Chad

		2007	2008	2009	2010	2011	2015	2016	2017
User's accuracy	Urban area	100.0 %	100.0 %	100.0 %	100.0 %	98.5 %	99.2 %	100.0 %	100.0 %
	Bare soil	82.6 %	84.5 %	84.7 %	85.4 %	82.1 %	76.1 %	79.3 %	82.5 %
	Bare rock	97.3 %	95.3 %	99.3 %	97.2 %	94.1 %	95.9 %	94.0 %	95.9 %
	Grassland	63.1 %	61.4 %	64.6 %	62.8 %	64.7 %	57.8 %	59.3 %	57.6 %
	Shrubland	83.7 %	84.8 %	85.7 %	82.3 %	82.5 %	80.5 %	80.5 %	78.4 %
	Forest	89.8 %	82.3 %	90.6 %	92.9 %	89.7 %	84.2 %	93.2 %	87.3 %
	<b>Overall accuracy</b>	<b>84.4 %</b>	<b>83.3 %</b>	<b>85.7 %</b>	<b>85.0 %</b>	<b>84.0 %</b>	<b>80.3 %</b>	<b>82.3 %</b>	<b>81.4 %</b>
	Kappa	0.81	0.80	0.83	0.81	0.81	0.76	0.78	0.77

### 3.3.3.4 Development of an index for environmental impact

As explained above, pixel-based change detections of SAR imagery can lead to false conclusions in cases when single wrongly classified pixels appear as changes in land cover of areas which did not undergo any changes. Furthermore, the simple description of transitions from one class into another does not allow for implications on the severity of these changes and their consequences for the environment. For this reason, an index for natural resource depletion was developed by Hagenlocher et al. (2012) which aggregates LULC classes at a coarser scale and integrates expert-based weights for a distinct and clear representation of the real impact of changes in a study area. It was originally designed for VHR optical imagery but in this study adapted for radar data.

In a first step, interviews are conducted with experts to retrieve weights of each LULC class in respect to its environmental integrity (EnvInt) and human security (HumSec) in the study area. Two regional experts from the humanitarian domain with ecological background were interviewed to derive the index values of natural resources (NR) as shown in Table 20. Because our study focuses on the human-induced aspects of landscape, a ratio of 0.35/0.65 was used for the calculation of NR to place emphasis on the socio-economic impacts in the study area.

Table 20: Importance of selected LULC classes for the study area in eastern Chad

Class	EnvInt 35 %	HumSec 65 %	NR 100 %
Urban area	0.00	0.50	0.313
Bare soil	0.30	0.35	0.331
Bare rock	0.20	0.25	0.231
Grassland	0.50	0.45	0.469
Shrubland	0.70	0.75	0.731
Forest	0.95	0.90	0.919

Subsequently, a NR value is calculated for a hexagon grid with a diameter of one kilometer according to the composition of LULC classes in the covered area and their corresponding weights. The resulting value can then directly be interpreted as a percentage of resource depletion. An example of a grid cell including an increasing urban area surrounded by bare soil and shrubland is given in Figure 91. It shows that, caused by the loss of shrubland, the NR value decreases from 0.609 to 0.528, which results in an overall weighted natural resource depletion (NRD<sub>w</sub>) of -8.2%.

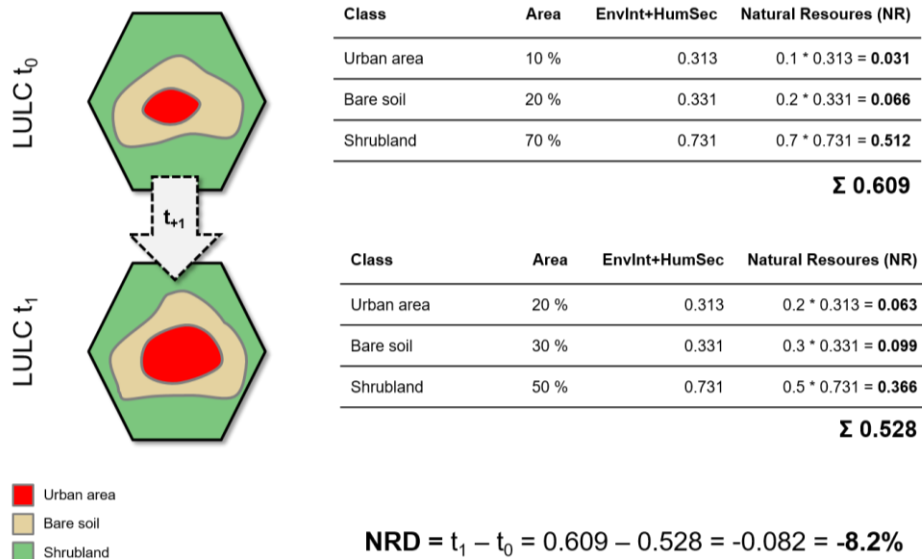


Figure 91: Calculation of the weighted Natural Resource Depletion (NRD<sub>w</sub>) Index

Figure 92 demonstrates the changes between 2007 and 2008 as an example. It shows that negative changes concentrate at three hot spots in the southeast, southwest and northwest while large parts of the study area remain comparably stable. The southern parts of Wadi Auada show a positive development for the given period.

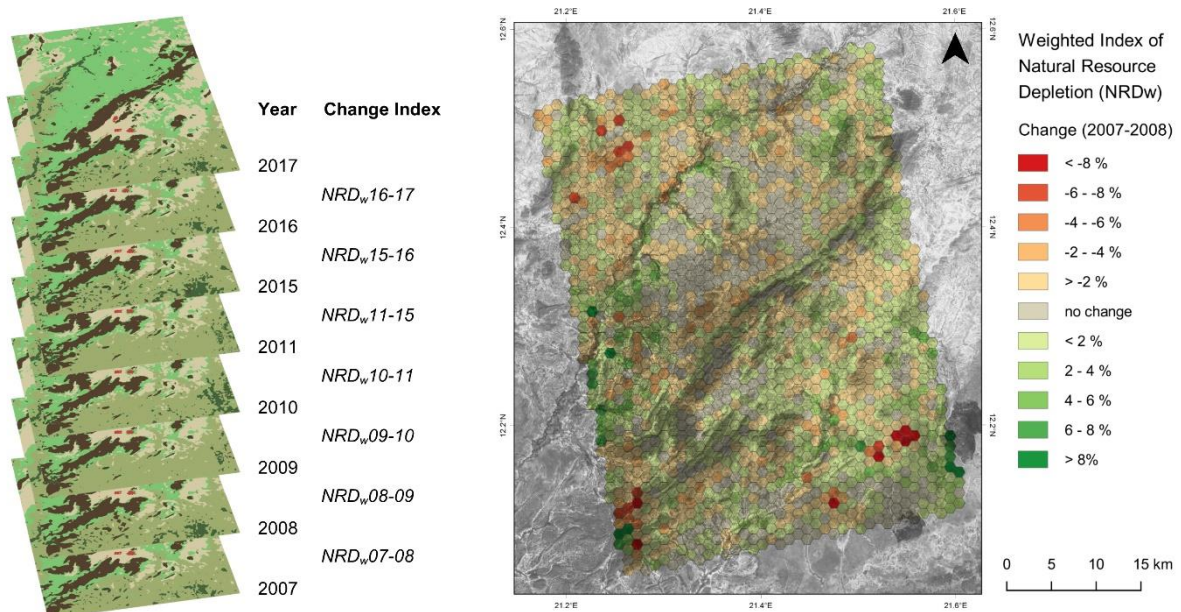


Figure 92: Resulting map of weighted Natural Resource Depletion (NRD<sub>w</sub>)

Simply comparing the start and end point of the acquired data would certainly miss one major point: Savannas show a high degree of biotic and abiotic variation at different spatial scales (Pickett et al. 2003). Additionally, the selection of the images is highly sensitive to smaller variations in phenology. This means that the sum of all changes within a given time should also be investigated and communicated.

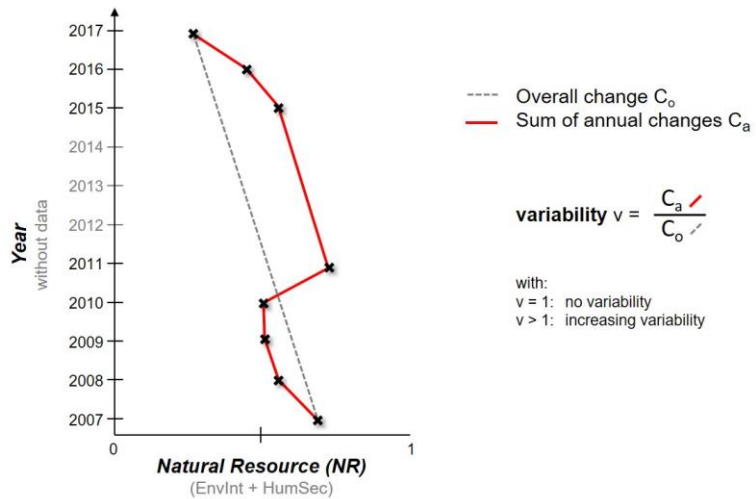


Figure 93: Calculation of the variability  $v$  of a grid cell

Therefore, a vector-based change detection was developed which includes both the overall change between the first and the last observation as well as the sum of all changes along this time-series. Here, variability  $v$  is defined as the ratio between the overall change  $C_o$  and the sum of annual changes  $C_a$  (Figure 93). If no changes happened in a grid cell besides the overall changes, it takes the value of 1. The more it exceeds this value, the larger is the variation of LULC classes within this cell during the investigated period. It consequently ranges between 1 and 7, which is the sum of maximum change ( $100\% \triangleq \text{NRDw} = \pm 1$ ) for all seven investigated years.

### 3.3.3.5 Results and discussion

Table 21 summarizes the statistical evaluation of all 1739 hexagon grid cells over the investigated period. Neither the mean ( $\text{NR}_{\text{mean}}$ ) nor the median ( $\text{NR}_{\text{median}}$ ) of natural resources in the study area show significant trends. The year 2015 seems to be the one with minimal natural resources, shown by the lowest  $\text{NR}_{\text{median}}$  and sum ( $\text{NR}_{\text{sum}}$ ), at least at the time of image acquisition. Largest resource depletion ( $\text{NRDw}_{\text{mean}} = -0.421\%$ ) can be observed for the span between 2011 and 2015 which is a consequence of missing annual data during this period (Table 17). The highest  $\text{NRDw}_{\text{mean}}$  of  $+0.379$  is found between 2015 and 2016 which either indicates a recovery of the landscape from the previous year or simply an adjustment of the phonologic variations. Based on these data it can be concluded that the overall environment integrity and human security did not significantly decrease during this decade.

Table 21: Natural resources (NR) and natural resource depletion (NRDw) between 2007 and 2017

	2007	2008	2009	2010	2011	2015	2016	2017
$\text{NR}_{\text{max}}$	91.9 %	91.5 %	90.7 %	90.1 %	91.4 %	91.7 %	89.5 %	88.6 %
$\text{NR}_{95\%}$	73.5 %	76.2 %	74.7 %	74.3 %	74.6 %	73.9 %	73.1 %	73.3 %
$\text{NR}_{\text{mean}}$	46.9 %	47.1 %	47.0 %	47.1 %	46.9 %	46.5 %	46.8 %	47.0 %
$\text{NR}_{\text{median}}$	45.7 %	45.4 %	45.9 %	45.9 %	45.8 %	44.3 %	45.6 %	45.1 %
$\text{NR}_{5\%}$	24.8 %	24.4 %	25.0 %	24.9 %	24.2 %	25.0 %	25.4 %	25.6 %
$\text{NR}_{\text{min}}$	23.1 %	23.1 %	23.1 %	23.1 %	23.1 %	23.1 %	23.1 %	23.1 %
$\text{NR}_{\text{sum}}$	840.8	844.6	843.5	843.8	840.7	833.1	839.9	842.8
$\text{NRDw}_{\text{mean}}$		0.187 %	-0.037 %	0.016 %	-0.175 %	-0.421 %	0.379 %	0.158 %
$\text{NRDw}_{\text{net}}$		3.36	-0.65	0.28	-3.14	-7.55	6.79	2.83

Figure 94 shows the NRDw maps for all time intervals. At first sight, no clear trend can be identified. Especially around the settlements of Djabal and Goz Beida in the south and Koufoufou in the north, no depletion of resources is shown. Additionally, the Hadjer Arkop massif shows stable values throughout the investigated period. Variations in NR can be identified around Wadi Auada and its surrounding forested areas, extending into both positive and negative values. It cannot be determined if these indicate a gradually changing ecosystem or if they are caused by seasonal variations alone. This will be pursued later. The areas of strongest impacts can be addressed to the shrublands in the southeast and the grassland plains in the north.

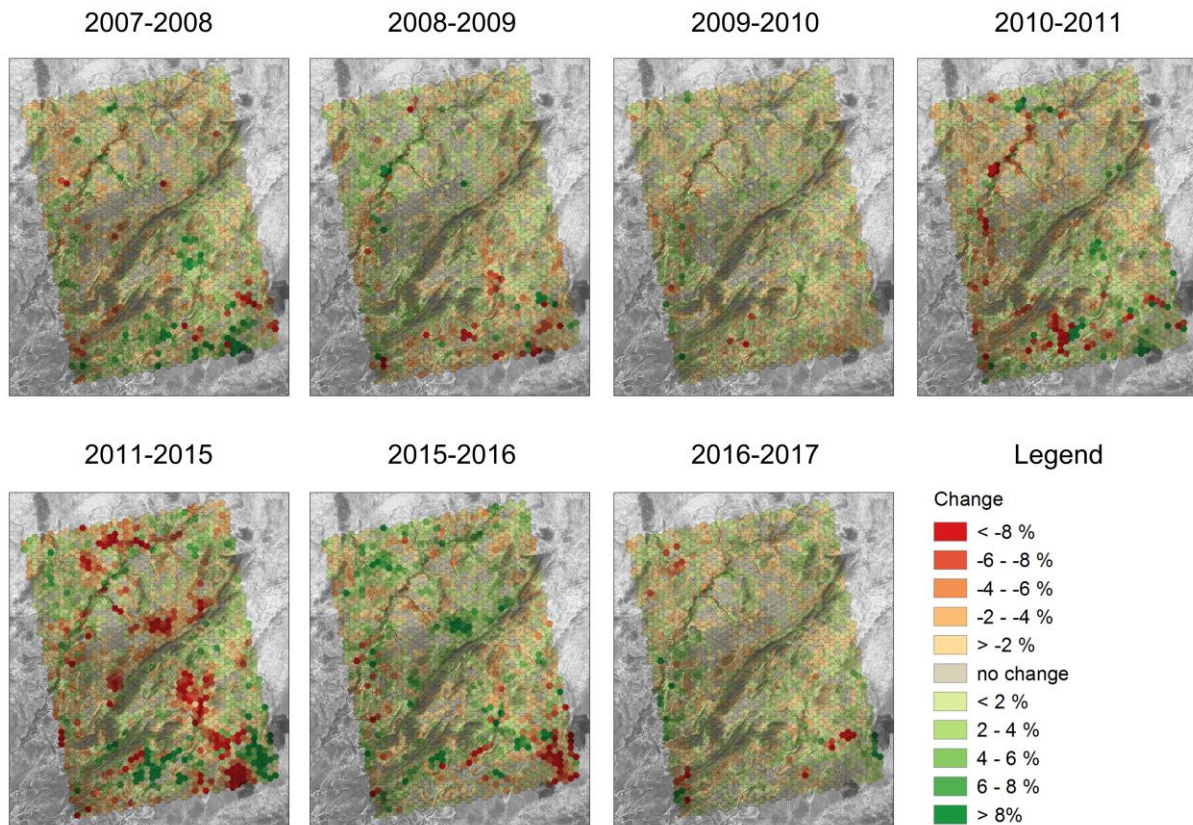


Figure 94: Spatial representation of weighted natural resource depletion (NRDw)

Figure 95 shows the final map summarizing the overall values of weighted natural resource depletion (NRDw) including the variability  $v$  as hachures of the single hexagon grid cells. Both measures together help to put the findings into a clearer context. While the colors indicate the severity of changes between 2007 and 2017, the hachures mark the general affinity of an area towards changes. For example, if an area shows low to moderate overall change in natural resources but has a high variability, this area is more likely to be affected by seasonal or inter-annual changes. This is often the case for shrublands or grasslands. In turn, if an area has a low variability ( $v < 1.5$ ) the underlying changes are rather of long-term nature, such general trends occur because of natural land degradation (or recovery) or human impact, for example, especially if urban areas or bare soil are involved in these changes.

In general, no clear trends of change can be determined. This supports the indications made based on Table 21. No impact goes out from the urban areas, neither does Wadi Auada underly significant changes. Its variability values are mostly above 2.0, indicating that it is rather subject to inter-annual and seasonal dynamics. Strongest NRDw values in both positive and negative direction are

accumulated in the southeast of the study area. They can be attributed to the transition between forest and shrubland, but again, based on their variability values, these are more likely caused by shifts in the phenology between the acquisition dates instead of long-term trends.

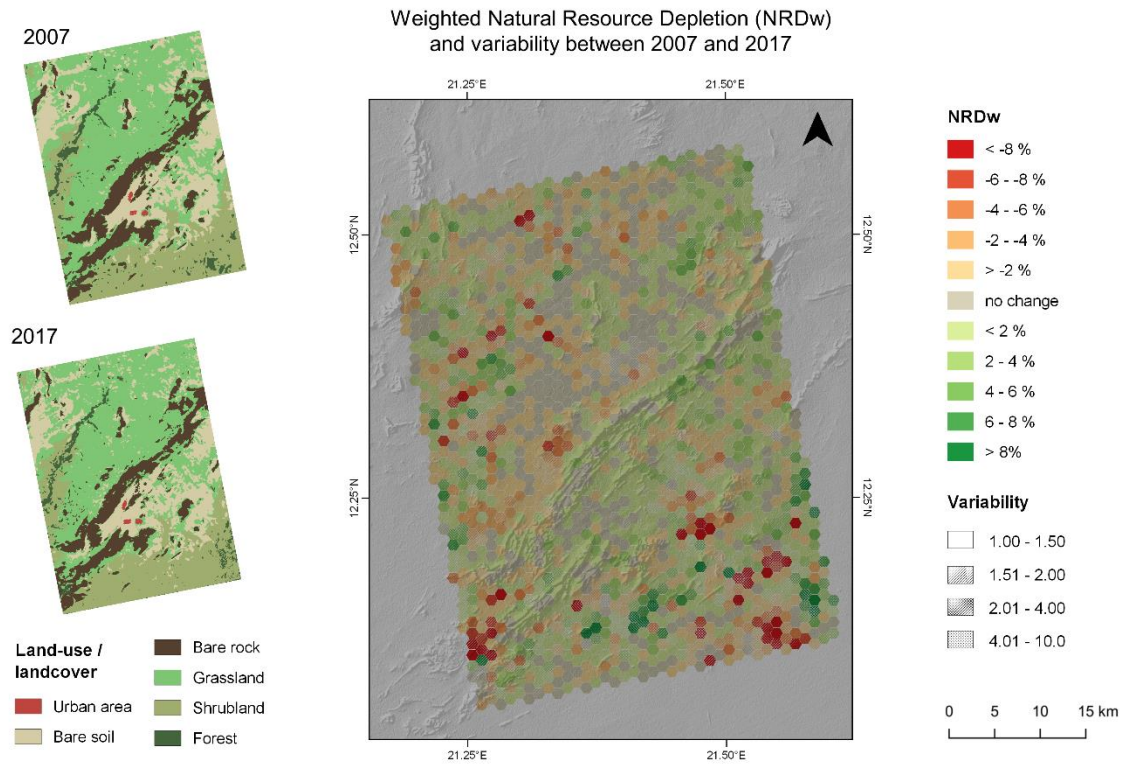


Figure 95: Overall weighted natural resource depletion (NRDw) and variability

Figure 96 shows the frequency of variabilities of all 1739 analyzed hexagon grid cells plotted against their NDRw values and allows to draw final conclusions from this study.

In general, areas of low variability ( $v < 2.0$ ) form major parts of the study area, but they mainly show subtle to no changes. These are the areas which underly a general trend rather than indifferent variations. Furthermore, areas with slight changes ( $\text{NRDw} \pm 2\%$ ) are more frequent than areas with no change, especially for higher variabilities. Consequently, the study area does show some long-term dynamics which are slightly stronger at the negative side ( $\text{NRDw} < 4\%$ ).

On the other hand, areas with moderate variability ( $v = 2.0 - 4.0$ ,  $n=292$ ) are the ones which are subject to subtle changes and relatively unsteady development. As found above, these are probably areas in transition between grassland and shrubland or shrubland and forest. Lastly, hexagon cells with distinctively high variability ( $v > 4.00$ ,  $n=48$ ) are very rare and don't play a significant role in the study area.

As shown, NRDw values are normally distributed in each variability class with exceptions for very high or very low developments ( $\text{NRDw} > 8\%$  and  $< -8\%$ ). Statistical outliers become especially visible in the class of highest variability ( $v > 4.00$ ) where strong positive changes ( $\text{NRDw} > 8\%$ ) constitute the majority. These extreme values outside the gaussian distribution are likely to result from misclassifications at areas which are hard to classify and therefore cause constant changes between classes at each observed interval.

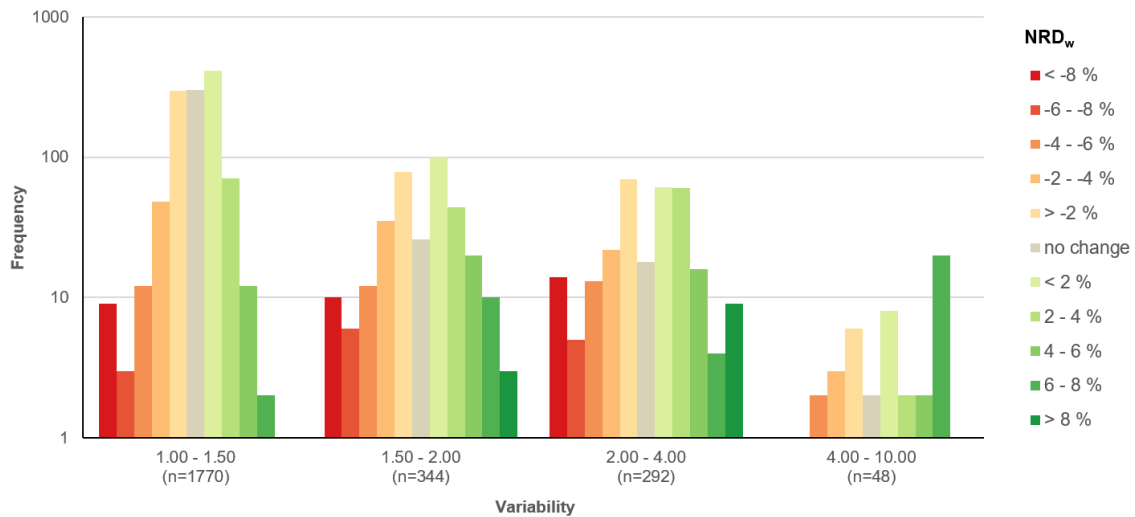


Figure 96: Frequency distribution of grid cell variability within the study area compared to their NRDw index for the time between 2007 and 2017. Note the logarithmic scaling of the y-axis

Altogether, the proposed approach shows how to derive detailed change maps based on time-series of SAR imagery which include the knowledge of experts and are easy to read. However, some things can be discussed.

One crucial finding is that the landscape in the study area did not undergo large-scale changes during the investigated period. Hot-spots can be identified (Figure 94) but they do not add up to a long-term pattern (Figure 95). It is notable that none of the settlements contributed to landscape degradation, but according to various sources, these settlements did not grow significantly during the observed decade (Farman-Farmaian & Ndakass 2014; Monier 2009; UNHCR 2005). Another reason for the stability of resources in the area could be the large proportion of bare soil as a part of the described agricultural use. As their NR value is already low (Table 20), only changes to human settlements or bare rock would have caused negative NRDw values. It could not be ultimately detected if the changes around Wadi Aouada were caused by seasonal variations or long-term developments. As it is the area of the highest resource concentration, its NRDw is particularly sensitive to smaller changes. At least it can be remarked that its core area remained stable during the whole investigated period.

On the methodological side, some points must be addressed. It is clear that a time-series consisting of more than eight SAR scenes would have given a clearer image on the temporal development of the study area. Also, the gap of three years in between when no ALOS acquisitions were made is not the ideal case. In particular, the measure of variability would have needed a longer baseline to be more reliable. These issues will be reduced in the future when ALOS-2 and TanDEM-L will constantly deliver images over longer time periods. Also, the VH configuration of Sentinel-1 might be of use in future times.

Regarding the input classifications, grassland was the class which resulted in the lowest accuracy values (Table 19). This is because of its limited interaction with L-band microwaves. Combinations of short and long wavelengths would increase the classification accuracy here but would also make the process more complex and reduce its potential for operationalization.

Including image textures enriched the feature space to a sufficient degree for the use as input in a random forest classifier but, as with all radar information, produced results with granular patterns which led to the misclassification of single pixels. However, aggregating pixels to hexagon grids of

1 km clearly reduced the impact of these pixels and increased the interpretability of the map at the same time.

### 3.3.3.6 Scientific conclusions and practice recommendations

The following general remarks can be given for the application of SAR data for environmental impact assessments in a humanitarian context:

- The definition of **target classes** is a crucial step at the beginning of the study. It is advised that it is done in collaboration with regional experts who know which LULC types are relevant in the study area, which of them are prone to changes and what is their relative importance to environmental integrity and human security.
- Krueger et al. (2012) discuss the **role of experts** in environmental studies and highlight the necessity for a careful selection in order to get unbiased results. Ahlroth et al. (2011) even suggest predefined generic sets of weights to be able to correctly integrate the expertise and opinion of people with different background. This seems especially reasonable in a humanitarian context where parties with often oppositional interests come together.
- The spatial resolution of the SAR sensors is not of main importance. Decisive is the **temporal availability** of images from the same time of the year (preferably the same month to minimize the effect of phenologic variations) over a longer time. Images from at least six years are suggested to be able to make assumptions on long-term trends. Otherwise, the discrimination of random variations from actual trends is difficult, especially when working with SAR data which contains speckle. Capstick & Harris (2001) investigated the effect of speckle filtering on LULC classification and found that filtered data can yield up to 38 % higher accuracies compared to unfiltered data. In this study, filtering was disregarded and mitigated by aggregating the classified results.
- The level of **spatial aggregation** has to be defined with care. If it is too large, target classes might vanish in the mixed information of a hexagon cell. If it is too small, the map becomes less readable and misclassifications might dominate the information of a grid cell. Finding the perfect level of spatial aggregation for ecological studies based on satellite imagery was empirically investigated by He et al. (2002) who use several indices to assess the effects of aggregation on the final results. Such initial analyses are recommended when the user has little information on the study area and is insecure about a suitable level of aggregation.
- In terms of **operationalization** and monitoring, a database with training samples could be favorable so that the step of training the classifier no longer needs repeating. This would allow continuing with existing datasets as soon as new satellite imagery becomes available. In this context, convolutional neural networks and methods of deep learning are the most promising advances for the near future (Gong et al. 2017; Gong et al. 2016).

### 3.3.4 Estimation of biomass (Sénégal)

Note: This study was published by Braun et al. (2018) as an open access article distributed under the Creative Commons Attribution License which permits unrestricted use, distribution, and reproduction in any medium, provided the original work is properly cited (CC BY 4.0). The reader is advised to consult this publication for a more detailed description of this study. The contribution of all authors is listed in chapter 1.4.

#### 3.3.4.1 Background and aims

Above-ground biomass (AGB) is a key resource for displaced people because it allows them to cover their need for construction materials for their dwellings and firewood for cooking (Barbieri et al. 2017; Rivoal & Haselip 2017; Wilson 1992). Its spatial quantification with respect to the settlement is therefore an important information which can be covered by methods of remote sensing. Although the relationship between vegetation volume and radar backscatter intensity is widely understood (Dobson et al. 1992; Ghasemi et al. 2011; Sinha et al. 2015), one main constraint is the availability of in-situ measurements on the ground. Whenever quantitative information on the amount of biomass is to be retrieved from SAR imagery, their mathematic relationship needs to be analyzed first, because each vegetation type and community produces different backscatter, as a function of crown volume, the density of branches, and the size and orientation of stems (Ulaby et al. 1986).

Initiated by the GIS unit of the MSF Operational Center Geneva in Switzerland, contacts were established to Action Contre la Faim (ACF), an NGO which, amongst other tasks, creates maps of biomass production and anomalies for large parts of the Sahel at a spatial resolution of 1 kilometer (Fillol 2018). Their service is operational and widely used for agricultural yield prognoses, the management of grazing and the monitoring of climate change effects. However, as it is based on optical imagery of PROBA-V, the maps are mainly representative of the cloud-free and dry summer season. Information about biomass availability in the rainy winter season would substantially improve the value of these products and increase the understanding of sub-Saharan ecosystems. This study demonstrates a novel approach on the integration of radar imagery of medium to low resolution for the operational mapping of biomass.

Sénégal was selected as a case study because it ranges along the transition between sub-tropical ecosystems in the south and the deserts of the Sahel zone in the north (Figure 97, top left). To provide nation-wide biomass information, acquisition modes cover larger areas, such as the ScanSAR mode presented in Figure 32. However, an increased footprint of the radar image entails a coarser spatial resolution. But as the study investigates AGB at the regional to national scale, spatial resolutions of 100 meters or below are completely sufficient.

#### 3.3.4.2 Data sources and pre-processing

As summarized by Sinha et al. (2015) and Ghasemi et al. (2011), best results can be achieved when SAR backscatter of different wavelengths are combined. One of the few sensors which provide largely archived images in ScanSAR mode are ALOS PALSAR (L-band) and ENVISAT ASAR (C-band). The assumption is that different wavelengths interact more effectively with different types of vegetation. However, their sensitivity towards grasslands and steppe landscapes with scattered vegetation is limited (Ranson & Sun 1994). For this reason, passive microwave data from the Special Sensor Microwave/Imager (SSM/I), representing surface brightness at a spatial resolution of 12.5 kilometers was additionally used in this study (Armstrong et al. 1994). It has a revisit frequency of one day at nearly global coverage. For this reason, monthly average values were calculated (Table 22).

In-situ measurements of AGB were collected and provided by the Centre de Suivi Écologique CSE (Dakar, Senegal). These data were collected at an annual basis between 1987 and 2015 at the sites

shown as black circles in Figure 32. Measurements were undertaken between September and October based on destructive and non-destructive samplings along representative transects of 200 meters at each identified site as documented by Yameogo et al. (2004). Total biomass was then calculated based on allometric equations given by Cissé (1980).

The common spatial extent of the SAR missions is shown in Figure 97 (red polygon), as well as the locations of the ground sampling points (black circles). Because no sampling points were available south of the Saloum river delta and because of the limited footprint of the SAR images, the southernmost subdivisions of Sénégal could not be included in the study. The whole study area still ranges over 300 kilometers in north-south direction and covers different types of ecosystems and climate zones.

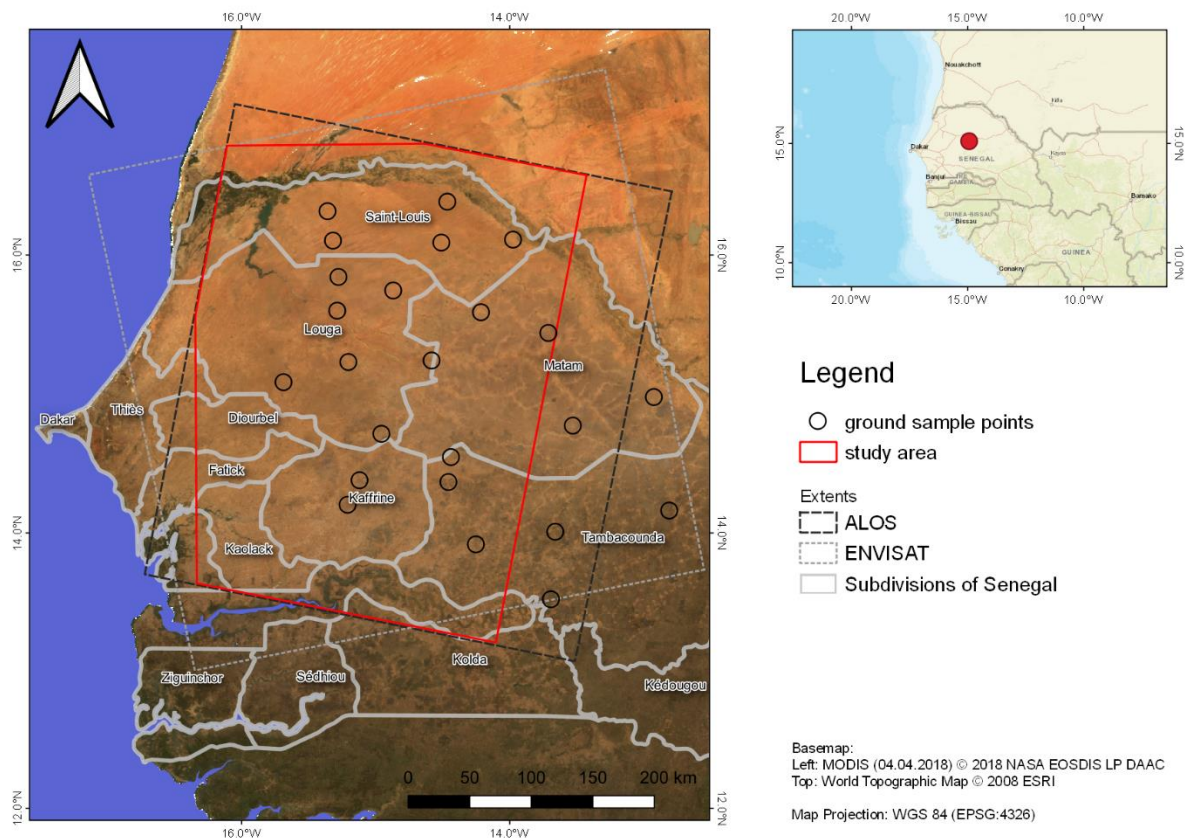


Figure 97: Study area for biomass estimates in Senegal

Although the biomass measurements were undertaken at a yearly interval, only three years were analyzed in this study because of the following reasons:

- a) Inconsistency: Data of these years were the most complete. Years where one of the sample points was left out were not considered for this study to keep the number of available measurements as high as possible. The measurements shown in Figure 97 are the ones which were available in all three years.
- b) Data availability: ENVISAT ASAR and ALOS PALSAR data taken in November or December of each corresponding year was required. Only years where both satellites provided images in ScanSAR mode could be used for this study.

These criteria left the years 2006, 2009 and 2010 as a usable base for this study. The exact dates of the images are shown in Table 22. Because of the aforementioned reasons of data availability, a

consistent polarization for all satellite images could not be found. For this reason, SSM/I data was downloaded in both horizontal and vertical polarization, so it could later be combined with data of either polarization. The basic assumption is that the wavelengths of the active radar systems interact with different parts of the vegetation cover and a combination of both reveals more about the presence of biomass than one sensor alone. While microwaves of ENVISAT ( $\lambda = 5.66$  cm) have stronger interactions with grassland and tree crowns, the long waves of ALOS ( $\lambda = 23.62$ cm) can penetrate canopies or leaves and are backscattered by branches and stems. Furthermore, the integration of passive radar emissions provides complementary information which is not measurable by spaceborne SAR systems. While this combination is already successfully applied to soil moisture mapping (Das et al. 2011; Entekhabi et al. 2010), its application in biomass estimation is not yet tested.

Data of ENVISAT and ALOS were radiometrically calibrated, topographically normalized, and geometrically corrected using a 30-meter digital elevation model of the SRTM mission (chapter 2.3). Sigma0 values were then connected to dB scale for better contrasts over the whole value range, SSM/I products were used as provided by the NSIDC because of its extensive and accurate internal calibration (Hollinger et al. 1990; Wentz 2013).

For the later fusion of all three sensors, images were additionally transformed to 8-bit integer data for a principal component analysis (PCA, Geladi et al. 1989).

Table 22: Satellite data used for biomass estimations in Sénégal

Year	Sensor	Date	frequency [GHz]	polarization
2006	ENVISAT ASAR	19.12.2006	5.3	HH
	ALOS PALSAR	23.12.2006	1.27	HH
	SSM/I	12.2006	85	H
	SSM/I	12.2006	85	V
2009	ENVISAT ASAR	20.12.2009	5.3	VV
	ALOS PALSAR	31.12.2009	1.27	HH
	SSM/I	12.2009	91	H
	SSM/I	12.2009	91	V
2010	ENVISAT ASAR	29.11.2010	5.3	VV
	ALOS PALSAR	18.11.2010	1.27	HH
	SSM/I	12.2010	91	H
	SSM/I	12.2010	91	V

### 3.3.4.3 Correlation analysis

Backscatter values of ALOS and ENVISAT images were extracted in a radius of 3 kilometers around the sampling point and averaged to a mean value to reduce the effect of speckle on single pixels and to get a representative value for the sampled site. Because of their low spatial resolution, SSM/I values were directly extracted at the sampling points without further spatial averaging.

AGB measurements of the years 2006, 2009 and 2010 were then correlated to the values of the images of the sensors' images of the respective years. Additionally, multiple combinations of values from ALOS (A), ENVISAT (E), and SSM/I (S) were computed to investigate their relationships and their correlation with biomass measurements.

A selection of representative results is given in Table 23. The strength of the relationship between the derived radar measures and the underlying AGB values was calculated by the coefficient of determination ( $R^2$ ). It explains how well the depending variable (biomass) can be explained by the

independent variable (radar information) and ranges between 0 (no correlation) and 1 (radar data fully explains the biomass variations). Furthermore, the root mean square error (RMSE) was assessed based on a 10-fold-cross validation which compares the measured values with the ones predicted by the regression (Kohavi 1995).

The relationships were then expressed as an exponential function of the following structure:

$$y = a * b \cdot e^x \quad (24)$$

where y is the biomass, x is the radar measure and a and b are equation coefficients.

Scatter plots of the radar measures against the AGB values are shown in Figure 98. The plot letters indicate the corresponding regression as given in Table 23.

Table 23: Correlation analysis between AGB and radar measures

Plot	Radar system	Variable(s)	Regression	R <sup>2</sup>	RMSE	Samples
a	ALOS (A)	HH	$23286.569 * e^{0.118*A}$	0.313	2308.15	n=60
b	ENVISAT (E)	HH & VV	$35387.901 * e^{0.177*E}$	0.371	2286.31	n=60
c	ENVISAT ALOS	$E - (5 * (E/A))$	$75722.369 * e^{0.180 * (E - 5 * \frac{E}{A})}$	0.375	2117.09	n=60
d	SSM/I (S)	H only	$0.000238 * e^{0.0059*S}$	0.130	2593.15	n=61
e	ENVISAT SSM/I	E/S 2006 H	$46335.014 * e^{583.855 * \frac{E}{S}}$	0.498	1500.5	n=21
f	ALOS SSM/I	A/S 2006 H	$25422.691 * e^{388.723 * \frac{A}{S}}$	0.501	1692.82	n=21
g	ENVISAT ALOS SSM/I	PC1 2006 H only	$428.721 * e^{-0.007 * PCA1(2006)}$	0.519	1657.23	n=21
h	ENVISAT ALOS SSM/I	PC1 2009 H & V	$1714.262 * e^{0.003 * PCA1(2009)}$	0.308	1384.03	n=22
i	ENVISAT ALOS SSM/I	PC1 2010 H & V	$6117.281 * e^{0.003 * PCA1(2010)}$	0.353	2512.59	n=23

It can be stated that relationships exist between AGB and images of active radar sensors, whereby ENVISAT shows slightly higher R<sup>2</sup> (0.371) than ALOS (0.313). This can again be explained by the fact that many of the investigated areas feature open landscapes with sparse tree cover and dominating grassland, which interacts stronger with the short waves of ENVISAT. In the spatial representation (Figure 98, plot 2) the differences between low and high biomass areas are more pronounced, especially along the Sénégal river in the north. As it turned out, the ratio between ENVISAT and ALOS backscatter describes the differences in vegetations quite well. If this ratio is added to the backscatter of ENVISAT (plot c) the variation of AGB can be explained even better (R<sup>2</sup>). The benefit of combining imagery of different wavelengths was also found by Omar et al. (2017) for Sentinel-1 and ALOS-2 data and by Englhart et al. (2011) for TerraSAR-X and ALOS PALSAR. Yet, in our study, the combination did not outperform the single data approaches significantly. Therefore, the introduced SSM/I data which, taken as only source, has a very low R<sup>2</sup> of 0.13. That means it cannot serve as an explanatory source for the spatial distribution of AGB alone. In fact, the spatial pattern generated by regression d is the inverse of what is expected in the study area. First when passive radar brightness from SSM/I is combined with ENVISAT and ALOS (plots e and f), the R<sup>2</sup> increases substantially to 0.498 and 0.501. The regressions based on the first principal component of the merged radar information (plots h, i and j) show an indifferent result. While the data of 2006 shows

an  $R^2$  of 0.519 which was the highest in this study, results from 2009 and 2010 did not bring any increase ( $R^2 = 0.308$  and  $0.353$ ). This resulted from the fact that the input data for 2006 was consistently horizontally polarized, while for 2009 and 2010 data of vertical and horizontal polarization had to be mixed because of limited availability (Table 22).

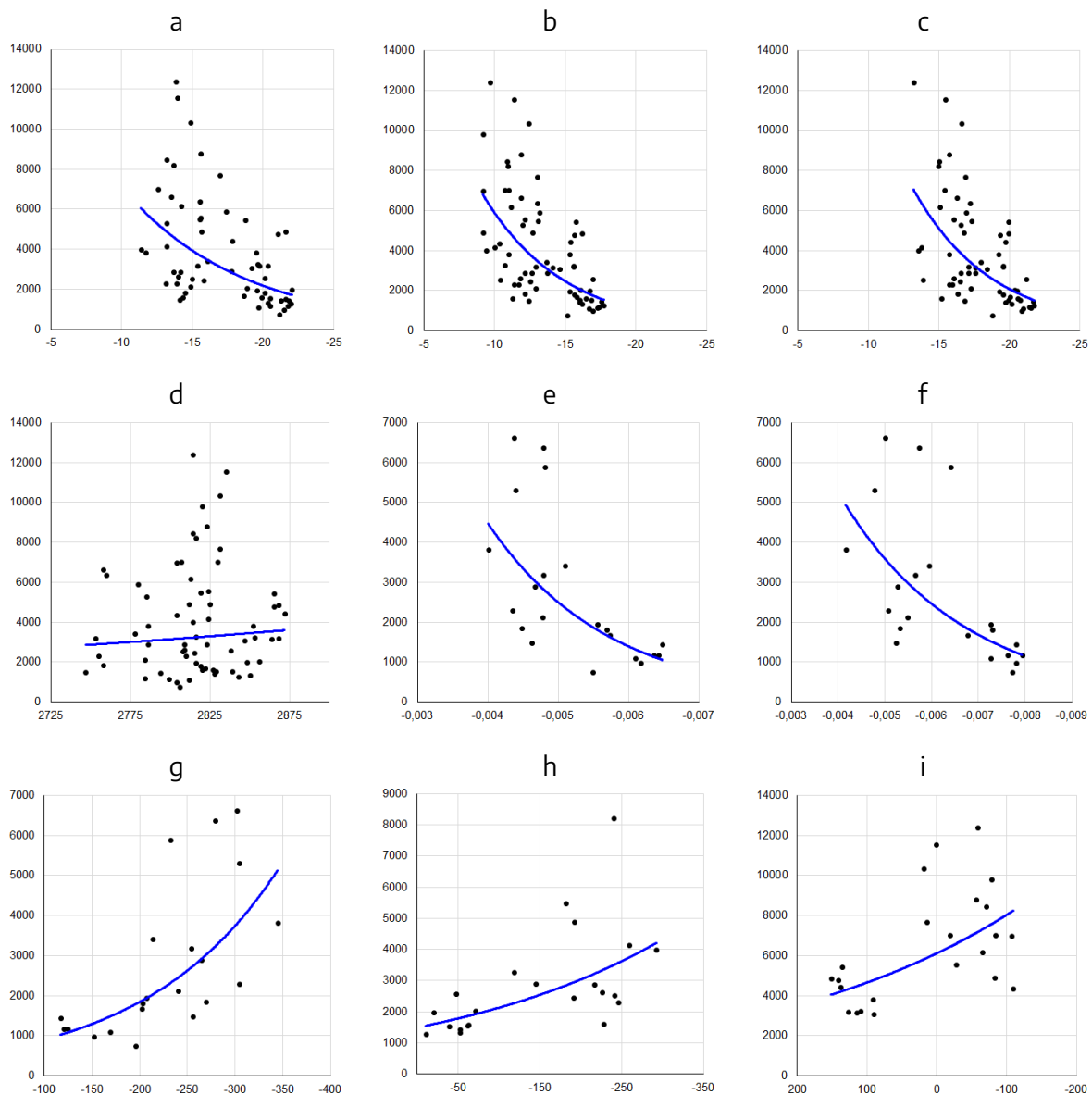


Figure 98: Selected relationships between AGB and radar measures  
*y*-axes: above-ground biomass [kg/ha], *x*-axes: selected radar measures (Table 23)

### 3.3.4.4 Results and discussion

The results shown in Table 23, Figure 98 and Figure 99 are a selection of the most representative findings in this study. As stated, many more combinations between ENVISAT, ALOS and SSM/I data are possible but many of them were found to be of comparable (or lower) significance.

The validation scores indicate that a combination of sensors of different wavelengths lead to better predictions. While the highest  $R^2$  was achieved by the PC1 of 2006, the lowest RMSE was observed

for the PC1 of 2009. Only the PC1 of 2010 led to low scores because it splits the samples into two populations which lack of a clear common trend.

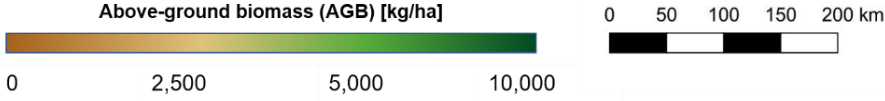
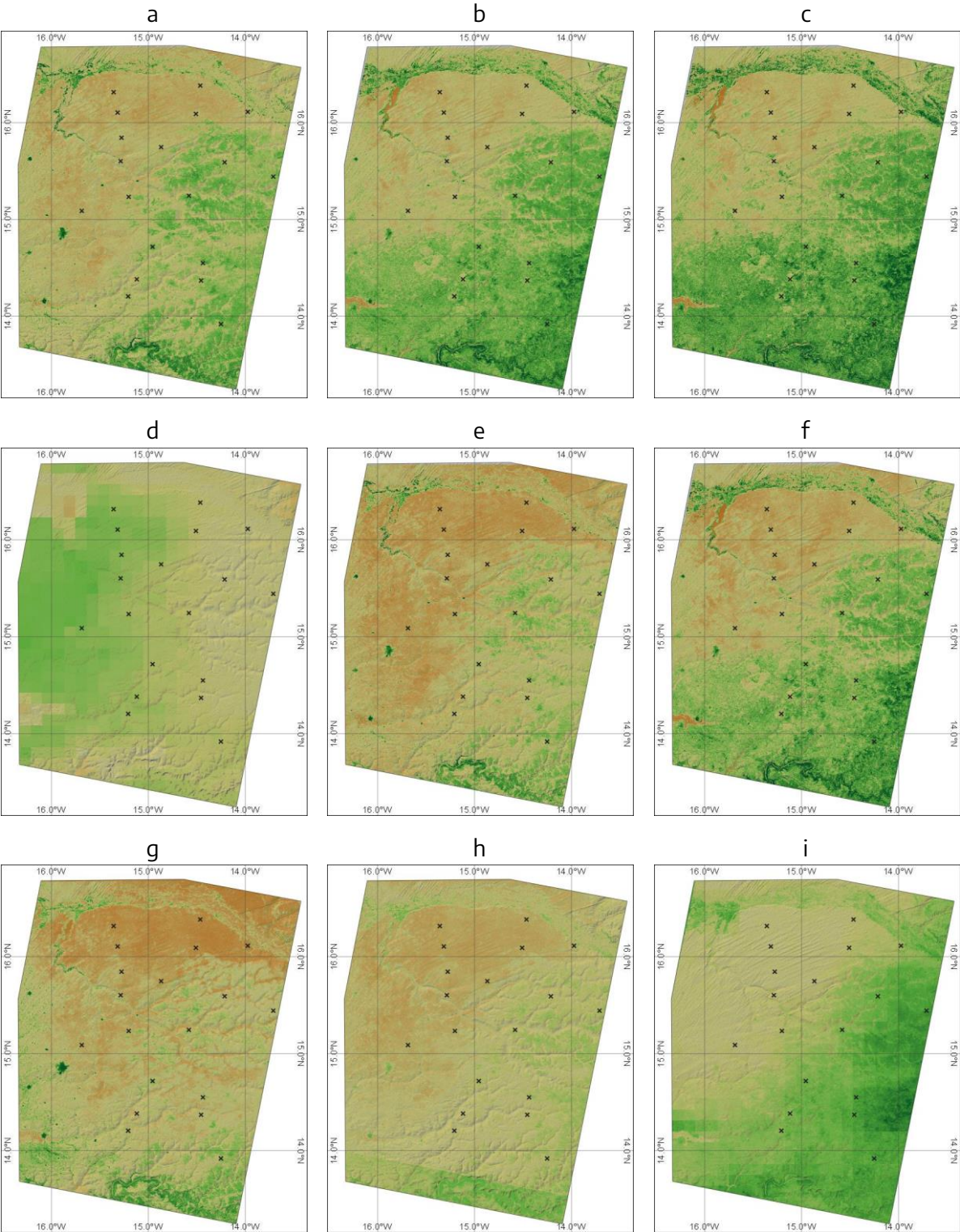


Figure 99: AGB maps produced by selected regression methods (Figure 98)

The basic principle of linking biomass to radar measures was applied successfully in this study. Except for plot d, all examples showed that there is a strong relationship between AGB and backscatter intensity. This fact itself is notable, given that there are only a few studies providing biomass estimates in areas with values below 10 t/ha. However, this relationship was subject to various factors which will be discussed as follows:

The highest  $R^2$  of simple combinations of active and passive radar information was achieved for the combination of ALOS and SSM/I in only horizontal polarization (plot f). This indicates that the information of both is complementary: While the long wavelength of ALOS is sensitive to massive vegetation structures, such as stems and large branches, the passive radar brightness might better reflect the herbaceous layer below. Both components form the typical savanna landscape in this area.

It was common in all cases that none of the regressions were able to reproduce the maximum values of > 12 t/ha. In turn, the minimum values of around 1 t/ha were correctly represented by both ALOS ( $\text{Sigma0} < 20$  dB) and ENVISAT ( $\text{Sigma0} < -15$  dB). As shown in plots a, b and c, ENVISAT had a slightly stronger correlation than ALOS, probably because of the already mentioned reason that some of the lighter vegetation cover is partially penetrated by the long wavelengths of ALOS PALSAR and therefore no longer a suitable radar target. In turn, the areas of more wooden vegetation have a potentially stronger interaction with sensors of large wavelengths. While the low-biomass areas in the center of the study area seem more pronounced in plot d, the higher AGB values are reached in the area along the river in the north in plot e.

Regarding the regressions based on the principal component analysis (PCA), a clear increase of prediction quality can be observed for the year 2006 ( $R^2 = 0.519$ ), while the ones for the years 2009 and 2010 were comparably low. One reason is that the relationship between PCA and AGB for the year 2006 is clearly exponential and can therefore be expressed as a regression curve while the point distributions for the years 2009 and 2010 show fewer clear trends (Figure 98 g-i). The unavailability of radar images from further years did not allow the drawing of final conclusions regarding if the measurements of 2006 were more representative for the spatial biomass distribution or if the lower accuracy of the other two years was influenced by other factors (phenologic shifts, unsuitable radar imagery). The results however indicate that PCAs based on a common polarization (2006: horizontal only) are more favorable than ones with mixed polarizations (2009 and 2010: horizontal and vertical data) because they address the same scattering mechanism. More consistent pairs of field measurements with imagery of all three sensors are needed to proof this presumption.

One main point of concern is that the sample size of field measurements which were used for the regression analysis was not consistent over all plots. This was because of partially limited coverage of single scenes (as shown in Figure 97, not all usable points lie within all radar scenes) and missing data of the same polarization. Thus, the increased accuracy of sensor combinations (plots d-j) towards the single scene regressions (a-c) could also partially be explained by the lower basic population ( $n=21$  of 60 available measurements).

As most studies deal with tropical biomass and the presented results are among the first which present relationships of biomass with radar measures in areas with sparse vegetation cover ( $\text{AGB} < 15$  t/ha), these findings should therefore be used as a starting point for further analyses. Increased data availability is given since Sentinel-1 (C-band) and ALOS-2 (L-band) cover swaths of up to 450 km (Table 32) and acquire images at regular intervals.

### 3.3.4.5 Scientific conclusions and practice recommendations

The derivation of AGB values from radar imagery is not new. However, the following recommendations can be given based on the findings provided above.

- A sufficient number of homogeneously collected **field measurements** is required for each large-scale mapping of biomass. Although many relationships exist between different sensors' backscatter and AGB it is not advisable to simply adapt these regressions because they rely on the scattering mechanisms of different surfaces and vegetation types which are not directly comparable between different landscapes.
- **P-band L-band** systems show stronger relationships to forest biomass and dense shrubs because of their higher wavelength which is partially able to penetrate canopies (Schmullius & Evans 1997). The emitted waves often interact with the stems which are a suitable indicator for the overall biomass of an area.
- In turn, microwaves of C-band or X-band systems end at the canopies and have a lower saturation (section 3.3.1), but they are able to detect **finer differences** in grasslands and areas of sparse vegetation.
- Any actively acquired radar imagery should be **carefully calibrated** for radiometric distortions based on topography and incidence angle, especially for scenes over a wide range (Figure 14). Villard & Le Toan (2015) have investigated the effect of radiometric corrections of local incidence angles and scattering mechanisms on the accuracy of biomass regressions based on P-band SAR intensity. They report that the sensitivity of the calibrated measure to AGB can be nearly twice as high compared to less carefully calibrated data, thus increasing the correlation coefficient from 0.3 to 0.68.
- If the study area ranges over various ecosystems, it is advisable to base regressions on **multiple sensors**, preferably of short and long wavelengths. Integration of passive radar of considerably lower spatial resolution can bring additional accuracy, but only if the study area is large enough to reveal land cover-related patterns in the radar brightness of passive systems.
- **Passive radar** emittances are affected by atmospheric disturbances and should therefore be averaged over several acquisitions to retrieve representative values as shown in this study. This was done in studies on sea ice concentration (Schweitzer 1995) and wind speed (Halpern et al. 1995) but not yet in ecological studies.
- If several systems are used for the prediction of biomass, it is advisable to use images of the same **polarization** (horizontal or vertical) throughout all image acquisitions whenever possible to reduce the impact of wave polarization on backscatter variation.

### 3.4 Summary of the most important results

This chapter shortly summarizes the most important findings gained in the presented case studies. For the sake of readability, the presented case studies are abbreviated as suggested in Table 24.

Table 24: Case studies presented in this thesis

Section	Abbreviation	Aim and result
3.1.2	POP-TSX-KEN	Estimation of building density in camp Dagahaley (Kenya) based on TerraSAR-X data. Map of dwelling numbers within a radius 100 meters.
3.1.3	POP-A2-NGA	Estimation of building density in the city of Maiduguri (Nigeria) based on ALOS-2 and TanDEM-X data. Map of dwelling density aggregated in hexagons of 250 meters.
3.1.4	POP-S1-BGD	Description of growth of camp Kutupalong (Bangladesh) based on Sentinel-1 data. RGB map of growth and map of forest decrease between 2017 and 2018.
3.1.4	POP-TSX-BGD	Assessment of building changes in camp Kutupalong (Bangladesh) based on RGB composites of VHR imagery of TerraSAR-X between 09/2017 and 08/2018.
3.1.5	INF-S1-GIN/ETH	Identification of villages around Guéckédou (Guinea) and roads in the region of Gambella (Ethiopia) with multi-temporal Sentinel-1 data. Maps at regional scale.
3.1.6	INF-S1-SYR	Assessment of building damages in Raqqqa (Syria) as a result of the civil war based on Sentinel-1 time-series data. Map of spatial distribution of damages.
3.2.2	HYD-S1-BGD	Evaluation of the effect of sea-level changes on Bhasan Char (Bangladesh) with ERS-1/2, ENVISAT, and Sentinel-1, data. Maps/statistics for multiple dates since 1996.
3.2.3	HYD-S1-LAO	Water body mapping for the Attapeu dam break (Laos) based on Sentinel-1 data. Maps of flood extents for multiple dates before and after the incident.
3.2.4	HYD-TDX-BGD	Derivation of a DEM of the area around camp Kutupalong (Bangladesh) based on a TanDEM-X image pair. Maps of surface runoff for risk assessment within the camp.
3.3.2	ENV-A2-MLI	Recommendations for new groundwater drilling sites around the city of Kidal (Mali) based on ALOS-2, TanDEM-X and Sentinel-1 data. Maps and local recommendations.
3.3.3	ENV-A2-TCO	Monitoring of the environmental impact of the refugee camp Djabal (Chad) based on ALOS data. Assessment of weighted impacts aggregated in hexagons of 1 kilometer.
3.3.4	ENV-A1-SEN	Derivation of aboveground biomass for large parts of Sénégal based on ENVISAT, ALOS PALSAR and SSM/I data. Biomass maps [t/ha] at 100 meters resolution.

Note: The abbreviation contains the domain (POP=population, INF=infrastructure, HYD=hydrology, ENV=environment/resources), the sensor which was mainly used in the study, and the official three letter code of each state as also used by the United Nations (ISO 3166-1 alpha-3).

Referring back to the dimensions of humanitarian aid (Figure 3), the presented case studies were rated according to the emergency situation which they provide information for, taking into account three aspects of user requirements: the temporal dimension of the aid to be delivered (short-term to long-term), the spatial extent of the affected area (local to regional scale), and the degree of specialization required from the humanitarian staff in the respective situation (basic services to highly-specialized aid). As demonstrated in Table 25 (first columns), the case studies cover emergencies of all spatial and temporal dimensions, as well as situations which require different levels of specialized response. The applications range from local mapping of camp changes to the long-term and nation-wide assessment of environmental resources. While the tasks linked to population monitoring are of rather general nature, there are also studies which provide information the intervention of highly specialized forces, such as damage mapping or groundwater drilling. As also shown in the figure, the degree of specialization is mostly either very high or very low. More generally speaking, information derived from SAR data is suitable to be used in nearly any setting and dimension of humanitarian aid.

As also shown in Table 25 (middle columns), the presented case studies have different requirements to the user in the respective situation: some of the tasks are take long time-consuming and require

highly-skilled staff, while others can be performed by laymen within comparably short time. In this context, the factor of time is rather influenced by preparatory tasks and a proper evaluation of the results, than the actual processing of the data itself. These aspects involve the selection and retrieval of suitable data, the definition and weighting of target classes (ENV-A2-TCD), or the interpretation of the generated information by experts, such as the identification of groundwater drilling sites (ENV-A2-MLI). For some organizations, also the factor of data acquisition costs plays a crucial role. Wherever VHR SAR data is required, commercial satellites become inevitable, but especially the studies which focus larger areas at spatial resolutions above 10 meters essentially profit from the open access to Sentinel-1 data.

From a technical and scientific side (Table 25, last columns), the studies also differ regarding the volume of exploited data and the computational capacities which are required to process them into usable information. Again, monitoring or big data approaches are of higher requirements than the analysis of single scenes. With the development of cloud-based tools and online processing services (discussed in chapter 4.2), both scientists and users will have less technical barriers to conduct such tasks. Finally, the degree of scientific quality and innovation ranges widely within the studies. The more application-oriented studies aim at the quick and easy derivation of information, for example by interpreting visually enhanced products (SINF-S1-GIN, ENV-A2-MLI) or identification of changes in RGB images (POP-TSX-BGD). More sophisticated approaches used methods of automated image classification (POP-S1-BGD, HYD-S1-LAO), numerical regression (POP-TSX-KEN, ENV-A1-SEN), or SAR-specific processing (INF-S1-SYR, HYD-TDX-BGD). Highest scientific innovation was involved in the estimation of population density by integrated use of normalized elevation data (POP-A2-NGA), the estimation of damages in Sentinel-1 time-series (INF-S1-SYR), the automated evaluation of ecosystem degradation using automated training areas and expert-based weights (ENV-A2-TCD) and the estimation of biomass by the integration of passive radar images (ENV-A1-SEN).

Table 25: Case studies rated according to information content, requirements and technical aspects

Study	Requirements by the user			Requirements from the user			Technical / scientific aspects		
	temporal dimension	spatial dimension	degree of specialization	time-consuming	cost-intensive	technical skills	data volume	computation capacity	scientific innovation
POP-TSX-KEN									
POP-A2-NGA									
POP-S1-BGD									
POP-TSX-BGD									
INF-S1-GIN/ETH									
INF-S1-SYR									
HYD-S1-BGD									
HYD-S1-LAO									
HYD-TDX-BGD									
ENV-A2-MLI									
ENV-A2-TCD									
ENV-A1-SEN									

Black circle: high/large/strong, white circle: low/small/weak. Note that the study on damage assessment delivers information for both short-term requirements (evacuation) and long-term aims (reconstruction/advocacy).

## 4 Conclusions

This last part of the thesis serves as both a summary and outlook discussing the role of radar remote sensing in the field of humanitarian relief action. Chapter 4.1 compiles the overall findings regarding the benefits of SAR imagery identified within the case studies in a systematic way. It refers to both widely acknowledged practice and untapped potential within the humanitarian domain and also reflects on the limitations which were revealed during the case studies. These limitations are of technical, structural, and organizational nature and are expounded in chapter 4.2 which consolidates both preceding chapters against the background of future developments. It notes challenges to address in the future and raises questions for further research.

### 4.1 Potential and limitations of radar data

This chapter groups the main findings from the case studies into different topics which primarily expresses both advantages and limitations. A comparison of these points for the application domains presented in this study is given in the last section.

#### 4.1.1 In/dependency

90% of all persons interviewed in the survey (Appendix 1) named independency from cloud cover as a main advantage of radar data. In fact, incomplete data or outdated images are a main limitation for the reliable and thorough extraction of information. This affects nearly all applications and is especially important for time-critical tasks. The time to wait for cloud-free conditions is often not given in humanitarian emergencies, especially for health-related tasks and risk assessments (mapping of roads and rural settlements for logistics and vaccination campaigns [INF-S1-GIN/ETH], and flood mapping [HYD-S1-LAO]). As a matter of fact, flooding is mostly accompanied by heavy rainfalls and thick cloud cover over several days, making optical data unusable. The benefits of radar data became evident in section 3.2.3, not only because of the **availability of images** close to the incident (dam break), but also because of the comparably easy and automated binarization of SAR images to automatically distinguish water and land surfaces (also shown in section 3.2.2). For these cases, the high value of radar data does not lie in their spatial, but their temporal resolution and the accessibility of archived images. A point that is often neglected is the fact that radar sensors do not need sunlight, so the chance to acquire an image of a certain area within a given time is proportionately twice as high as for optical images, thus enabling humanitarian organizations to react faster on emergencies.

At the same time, using radar data makes the user dependent: As the images do not contain natural colors, the interpretation of data from previously unknown areas is significantly harder (Lillesand et al. 2008). Accordingly, optical imagery or information acquired in the field is required to understand the backscatter intensity images. Any task dealing with visual image analysis and manual information extraction (mapping of geologic structures [ENV-A2-MLI], identification of camp sizes [POP-S1-BGD], and dwelling changes [POP-TSX-BGD]) relies on the **availability of secondary information**, such as thematic maps, existing geodata, or VHR optical reference images. If these are not available, the applicability of radar imagery is restricted.

Lastly, the quality of the derived results can only be assessed if some validation data is at hand. This relationship was called the “paradox of remote sensing” by Lang (2014), because unvalidated results are practically useless while having sufficiently available validation data, in turn, makes remote sensing unnecessary. So, this limitation is not strictly constrained to SAR data, but any effort to highlight their potential is restricted by a **proper validation** using independent secondary data

sources of similar spatial coverage and temporal validity. In this study, this challenge was tackled by including freely available sources, such as OpenStreetMap (POP-A2-NGA) or independently collected reference data from optical images (ENV-S2-TCD), or by splitting reference data into training and validation subsets (ENV-A1-SEN).

Concludingly, the integration of SAR data makes users in the humanitarian domain more independent in terms of fast image delivery and quick response, but brings limitations regarding the visual interpretation when no a-priori or additional information are available.

#### 4.1.2 Information content

As demonstrated in chapter 2.2 (especially in Figure 15) and in the many case studies of part 3 of this thesis, the information content of radar images is different from optical images – which provide information that is more closely related to the human vision. This brings both advantages and limitations for their use within the humanitarian domain.

The most striking difference which is still not sufficiently acknowledged is the fact that radar sensors measure **characteristics of surfaces** instead of their appearance. The numerous case studies showed how backscatter intensity can be used to describe, quantify or classify phenomena at the earth's surface. For the mapping of settlements, the high backscatter caused by solid vertical structures (double bounce) and metal materials (high dielectricity) can be used as proxy for the presence of houses (POP-TSX-KEN, POP-A2-NGA). This relationship was also exploited for the identification of rural settlements which are highlighted as bright spots in Sentinel-1 data which turned out as a valid alternative to often costly or outdated VHR optical data (INF-S1-GIN). This independency from optical imagery also turned out to be of high informative value for the rapid assessment of damages in urban environments or ecosystems where a decrease in backscatter intensity indicates the damage of infrastructural features (INF-S1-SYR) or the loss of forest areas (POP-S1-BGD). In turn, smooth water surfaces cause little or no backscatter because the incoming signal is reflected away from the sensor. This makes them easily identifiable for hydrologic purposes, such as flood mapping (HYD-S1-BGD, HYD-S1-LAO).

As the spectral variety of SAR imagery is limited compared to optical data, **image textures** were used in this work to increase the feature space for image classification (ENV-A2-TCD) and spatial regression (POP-S2-NGA). Especially calculating these textures with multiple window sizes helps to describe and detect phenomena at different spatial scales (Woodcock & Strahler 1987). As for dwelling estimates, this scale-dependency was exploited by extensive multi-looking of high-resolution SAR images which led to a clear distinction between the camp area and its surroundings in products of multiple looks, while maintaining the variations within the camp in products of fewer looks (POP-TSX-KEN).

Signals emitted by radar sensors are able to **penetrate materials** or surfaces as a function of their wavelength plus the structure and water content of the respective surface (Ulaby et al. 1986). Although this penetration depth is often limited to a couple of centimeters, it is useful for the identification and discrimination of geomorphologic features and geologic structures in arid environments (ENV-A2-MLI). Furthermore, as shown in the study on biomass (ENV-A1-SEN), the interaction of microwaves with surfaces strongly depends on their wavelength. This allows the systematic use of sensors to address specific vegetation features (e.g. canopies, branches, and stems). Although the interaction of wavelengths with surfaces and materials is a unique feature of radar sensors and also well investigated, only 50 % of the interviewed persons considered the “capability to penetrate materials” as an attractive capability (Appendix 1). One reason could be that this feature is most exploitable in environmental studies and of lesser importance for the analysis

of camps and emergencies. But the answer also indicates that the ability of microwaves to penetrate materials is probably not sufficiently acknowledged yet in the application domain.

Lastly, interferometric and polarimetric information is a unique feature of SAR imagery. It reveals even higher details of **structures at sub-pixel precision**, such as the presence and absence of solid objects, (e.g. buildings, INF-S1-SYR), or the composition of surfaces regarding the various scattering mechanisms contributing to the signal (urban density, POP-A2-NGA). These information types are useful in both urban and environmental applications and cannot be provided by optical imagery. A further benefit is the measurement of topography or ground motion at the centimeter scale which also provides considerable potential for humanitarian applications. Besides the generation of precise digital elevation models (HYD-TSX-BGD), relevant information is mostly required in risk-related fields, such as subsidence caused by groundwater extraction or tectonic movement (Tomás et al. 2014).

On the downside, it has to be remarked that a single radar image provides fewer **visual details** than an optical image of the same resolution in most cases. This is mainly a consequence of speckle effects and less sensitivity of microwaves to visually distinctive surfaces. Furthermore, the imaging geometry tends to overlook objects which are located in the signal shadow (Figure 16). This prevents, for instance, the automated delineation of dwelling footprints in images acquired at large incidence angles. Even the visual identification is difficult because walls facing towards the sensor are predominantly imaged while the rest of the dwelling is nearly invisible (Figure 50). A robust and transferable method for an automated building extraction, such as provided by object-based image analysis approaches of VHR optical data over refugee camps (Hagenlocher et al. 2012; Lang & Füreder 2015; Spröhnle et al. 2017; Tiede et al. 2017), is not yet developed. As demonstrated in chapter 3.1, the identification of changes at the building level is possible with radar data (Figure 106, POP-TSX-BGD, INF-S1-SYR) but it has to be kept in mind that there also changes which do not cause significant increase or decrease of backscatter intensity, such as burnt dwellings or partially missing building parts. Accordingly, these changes are not measurable by SAR satellites. Lastly, some environments are not suitable for observation by SAR satellites: dense canopies cannot be penetrated by non-military sensors to detect dwellings underneath. Also extreme topographic features can only be radiometrically corrected if a high-resolution DEM is available.

Despite these limitations, only 10 % of the interviewed persons state that they generally prefer optical images towards radar data (Appendix 1), which indicates that these benefits have been recognized and most users are open towards these data.

### 4.1.3 Temporal coverage

As already mentioned, the active nature of SAR sensors allows the acquisition of images at both day and night-time, and independent from cloud cover. Accordingly, the share of **archived images** which are usable for specific tasks is potentially higher than is the case for optical data. In fact, the usability of radar images exponentially rises as more images are available.

The most evident benefit in having a large time-series of images of an area is the dense **monitoring** of changes. It allows to determine the pace of dynamics, such as ecosystem degradation (ENV-A2-TCD) or the spatial distribution of flooded areas (HYD-S1-LAO). With the launch of Sentinel-1, the outstanding archive of ERS-1/2 and ENVISAT ASAR was continued, allowing for the precise and consistent investigation of nearly any land area since 1991 (Figure 101). As many areas are covered at a monthly interval, the description of seasonal phenomena is possible as well as developments ranging over decades. In a humanitarian context, the environment of potential reception sites can be analyzed regarding their long-term suitability as a safe livelihood (e.g. regular occurrence of

floods [HYD-S1-BGD, INF-S1-ETH]), as well as regarding the impact of already existing camps on the integrity of ecosystems (ENV-A2-TCD). This potential is acknowledged among the surveyed users, who see SAR data valuable for the mapping water bodies and other resources (80 %), the provision of images at regular intervals (60 %) and the mapping of landcover / land-use and its dynamics (55 %, Appendix 1).

Furthermore, large image archives provide the possibility to generate **multi-date averages**. As shown in section 3.1.5, a very clear image with nearly zero speckle remains after temporally averaging images of multiple dates (Figure 52). Although such average products no longer refer to a specific date or period, and cannot therefore be used for temporal analyses, their level of detail is significantly increased which makes them suitable for the mapping of persistent phenomena, such as rural settlements (INF-S1-GIN) and road networks (INF-S1-ETH) in unmapped areas. And besides the average backscatter, additional statistics, such as the temporal standard deviation, give further insights on seasonal variations or long-term developments (Santoro & Wegmüller 2014; Schotten et al. 1995).

Another important aspect of archived imagery is the chance to **date specific incidents** in a retrospective. As demonstrated in section 3.1.6, the availability of time-series data allows identifying the exact moment when buildings in an area were damaged or destroyed (INF-S1-SYR). This not only helps to reconstruct the course of conflicts, for example by the provision of situation maps (Gunawan et al. 2011), but also can assist to pursue justice, advocacy, and accountability when it comes to the violation of human rights (Geis & Schlag 2017; Sulik & Edwards 2010). The aspect of time was also confirmed by 50 % of the interviewed people (Appendix 1) who named the tasking of images of specifically defined dates as practical for their work within the humanitarian domain.

The **limitations** of time-series analysis are evident: Many operational satellites acquire images at regular intervals, but they are subject to variations. Some of them are intentional, such as regional focus areas defined in the acquisition plans (Potin et al. 2018), while others are of technical nature, for example, when satellites fail to acquire images or cease to operate. As also shown in Figure 101, a gap exists between March 2011 (failure of ALOS PALSAR) and June 2014 (first images of ALOS-2) where no archived L-band data is available. Unfortunately, a similar period is affected regarding the C-band missions of the European Space Agency (ESA) between the end of operation of ERS-1/2 in July 2011 and the first images of Sentinel-1 in October 2013. Despite the presence of RADARSAT-2 and TerraSAR-X, a generally lower availability of SAR images during this period can limit some long-term applications. However, these limitations are calculable for retrospective analyses because the availability of data can quickly be assessed before starting an analysis. According to this, Davis & Lambert (2007) recommend pilot studies before starting large-scale data collection for emergencies. As shown in section 3.1.6, persistent scatterer analyses for damage mapping (INF-S1-SYR) is only possible with large series of SAR data. Otherwise, backscatter anomalies along a time series cannot be identified to a sufficient certainty.

One key requirement for time-series analysis of SAR images is a careful **radiometric calibration** (section 2.3.1) to remove the effects of incidence angle, wavelength, and sensor characteristics. Otherwise, smaller variations in backscatter could be falsely identified as changes. Another important issue is the treatment of speckle. As filtering is largely dependent from pixel size and overall image noise, a multi-temporal speckle filter should be preferred so that all images are filtered equally and the emergence of pseudo-patterns by the effect of filters on single images is prevented (Maghsoudi et al. 2011). Additionally, if no digital elevation model of high spatial resolution and quality is present, the effect of correction of topographically-induced radiometric distortions is restricted (van Zyl et al. 1993). Currently, freely available DEMs have spatial resolutions of 30 meters

(Bayburt et al. 2017) which is roughly 10 times lower than the pixel size of Sentinel-1 GRD products (Table 32, Appendix 2) and thus, not ideal for their radiometric and geometric terrain correction.

Lastly, the amount of acquired Sentinel-1 images reached, as expected, technical limits when it comes to the provision of data. Since September 2018, the long-term archive has been activated which moves images older than one year into an archive where they can be stored more effectively and sustainably (ESA 2018). Access to these images is still possible and free of charge but unavoidably connected to an active ordering and delivery process which can take several hours until the desired products are made available for download. This will not affect emergencies, such as flooding, where a few pre and post-disaster images are required, but whenever larger time-series are required to respond to sudden events (such as presented in INF-S1-SYR), the access to all historic images can be subject to delays.

#### 4.1.4 Efficiency and operational use

The aforementioned points summarize how the use of SAR data can assist the work of humanitarian aid regarding independency, information, and retrospective. At the same time, this work showed that it can often be effectively integrated into working routines.

In terms of **financial efficiency**, two aspects are worthy of mention. Firstly, the launch of Sentinel-1 can be considered as a new era for radar remote sensing because it provides images at regular intervals free of charge. This allows humanitarian organizations to conduct cost-effective studies without financial risks. The provision of data at no costs is considered attractive by 45 % of the interviewed persons for their work within humanitarian organizations (Appendix 1). Furthermore, archives of other SAR satellite missions are increasingly opened for public use (ESA 2010; Olthof & Tolszczuk-Leclerc 2018; Shimada et al. 2014). Secondly, although this declaration might not be universally valid, radar images are reported as being cheaper than optical data in many studies (Gimeno et al. 2004; Ozden et al. 2016; Sinha et al. 2015; Slater & Brown 2000). However, the fact that only 30 % of the interviewed persons appreciate the lower price of SAR data indicates that, for organizations which are able to pay for remote sensing imagery, the price is a secondary criterion, as long as the images deliver the required information.

Of higher importance is the aspect of **time efficiency** which is provided by SAR data. It was demonstrated that water bodies (HYD-S1-BGD, HYD-S1-LAO), hydrogeologic features (ENV-A2-MLI), as well as settlements and road infrastructures (HYD-S1-BGD, INF-S1-ETH) can quickly be delineated from the images. Furthermore, the localization of resources based on radar data can be achieved with simple methods (ENV-A1-SEN) and is capable of being integrated into existing routines based on optical data (Filloi 2018).

As most images are delivered to the user, at the latest, one day after their acquisition, rapid response within short times becomes possible. The aspect of time is especially valuable in cases of emergencies when quick information is required for decisions on evacuation, medical care or the provision of foods or accommodation. From an application point of view, it makes little difference if an information is extracted automatically or by **visual inspection and manual digitization**, as long as the time required for it is short. Witmer (2015) reports that most studies on remote sensing of conflict areas still prefer visual interpretation because it is faster. However, from a technical perspective, it is prone to errors related to different users' perception, level of objectivity, and their tendency to become exhausted during the mapping process (Ramchurn et al. 2016). Furthermore, the true value of an approach can only be assessed if it is transparent, reproducible, and transferable. It should be therefore of main interest, to develop workflows which are standardized and, at least partly, automatable. Again, the domain with the highest potential for automation are

water body mapping (HYD-S1-LAO) and automated change detection (POP-S1-BGD, INF-S1-SYR). While from a scientific point, only automated workflows are significant, it is the task of the users in humanitarian organizations to decide about the methods to derive the required information, especially regarding speed, reliability, and their level of replicability.

Unfortunately, some aspects of radar data are also obstructive in terms of efficiency and operationalization. Image analysis in some domains still requires careful **preparation** and **user input** which cannot be automated: for example, assessing the impact of changes on ecosystem integrity and human security (ENV-A2-TCH) require the careful definition of LULC classes as well as their weighting by experts. These steps can be integrated in an operational routine, for example by the preparation of a catalogue of classes and weights for different environments, but it is still not advisable to leave crucial decisions to an algorithm. On the other hand, the automated selection of training areas for the supervised classification by predefined criteria (Figure 90) reduces the amount of user input and increases transferability.

As another example, most tasks related to the identification of groundwater (ENV-A2-MLI) are time-consuming and not automatable. Many studies exist on the automated extraction of lineaments (Corgne et al. 2010; Filho & Rossetti 2012; Flores-Prieto et al. 2015; Koch & Mather 1997), but it is the duty of the user to select those relevant to subsurface discharge processes. As demonstrated in section 3.3.2, some of the linear structures highlighted by the radar images were volcanic dyke intrusions without larger impact on the aquifer. Again, the only option to assist operational workflows is to **prepare systematic mapping guidelines** to be followed, as suggested in Figure 83, so different mappers come to similar and comparable results in their areas.

Finally, the derivation of operational or automated routines can also be harmful, because they can make users too comfortable with their standards which bears the risk of being “locked-in” and missing **technological advancements** and new opportunities (Pentland et al. 2011). A balance between the efficient use of SAR data within operational routines and openness towards change is to be found. Furthermore, as shown in the studies on dwelling estimation (POP-TSX-KEN, POP-A2-NGA), the integration of additional training data can increase the prediction quality. With each passing year, **reference data** has to be updated or extended. Otherwise, the classifier is ill-trained on the newly acquired SAR image which already contains these changes. A similar issue is related to the derivation of biomass by field reference data (ENV-A1-SEN): although stable relationships between backscatter intensities and above ground biomass were found (Table 23). If no more measurements are collected in subsequent years, the potential to increase the predictability of the model is lost. Generally, an easy way of adding new findings, opinions, measurements or other data sources to existing approaches must be found in order to make full and efficient use of operational pipelines. One solution is potentially provided by self-taught image classification approaches which rely on the flexible input of reference data (Zhu et al. 2017).

Concludingly, only 20 % of the interviewed people see SAR data as an attractive input for operational routines. This study showed their potential for a time-efficient extraction of desired information and can be the beginning of further discussions on the operational use of SAR data in the humanitarian domain. Still, it must be denoted that some of the presented case studies are not automatable yet because they require a higher degree of user input but are still ready for operational use. Most of the restrictions mentioned above are not directly linked to the nature of SAR data, but rather refer to general constraints regarding data acquisition, expert-based interpretation, project management and processing strategies. This argument is confirmed by Zhang & Kerle (2008) who identified **structural hurdles** in data handling as one main barrier for effective emergency response, even if these data are provided in near-real time.

### 4.1.5 Synthesis

As shown in the previous section, images from radar satellites have certain features which make them attractive as inputs for analyses in a humanitarian context. The most important ones are the degree of information, the availability within long-time archives, as well as the potential to be integrated into operational routines for rapid disaster response. These aspects also have their downsides or bring new challenges. They are summarized in Table 26 which systematically lists these features and rates them regarding their advantageous and limiting aspects with respect to the use of SAR imagery for different fields of use in the humanitarian domain. The symbols are defined as follows:

- ▲ clearly advantageous factor
- △ predominantly advantageous factor
- factor has no or only little effect in this domain
- ▽ potentially limiting factor
- ▼ clearly limiting factor

It has to be noted that many aspects have both positive and negative implications and the intention of the table is to provide an overview which is comparably easy to read. The sometimes contradicting properties of SAR images were carefully discussed in the previous section.

Table 26: Potential and limitations of SAR images for humanitarian operations

Fields of use \ Features of SAR images		Mapping camps and dwellings	Mapping infrastructures	Monitoring camp dynamics	Identification of damages	Mapping water bodies / floods	Measuring topography	Allocating groundwater	Assessing environmental impacts	Continuous biomass estimates
Information	cloud-free images	△	△	▲	▲	▲	△	△	▲	△
	image texture and scale	▲	▲	△	△	▲	-	△	▲	△
	speckle effects	▽	▼	▼	▼	▽	-	▽	▽	▽
	geometric effects	▼	▽	▽	▼	-	▲	-	-	▽
	InSAR: phase information	△	△	△	▲	-	▲	-	△	-
	PolSAR: wave polarization	△	△	△	△	△	-	▲	▲	▲
Time	long-term archives	△	△	▲	▲	▲	-	△	▲	▲
	dense image series	△	▲	▲	▲	▲	△	△	△	△
	tasking specific dates	▲	△	▲	▲	▲	-	-	-	△
Use	automatable	△	△	▽	▲	▲	▲	▼	▽	▽
	operationable	△	△	▽	▽	△	▲	△	△	▲
	rapid response	△	△	△	▲	▲	-	-	-	△
	techn. easy to perform	△	▲	▲	▼	△	▼	▽	▽	▽

## 4.2 Future challenges and developments

Based on the findings from the case study, as well as on the previously identified potentials and limitations, this chapter

- identifies challenges which were not solved within this work,
- defines points which must be improved to make SAR images more useful for humanitarian operations, and
- discusses developments which will provide new opportunities in the future.

### 4.2.1 Dissemination and scientific demand

As demonstrated in chapter 1.3, there are not many studies which use radar remote sensing as a direct input for the derivation of information for humanitarian purposes. Over 16 years after Wegmüller et al. (2002) presented the potential of radar imagery for disaster management and humanitarian relief, only a few concrete case studies followed which actually made use of this potential. It has to be mentioned that, at this time, there was a general skepticism towards remote sensing for humanitarian purposes: Kelly (1998) reports of a culture which sees ‘flying around in aircraft’ as a waste of money that is better spent by directly helping people in need. Twenty years later, many of these doubts are already eliminated, but a general barrier lays in the different interests between the scientific community and those who might make practical use of their findings: while scientists predominantly pursue developing innovative techniques, humanitarian aid seeks for reliable and field-tested approaches. Accordingly, the **aspect of novelty and innovation** seems to be desirable for the scientific side while it is rather unattractive and connected to risks for the humanitarian side. However, as indicated by the survey conducted among people working in the humanitarian domain, 80 % of the interviewed persons named optical remote sensing images as a frequently used source of information for their work, while only 10 % of them make regular use of SAR data. On the other hand, 90 % called themselves ‘curious or interested’ regarding radar data (Appendix 1). This clearly testifies that the original skepticism towards remote sensing is progressively retrenched, but progress seems to be slower in the case of radar imagery.

The survey indicates a general openness towards new information sources and methods, but not enough **successful examples** are provided yet to the humanitarian community which demonstrate the practical use of SAR data for their work. A honorable attempt to increase the attractiveness of radar images was made by Amitrano et al. (2013) who presented their work on SAR data for humanitarian purposes on the ‘Global Humanitarian Technology Convergence’. Such events, where engineers, scientists and humanitarian professionals come together, are crucial for both sides, because they allow to the raising of questions, discuss various points, find similar interests, identify wasted potential, and finally reduce doubts regarding previously unused methods.

The only way for SAR imagery to find its way “from theory to applications“ (Ulaby et al. 1990) is the provision of more case studies for concrete situations, such as presented in this work. In the following, lack of research is defined, and five concrete topics are suggested for future investigations, which are ideally disseminated outside the radar community.

**Object-based SAR analysis for dwelling detection:** While object-based methods on VHR optical images are widely investigated and applied in humanitarian context (Hagenlocher et al. 2012; Lang et al. 2018; Tiede et al. 2017; Tiede et al. 2010), their application on radar images is still a challenge. Currently missing are adaptable workflows which use segmentation techniques to aggregate pixels of radar images to analyze and classify them as image objects, such as suggested by Boldt et al. (2014). As the spatial resolution of SAR sensors successively reaches similar levels of detail, their potential for the delineation and counting of dwellings within camps is immense.

**Backscatter signature analyses of light construction materials:** As demonstrated in the case studies of chapter 3.1, the light construction materials of informal settlements and makeshift dwellings are not ideal targets for microwaves, especially when compared to solid buildings of urban areas. Not enough studies exist which investigate the subtle interactions of these materials with radar signals of different wavelengths. One example is given by Kempf et al. (2007) who generally compare the variety of backscatter signatures within urban areas. The methods are already developed involving simple textural measures (Voisin et al. 2013), the SAR simulation of built-up objects (Auer et al. 2010; Franceschetti et al. 1995), polarimetric analyses (Zhai et al. 2016) or multi-temporal tomographic approaches (Porfiri et al. 2015). However, no studies so far exist in refugee camp environments.

**Template matching for automated identification of infrastructures:** Similar to the object-based approaches mentioned above, template matching is widely acknowledged for VHR optical imagery, for example, with the automated extraction of dwellings in refugee camps (Ghorbanzadeh et al. 2018) or the mapping of roads (Lin et al. 2012). Their potential for applications in the humanitarian domain is manifold, but only a few use radar images as an input. One reason was the distortion of fine details by speckle effects which limit the precise generation and detection of templates. But as shown in section 3.1.5, the effect of speckle can be completely removed from images when long time-series are combined in a temporal average. The nearly unlimited availability of Sentinel-1 data brings new opportunities for template matching which makes it a valuable input for humanitarian applications in previously unmapped areas. Furthermore, the degree of objectivity can clearly be increased towards the manual identification demonstrated in section 3.1.5.

**Automated replacement of cloud-induced gaps:** As the survey showed, most users feel more comfortable with optical data. Whenever their analysis is limited by patches of cloud cover, SAR data can be used to fill these gaps. This was already successfully demonstrated by Eckardt et al. (2013) and Braun et al. (2016a) but no automated approaches exist so far. As they would be applicable to any thematically classified product, their application spectrum within humanitarian operations is wide: reconstructing dwelling densities within camps, closing gaps in land-use or landcover classifications for the monitoring of resources or mapping water bodies which are partially covered by clouds.

**Integration of passive radar imagery for regional studies:** As shown in section 3.3.4, the integration of passive radar data can increase the prediction accuracy of regional analyses. Although collected at a lower spatial resolution, their information content was proven complementary because their wavelengths are considerably outside the range of active SAR systems. Their acquisition principles allow high repetition rates and therefore the precise temporal monitoring of rapidly occurring changes at the ecosystem scales. Classical approaches are surface temperature, soil moisture, and precipitation rates (Das et al. 2011; Ulaby et al. 1990) but in the humanitarian domain, they could be integrated into existing approaches on natural resources (e.g. biomass, section 3.3.4), large-scale ecosystem degradation (Berry 2008; Lonergan 1998), and food security (Caniato et al. 2017; Thenkabail et al. 2010).

**Sentinel-1 for emergency response:** One of the key tasks of the Sentinel-1 mission within the Copernicus program is the assessment of risks and natural disasters (Aschbacher 2017). While its analytical and scientific contribution to hazard mapping is already widely investigated (sections 3.2.1 and 3.3.1), only a few studies present their use for short-term derivation of information in cases of emergencies. To gain trust and credibility in the humanitarian community, this needs to be addressed by scientists providing more examples with an application focus on rapid response.

## 4.2.2 Data availability and handling

Besides analyzing the data, a large need for concepts was identified in this study which grant an efficient handling of the data within organizations. These concepts have to address the aspect of file size, legal restrictions, and the management of data flows. The main challenges are discussed in the following.

No data – no information. While this statement seems obvious, it refers to several aspects which are related to obstacles and opportunities for the use of SAR data by humanitarian organizations. Firstly, high and very high-resolution radar images are provided by commercial providers and acquisition costs are not affordable to smaller organizations. Also, not all organizations are **experienced** in the tasking, ordering, and retrieval of such data in emergency situations where time is scarce. For this reason, the International Charter on Space & Major Disasters was established in 2000 as an agreement among major space agencies to provide free satellite data upon tasking in the case of an emergency (Jones et al. 2015). Of the currently 28 satellite missions included, only 5 are SAR satellites (ALOS-2, Kompsat-5, RADARSAT-2, Sentinel-1, TerraSAR-X). For the year 2017, it was activated 44 times (International Charter 2018), mostly in the context of flooding (18) and ocean storms (18), but also for earthquakes (7), wildfires (5), search and rescue operations (2), and landslides (1), providing a total of 3,628 images in 2017 of which 23.5 % were radar images. As shown in this work, flooding is particularly well-suited to be assessed with SAR images, given that images proximal to the incident are available. To increase their availability for a more effective response, it would be beneficial if other radar sensors, such as CosmoSkyMed, RISAT-2, or PAZ, as well as future missions (chapter 4.2) would also be part of the charter. To achieve this, their involvement has to be assured already during the planning and financing phase of upcoming satellites. This was again emphasized by Teeuw et al. (2013) who stated that “the provision of free satellite data needs to be improved”.

Even if the data is not provided for free, the **financial efforts** seem manageable: The tasking of new high-resolution radar imagery of the ten largest refugee camps costs between 30,000 and 187,000 Euro, depending on the selected sensor and imaging mode (Appendix 15). As these already host 2.2 million displaced people, the price per person lies between 0.015 and 0.088 Euro. Having SAR images of large camps at annual intervals would significantly increase this contribution to humanitarian aid and foster their integration into monitoring and response routines. Additionally, a comparably up-to-date pre-disaster image would be available in cases of emergencies, for example for the mapping of damages or floods. According to estimates of the UNHCR (2018b), about 20 million people lived within refugee or IDP camps. Extrapolating the numbers from above, roughly between 300,000 and 2 million Euro were required to cover these refugee camps at an annual basis for a better preparedness. While this sum seems much at first glance, its share of the total funding for humanitarian assistance of 27.3 billion US dollars for the year 2017 (Urquhart & Tüchel 2018) is rather small. For the future, procedures for joint funding or collaborations with distributors of spaceborne SAR imagery might be a worthwhile discussion among organizations, institutions and governments.

Furthermore, there are portals, services, and programs which already provide information derived from remote sensing imagery to humanitarian organizations, such as UNOSAT (Schaeffer 2016), UN Spider (Backhaus et al. 2010), SERTIT (Tholey et al. 2011), ReliefWeb (Wolz & Park 2006), or the Geohazards Exploitation Platform (Laur et al. 2016). They are experienced with the rapid response to emergencies and can shorten the time required to deliver useful information. This is also confirmed by Zhang & Kerle (2008) who state that “the time-consuming aspect is not the data acquisition itself, but rather the transfer, processing and dissemination of useful products to

emergency response personnel in the field, a requirement well served by Charter-like activities”. So, even if the data is not processed by humanitarian organizations themselves, the effective use of remote sensing products is fostered. In return, the operators and providers of the satellite data have potential benefit because their contribution to such collaborations is publicly credited for directly assisting to solutions for current societal problems. As an example, ASTRIUM (2011) published a document demonstrating the use of TerraSAR-X for the retrieval of information within the Dagahaley refugee camp. Again, a stronger integration of SAR imagery in such processes should be aspired. This can be tackled at several levels of technical complexity:

1. **Basic integration:** As a minimum level of operationalization, SAR data can be used for the quick and manual derivation of information, for example for the mapping of floods (section 3.2.3). This can be done by the humanitarian organizations themselves by following standardized mapping protocols in the case of an emergency. In-house interpretation of the data reduces the time required for communication with the aforementioned service providers and allows quicker decisions. As another example, SAR data could be integrated into humanitarian mapathons, for example when it comes to the mapping of infrastructures for medical field campaigns, as presented in section 3.1.4. Although manual derivation of information is mainly suited for time-critical decisions, it can also be used to get a general understanding of situations, such as gradual changes around refugee camps (section 3.1.4).
2. **Standard integration:** A more advanced level of operational SAR usage is the preparation of ready-to-used work flows to derive standardized products upon request. This is how most of the aforementioned services operate to provide reliable information in a transparent and automated or semi-automated way. (Boccardo & Tonolo 2015). These workflows include the steps of image acquisition, information extraction and visualization. According to Voigt et al. (2016), the pure availability of earth observing satellite systems has significantly increased during the past 15 years and therefore is no longer a limitation to operational routines. As already stated in the previous section, the main challenge will be to work on automatable and transferable workflows based on SAR data to contribute to this development.
3. **Holistic integration:** To make the most efficient use of SAR data in cases of emergencies, not only the derivation of information has to be automated but also the provision of ready-to-use information products to the end user. This aspect clearly goes beyond the compilation of maps and involves the careful selection of data formats, the transfer of information, and the adapted presentation to the workers in the field. Füreder et al. (2012) suggest GoogleEarth kml files instead of commonly used PDF maps, because they allow viewing the data in a spatial context which can be adjusted by the user. Also, web-based applications are of greater value, especially when users can contribute to the available data and keep it updated (Knoth et al. 2018). Especially in this holistic approach, it is no longer important if data was derived from optical data or microwave sensors, and focus is shifted towards the effective provision of information. The only limitation which remains in this context is a stable and powerful internet connection which is still a constraint in many parts of the world, especially in remote areas, such as refugee camps (Teeuw et al. 2013).

### 4.2.3 Collaboration and transfer of knowledge

As argued in the previous sections, a successful integration of SAR imagery into humanitarian aid requires mutual interest between Scientific communities and relief organizations. Even if both sides have the same interest, namely finding solutions for specific questions, the way of communication seems fragmentary: scientific achievements are published in technically-oriented journals, while humanitarian aid is communicated via organizational reports and public media. And

neither group belongs to the common audience for the aims and achievements of the other. This is confirmed by Papp & Barclay (2018) who report that “the space industry and research institutes rarely give presentations at NGO conferences” and, in turn, “NGOs frequently have a lack of presence in workshops and congresses on new technologies”. This point refers to the arguments given in section 4.2.1, namely that stimulated **inter-disciplinary communication** could increase the benefit of SAR data in the humanitarian domain. Above that, they argue for officially arranged partnerships to overcome these rather structural barriers. This could be fostered from the side of humanitarian organizations who, once the potential and limitations of radar images are understood, could be more aggressively involved in the definition of needs, the selection of methods, and the creation of results. Thus, they would no longer be seen as mere customers of these products, but rather be a part of the processing chain and the development of new techniques and products. In turn, technologically-oriented research has to place more emphasis on the understanding of needs and the usability of their work (discussed with more detail later in part 4). Furthermore, Papp & Barclay (2018) state that “change in NGOs comes from bottom up-demands”, which underlines that workers in the field have to understand how results were generated to express constructive feedback and re-phrase their exact needs. This is directly confirmed by an open answer retrieved in the survey (Appendix 1):

*“I am not particularly well versed on the technical side of radar imagery (or remote sensing in general). So, lots of these sound useful to me but I need to be educated on the limitations and appropriate usage of radar data. It's very easy to grab data and go in humanitarian settings without properly understanding where you should be cautious using it.”*

This answer again underlines that an **understanding of the technical aspects** on the user side is a key requirement for the integration of SAR products and can increase their usefulness. Above that, stronger collaborations within relief teams (workers in the field and data analysts) but also between organizations can truly boost the development of processing pipelines, data handling strategies, and monitoring routines (Cowan 2011).

As strategies, humanitarian NGOs have their own GIS units which not only work on the development of geospatial solutions for their colleagues, but also facilitate the **exchange** with external parties when it comes to the transfer and adaptation of scientific innovations. Another form of **involvement** lies in the provision of field information: as many of the investigated areas are not easily accessible or dangerous for people outside the humanitarian domain, relief workers can be closely integrated into the process of data analysis by providing in-situ data to facilitate the interpretation, calibration, and validation of information retrieved from the radar images. Possible ways are photographs, measurements, surveys, samples, or GPS points and tracks, although their collection can be time-consuming and is sometimes legally restricted (Beaudou et al. 1999). By contributing to data acquisition, relief workers can actively participate in the process of information generation and design of the study, thus being able to express or refine their requests, and gaining a better understanding of the final products. This is confirmed by Bjørge (1999) who states that, “in order to streamline image acquisition, analysis and information dissemination it is important to develop relationships among image providers, value adding companies and relief agencies”. It will be one major challenge in future studies, to define, manage, and maintain these relationships among all involved parties.

Finally, besides the sheer publication of relevant studies, the scientific community has to foster the **transfer of knowledge** and practical skills into the humanitarian domain. As underlined by the statement from the survey cited above, there is a clear demand for educational resources, practical

workshops, and other forms of capacity development which assist organizations, not only to adapt the proposed techniques, but also to contribute to the development of innovative and integrated methods. This also applies for volunteered geographic information, as suggested in section 4.2.2, only if SAR-related characteristics, such as speckle, backscattering, polarization, and geometric effects, are well understood, radar imagery can be integrated into working routines of both experts and volunteers. This demand is underlined by Teeuw et al. (2013) who state that "the 'peopleware' component of geoinformatics needs to be strengthened, with the provision of free training materials that use disaster management examples". For this reason, many forms of capacity development were established during the last decade. A brief summary of existing resources and efforts is given in Table 34 (Appendix 14). It demonstrates the multitude of strategies to impart knowledge on SAR remote sensing, ranging from materials for self-study, over online webinars which allow direct contact to lecturers via blended learning, as well as on-site teachings of specialized topics and applications. Yet, training activities specialized on the application of radar imagery in humanitarian settings do not exist yet. These would surely boost the transfer of this technology into the work of relief agencies, NGOs, and regional administrations. The responses of the survey (Table 28, Appendix 1) indicate that there is large interest in SAR data but workers in the humanitarian domain are mostly lacking the technical expertise or the time to acquire it.

Concludingly, the main challenges in the future lay in the way scientists and experts from the humanitarian field work together regarding the definition of problems and information demands, the joint selection, preparation and analysis of the data, plus the bi-directional communication of skills for a better mutual understanding of each side's expertise.

#### 4.2.4 New sensors and technologies

Under the currently observable pace of technological innovations, this outlook can only be a snapshot. It will therefore focus on three major points: satellites, tools, and innovations, with none of them being covered in entirety. Still, the most important trends and their impact on the scientific development of radar-based methods and humanitarian action shall be shortly described here.

We currently face the most prosperous decade regarding spaceborne remote sensing. Not only are more imaging satellites orbiting the earth than ever, but with the Copernicus program having revolutionized the provision of free imagery, earth observation has turned into a big data business (Ma et al. 2015; Sudmanns et al. 2019). That means, the availability of suitable data and its access for concrete information needs will play a **minor role** in the future. And with the aforementioned Copernicus program and the NASA Earth Sciences Disaster program, civil protection and disaster response have been manifested into institutional frameworks (Freilich 2018).

Currently, Sentinel-1 A and B deliver images at repeat cycles of 6 days, and revisit times up to one day in suitable regions. Their successors, Sentinel-1 C and D will be launched successively as soon as either 1-A or 1-B fails to guarantee a long-term continuation of the mission, and therefore all related operational services (Potin et al. 2018). Data availability is ensured within 24 hours after image acquisition and even within three hours for selected priority areas (Potin et al. 2018). Including regions with high flood recurrence and high social vulnerability into this **near real-time** (NRT) concept would be an immense achievement for humanitarian flood mapping and emergency response.

As for commercial satellites, TerraSAR-X and TanDEM-X have not only doubled their expected lifetime since their launch in 2007 and 2010 respectively, their fuel levels currently allow an operation for the next 3 or 4 years (Buckreuss et al. 2018). Because they were used to globally map every land surface between January 2010 and December 2015 (Zink et al. 2017), an excellent **archive**

of images was collected to be used as pre-disaster information for emergency response within cities as discussed in section 3.1.6.5. They are complemented by the PAZ satellite, launched in February 2018, within a cooperation between Hisdesat and Airbus to provide a constellation of three sensors of similar configuration to reduce their revisit time up to 4 days, thus enabling faster disaster response and higher potential for repeat-pass interferometry (Bach et al. 2018). Radarsat-2 will also be followed by the Radarsat constellation mission (RCM) to be launched in early 2019, consisting of three C-band SAR satellites, with a strong focus on data continuity and enhanced operational use (Lisle et al. 2018). As Radarsat-2 is already participating in the disaster charter mentioned in section 4.2.2, it can be expected that this mission will also be available for emergency response. Lastly, CosmoSkyMed is followed by the second generation (CSG) which consists of two satellites (together with SAOCOM) which will be operating from 2020 and 2021 under various standard and experimental imaging modes (Mari et al. 2018).

Further upcoming missions are following the Smallsat concept, which aims at the launch of several SAR satellites of comparably low cost for significantly higher coverage rates (Freeman 2018). Examples are NovaSAR-S, a spaceborne S-band radar sensor which was launched in late 2018 (Márquez-Martínez et al. 2017), or ICEYE, the world's first SAR satellite with a launch mass of under 100 kilograms (Werner 2018). These missions are still in their calibration phase and their contribution to humanitarian action is still unknown, but they potentially increase the **availability** of imagery for different kinds of information requirements.

A last kind of future SAR missions are based on new technologies and highly specialized towards the observation of **environmental systems**: TanDEM-L is an upcoming bistatic SAR constellation of two L-band sensors with swath widths of up to 350 kilometers at spatial resolutions of three meters (Moreira et al. 2018). Because of its large wavelength, it is sensitive towards vegetation and forest biomass and will be of high use for environmental monitoring, such as the impact assessment demonstrated in chapter 3.3.3 and the large-scale estimation of biomass (chapter 3.3.4). Its launch is expected in 2020 with expected downlink volumes of up to 7 TBs per day (Moreira et al. 2018). This will not only lead to unprecedented amounts of data, but also bring the necessity for internet-based cloud processing techniques for its users. This point will be discussed later in this chapter. The same applies for the Biomass mission to be launched in 2021 which aims at a global and systematic derivation of forest biomass at a spatial scale of 4 ha and deforestation patterns at 0.25 ha. It employs a P-band transmitter and will be the first spaceborne tomographic mission, thus allowing the analysis of vertical structures of forest bodies (Fügen et al. 2018). Both TanDEM-L and Biomass are highly innovative techniques and will provide new possibilities in earth observation which will also be useful in the humanitarian domain or for emergency response.

As already indicated above, the increased availability of SAR data leads to a demand for **effective processing strategies**. The most traditional way is the processing with specialized software on local computers, which can be costly to acquire and maintain. Regarding software, Teeuw et al. (2013) demanded, "we need more free geoinformatic software for disaster management application". This issue has been addressed by various free or open-source programs or packages for the processing of radar data, such as *ESA SNAP*, *PolSARpro-BIO*, *GMTSAR*, *ASF MapReady*, *WinSAR/ISCE*, *DORIS*, *StaMPS*, or the *Orfeo Toolbox*, and substantial progress must be attested for the last decade. The free access to processing frameworks for radar imagery has essentially lowered the barriers for people to enter the field of SAR analysis for many kinds of applications. However, they differ regarding their potential to develop operational routines or services, and it often takes advanced skills to automate processes for a more efficient data handling.

For this case, several platforms were established in the last years which assist users in the retrieval of operational services for specific information needs. The most famous is probably the *Copernicus Emergency Management Service* which can be activated by EU member states, associated countries, as well as by humanitarian aid organizations, in the case of natural and technical disasters and, as explicitly mentioned, humanitarian crises (Ajmar et al. 2017). Upon request, rapid maps delineating or evaluating the respective events are created based on Sentinel-1 imagery and other suitable Copernicus data. As another example, *HYP3* was developed by the Alaska Satellite Facility (ASF, Arko et al. 2016) where users can define an area of interest to receive geocoded Sentinel-1 products whenever new images were acquired, which can then be used for the detection of landcover or surface elevation changes. Cloud-based portals for the response to natural hazards are the *Geohazards Thematic Exploitation Platform* (G-TEP, Laur et al. 2016) which allows the derivation of SAR-based information for earthquake response and landslide analysis, or the *SARVIEWS Hazard Platform* of the ASF (Meyer 2017) for the automated generation of maps on natural hazards. All these platforms and portals facilitate the access to SAR data and value-added products for rapid response. Given by the nature of SAR data to be independent from cloud-cover, radar imagery plays an inherent part already. With the increased availability of new image products delineated above, the foundation of these portals will be strengthened.

On the scientific side, the dependency of SAR data from ancillary information described in section 4.1.1 can be addressed by the integration of crowd-sourced or volunteered **geographic information** (Sui et al. 2013) as an important complementary part. This integration must be facilitated by user-friendly online portals, effective cloud infrastructures and mobile apps, for a standardized and decentralized data injection as an official input into scientific development of innovative methods. Mulder et al. (2016) outline how the information flow between affected people, data collectors, translators, data analysts, data processors, and decision makers must be organized for an effective and inclusive humanitarian response and not only highlight the potential but also threats of crisis mapping. Two examples are the “Digital Humanitarian Network” which is a platform to coordinate and facilitate the collaboration between professional humanitarians and private digital volunteers (Meier 2015), or the “Humanitarian OpenStreetMap Team” (Palen et al. 2015) which consists of over 150,000 participants who map buildings and roads to assist relief operations. As already suggested in section 4.2.4, SAR data needs to be part of this process.

Lastly, big data approaches and methods of machine learning, such as convolutional neural networks and deep learning, must be **optimized** to match the characteristics and peculiarities of SAR data. As indicated above, the amount of data will continue to increase to an extent which is no longer processible by traditional methods of image analysis. Both the number of images and their file size resulting from large footprints and increased spatial resolution will require automated methods based on intelligent learning (Gong et al. 2017) and distributed-processing, such as the Google Earth Engine (GEE), NASA Earth Exchange (NEX), the Australian geoscience data cube (AGDC), or the JRC Earth Observation Data and Processing Platform (JEODPP, Soille et al. 2018). Currently, only GEE and JEODPP feature access to radar data, and it is the duty of the space agencies, governments, and data distributors to stimulate the integration of current and upcoming SAR missions into these portals for capable academic involvement and innovative solutions.

#### 4.2.5 Utility and data ethics

This last chapter addresses key questions raised in the scope of humanitarian remote sensing with a special focus on radar data. As shown in this work, the transfer of SAR images, and technical solutions in general, into the world of humanitarian aid is slow and longsome. While the main aim

of this thesis was to lay a solid groundwork and to demonstrate their applicability, this section addresses two less technical aspects which might be further reasons for the limited use of radar in the humanitarian domain.

The first addresses the fact that information might be a key requirement in humanitarian crises, but especially in cases of emergency, the rapid delivery of help outranks the development of deliberate strategies derived from carefully investigated information. In other words: Understandably, in urgent situations priorities rather lay on the provision of aid than on the preparation, application, and validation of geospatial techniques, especially if the techniques are not fully developed yet (Monaco 2014). Accordingly, the use of radar imagery, and earth observation methods in general, can bring substantial benefit to crisis situations, but only if the financial and human resources allow it. Paul Carrion, a humanitarian aid worker with over a decade of field experience in various emergencies, raises the legitimate question, “If all you have is a hammer... how useful is humanitarian crowdsourcing?” (Carrion 2015). He certifies high potential for geospatial methods in the humanitarian domain, but states that simply increasing the quantity of data does not necessarily bring a significant improvement or benefit, especially for large-scale humanitarian emergencies. A set of **validation criteria** for Copernicus services in the domain of human security was developed by d’Oleire-Oltmanns et al. (2015) which includes relevance, readability, impact, and transferability. It allows users of geospatial products or services to give a distinct feedback and to improve the utility and usability of the provided information. This feedback is strongly required, so that the delivered products are not only correct, but also useful.

Besides that, as shown in this work, radar imagery is often prone to misinterpretation and derived products need to be discussed and explained regarding their information content and possible error sources. If these are not communicated to the users, the utility of an information, for example a map, is limited. Consequently, the development of SAR-based approaches for humanitarian action needs to be balanced regarding correctness, quick delivery, and utility for the user. This is also emphasized by Cowan (2011) who stated that, “Before geospatial analysis can become a consistently beneficial and reliable tool for responders, a re-design and multi-agency adoption of a standardized assessment product [...] is necessary. This product should come on the heels of a comprehensive framework that not only assesses spatially referenced needs, but equates resources mobilized to meet those needs”. This again underlines the appeal from section 4.2.3 that users must not be seen as pure customers, but rather be an **integrated part** in the development and validation of methods. This again would help academia to shed the public opinion that scientific research is done in an ivory tower and not really a contribution to society (Wiek et al. 2012). The true point here is that the need for innovation and novelty often results in a loss of focus for the real problem. This was nicely quoted in the field guide to humanitarian mapping by MapAction (2011), stating “forget GIS – I just need a map!”. This means, if the result is not sufficiently usable by the persons in the field, any technique is futile. Again, this applies for SAR in peculiar where solutions for distinct problems are still to be found (see the call for research topics in section 4.2.1) and the technological progress outlined in section 4.2.4 which requires the development of new approaches. Lastly, with increasing amounts of imagery and new processing strategies becoming accessible to nearly anyone, researchers should not lose focus on the spatial component of the used data and its interpretation within a wider thematical context (Shook et al. 2018).

Besides a geographical and societal focus, automated image analysis should consider ethical aspects: Describing the surface of the earth by methods of remote sensing and data analysis seems to be a rather objective and neutral process, but in fact it contains several highly contested aspects and can have far-reaching social implications (Mulder et al. 2016). Most of them result from the fact

that earth observation is by definition a top-down approach to the support of decisions and the development of strategies. This can lead to a strong **power asymmetry** between the ones who map an area and the ones being mapped, which are mostly not involved in the process, nor are they asked for their permission (Kuffer et al. 2018). While this is a serious issue for VHR optical data, radar imagery does not reveal too much details pertaining to single persons or their private properties at first sight. Still, it becomes a problem as soon as the information is harmful to the persons living within a certain area. For example, the mapping of slum areas in cities, as described in section 3.1.1, can lead to the stigmatization or criminalization of entire groups of people as low-income classes living in informal or even illegal buildings (Gilbert 2007). Instead of assisting sustainable urban development and integrated planning, studies report how results retrieved from remote sensing were used for forced evictions of such deprived areas (Kuffer et al. 2018; Mahabir et al. 2018; Patel et al. 2015). Special care has therefore been taken by scientists to **avoid stereotyping** and to find a healthy balance between scientific terminology and undiscriminating language. As another linguistic aspect, Ciesla (1991) argues that the term of “ground truth” is not ideal because of its absolute and judgmental nature, and suggests to see it as a “as a periodic reassessment of values”.

Security implications of remote sensing also arise in refugee camps where often ethnic minorities are gathered seeking shelter from forceful displacement. Mapping these camps as described in chapter 3.1 might be helpful to those providing basic services and medical aid, but brings additional danger to the already exposed and **vulnerable inhabitants** which are often not protected by national laws (Carlin 1990). This also applies for environmental impact assessments of refugee camps as suggested in section 3.3.3: While the neutral description of changing ecosystems aims to assist sustainable land management and to avoid uncontrolled degradation, environmental impacts were misused by both societies and politics to argue against hosting refugees in general for reasons of national resource protection (Martin 2005; Rutinwa 2017). Misleading interpretation cannot completely be avoided, but has to be considered when conducting ecological studies in a humanitarian context. At larger scales, remote sensing of natural resources can generally violate the territorial sovereignty of states: Wasowski (1991) argues that especially developing countries are politically and economically pressured by the international community to control large-scale clearance of their tropical rainforests because global climate interests, without assuring financial or technical aid, also neglecting their economic dependency and often limited capabilities to control these processes. Against the background of the expected global biomass estimates derived from upcoming SAR missions (section 4.2.4), this aspect should be considered and discussed along with the ongoing discussion of changing environments.

Lastly, the aspect of crowdsourced geographic information, which was praised at many times in this work as an ideal complementary information contributing to the validation of radar analyses can have its downsides as well: while its **decentralized structure** and low technical barriers for new entrants brings large potential for the rapid and joint mapping of information, it still lacks reliable validation mechanisms which grant that the collected data is correct (Meier 2015). Moreover, as any technology it is vulnerable to manipulation in favor of certain political opinions or mobilization. Crowdsourced information has therefore to be integrated with care and ideally checked against manipulation and systematic bias.

All of these questions on utility and ethics raised above are not to be easily answered, but it becomes clear that solutions can only be found in an inter-disciplinary and inter-cultural discourse and it should be the duty of the scientific community to jointly initiate and moderate this dialogue. Furthermore, geospatial scientists should more intensely engage in the discussion and

interpretation of their own results, instead of simply providing maps to their clients from the humanitarian domain.

### 4.3 Final remarks

This work demonstrated the multitude of possibilities to integrate SAR into the humanitarian domain to facilitate planning, decision making, and the provision of aid. The survey showed that radar images are known to those working with geospatial data in this field, but it is still mainly considered as an alternative when no optical images are available. As demonstrated in the case studies, radar imagery can be more than just a necessary evil, provided that its potential is fully exploited, and its limitations are understood. This work showed both aspects and communicated that there is a need for specifically developed methods for radar information. Consequently, the expectation that workflows applicable to optical imagery can simply be transferred to SAR data has to be dispelled. On the other hand, the survey also indicated large interest and openness towards radar images and named time limitations and technical complexity as the main barriers. Although this work does not intend to serve as a training manual for beginners, it still elaborates the most relevant aspects for the field of humanitarian action, and thus, serves as a potential starting point for people which are interested to engage in this field.

Referring back to the scientific gaps identified in section 1.3.4, this work tackles most of the currently existing problems: It communicates the interpretation of backscatter intensity and its manifold use by innovative methods, and reduces its inherent complexity within tangible use cases. In this context, classical forms of data processing (image interpretation, binarization or classification) are involved as well as new technical developments (cloud computing, open-source software, big-data solutions). While the application of traditional methods underlines the potential integration of radar data into existing frameworks, the aspect of technical progress constitutes SAR data as a key component ready for future implementation.

The highest interest of humanitarian action lies in the spatial and temporal resolution provided by SAR data. VHR radar images gradually catch up with the spatial resolution of optical images, which makes them most useful for the focused and in-depth inspection of small areas. Here, this work showed how this new level of detail can be handled efficiently. On the other hand, the high repetition rates of operational missions, such as Sentinel-1 or ALOS-2 allow the unprecedented extraction of information on dynamics and the monitoring of even subtle changes independently from cloud cover, accordingly, in any part of the world. One major challenge for operational tasks will be to find a balance between the level of detail, the coverage, and the price of imagery when it comes to the selection of a suitable data source, especially for long-term tasks.

Additional to these advantages regarding resolution, the utility of SAR data is completed by the sensitivity of the waves towards surfaces characteristics. Their potential to map man-made structures, vegetation volume, topographic variations, or water surfaces makes them a key source of information for humanitarian operations.

To achieve a sustainable and useful integration of radar data for humanitarian work, people at the interlinkage between science and application take a key role. Not only do they need the technical expertise to establish workflows to provide information, but also will they have to moderate the needs of the workers in the field and the academic sector which develops new techniques and solutions. This is especially important because technologic progress will continuously develop new satellites, data processing strategies, and ways of communication. This fact will make it even more important that solutions are developed in close collaboration with all involved parties and that the ones in charge of processing the data can elaborate on the selection of suitable methods, and are

capable of spatial thinking and interdisciplinary communication (Shook et al. 2018). Only then, the derived information is useful and can assist persons in charge in making good decisions.

Lastly, with all the focus on technological contribution to humanitarian aid, it needs to be noted again that radar imagery, or remote sensing in general, is no universal remedy for crisis situations. It is a suitable approach for the quick and objective retrieval of information, which in fact can be decisive in cases of emergency. The actual aid is delivered by humanitarian organizations and their tireless workers and much more politically and scientifically dependent. This thesis proposes SAR as a tool for shorter response times, more transparency, and higher quality information to hopefully make their work easier someday.

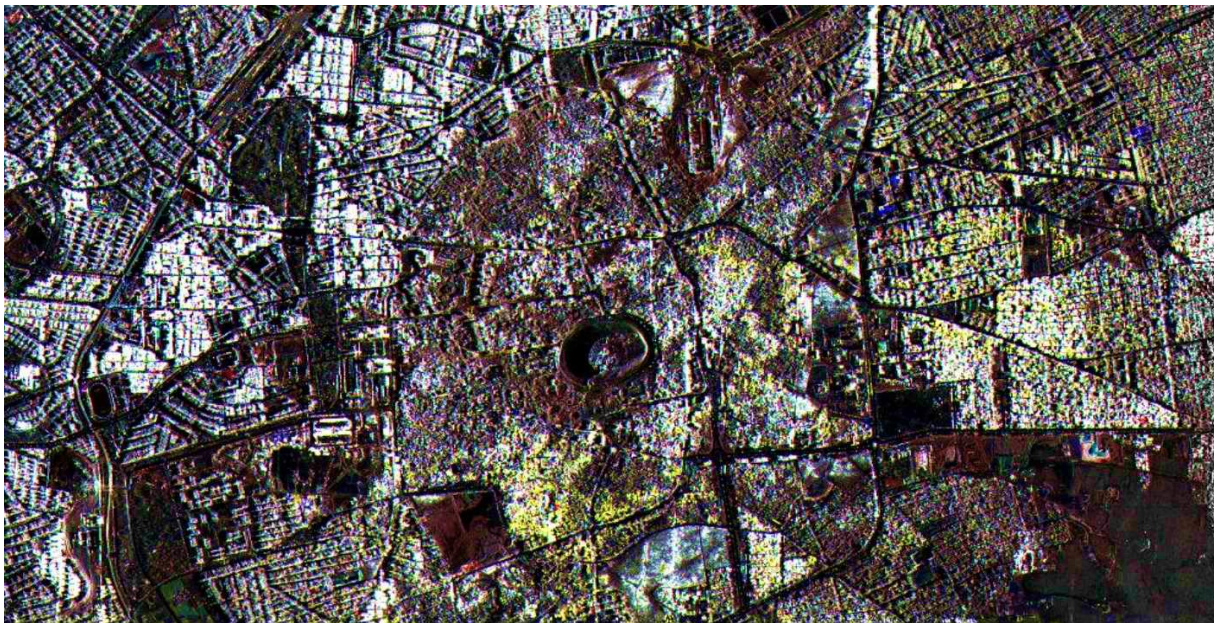


*Figure 100: Change of backscatter intensity (TerraSAR-X ST) in Aleppo during the Syrian civil war  
Red: 24.09.2016, (30.09.2016 airstrike), green: 07.11.2016, (16.11.2016 barrel bombs), blue: 21.12.2016*

## References

- Abdelsalam, M. G. & El-Baz, F. (2015): Analyses of optical images and radar data reveal structural features and predict groundwater accumulations in the central eastern desert of Egypt. *Arabian Journal of Geosciences* 8 (5), 2653–2666.
- Abdelsalam, M. G., Robinson, C., El-Baz, F. & Stern, R. J. (2000): Applications of orbital imaging radar for geologic studies in arid regions: The Saharan testimony. *Photogrammetric Engineering & Remote Sensing* 66 (6), 717–726.
- Abdelsalam, M. G. & Stern, R. J. (1996): Mapping Precambrian structures in the Sahara desert with SIR - C/X - SAR radar: The Neoproterozoic Keraf Suture, NE Sudan. *Journal of Geophysical Research: Solid Earth* 101 (E10), 23063–23076.
- Abou Fadel, L. (2016): Civilians rise up against ISIS rule in Raqqa city: government. *AMN*, March 06. <https://www.almasdarnews.com/article/civilians-rise-isis-rule-raqqa-city-government/> (15.01.2018).
- Afifi, T. & Jäger, J. (2010): *Environment, forced migration and social vulnerability*. Springer, Heidelberg.
- Agier, M. (2002): Between war and city: Towards an urban anthropology of refugee camps. *Ethnography* 3 (3), 317–341.
- Aherne, F. J., Thacker, N. A. & Rockett, P. I. (1998): The Bhattacharyya metric as an absolute similarity measure for frequency coded data. *Kybernetika* 34 (4), [363]–368.
- Ahlroth, S., Nilsson, M., Finnveden, G., Hjelm, O. & Hochschorner, E. (2011): Weighting and valuation in selected environmental systems analysis tools: Suggestions for further developments. *Journal of Cleaner Production* 19 (2-3), 145–156.
- Airbus (2014): TerraSAR-X services: International price list. Issue 6.0. [http://spot-ads2.occterra.net/files/pmedia/public/r463\\_9\\_itd-0508-cd-0001-tsx\\_international\\_pricelist\\_en\\_issue\\_6.00.pdf](http://spot-ads2.occterra.net/files/pmedia/public/r463_9_itd-0508-cd-0001-tsx_international_pricelist_en_issue_6.00.pdf) (15.01.2019).
- Airbus (2015): TerraSAR-X image product guide: Basic and enhanced radar satellite imagery. Issue 2.1. [https://www.intelligence-airbusds.com/files/pmedia/public/r459\\_9\\_20171004\\_tsxx-airbusds-ma-0009\\_tsx-productguide\\_i2.01.pdf](https://www.intelligence-airbusds.com/files/pmedia/public/r459_9_20171004_tsxx-airbusds-ma-0009_tsx-productguide_i2.01.pdf) (15.02.2019).
- Ajmar, A., Boccardo, P., Broglia, M., Kucera, J., Giulio-Tonolo, F. & Wania, A. (2017): Response to flood events: The role of satellite - based emergency mapping and the experience of the Copernicus emergency management service. In: Molinari, D., Ballio, F. & Menoni, S. (Eds.): *Flood damage survey and assessment: New insights from research and practice*. Wiley, Washington, D.C., 213–228.
- Akhtar, P., Marr, N. E. & Garnevskaja, E. V. (2012): Coordination in humanitarian relief chains: Chain coordinators. *Journal of Humanitarian Logistics and Supply Chain Management* 2 (1), 85–103.
- Al-Adamat, R.A.N., Foster, I.D.L. & Baban, S.M.J. (2003): Groundwater vulnerability and risk mapping for the basaltic aquifer of the Azraq basin of Jordan using GIS, remote sensing and DRASTIC. *Applied Geography* 23 (4), 303–324.
- Alfieri, L., Salamon, P., Pappenberger, F., Wetterhall, F. & Thielen, J. (2012): Operational early warning systems for water-related hazards in Europe. *Environmental Science & Policy* 21, 35–49.
- Alganci, U., Besol, B. & Sertel, E. (2018): Accuracy assessment of different digital surface models. *ISPRS International Journal of Geo-Information* 7 (3), 114.
- Ali, I., Naeimi, V., Cao, S., Elefante, S., Bauer-Marschallinger, B. & Wagner, W. (2017): Sentinel-1 data cube exploitation: Tools, products, services and quality control. In: *BiDS 2017*. Big Data from Space, 28 - 30 November 2017, Toulouse, France, 40–43.
- Aljazeera (2013): Syria rebels capture northern Raqqa city. *Al Jazeera*, March 05. <http://www.aljazeera.com/news/middleeast/2013/03/201334151942410812.html> (04.01.2018).
- Al-Khatib, I. A., Ju'ba, A., Kamal, N., Hamed, N., Hmeidani, N. & Massad, S. (2003): Impact of housing conditions on the health of the people at al-Ama'ri refugee camp in the West Bank of Palestine. *International Journal of Environmental Health Research* 13 (4), 315–326.

- Allan, N. J. R. (1987): Impact of Afghan refugees on the vegetation resources of Pakistan's Hindukush-Himalaya. *Mountain Research and Development* 7 (3), 200.
- Alnsour, J. & Meaton, J. (2014): Housing conditions in Palestinian refugee camps, Jordan. *Cities* 36, 65–73.
- Amitrano, D., Di Martino, G. & Iodice, A. et al. (2013): Synthetic aperture radars for humanitarian purposes: Products and opportunities. In: Moore, K. (Ed.): *GHT 2013: 20 - 23 Oct. 2013, San Jose, California, USA*. Global Humanitarian Technology Conference, 20 - 23 October 2013, San Jose, CA, USA, 457–462.
- Andrade, E. (1959): Doppler and the Doppler effect. *Endeavour* 18 (69), 14–19.
- Antoniou, V. (2018): A chimera of VGI, citizen science and mobile devices. In: Bordogna, G. & Carrara, P. (Eds.): *Mobile information systems leveraging volunteered geographic information for earth observation*. Springer International Publishing, Basel, 133–149.
- Antonova, S., Kääh, A., Heim, B., Langer, M. & Boike, J. (2016): Spatio-temporal variability of X-band radar backscatter and coherence over the Lena river delta, Siberia. *Remote Sensing of Environment* 182, 169–191.
- Aravena Pelizari, P., Spröhnle, K., Geiß, C., Schoepfer, E., Plank, S. & Taubenböck, H. (2018): Multi-sensor feature fusion for very high spatial resolution built-up area extraction in temporary settlements. *Remote Sensing of Environment* 209, 793–807.
- Arciniegas, G. A., Bijker, W., Kerle, N. & Tolpekin, V. A. (2007): Coherence- and amplitude-based analysis of seismogenic damage in Bam, Iran, using Envisat ASAR data. *IEEE Transactions On Geoscience And Remote Sensing* 45 (6), 1571–1581.
- Ardizzone, F., Bonano, M. & Giocoli, A. et al. (2012): Analysis of ground deformation using SBAS-DInSAR technique applied to COSMO-SkyMed images, the test case of Roma urban area. In: Notarnicola, C., Paloscia, S. & Pierdicca, N. (Eds.): *SPIE 8536. SAR Image Analysis, Modeling, and Techniques XII*, 26 - 29 September 2012, Edinburgh, United Kingdom, 85360D.
- Argialas, D. P. & Mavrantza, O. D. (2000): Comparison of edge detection and hough transform techniques for the extraction of geologic features. *International Archives of Photogrammetry and Remote Sensing* (34).
- Argyriou, G., Papadakis, G. & Stamoulis, G. et al. (2018): GeoSensor: On-line scalable change and event detection over big data. In: *WWW 2018. The Web Conference 2018*, 23 - 27 April 2018, Lyon, France, 223–226.
- Arko, S. A., Hogenson, R., Geiger, A., Herrmann, J., Buechler, B. & Hogenson, K. (2016): Sentinel-1 archive and processing in the cloud using the Hybrid Pluggable Processing Pipeline (HyP3) at the ASF DAAC. In: *AGU 2016. American Geophysical Union, Fall Meeting*, 06 - 12 December, San Francisco, USA.
- Armstrong, R., Knowles, K., Brodzik, M. J. & Hardman, M. A. (1994): DMSP SSM/I-SSMIS pathfinder daily EASE-grid brightness temperatures: Version 2. Updated 2018.
- Aschbacher, J. (2017): ESA's Earth observation strategy and Copernicus. In: Onda, M. & Young, O. R. (Eds.): *Satellite earth observations and their impact on society and policy*. Springer, Heidelberg, 81–86.
- Ashman, K. M., Bird, C. M. & Zepf, S. E. (1994): Detecting bimodality in astronomical datasets. *Astronomical Journal* (108), 2348–2361.
- Askne, J. & Hagberg, J. O. (1993): Potential of interferometric SAR for classification of land surfaces. In: *IGARSS 1993. IEEE International Geoscience and Remote Sensing Symposium*, 18 - 21 August 1993, Tokyo, Japan, 985–987.
- ASTRIUM (2011): Observation of Dadaab (Kenya) refugee camp based on TerraSAR-X data. [https://www.intelligence-airbusds.com/files/pmedia/public/r2337\\_9\\_201108\\_astriumgeo\\_terrasarx\\_dadaab\\_refugee\\_camp.pdf](https://www.intelligence-airbusds.com/files/pmedia/public/r2337_9_201108_astriumgeo_terrasarx_dadaab_refugee_camp.pdf) (21.01.2019).
- Atmanand, M. A. (2003): Insurance and disaster management: The Indian context. *Disaster Prevention and Management: An International Journal* 12 (4), 286–304.
- Atzberger, C. (2013): Advances in remote sensing of agriculture: Context description, existing operational monitoring systems and major information needs. *Remote Sensing* 5 (2), 949–981.

- Auer, S., Balz, T., Becker, S. & Bamler, R. (2010): 3D SAR simulation of urban areas based on detailed building models. *Photogrammetric Engineering & Remote Sensing* 76 (12), 1373–1384.
- Austin, J. M., Mackey, B. G. & van Niel, K. P. (2003): Estimating forest biomass using satellite radar: An exploratory study in a temperate Australian Eucalyptus forest. *Forest Ecology and Management* 176 (1-3), 575–583.
- Aylward, B., Barboza, P. & Bawo, L. et al. (2014): Ebola virus disease in West Africa - the first 9 months of the epidemic and forward projections. *The New England Journal of Medicine* 371 (16), 1481–1495.
- Bach, K., Kahabka, H., Fernando, C. & Perez, J. C. (2018): The TerraSAR-X/PAZ constellation: post-launch update. In: *EUSAR 2018*. 12th European Conference on Synthetic Aperture Radar, 04 - 07 June 2018, Aachen, Germany, 1–3.
- Backhaus, R., Czarán, L. & Epler, N. et al. (2010): Support from space: The United Nations platform for space-based information for disaster management and emergency response (UN-SPIDER). *Geoinformation for Disaster and Risk Management: Examples and Best Practices*, 103–113.
- Bai, X., Sun, J., Hong, W. & Mao, S. (2010): On the TOPS mode spaceborne SAR. *Science China Information Sciences* 53 (2), 367–378.
- Baize, S., Pannetier, D. & Oestereich, L. et al. (2014): Emergence of Zaire Ebola virus disease in Guinea. *New England Journal of Medicine* 371 (15), 1418–1425.
- Baldwin, C. & Marshall, A. (2018): Monsoon floods and landslides threaten 100,000 Rohingya refugees in Bangladesh: 09.03.2018. <https://www.reuters.com/article/us-myanmar-rohingya-monsoon/monsoon-floods-and-landslides-threaten-100000-rohingya-refugees-in-bangladesh-idUSKCN1GL210> (12.09.2018).
- Ballester-Berman, J. D., López-Sánchez, J. M. & Fortuny-Guasch, J. (2005): Retrieval of biophysical parameters of agricultural crops using polarimetric SAR interferometry. *IEEE Transactions On Geoscience And Remote Sensing* 43 (4), 683–694.
- Balling, R. C. & Brazel, S. W. (1988): High-resolution surface temperature patterns in a complex urban terrain. *Photogrammetric Engineering & Remote Sensing* 54 (9), 1289–1293.
- Bamler, R. (1992): A comparison of range-Doppler and wavenumber domain SAR focusing algorithms. *IEEE Transactions On Geoscience And Remote Sensing* 30 (4), 706–713.
- Bamler, R. & Hartl, P. (1998): Synthetic aperture radar interferometry. *Inverse problems* 14 (4), R1.
- Band, L. E. (1986): Topographic partition of watersheds with digital elevation models. *Water Resources Research* 22 (1), 15–24.
- Barbieri, J., Riva, F. & Colombo, E. (2017): Cooking in refugee camps and informal settlements: A review of available technologies and impacts on the socio-economic and environmental perspective. *Sustainable Energy Technologies and Assessments* 22, 194–207.
- Bastiaanssen, W. G. M. (1998): *Remote sensing in water resources management: The state of the art*. International Water Management Institute, Colombo, Sri Lanka.
- Bates, D. C. (2002): Environmental refugees? Classifying human migrations caused by environmental change. *Population and Environment* 23 (5), 465–477.
- Bayburt, S., Kurtak, A. B., Büyüksalih, G. & Jacobsen, K. (2017): Geometric accuracy analysis of WorldDEM in relation to AW3D30, SRTM and ASTER GDEM2. *International Archives of Photogrammetry and Remote Sensing* 42 (1W1), 211–217.
- Bayer, T., Winter, R. & Schreier, G. (1991): Terrain influences in SAR backscatter and attempts to their correction. *IEEE Transactions On Geoscience And Remote Sensing* 29 (3), 451–462.
- Bazi, Y., Bruzzone, L. & Melgani, F. (2007): Image thresholding based on the EM algorithm and the generalized Gaussian distribution. *Pattern Recognition* 40 (2), 619–634.
- Beaudou, A. G. & Cambrézy, L. (1999): *Refugee Camps and Environment: Landscape and deforestation in Dadaab region (Kenya)*. UNHCR–IRD, Marseille.
- Beaudou, A. G., Cambrézy, L. & Souris, M. (1999): Environment, cartography, demography and geographical information system in the refugee camps Dadaab, Kakuma - Kenya: Final report. Major findings. [http://www.cartographie.ird.fr/publi/Refugies/Final\\_report.pdf](http://www.cartographie.ird.fr/publi/Refugies/Final_report.pdf) (15.12.2018).
- Bell, J. R., Schultz, L. A. & Jones, M. et al. (2017): Near real-time use of optical remote sensing and Synthetic Aperture Radar for response to central US flooding in late April-early May 2017. In:

- AGU Fall Meeting Abstracts*. American Geophysical Union, Fall Meeting, 07 - 15 December, New Orleans, USA, IN31C-0094.
- Benallegue, M., Taconet, O., Vidal-Madjar, D. & Normand, M. (1995): The use of radar backscattering signals for measuring soil moisture and surface roughness. *Remote Sensing of Environment* 53 (1), 61–68.
- Berry, L. (2008): The impacts of environmental degradation on refugee - host relationships. *African Security Studies* 17 (3), 125–131.
- Beven, K. J. & Kirkby, M. J. (1979): A physically based, variable contributing area model of basin hydrology: Un modèle à base physique de zone d'appel variable de l'hydrologie du bassin versant. *Hydrological Sciences Bulletin* 24 (1), 43–69.
- Bhattacharya, A. & Mukherjee, K. (2017): Review on InSAR based displacement monitoring of Indian Himalayas: Issues, challenges and possible advanced alternatives. *Geocarto International* 32 (3), 298–321.
- Bi, C., Wang, H. & Bao, R. (2014): SAR image change detection using regularized dictionary learning and fuzzy clustering. In: *CCIS 2014*. 3rd International Conference on Cloud Computing and Intelligence Systems, 20 - 21 May 2013, London, UK, 327–330.
- Biggin, D. S. (1996): A comparison of ERS - 1 satellite radar and aerial photography for river flood mapping. *Water and Environment Journal* 10 (1), 59–64.
- Birkmann, J., Garschagen, M., van Tuan, V. & Binh, N. T. (2012): Vulnerability, coping and adaptation to water related hazards in the Vietnamese Mekong delta. In: Renaud, F. G. & Kuenzer, C. (Eds.): *The Mekong delta system: Interdisciplinary analyses of a river delta*. Springer Netherlands, Dordrecht, 245–289.
- Bitelli, G., Franci, F., Luppi, M., Mandanici, E. & Tonolo, F. G. (2015): Utilizzo di immagini satellitari multispettrali ad alta risoluzione nella gestione di emergenze umanitarie. In: *ASITA 2015: Vol. 131*. XIX Conferenza Nazionale, 29 September - 01 October 2015, Milano, Italy, 131–138.
- Bjørøgo, E. (1999): Very high resolution satellites: A new source of information in humanitarian relief operations. *Bulletin of the American Society for Information Science and Technology* 26 (1), 22–24.
- Bjørøgo, E. (2000a): Refugee camp mapping using very high spatial resolution satellite sensor images. *Geocarto International* 15 (2), 79–88.
- Bjørøgo, E. (2000b): Using very high spatial resolution multispectral satellite sensor imagery to monitor refugee camps. *International Journal of Remote Sensing* 21 (3), 611–616.
- Blackwell, T. H. & Kaufman, J. S. (2002): Response time effectiveness: Comparison of response time and survival in an urban emergency medical services system. *Academic Emergency Medicine* 9 (4), 288–295.
- Blumberg, D. G. (1998): Remote sensing of desert dune forms by polarimetric synthetic aperture radar (SAR). *Remote Sensing of Environment* 65 (2), 204–216.
- Boccardo, P. (2013): New perspectives in emergency mapping. *European Journal of Remote Sensing* 46 (1), 571–582.
- Boccardo, P. & Tonolo, F. G. (2015): Remote sensing role in emergency mapping for disaster response. In: Lollino, G., Manconi, A., Guzzetti, F., Culshaw, M., Bobrowsky, P. & Luino, F. (Eds.): *Engineering geology for society and territory: Urban geology, sustainable planning and landscape exploitation*. Springer International Publishing, Cham, 17–24.
- Böhner, J. & Selige, T. (2006): Spatial prediction of soil attributes using terrain analysis and climate regionalisation. *Göttinger Geogr. SAGA-Analyses and Modelling Applications. Abh* (115).
- Boldt, M., Thiele, A., Schulz, K. & Hinz, S. (2014): SAR image segmentation using morphological attribute profiles. *International Archives of Photogrammetry and Remote Sensing* 40 (3), 39.
- Boni, G., Ferraris, L. & Pulvirenti, L. et al. (2016): A prototype system for flood monitoring based on flood forecast combined with COSMO-SkyMed and Sentinel-1 data. *IEEE Journal of Selected Topics in Applied Earth Observations and Remote Sensing* 9 (6), 2794–2805.
- Bonner, P. C., Schmidt, W.-P., Belmain, S. R., Oshin, B., Baglolle, D. & Borchert, M. (2007): Poor housing quality increases risk of rodent infestation and Lassa fever in refugee camps of Sierra Leone. *The American journal of tropical medicine and hygiene* 77 (1), 169–175.

- Born, G. H., Dunne, J. A. & Lame, D. B. (1979): Seasat mission overview. *Science* 204 (4400), 1405–1406.
- Bouchardy, J.-Y. (2005): Radar images and geographic information helping identify water resources during humanitarian crisis: The case of Chad/Sudan (Darfur) emergency. In: Bobylev, L. P. (Ed.): *Global monitoring for sustainability and security*. 31st International Symposium of Remote Sensing & the Environment, 20 - 24 June 2005, St. Petersburg, Russian Federation.
- Bouchemakh, L., Smara, Y., Boutarfa, S. & Hamadache, Z. (2008): A comparative study of speckle filtering in polarimetric radar SAR images. In: *ICTTA 2008: From theory to applications*. 3rd International Conference on Information and Communication Technologies, 7 - 11 April 2008, Damascus, Syria.
- Bouvet, A., Mermoz, S. & Le Toan, T. et al. (2018): An above-ground biomass map of African savannahs and woodlands at 25 m resolution derived from ALOS PALSAR. *Remote Sensing of Environment* 206, 156–173.
- Bovolo, F. & Bruzzone, L. (2007): A split-based approach to unsupervised change detection in large-size multitemporal images: Application to tsunami-damage assessment. *IEEE Transactions On Geoscience And Remote Sensing* 45 (6), 1658–1670.
- Bowles, E. (1998): From village to camp: Refugee camp life in transition on the Thailand-Burma border. *Forced Migration Review* 2, 11–14.
- Bradshaw, C. J. A., Sodhi, N. S., Peh, K. S. & Brook, B. W. (2007): Global evidence that deforestation amplifies flood risk and severity in the developing world. *Global Change Biology* 13 (11), 2379–2395.
- Brakenridge, G. R. & Kettner, A. J. (2018): DFO flood event 4658 Laos: Maximum observed flooding. <http://floodobservatory.colorado.edu/Events/4658/2018Laos4658.html> (10.09.2018).
- Brakenridge, G. R., Tracy, B. T. & Knox, J. C. (1998): Orbital SAR remote sensing of a river flood wave. *International Journal of Remote Sensing* 19 (7), 1439–1445.
- Braun, A. (2018a): Assessment of building damage in Raqqa during the Syrian civil war using time-series of radar satellite imagery. *Journal for Geographic Information Science* 1, 228–242.
- Braun, A. (2018b): Spatial data in humanitarian assistance: Online survey (unpublished results). <https://www.surveymonkey.de/r/853QCSK> (08.12.2018).
- Braun, A., Hagensieker, R. & Hochschild, V. (2016a): Filling of cloud-induced gaps for land use and land cover classifications around refugee camps. In: Ouwehand, L. (Ed.): *LPS 2016*. ESA Living Planet Symposium, 9 - 13 May 2016, Prague, Czech Republic.
- Braun, A. & Hochschild, V. (2015): Combined use of SAR and optical data for environmental assessments around refugee camps in semiarid landscapes. *International Archives of Photogrammetry and Remote Sensing XL-7/W3*, 777–782.
- Braun, A. & Hochschild, V. (2017a): A SAR-based index for landscape changes in African savannas. *Remote Sensing* 9 (4), 359–382.
- Braun, A. & Hochschild, V. (2017b): Potential and limitations of radar remote sensing for humanitarian operations. *Journal for Geographic Information Science* 1, 228–243.
- Braun, A., Lang, S. & Hochschild, V. (2016b): Impact of refugee camps on their environment. A case study using multi-temporal SAR data. *Journal of Geography, Environment and Earth Science International* 4 (2), 1–17.
- Braun, A., Wagner, J. & Hochschild, V. (2018): Above-ground biomass estimates based on active and passive microwave sensor imagery in low-biomass savanna ecosystems. *Journal of Applied Remote Sensing* 12 (4), 46027.
- Breiman, L. (2001): Random forests. *Machine Learning* 45 (1), 5–32.
- Breiman, L., Friedman, J. H., Olshen, R. A. & Stone, C. J. (1984): Classification and regression trees. *Wadsworth International Group*.
- Brenner, A. R. & Roessing, L. (2008): Radar imaging of urban areas by means of very high-resolution SAR and interferometric SAR. *IEEE Transactions On Geoscience And Remote Sensing* 46 (10), 2971–2982.
- Bromley, J., Brouwer, J., Barker, A. P., Gaze, S. R. & Valentine, C. (1997): The role of surface water redistribution in an area of patterned vegetation in a semi-arid environment, south-west Niger. *Journal of Hydrology* 198 (1-4), 1–29.

- Brown, W. M. (1967): Synthetic Aperture Radar. *IEEE Transactions on Aerospace and Electronic Systems* AES-3 (2), 217–229.
- Brunner, D., Lemoine, G. & Bruzzone, L. (2010): Earthquake damage assessment of buildings using VHR optical and SAR imagery. *IEEE Transactions On Geoscience And Remote Sensing* 48 (5), 2403–2420.
- Buckreuss, S., Schättler, B. & Fritz, T. et al. (2018): Ten years of TerraSAR-X operations. *Remote Sensing* 10 (6), 873.
- Burns, B. L. & Cordaro, J. T. (1994): SAR image-formation algorithm that compensates for the spatially variant effects of antenna motion. *International Society for Optics and Photonics* 2230.
- Burrows, G., Braun, A. & Wendt, L. (2017): Briefing note – water supply in Kidal, Mali: EO4HumEn+ report. 20.05.2017.
- Buscaïl, F. & Caby, R. (2004): Kidal - Anefif Est: Carte géologique de l'Adrar des Iforas (d'après J. Fabre, 1982, modifié). Échelle: 1 200.000.
- Bütthe, T., Major, S. & Souza, A. d. M. (2012): The politics of private foreign aid: Humanitarian principles, economic development objectives, and organizational interests in NGO private aid allocation. *International Organization* 66 (4), 571–607.
- Butt, T. A., McCarl, B. A. & Kergna, A. O. (2006): Policies for reducing agricultural sector vulnerability to climate change in Mali. *Climate Policy* 5 (6), 583–598.
- Caniato, M., Carliez, D. & Thulstrup, A. (2017): Challenges and opportunities of new energy schemes for food security in humanitarian contexts: A selective review. *Sustainable Energy Technologies and Assessments* 22, 208–219.
- Capstick, D. & Harris, R. (2001): The effects of speckle reduction on classification of ERS SAR data. *International Journal of Remote Sensing* 22 (18), 3627–3641.
- Carlin, J. E. (1990): Refugee and immigrant populations at special risk: Women, children and the elderly. In: Holtzman, W. H. & Bornemann, T. H. (Eds.): *Mental health of immigrants and refugees*, Austin, Texas, 224–233.
- Carlson, B. C. (1966): Some inequalities for hypergeometric functions. *Proceedings of the American Mathematical Society* 17 (1), 32.
- Carrion, P. (2015): “If all you have is a hammer...” - How useful is humanitarian crowdsourcing? 05.09.2015. <https://medium.com/@paulcurrion/if-all-you-have-is-a-hammer-how-useful-is-humanitarian-crowdsourcing-fed4ef33f8c8> (20.01.2019).
- Castañeda, C., Gutiérrez, F., Manunta, M. & Galve, J. P. (2009): DInSAR measurements of ground deformation by sinkholes, mining subsidence, and landslides, Ebro river, Spain. *Earth Surface Processes and Landforms* 34 (11), 1562–1574.
- Catani, F., Farina, P., Moretti, S., Nico, G. & Strozzi, T. (2005): On the application of SAR interferometry to geomorphological studies: Estimation of landform attributes and mass movements. *Geomorphology* 66 (1-4), 119–131.
- CCCM (2014): Camp closure guidelines. [https://www.globalccmcluster.org/system/files/publications/Camp\\_Closure\\_Guidelines.pdf](https://www.globalccmcluster.org/system/files/publications/Camp_Closure_Guidelines.pdf) (10.11.2018).
- CCCM (2016): Muna Garage El Badawe temporary formally-managed settlement, Jere LGA: Action points, shelter site plan and decongestion standard operating. Procedures I December 2016. [https://reliefweb.int/sites/reliefweb.int/files/resources/nga\\_shelter\\_cccm\\_i\\_decongestion\\_and\\_site\\_improvement\\_standard\\_operating\\_procedures\\_i\\_mu\\_na\\_garage\\_el\\_badawee\\_-\\_december\\_2016\\_-\\_january\\_2017.pdf](https://reliefweb.int/sites/reliefweb.int/files/resources/nga_shelter_cccm_i_decongestion_and_site_improvement_standard_operating_procedures_i_mu_na_garage_el_badawee_-_december_2016_-_january_2017.pdf) (15.10.2018).
- Chambers, J., Eddy, W. & Härdle, W. et al. (1996): *Numerical Bayesian methods applied to signal processing*. Springer New York, New York, NY.
- Chan, E. Y. Y., Chiu, C. P. & Chan, G. K. W. (2018): Medical and health risks associated with communicable diseases of Rohingya refugees in Bangladesh 2017. *International Journal of Infectious Diseases* 68, 39–43.
- Chander, G., Markham, B. L. & Helder, D. L. (2009): Summary of current radiometric calibration coefficients for Landsat MSS, TM, ETM+, and EO-1 ALI sensors. *Remote Sensing of Environment* 113 (5), 893–903.

- Chatterjee, R. S., Fruneau, B. & Rudant, J. P. et al. (2006): Subsidence of Kolkata (Calcutta) City, India during the 1990s as observed from space by differential synthetic aperture radar interferometry (D-InSAR) technique. *Remote Sensing of Environment* 102 (1-2), 176–185.
- Checchi, F., Stewart, B. T., Palmer, J. J. & Grundy, C. (2013): Validity and feasibility of a satellite imagery-based method for rapid estimation of displaced populations. *International Journal of Health Geographics* 12 (1), 4.
- Chen, C. W. & Zebker, H. A. (2001): Two-dimensional phase unwrapping with use of statistical models for cost functions in nonlinear optimization. *Journal of the Optical Society of America* 18 (2), 338–351.
- Chen, J., Lin, H., Huang, C. & Fang, C. (2009): The relationship between the leaf area index (LAI) of rice and the C - band SAR vertical/horizontal (VV/HH) polarization ratio. *International Journal of Remote Sensing* 30 (8), 2149–2154.
- Chen, S.-W. & Sato, M. (2013): Tsunami damage investigation of built-up areas using multitemporal spaceborne full polarimetric SAR images. *IEEE Transactions On Geoscience And Remote Sensing* 51 (4), 1985–1997.
- Chen, S.-W., Wang, X.-S. & Xiao, S.-P. (2018): Urban damage level mapping based on co-polarization coherence pattern using multitemporal polarimetric SAR data. *IEEE Journal of Selected Topics in Applied Earth Observations and Remote Sensing* 11 (8), 2657–2667.
- Cheng, R., Mantovani, A. & Frazzoli, C. (2017): Analysis of food safety and security challenges in emerging African food producing areas through a one health lens: The dairy chains in Mali. *Journal of Food Protection* 80 (1), 57–67.
- Chini, M., Hostache, R., Giustarini, L. & Matgen, P. (2017): A hierarchical split-based approach for parametric thresholding of SAR images: Flood inundation as a test case. *IEEE Transactions On Geoscience And Remote Sensing* 55 (12), 6975–6988.
- Chini, M., Piscini, A., Cinti, F. R., Amici, S., Nappi, R. & DeMartini, P. M. (2013): The 2011 Tohoku (Japan) Tsunami inundation and liquefaction investigated through optical, thermal, and SAR data. *IEEE Geoscience and Remote Sensing Letters* 10 (2), 347–351.
- Chkam, H. (2016): Aid and the perpetuation of refugee camps: The case of Dadaab in Kenya 1991-2011. *Refugee Survey Quarterly* 35 (2), 79–97.
- Chowdhury, M. H. (2017): Island chosen to relocate Rohingya refugees not fit for habitation, says Bangladesh forest department. *BD News*, February 18.  
<https://bdnews24.com/bangladesh/2017/02/18/island-chosen-to-relocate-rohingya-refugees-not-fit-for-habitation-says-bangladesh-forest-department> (11.08.2018).
- Cian, F., Marconcini, M. & Ceccato, P. (2018): Normalized Difference Flood Index for rapid flood mapping: Taking advantage of EO big data. *Remote Sensing of Environment* 209, 712–730.
- Ciesla, W. (1991): Ethics in photogrammetry and remote sensing. A perspective from a natural resource specialist. *Photogrammetric Engineering & Remote Sensing* 57 (3), 281–282.
- Cigna, F. & Tapete, D. (2018): Tracking human-induced landscape disturbance at the Nasca lines UNESCO world heritage site in Peru with COSMO-SkyMed InSAR. *Remote Sensing* 10 (4), 572.
- Cimy, F. C. (1977): Refugee camps and camp planning: The state of the art. *Disasters* 1 (2), 125–143.
- Cindrich, I., Marks, J. & Klooster, A. (1977): Coherent optical processing of Synthetic Aperture Radar data. In: Vatz, B. W. (Ed.): *SPIE 0128. Effect Utilization of Optics in Radar Systems*, 27 September 1977, Huntsville, 128–143.
- Cissé, M. I. (1980): The browse production of some trees of the Sahel: Relationships between maximum foliage biomass and various physical parameters. *Browse in Africa*, 205–210.
- Clark, J. & Tan, V. (2004): Hundreds flee new fighting in Darfur. UNHCR opens 8th camp in Chad. <http://www.unhcr.org/print/40c081119.html> (15.11.2016).
- Clausi, D. A. (2014): An analysis of co-occurrence texture statistics as a function of grey level quantization. *Canadian Journal of Remote Sensing* 28 (1), 45–62.
- Cloude, S. R. & Pottier, E. (1996): A review of target decomposition theorems in radar polarimetry. *IEEE Transactions On Geoscience And Remote Sensing* 34 (2), 498–518.
- Cloude, S. R. & Pottier, E. (1997): An entropy based classification scheme for land applications of polarimetric SAR. *IEEE Transactions On Geoscience And Remote Sensing* 35 (1), 68–78.

- Colin-Koeniguer, E. & Trouvé, N. (2011): POLSARP: Investigating the benefits of polarimetry for urban applications using X-band SAR images. [https://earth.esa.int/c/document\\_library/get\\_file?folderId=409266&name=DLFE-5576.pdf](https://earth.esa.int/c/document_library/get_file?folderId=409266&name=DLFE-5576.pdf) (12.06.2015).
- Collins, M. J., Wiebe, J. & Claudi, D. A. (2000): The effect of speckle filtering on scale-dependent texture estimation of a forested scene. *IEEE Transactions On Geoscience And Remote Sensing* 38 (3), 1160–1170.
- Colwell, R. N. (1968): Remote sensing of natural resources. *Scientific American* 218 (1), 54–71.
- Cook, A. D. B. & Ne, F. Y. (2018): *Complex humanitarian emergencies and disaster management in Bangladesh: The 2017 Rohingya exodus*. NTS Report No. 11. Centre for Non Traditional Security Studies, Singapore.
- Corgne, S., Magagi, R., Yergeau, M. & Sylla, D. (2010): An integrated approach to hydro-geological lineament mapping of a semi-arid region of West Africa using Radarsat-1 and GIS. *Remote Sensing of Environment* 114 (9), 1863–1875.
- Corsellis, T. (2001): *The selection of sites for temporary settlements for forced migrants*. Dissertation. University of Cambridge UK.
- Covello, F., Battazza, F. & Coletta, A. et al. (2010): COSMO-SkyMed an existing opportunity for observing the earth. *Journal of Geodynamics* 49 (3-4), 171–180.
- Cowan, N. M. (2011): A geospatial data management framework for humanitarian response. In: *ISCRAM Conference 2011*. 8th International Conference on Information Systems for Crisis Response and Management, 8 - 11 May, Lisbon, Portugal, 1–5.
- Cowan, N. M. (2014): Building a geospatial data model for humanitarian response. *Journal of Emergency Management* 12 (5), 383–390.
- Cozzolino, A. (2012): *Humanitarian logistics: Cross-sector cooperation in disaster relief management*. Springer Science & Business Media, Berlin.
- Crosetto, M. (2002): Calibration and validation of SAR interferometry for DEM generation. *ISPRS Journal of Photogrammetry and Remote Sensing* 57 (3), 213–227.
- Cumming, I. G. & Wong, F. H. (2005): Digital processing of Synthetic Aperture Radar data. *Artech house* 1 (2), 3.
- Curlander, J. C. (1982): Location of spaceborne SAR imagery. *IEEE Transactions On Geoscience And Remote Sensing* GE-20 (3), 359–364.
- Czubski, K., Kozak, J. & Kolecka, N. (2013): Accuracy of SRTM-X and ASTER elevation data and its influence on topographical and hydrological modeling: Case study of the Pieniny mountains in Poland. *International Journal of Geoinformatics* 9 (2).
- d'Oleire-Oltmanns, S., Riedler, B., Pernkopf, L., Weinke, E. & Lang, S. (2015): Validation strategy for user-specific map products for the European Copernicus security service. *Journal for Geographic Information Science* 1.
- Dabbagh, A. E., Al-Hinai, K. G. & Khan, M. A. (1997): Detection of sand-covered geologic features in the Arabian Peninsula using SIR-C/X-SAR data. *Remote Sensing of Environment* 59 (2), 375–382.
- Daida, J. M., Onstott, R. G., Bersano-Begey, T. F., Ross, S. J. & Vesecky, J. F. (1996): Ice roughness classification and ERS SAR imagery of Arctic sea ice: Evaluation of feature-extraction algorithms by genetic programming. In: *IGARSS 1996*. IEEE International Geoscience and Remote Sensing Symposium, 27–31 May 1996, Lincoln, NE, USA, 1520–1522.
- Danklmayer, A., Doring, B. J., Schwerdt, M. & Chandra, M. (2009): Assessment of atmospheric propagation effects in SAR images. *IEEE Transactions On Geoscience And Remote Sensing* 47 (10), 3507–3518.
- Darcy, J. & Hofman, C.-A. (2003): *According to need?: Needs assessment and decision-making in the humanitarian sector*. HPG report 15, September 2003, London.
- Das, N. N., Entekhabi, D. & Njoku, E. G. (2011): An algorithm for merging SMAP radiometer and radar data for high-resolution soil-moisture retrieval. *IEEE Transactions On Geoscience And Remote Sensing* 49 (5), 1504–1512.
- Dasgupta, S., Huq, M. & Khan, Z. H. et al. (2014): Cyclones in a changing climate: The case of Bangladesh. *Climate and Development* 6 (2), 96–110.

- Davis, J. & Lambert, R. (2007): *Engineering in emergencies: A practical guide for relief workers*, 2. ed. Practical Action Publications, Bourton on Dunsmore, Rugby, Warwickshire.
- de Vries, C. G., Hixson, A. N. & Liss, B. M. et al. (2017): *An investigative environmental impact assessment for Kutupalong refugee camp and surroundings, Bangladesh: Preliminary research, analysis, recommendations, and work breakdown structure for in situ EIA team*.
- de Vries, F. P. (1998): *Speckle reduction in SAR Imagery by various multi-look techniques*, Den Haag.
- Dekker, R. J. (1998): Speckle filtering in satellite SAR change detection imagery. *International Journal of Remote Sensing* 19 (6), 1133–1146.
- Dekker, R. J. (2003): Texture analysis and classification of ERS SAR images for map updating of urban areas in the netherlands. *IEEE Transactions On Geoscience And Remote Sensing* 41 (9), 1950–1958.
- Dekker, R. J. (2005): SAR change detection techniques and applications. In: *EARSeL 2005*. 25th Symposium of the European Association of Remote Sensing Laboratories, 6-11 June 2005, Porto, Portugal, 63–69.
- Dell'Acqua, F. & Gamba, P. E. (2012): Remote sensing and earthquake damage assessment: Experiences, limits, and perspectives. *Proceedings of the Institute of Electrical and Electronics Engineers* 100 (10), 2876–2890.
- Deng, G., Cahill, L. W. & Tobin, G. R. (1995): The study of logarithmic image processing model and its application to image enhancement. *IEEE Transactions on Image Processing* 4 (4), 506–512.
- Deng, X., López-Martínez, C., Chen, J. & Han, P. (2017): Statistical modeling of polarimetric SAR data: A survey and challenges. *Remote Sensing* 9 (4), 348.
- Deroin, J.-P., Company, A. & Simonin, A. (1997): An empirical model for interpreting the relationship between backscattering and arid land surface roughness as seen with the SAR. *IEEE Transactions On Geoscience And Remote Sensing* 35 (1), 86–92.
- Derrode, S., Mercier, G. & Pieczynski, W. (2004): Unsupervised change detection in SAR images using a multicomponent HMC model. In: Smits, P. & Bruzzone, L. (Eds.): *Analysis of multi-temporal remote sensing images: Series in remote sensing: Volume 3*. World Scientific, Trento, 195–203.
- Di Traglia, F., Nolesini, T. & Intrieri, E. et al. (2014): Review of ten years of volcano deformations recorded by the ground-based InSAR monitoring system at Stromboli volcano: A tool to mitigate volcano flank dynamics and intense volcanic activity. *Earth-Science Reviews* 139, 317–335.
- Ding, X. & Li, X. (2011): Monitoring of the water-area variations of Lake Dongting in China with ENVISAT ASAR images. *International Journal of Applied Earth Observation and Geoinformation* 13 (6), 894–901.
- Ding, X.-l., Li, Z.-w., Zhu, J.-j., Feng, G.-c. & Long, J.-p. (2008): Atmospheric effects on InSAR measurements and their mitigation. *Sensors* 8 (9), 5426–5448.
- Dinguirard, M. & Slater, P. N. (1999): Calibration of space-multispectral imaging sensors: A review. *Remote Sensing of Environment* 68 (3), 194–205.
- Dittus, M., Quattrone, G. & Capra, L. (2017): Mass participation during emergency response: Event-centric crowd-sourcing in humanitarian mapping. In: *CSCW 2017*. ACM Conference on Computer Supported Cooperative Work and Social Computing, 25 February - 01 March 2017, Portland, Oregon.
- Dobson, M. C., Ulaby, F. T., LeToan, T., Beaudoin, A., Kasischke, E. S. & Christensen, N. (1992): Dependence of radar backscatter on coniferous forest biomass. *IEEE Transactions On Geoscience And Remote Sensing* 30 (2), 412–415.
- Dong, Y., Forster, B. C. & Ticehurst, C. (1997): Radar backscatter analysis for urban environments. *International Journal of Remote Sensing* 18 (6), 1351–1364.
- Dong, Y., Milne, A. K. & Forster, B. C. (2000): A review of SAR speckle filters: Texture restoration and preservation. In: *IGARSS 2000*. IEEE International Geoscience and Remote Sensing Symposium, 24 - 28 July 2000, Honolulu, HI, USA, 633–635.
- d'Ozouville, N., Deffontaines, B., Benveniste, J., Wegmüller, U., Violette, S. & Marsily, G. de (2008): DEM generation using ASAR (ENVISAT) for addressing the lack of freshwater ecosystems

- management, Santa Cruz Island, Galapagos. *Remote Sensing of Environment* 112 (11), 4131–4147.
- Drury, S. A. (2001): *Image interpretation in geology*, 3<sup>rd</sup> edn. Blackwell Science, Malden, MA.
- Du, P., Liu, P. & Xia, J. et al. (2014): Remote sensing image interpretation for urban environment analysis: Methods, system and examples. *Remote Sensing* 6 (10), 9458–9474.
- Dumitru, C. O., Schwarz, G., Cui, S., Espinoza-Molina, D. & Datcu, M. (2016): Semi-automated semantic annotation of big archives of high resolution SAR images. In: *EURSAR 2016*. 11th European Conference on Synthetic Aperture Radar, 06 - 09 June 2016, Hamburg, Germany.
- Dutra, L. V. (1999): Feature extraction and selection for ERS-1/2 InSAR classification. *International Journal of Remote Sensing* 20 (5), 993–1016.
- Eckardt, R., Berger, C., Thiel, C. & Schmullius, C. (2013): Removal of optically thick clouds from multi-spectral satellite images using multi-frequency SAR data. *Remote Sensing* 5 (6), 2973–3006.
- e-geos (2017): Price list: BDS-COM-17-002. [http://www.e-geos.it/images/documents/Pricelist-nov17/BDS-COM-17-002\\_e-GEOS%20Official%20Pricelist\\_October%2020th\\_2017.pdf](http://www.e-geos.it/images/documents/Pricelist-nov17/BDS-COM-17-002_e-GEOS%20Official%20Pricelist_October%2020th_2017.pdf) (15.01.2019).
- Ehrlich, D., Lang, S., Laneve, G., Mubareka, S., Schneiderbauer, S. & Tiede, D. (2009): Can earth observation help to improve information on population?: Indirect population estimations from EO derived geo-spatial data: Contribution from GMOSS. In: Jasani, B., Pesaresi, M., Schneiderbauer, S. & Zeug, G. (Eds.): *Remote sensing from space: Supporting international peace and security*. Springer, Dordrecht, 211–237.
- Eineder, M. (2003): Problems and solutions for InSAR digital elevation model generation of mountainous terrain. In: *Fringe 2003*. Proceedings of Fringe Workshop, Frascati, Italy.
- Eklund, L., Degerald, M., Brandt, M., Prishchepov, A. V. & Pilesjö, P. (2017): How conflict affects land use: Agricultural activity in areas seized by the Islamic State. *Environmental Research Letters* 12 (5), 54004.
- Eldhuset, K., Andersen, P. H., Hauge, S., Isaksson, E. & Weydahl, D. J. (2003): ERS tandem InSAR processing for DEM generation, glacier motion estimation and coherence analysis on Svalbard. *International Journal of Remote Sensing* 24 (7), 1415–1437.
- Engdahl, M., Borgeaud, M. & Rast, M. (2001): The use of ERS-1/2 tandem interferometric coherence in the estimation of agricultural crop heights. *IEEE Transactions On Geoscience And Remote Sensing* 39 (8), 1799–1806.
- Engdahl, M. & Hyyppä, J. (2000): Temporal averaging of multitemporal ERS-1/2 tandem InSAR data. In: *IGARSS 2000*. IEEE International Geoscience and Remote Sensing Symposium, 24 - 28 July 2000, Honolulu, HI, USA, 2224–2226.
- Englhart, S., Keuck, V. & Siegert, F. (2011): Aboveground biomass retrieval in tropical forests: The potential of combined X- and L-band SAR data use. *Remote Sensing of Environment* 115 (5), 1260–1271.
- Engman, E. T. & Chauhan, N. (1995): Status of microwave soil moisture measurements with remote sensing. *Remote Sensing of Environment* 51 (1), 189–198.
- Entekhabi, D., Njoku, E. G. & O'Neill, P. E. et al. (2010): The soil moisture active passive (SMAP) mission. *Proceedings of the Institute of Electrical and Electronics Engineers* 98 (5), 704–716.
- EODC (2018): Sentinel-1 coverage maps: 2018-11-09. <https://eomex.eodc.eu/cm> (10.11.2018).
- Eriksen, S. H. & O'Brien, K. (2007): Vulnerability, poverty and the need for sustainable adaptation measures. *Climate Policy* 7 (4), 337–352.
- ESA (2010): Revised ESA earth observation data policy: 29 July 2010. <https://earth.esa.int/web/guest/-/revised-esa-earth-observation-data-policy-7098> (12.12.2018).
- ESA (2018): Activation of Long Term Archive (LTA) access: 10.09.2018. <https://earth.esa.int/web/sentinel/thematic-content/-/article/activation-of-long-term-archive-lta-access> (10.01.2019).
- Esch, T., Heldens, W. & Hirner, A. (2018): The Global Urban Footprint. In: Weng, Q., Quattrochi, D. & Gamba, P. E. (Eds.): *Urban remote sensing*. CRC Press, Boca Raton, 3–14.

- Esch, T., Marconcini, M. & Felbier, A. et al. (2013): Urban footprint processor—Fully automated processing chain generating settlement masks from global data of the TanDEM-X mission. *IEEE Geoscience and Remote Sensing Letters* 10 (6), 1617–1621.
- Esch, T., Thiel, M., Schenk, A., Roth, A., Muller, A. & Dech, S. (2010): Delineation of urban footprints from TerraSAR-X data by analyzing speckle characteristics and intensity information. *IEEE Transactions On Geoscience And Remote Sensing* 48 (2), 905–916.
- Etang-Ndip, A., Hoogeveen, J. & Lendorfer, J. (2015): *Socioeconomic impact of the crisis in North Mali on displaced people: Policy Research working paper WPS 7253*. The World Bank, Washington DC.
- Ezeoke, M. & Tong, K. (2012): Synthetic Aperture Radar signature for oil sands exploration. In: *EMS 2012. Sixth UKSim/AMSS European Symposium on Computer Modeling and Simulation*, 14 - 16 November 2012, Malta, Malta, 455–460.
- Fairfield, J. & Leymarie, P. (1991): Drainage networks from grid digital elevation models. *Water Resources Research* 27 (5), 709–717.
- Falkenmark, M. (1990): Global water issues confronting humanity. *Journal of Peace Research* 27 (2), 177–190.
- Farman-Farmaian, M. & Ndakass, V. (2014): UNHCR Chad at a glance. <http://reliefweb.int/sites/reliefweb.int/files/resources/UNHCR%20Chad%20at%20a%20Glance-30April2014.pdf> (31.01.2017).
- Farr, T. G., Rosen, P. A. & Caro, E. et al. (2007): The shuttle radar topography mission. *Reviews of Geophysics* 45 (2).
- Fast, L. (2014): *Aid in danger: The perils and promise of humanitarianism*. University of Pennsylvania Press, Pennsylvania.
- Fernandez Galarreta, J., Kerle, N. & Gerke, M. (2015): UAV-based urban structural damage assessment using object-based image analysis and semantic reasoning. *Natural Hazards and Earth System Sciences* 15 (6), 1087–1101.
- Ferretti, A., Monti-Guarnieri, A., Prati, C. & Rocca, F. (2007a): *InSAR processing: Part B: A practical approach*. ESA Publications, Noordwijk, The Netherlands.
- Ferretti, A., Monti-Guarnieri, A., Prati, C. & Rocca, F. (2007b): *InSAR processing: Part C: A mathematical approach*. ESA Publications, Noordwijk, The Netherlands.
- Ferretti, A., Monti-Guarnieri, A., Prati, C., Rocca, F. & Massonnet, D. (2007c): *InSAR principles: Part A: Guidelines for SAR interferometry processing and interpretation*. ESA Publications, Noordwijk, The Netherlands.
- Ferretti, A., Prati, C. & Rocca, F. (2001): Permanent scatterers in SAR interferometry. *IEEE Transactions On Geoscience And Remote Sensing* 39 (1), 8–20.
- Filho, C. d. O. A. & Rossetti, D. d. F. (2012): Effectiveness of SRTM and ALOS PALSAR data for identifying morphostructural lineaments in northeastern Brazil. *International Journal of Remote Sensing* 33 (4), 1058–1077.
- Fillol, E. (2018): ACF biomass explorer: Interactive maps of biomass production anomaly. [www.sigsahel.info/index.php/pays/acf-biomass](http://www.sigsahel.info/index.php/pays/acf-biomass) (21.01.2019).
- Fisher, P. F. & Tate, N. J. (2006): Causes and consequences of error in digital elevation models. *Progress in Physical Geography* 30 (4), 467–489.
- Flores-Prieto, E., Quénéhervé, G., Bachofer, F., Shahzad, F. & Maerker, M. (2015): Morphotectonic interpretation of the Makuyuni catchment in Northern Tanzania using DEM and SAR data. *Geomorphology* 248, 427–439.
- Forkuor, G., Landmann, T., Conrad, C. & Dech, S. (2012): Agricultural land use mapping in the sudanian savanna of West Africa: Current status and future possibilities. In: *IGARSS 2012. IEEE International Geoscience and Remote Sensing Symposium*, 22 - 27 July 2012, Munich, Germany, 6293–6296.
- Forkuor, G. & Maathuis, B. (2012): Comparison of SRTM and ASTER derived digital elevation models over two regions in Ghana: Implications for hydrological and environmental modeling. In: Piacentini, T. & Miccadei, E. (Eds.): *Studies on environmental and applied geomorphology*. InTech, London.

- Forster, B. C. (1985): An examination of some problems and solutions in monitoring urban areas from satellite platforms. *International Journal of Remote Sensing* 6 (1), 139–151.
- Forzieri, G., Gardenti, M., Caparrini, F. & Castelli, F. (2008): A methodology for the pre-selection of suitable sites for surface and underground small dams in arid areas: A case study in the region of Kidal, Mali. *Physics and Chemistry of the Earth, Parts A/B/C* 33 (1-2), 74–85.
- Franceschetti, G., Guida, R., Iodice, A., Riccio, D., Ruello, G. & Stilla, U. (2007): Building feature extraction via a deterministic approach: Application to real high resolution SAR images. In: *IGARSS 2007*. IEEE International Geoscience and Remote Sensing Symposium, 23 - 28 July 2007, Barcelona, Spain, 2681–2684.
- Franceschetti, G., Migliaccio, M. & Riccio, D. (1995): The SAR simulation: An overview. In: *IGARSS 1995*. IEEE International Geoscience and Remote Sensing Symposium, 10 - 14 July 1995, Firenze, Italy, 2283–2285.
- Franklin, J. (1995): Predictive vegetation mapping: Geographic modelling of biospatial patterns in relation to environmental gradients. *Progress in Physical Geography* 19 (4), 474–499.
- Freeman, A. (1992): SAR calibration: An overview. *IEEE Transactions On Geoscience And Remote Sensing* 30 (6), 1107–1121.
- Freeman, A. (2018): Design principles for smallsat SARs. In: *AIAA/USU 2018*. 32nd Annual AIAA/USU Conference on Small Satellites, 04 - 09 August, Utah, USA, 1–10.
- Freeman, A. & Durden, S. L. (1998): A three-component scattering model for polarimetric SAR data. *IEEE Transactions On Geoscience And Remote Sensing* 36 (3), 963–973.
- Freilich, M. (2018): Looking down on the earth: Satellites, science, and societal benefit. In: *EGU General Assembly Conference Abstracts*. European Geosciences Union General Assembly, 4-13 April 2018, Vienna, Austria, 19863.
- Friesen, J., Taubenböck, H., Wurm, M. & Pelz, P. F. (2018): The similar size of slums. *Habitat International* 73, 79–88.
- Frost, V. S., Stiles, J. A., Shanmugan, K. S. & Holtzman, J. C. (1982): A model for radar images and its application to adaptive digital filtering of multiplicative noise. *IEEE Transactions on Pattern Analysis and Machine Intelligence* (2), 157–166.
- Fügen, T., Sperlich, E. & Heer, C. et al. (2018): The biomass SAR instrument: Development status and performance overview. In: *IGARSS 2018*. IEEE International Geoscience and Remote Sensing Symposium, July 22-27, Valencia, Spain, 8571-8574.
- Funning, G. J., Parsons, B., Wright, T. J., Jackson, J. A. & Fielding, E. J. (2005): Surface displacements and source parameters of the 2003 Bam (Iran) earthquake from Envisat advanced synthetic aperture radar imagery. *Journal of Geophysical Research: Solid Earth* 110 (B9).
- Füreder, P., Hölbling, D., Tiede, D., Zeil, P. & Lang, S. (2012): Monitoring refugee camp evolution and population dynamics in Dagahaley, Kenya, based on VHR satellite data. In: *AARSE 2012*. 9th African Association of Remote Sensing of the Environment, 29 October - 02 November 2012, El Jadida, Morocco.
- Füreder, P. & Rogenhofer, E. (2014): *User requirements for geospatial information products: Online survey conducted within the project EO4HumEn (unpublished)*, Salzburg.
- Gabriel, A. K., Goldstein, R. M. & Zebker, H. A. (1989): Mapping small elevation changes over large areas: Differential radar interferometry. *Journal of Geophysical Research: Solid Earth* 94 (B7), 9183–9191.
- Gagnon, L. & Jouan, A. (1997): Speckle filtering of SAR images: A comparative study between complex-wavelet-based and standard filters. *International Society for Optics and Photonics. Wavelet Applications in Signal and Image Processing* (3169), 80–92.
- Gamba, P. E., Dell'Acqua, F. & Lisini, G. (2006): Change detection of multitemporal SAR data in urban areas combining feature-based and pixel-based techniques. *IEEE Transactions On Geoscience And Remote Sensing* 44 (10), 2820–2827.
- Gatelli, F., Guamieri, A. M., Parizzi, F., Pasquali, P., Prati, C. & Rocca, F. (1994): The wavenumber shift in SAR interferometry. *IEEE Transactions On Geoscience And Remote Sensing* 32 (4), 855–865.
- Gauthier, Y., Bernier, M. & Fortin, J.-P. (1998): Aspect and incidence angle sensitivity in ERS-1 SAR data. *International Journal of Remote Sensing* 19 (10), 2001–2006.

- Gee, J. (2017): Bangladesh, Southeast Asia worried by Rohingya crisis. *The Washington Report on Middle East Affairs* 36 (7), 39–40.
- Geis, A. & Schlag, G. (2017): ‘The facts cannot be denied’: Legitimacy, war and the use of chemical weapons in Syria. *Global Discourse* 7 (2-3), 285–303.
- Geladi, P., Isaksson, H., Lindqvist, L., Wold, S. & Esbensen, K. (1989): Principal component analysis of multivariate images. *Chemometrics and Intelligent Laboratory Systems* 5 (3), 209–220.
- Gemenne, F. (2015): One good reason to speak of climate refugees!. *Forced Migration Review* 49, 70–71.
- Gens, R. & van Genderen, J. L. (1996): SAR interferometry: Issues, techniques, applications. *International Journal of Remote Sensing* 17 (10), 1803–1835.
- Gernhardt, S. & Bamler, R. (2012): Deformation monitoring of single buildings using meter-resolution SAR data in PSI. *ISPRS Journal of Photogrammetry and Remote Sensing* 73, 68–79.
- Geudtner, D., Prats-Iraola, P. & Yague-Martinez, N. et al. (2017): Sentinel-1: Constellation, SAR interferometry, performance, verification. In: *Fringe 2017*. 10th International Workshop on “Advances in the Science and Applications of SAR Interferometry and Sentinel-1 InSAR, 05 - 09 June 2017, Helsinki, Finland.
- Ghasemi, N., Sahebi, M. R. & Mohammadzadeh, A. (2011): A review on biomass estimation methods using synthetic aperture radar data. *International Journal of Geomatics and Geosciences* 1 (4), 776.
- Ghorbanzadeh, O., Tiede, D., Dabiri, Z., Sudmanns, M. & Lang, S. (2018): Dwelling extraction in refugee camps using CNN - first experiences and lessons learnt. *International Archives of the Photogrammetry, Remote Sensing and Spatial Information Sciences* XLII-1, 161–166.
- Giada, S., Groeve, T. de, Ehrlich, D. & Soille, P. (2003): Information extraction from very high resolution satellite imagery over Lukole refugee camp, Tanzania. *International Journal of Remote Sensing* 24 (22), 4251–4266.
- Gilbert, A. (2007): The return of the slum: Does language matter? *International Journal of Urban and Regional Research* 31 (4), 697–713.
- Giles, P. T. (2001): Remote sensing and cast shadows in mountainous terrain. *Photogrammetric Engineering & Remote Sensing* 67 (7), 833–840.
- Gimeno, M., San-Miguel-Ayanz, J. & Schmuck, G. (2004): Identification of burnt areas in Mediterranean forest environments from ERS-2 SAR time series. *International Journal of Remote Sensing* 25 (22), 4873–4888.
- Girard, P., Goulet, N. & Malo, M. (1998): Geologie du Mali: Synthèse des données géologiques et cartographie. Amélioration et modernisation du Centre de Documentation.
- Giustarini, L., Hostache, R., Matgen, P., Schumann, G., Bates, P. D. & Mason, D. C. (2013): A change detection approach to flood mapping in urban areas using TerraSAR-X. *IEEE Transactions On Geoscience And Remote Sensing* 51 (4), 2417–2430.
- Goering, D. J., Chen, H., Hinzman, L. D. & Kane, D. L. (1995): Removal of terrain effects from SAR satellite imagery of arctic tundra. *IEEE Transactions On Geoscience And Remote Sensing* 33 (1), 185–194.
- Goff, M. & Crow, B. (2014): What is water equity? The unfortunate consequences of a global focus on ‘drinking water’. *Water International* 39 (2), 159–171.
- Goldstein, R. M. & Werner, C. L. (1998): Radar interferogram filtering for geophysical applications. *Geophysical Research Letters* 25 (21), 4035–4038.
- Gong, L. (2018): Laos dam collapse: The Regional Response. RSIS Commentaries. <http://hdl.handle.net/10220/45650> (18.07.2018).
- Gong, M., Li, Y., Jiao, L., Jia, M. & Su, L. (2014): SAR change detection based on intensity and texture changes. *ISPRS Journal of Photogrammetry and Remote Sensing* 93, 123–135.
- Gong, M., Yang, H. & Zhang, P. (2017): Feature learning and change feature classification based on deep learning for ternary change detection in SAR images. *ISPRS Journal of Photogrammetry and Remote Sensing* 129, 212–225.
- Gong, M., Zhao, J., Liu, J., Miao, Q. & Jiao, L. (2016): Change detection in synthetic aperture radar images based on deep neural networks. *IEEE Transactions on Neural Networks and Learning Systems* 27 (1), 125–138.

- Goodman, J. W. (1976): Some fundamental properties of speckle. *Journal of the Optical Society of America* 66 (11), 1145–1150.
- Gorelick, N., Hancher, M., Dixon, M., Ilyushchenko, S., Thau, D. & Moore, R. (2017): Google Earth Engine: Planetary-scale geospatial analysis for everyone. *Remote Sensing of Environment* 202, 18–27.
- Grasso, D. N. (1993): Applications of the IHS color transformation for 1: 24,000-scale geologic mapping—A low cost SPOT alternative. *Photogrammetric Engineering & Remote Sensing* 59 (1).
- Gray, A. L., Mattar, K. E. & Vachon, P. W. et al. (1998): InSAR results from the Radarsat antarctic mapping mission data: Estimation of glacier motion using a simple registration procedure. In: *IGARSS 1998*. IEEE International Geoscience and Remote Sensing Symposium, 6 - 10 July 1998, Seattle, WA.
- Gray, A. L., Vachon, P. W., Livingstone, C. E. & Lukowski, T. I. (1990): Synthetic aperture radar calibration using reference reflectors. *IEEE Transactions On Geoscience And Remote Sensing* 28 (3), 374–383.
- GSC (2017): Bangladesh: Version 2 with sector inputs. 3 June 2017. [https://www.sheltercluster.org/sites/default/files/docs/tc\\_mora\\_17\\_bangladesh\\_initial\\_assessment\\_v2\\_3rd\\_june\\_2017\\_1.pdf](https://www.sheltercluster.org/sites/default/files/docs/tc_mora_17_bangladesh_initial_assessment_v2_3rd_june_2017_1.pdf) (10.09.2018).
- Guimaraes, U. S., Narvaes, I. d. S., Galo, B. T. & Lourdes, M. de (2017): ERS, ENVISAT and Sentinel data application for change detection in amazon coastal environments. *Revista Brasileira de Geomorfologia*, 257–278.
- Gunawan, L. T., Alers, H., Brinkman, W.-P. & Neerincx, M. A. (2011): Distributed collaborative situation-map making for disaster response. *Interacting with Computers* 23 (4), 308–316.
- Gupta, V. (1995): New satellite images for sale. *International Security* 20 (1), 94–125.
- Gustavsson, L. (2003): Humanitarian logistics: Context and challenges. *Forced Migration Review* 18 (6), 6–8.
- Gutenson, J. L., Follum, M. L., Snow, A. D. & Wahl, M. D. (2017): Large-scale flood inundation modeling in data sparse environments using TanDEM-X terrain data. *Open Water Journal* 4 (2), 4.
- Haack, B. N., Herold, N. D. & Bechdol, M. A. (2000): Radar and optical data integration for land-use/land-cover mapping. *Photogrammetric Engineering & Remote Sensing* 66 (6), 709–716.
- Haack, B. N. & Slonecker, T. (1994): Merged spaceborne radar and thematic mapper digital data for locating villages in Sudan. *Photogrammetric Engineering & Remote Sensing* 60, 1253–1257.
- Hagenlocher, M., Lang, S. & Tiede, D. (2012): Integrated assessment of the environmental impact of an IDP camp in Sudan based on very high resolution multi-temporal satellite imagery. *Remote Sensing of Environment* 126, 27–38.
- Hagensieker, R., Roscher, R., Rosentreter, J., Jakimow, B. & Waske, B. (2017): Tropical land use land cover mapping in Pará (Brazil) using discriminative Markov random fields and multi-temporal TerraSAR-X data. *International Journal of Applied Earth Observation and Geoinformation* 63, 244–256.
- Hailey, C. (2009): *Camps: A guide to 21st-century space*. MIT Press, Cambridge, Mass.
- Hajnsek, I., Jagdhuber, T., Schon, H. & Papathanassiou, K. (2009a): Potential of estimating soil moisture under vegetation cover by means of PolSAR. *IEEE Transactions On Geoscience And Remote Sensing* 47 (2), 442–454.
- Hajnsek, I., Kugler, F., Lee, S.-K. & Papathanassiou, K. (2009b): Tropical-forest-parameter estimation by means of Pol-InSAR: The INDREX-II campaign. *IEEE Transactions On Geoscience And Remote Sensing* 47 (2), 481–493.
- Halpern, D., Fu, L. & Knauss, W. et al. (1995): An atlas of monthly mean distributions of SSM/I surface wind speed, AVHRR/2 sea surface temperature, AMI surface wind velocity, TOPEX/POSEIDON sea surface height, and ECMWF surface wind velocity during 1993. <https://ntrs.nasa.gov/archive/nasa/casi.ntrs.nasa.gov/19950023922.pdf> (05.12.2018).
- Hansen, M. C. & Loveland, T. R. (2012): A review of large area monitoring of land cover change using Landsat data. *Remote Sensing of Environment* 122, 66–74.
- Hanson, T. (2018): Biodiversity conservation and armed conflict: A warfare ecology perspective. *Annals of the New York Academy of Sciences*.

- Hanssen, R. F. (1998): Atmospheric heterogeneities in ERS tandem InSAR. In: *CEOS SAR 1998. CEOS SAR Workshop*, 3 - 6 February 1998, Noordwijk, 1–5.
- Hanssen, R. F. (2001): *Radar interferometry: Data interpretation and error analysis*. Springer Science & Business Media, Dordrecht.
- Haralick, R. M. (1979): Statistical and structural approaches to texture. *Proceedings of the Institute of Electrical and Electronics Engineers* 67 (5), 786–804.
- Haralick, R. M., Shanmugam, K. & Dinstein, I.'H. (1973): Textural features for image classification. *IEEE Transactions on Systems, Man, and Cybernetics* 3 (6), 610–621.
- Haralick, R. M. & Shapiro, L. G. (1985): Image segmentation techniques. *Applications of Artificial Intelligence II* 548, 2–10.
- Hariharan, S., Tirodkar, S. & Bhattacharya, A. (2016): Polarimetric SAR decomposition parameter subset selection and their optimal dynamic range evaluation for urban area classification using Random Forest. *International Journal of Applied Earth Observation and Geoinformation* 44, 144–158.
- Harris, I., Jones, P. D., Osborn, T. J. & Lister, D. H. (2014): Updated high-resolution grids of monthly climatic observations: The CRU TS3.10 Dataset. *International Journal of Climatology* 34 (3), 623–642.
- Harrison, C. G. & Williams, P. R. (2016): A systems approach to natural disaster resilience. *Simulation Modelling Practice and Theory* 65, 11–31.
- Hassan, J. A. (2018): The dust of Kutupalong. *International Journal of Human and Health Sciences (IJHHS)* 2 (3), 176.
- Hassan, M. M., Smith, A. C., Walker, K., Rahman, M. K. & Southworth, J. (2018): Rohingya refugee crisis and forest cover change in Teknaf, Bangladesh. *Remote Sensing* 10 (5), 689.
- Havivi, S., Schvartzman, I., Maman, S., Rotman, S. R. & Blumberg, D. G. (2018): Combining TerraSAR-X and Landsat images for emergency response in urban environments. *Remote Sensing* 10 (5), 802.
- He, H. S., Ventura, S. J. & Mladenoff, D. J. (2002): Effects of spatial aggregation approaches on classified satellite imagery. *International Journal of Geographical Information Science* 16 (1), 93–109.
- Heldens, W., Esch, T. & Asamer, H. et al. (2017): Exploiting earth observation data pools for urban analysis: The TEP URBAN project. In: Erbertseder, T., Chrysoulakis, N., Zhang, Y. & Heldens, W. (Eds.): *Remote sensing technologies and applications in urban environments II*. International Society for Optics and Photonics, Bellingham.
- Heldens, W., Heiden, U., Esch, T., Stein, E. & Müller, A. (2011): Can the future EnMAP mission contribute to urban applications?: A Literature Survey. *Remote Sensing* 3 (9), 1817–1846.
- Helmer, M. & Hilhorst, D. (2006): Natural disasters and climate change. *Disasters* 30 (1), 1–4.
- Henderson, F. M. & Lewis, A. J. (2008): Radar detection of wetland ecosystems: A review. *International Journal of Remote Sensing* 29 (20), 5809–5835.
- Henry, J. - B., Chastanet, P., Fellah, K. & Desnos, Y.-L. (2006): Envisat multi - polarized ASAR data for flood mapping. *International Journal of Remote Sensing* 27 (10), 1921–1929.
- Herrera, G., Tomás, R. & López-Sánchez, J. M. et al. (2007): Advanced DInSAR analysis on mining areas: La Union case study (Murcia, SE Spain). *Engineering Geology* 90 (3-4), 148–159.
- Herz, M. (2013): *From camp to city: Refugee camps of the Western Sahara*. Lars Müller, Zürich.
- Hess, L. L., Melack, J. M. & Simonett, D. S. (1990): Radar detection of flooding beneath the forest canopy: A review. *International Journal of Remote Sensing* 11 (7), 1313–1325.
- Hildreth, W. B. a. (2009): The financial logistics of disaster: The case of Hurricane Katrina. *Public Performance & Management Review* 32 (3), 400–436.
- Hinse, M., Gwyn, Q. H.J. & Bonn, F. (1988): Radiometric correction of C-band imagery for topographic effects in regions of moderate relief. *IEEE Transactions On Geoscience And Remote Sensing* 26 (2), 122–132.
- Hirano, A., Welch, R. & Lang, H. (2003): Mapping from ASTER stereo image data: DEM validation and accuracy assessment. *ISPRS Journal of Photogrammetry and Remote Sensing* 57 (5-6), 356–370.

- Hoffmann, J. (2007): Mapping damage during the Bam (Iran) earthquake using interferometric coherence. *International Journal of Remote Sensing* 28 (6), 1199–1216.
- Hollinger, J. P., Peirce, J. L. & Poe, G. A. (1990): SSM/I instrument evaluation. *IEEE Transactions On Geoscience And Remote Sensing* 28 (5), 781–790.
- Holthuijsen, L. H. (2010): *Waves in oceanic and coastal waters*. Cambridge University Press, London.
- Hong, S. H. & Won, J. S. (2006): ERS-ENVISAT cross-interferometry for coastal DEM construction. In: Osten, W. (Ed.): *Fringe 2005: The 5th International Workshop on Automatic Processing of Fringe Patterns*. Springer, Berlin.
- Hoogeveen, J., Rossi, M. & Sansone, D. (2017): Leaving, staying or coming back? An analysis of the migration dynamics during the northern Mali conflict. Working Paper 167/17. [http://www.cerp.carloalberto.org/wp-content/uploads/2017/01/WP\\_167.pdf](http://www.cerp.carloalberto.org/wp-content/uploads/2017/01/WP_167.pdf) (13.07.2018).
- Hooper, A., Segall, P. & Zebker, H. A. (2007): Persistent scatterer interferometric synthetic aperture radar for crustal deformation analysis, with application to Volcán Alcedo, Galápagos. *Journal of Geophysical Research* 112 (B7), 993.
- Hua, H., Owen, S. E. & Yun, S. H. et al. (2017): Large-scale Sentinel-1 processing for solid earth science and urgent response using cloud computing and machine learning. In: *AGU Fall Meeting Abstracts*. American Geophysical Union, Fall Meeting, 07 - 15 December, New Orleans, USA.
- Huang, Y. & van Genderen, J. L. (1996): Evaluation of several speckle filtering techniques for ERS-1&2 imagery. *International Archives of Photogrammetry and Remote Sensing B* (31), 164–169.
- Hunsberger, C., Corbera, E. & Borrás Jr, S. M. et al. (2015): Land-based climate change mitigation, land grabbing and conflict: Understanding intersections and linkages, exploring actions for change. *MOSAIC Working Paper Series No 1*.
- Hyde, P., Nelson, R., Kimes, D. & Levine, E. (2007): Exploring LiDAR-RaDAR synergy: Predicting aboveground biomass in a southwestern ponderosa pine forest using LiDAR, SAR and InSAR. *Remote Sensing of Environment* 106 (1), 28–38.
- Hydro-R&D International & Proman (2011): Schema Directeur eau & assainissement ville de Kidal: Report. April 2011.
- Hydro-R&D International & Proman (2012): Sustainable regional development programme in the region of Kidal (DDRK): Phase 3. <http://proman.lu/project/sustainable-regional-development-programme-in-the-region-of-kidal-ddrk-phase-3> (13.08.2018).
- IEEE (1993): Standard definitions of terms for antennas. Reaffirmed 2004.
- Imhoff, M. L. (1993): Radar backscatter/biomass saturation: Observations and implications for global biomass assessment. In: *IGARSS 1993*. IEEE International Geoscience and Remote Sensing Symposium, 18 - 21 August 1993, Tokyo, Japan, 43–45.
- Infante, D., Confuorto, P., Di Martire, D., Ramondini, M. & Calcaterra, D. (2016): Use of DInSAR data for multi-level vulnerability assessment of urban settings affected by slow-moving and intermittent landslides. *Procedia Engineering* 158, 470–475.
- Inglada, J. (2003): Change detection on SAR images by using a parametric estimation of the Kullback-Leibler divergence. In: *IGARSS 2003*. IEEE International Geoscience and Remote Sensing Symposium, 21 - 25 July 2003, Toulouse, France, 4104–4106.
- INS (2017): Annuaire statistique 2016: Edition Novembre 2017. [http://www.stat-guinee.org/images/Publications/INS/annuelles/INS\\_annuaire\\_2016.pdf](http://www.stat-guinee.org/images/Publications/INS/annuelles/INS_annuaire_2016.pdf) (15.10.2018).
- INSTAT (2013): Recensement général de la population et de l'habitat du Mali de 2009 (RGPH): Resultats definitifs: Tome 0: Répertoire des villages. [http://www.instat-mali.org/contenu/rgph/repvil09\\_rgph.pdf](http://www.instat-mali.org/contenu/rgph/repvil09_rgph.pdf) (13.07.2018).
- International Charter (2018): Annual Report 2017: International charter "Space & Major Disasters". <https://disasterscharter.org/documents/10180/14622/17th+Annual+Report.pdf> (03.01.2018).
- IOM (2017): South Sudanese refugees relocated to camps since September 2016 top 100,000: 22 September 2017. <http://www.iom.int/news/south-sudanese-refugees-relocated-camps-september-2016-top-100000> (15.08.2018).
- ISCG (2018): Situation report: Rohingya refugee crisis: Cox's Bazar, 26 April 2018. [https://reliefweb.int/sites/reliefweb.int/files/resources/20180426\\_iscg\\_sitrep.pdf](https://reliefweb.int/sites/reliefweb.int/files/resources/20180426_iscg_sitrep.pdf) (10.09.2018).

- Jacobsen, K. (1997): Refugees' environmental impact: The effect of patterns of settlement. *Journal of Refugee Studies* 10 (1), 19–36.
- Jain, M., Knieling, J. & Taubenböck, H. (2015): Urban transformation in the National Capital Territory of Delhi, India: The emergence and growth of slums? *Habitat International* 48, 87–96.
- Jain, S. K., Singh, R. D., Jain, M. K. & Lohani, A. K. (2005): Delineation of flood-prone areas using remote sensing techniques. *Water Resources Management* 19 (4), 333–347.
- Jansen, B. J. (2008): Between vulnerability and assertiveness: Negotiating resettlement in Kakuma refugee camp, Kenya. *African Affairs* 107 (429), 569–587.
- Jarihani, A. A., Callow, J. N., McVicar, T. R., van Niel, T. G. & Larsen, J. R. (2015): Satellite-derived digital elevation model (DEM) selection, preparation and correction for hydrodynamic modelling in large, low-gradient and data-sparse catchments. *Journal of Hydrology* 524, 489–506.
- JAXA (2018): Flood resulting from Xe Namnoy Xe Pian dam collapse in Lao PDR: Map produced by Asian Disaster Preparedness Center (ADPC).  
[https://disasterscharter.org/image/journal/article.jpg?img\\_id=934665&t=1532691595767](https://disasterscharter.org/image/journal/article.jpg?img_id=934665&t=1532691595767) (21.01.2019).
- Jensen, J. R. & Cowen, D. C. (1999): Remote sensing of urban/suburban infrastructure and socio-economic attributes. *Photogrammetric Engineering & Remote Sensing* 65, 611–622.
- Jerneck, A. & Olsson, L. (2008): Adaptation and the poor: Development, resilience and transition. *Climate Policy* 8 (2), 170–182.
- Jin, X. & Davis, C. H. (2005): Automated building extraction from high-resolution satellite imagery in urban areas using structural, contextual, and spectral information. *Journal on Advances in Signal Processing* 2005 (14), 745309.
- Johannessen, O. M., Dalen, Ø. & Bjørgo, E. et al. (2001): Environmental monitoring of refugee camps using high-resolution satellite images (EnviRef): Final report.  
<https://www.nersc.no/nb/biblio/enviref-environmental-monitoring-refugee-camps-using-high-resolution-satellite-images> (12.08.2018).
- Jones, B. K., Stryker, T. S., Mahmood, A. & Platzeck, G. R. (2015): The International Charter 'Space and Major Disasters'. In: Lippitt, C. D., Stow, D. A. & Coulter, L. L. (Eds.): *Time-sensitive remote sensing*. Springer, New York, 79–89.
- Jordan, R. L., Huneycutt, B. L. & Werner, M. (1995): The SIR-C/X-SAR synthetic aperture radar system. *IEEE Transactions On Geoscience And Remote Sensing* 33 (4), 829–839.
- Joshi, N., Baumann, M. & Ehammer, A. et al. (2016): A review of the application of optical and radar remote sensing data fusion to land use mapping and monitoring. *Remote Sensing* 8 (1), 70.
- Joshi, N., Mitchard, E. T. A. & Broolly, M. et al. (2017): Understanding 'saturation' of radar signals over forests. *Scientific Reports* 7 (1), 3505.
- Joyce, K. E., Belliss, S. E., Samsonov, S. V., McNeill, S. J. & Glassey, P. J. (2009): A review of the status of satellite remote sensing and image processing techniques for mapping natural hazards and disasters. *Progress in Physical Geography* 33 (2), 183–207.
- Jung, J., Kim, D.-j., Lavallo, M. & Yun, S.-H. (2016): Coherent change detection using InSAR temporal decorrelation model: A case study for volcanic ash detection. *IEEE Transactions On Geoscience And Remote Sensing* 54 (10), 5765–5775.
- Jung, M., Yeom, J. & Kim, Y. (2018): Comparison of pre-event VHR optical data and post-event PolSAR data to investigate damage caused by the 2011 Japan tsunami in built-up areas. *Remote Sensing* 10 (11), 1804.
- Kadhim, N., Mourshed, M. & Bray, M. (2016): Advances in remote sensing applications for urban sustainability. *Euro-Mediterranean Journal for Environmental Integration* 1 (1), 7.
- Kakonge, J. O. (2000): A review of refugee environmental-oriented projects in Africa: A case for environmental impact assessment. *Impact Assessment and Project Appraisal* 18 (1), 23–32.
- Karimzadeh, S., Samsonov, S. V. & Matsuoka, M. (2017): Block-based damage assessment of the 2012 Ahar-Varzaghan, Iran, earthquake through SAR remote sensing data. In: *IGARSS 2017. IEEE International Geoscience and Remote Sensing Symposium*, 23 - 28 July 2017, Fort Worth, TX, USA, 1546–1549.

- Kariuki, J. G., Machua, J. M. & Luvanda, A.M. Kigomo J. (2008): Baseline survey of woodland utilization and degradation around Kakuma refugee camp: JOFCA/KEFRI project, technical report no. 1. <http://fornistest.metla.fi/content/baseline-survey-woodland-utilization-and-degradation-around-kakuma-refugee-camp> (01.12.2018).
- Kelly, C. (1998): Bridging the gap: Remote sensing and needs assessment. A field experience with displaced populations. *Safety Science* 30 (1-2), 123–129.
- Kempf, T., Peichl, M., Dill, S., Anglberger, H. & Suess, H. (2007): Microwave radar signature acquisition of urban structures. In: *ITG WFMN 2007. Wave Propagation in Communication, Microwave Systems and Navigation*, 4 - 5 July 2007, Chemnitz.
- Keogh, E. J., Lonardi, S. & Chiu, B. Y.-c. (2002): Finding surprising patterns in a time series database in linear time and space. In: Hand, D., Keim, D. A. & Raymond, N. G. (Eds.): *KDD 2002. Eighth ACM SIGKDD International Conference on Knowledge Discovery and Data Mining*, 23 - 25 July, Edmonton, Canada, 550–556.
- Khalil, R. Z. (2017): InSAR coherence-based land cover classification of Okara, Pakistan. *The Egyptian Journal of Remote Sensing and Space Science*.
- Khosravi, I., Safari, A., Homayouni, S. & McNairn, H. (2017): Enhanced decision tree ensembles for land-cover mapping from fully polarimetric SAR data. *International Journal of Remote Sensing* 38 (23), 7138–7160.
- Kim, Y., Jackson, T., Bindlish, R., Hong, S., Jung, G. & Lee, K. (2014): Retrieval of wheat growth parameters with radar vegetation indices. *IEEE Geoscience and Remote Sensing Letters* 11 (4), 808–812.
- Kimura, H. & Ito, N. (2000): ALOS/PALSAR: The Japanese second-generation spaceborne SAR and its applications. In: Wilheit, T. T., Masuko, H. & Wakabayashi, H. (Eds.): *Microwave remote sensing of the atmosphere and environment II. Second International Asia-Pacific Symposium on Remote Sensing of the Atmosphere, Environment, and Space*, 9 October 2000, Sendai, Japan, 110–119.
- Knoth, C., Slimani, S., Appel, M. & Pebesma, E. (2018): Combining automatic and manual image analysis in a web-mapping application for collaborative conflict damage assessment. *Applied Geography* 97, 25–34.
- Koch, M. & Mather, P. M. (1997): Lineament mapping for groundwater resource assessment: A comparison of digital Synthetic Aperture Radar (SAR) imagery and stereoscopic Large Format Camera (LFC) photographs in the Red Sea Hills, Sudan. *International Journal of Remote Sensing* 18 (7), 1465–1482.
- Kohavi, R. (1995): A study of cross-validation and bootstrap for accuracy estimation and model selection. In: *IJCAI 1995. Fourteenth International Joint Conference on Artificial Intelligence*, 20 - 25 August 1995, Montreal, Canada, 1137–1145.
- Kovács, G. & Spens, K. (2009): Identifying challenges in humanitarian logistics. *International Journal of Physical Distribution & Logistics Management* 39 (6), 506–528.
- Krogager, E. (1990): New decomposition of the radar target scattering matrix. *Electronics Letters* 26 (18), 1525.
- Krueger, T., Page, T., Hubacek, K., Smith, L. & Hiscock, K. (2012): The role of expert opinion in environmental modelling. *Environmental Modelling & Software* 36, 4–18.
- Kuffer, M. (2003): Monitoring the dynamics of informal settlements in Dar Es Salaam by remote sensing: Exploring the use of SPOT, ERS and small format aerial pPhotography. In: Schrenk, M. (Ed.): *CORP 2003. Information Technology in Urban and Spatial Planning*, 28 February - 1 March, Vienna, Austria, 473–483.
- Kuffer, M., Wang, J. & Nagenborg, M. et al. (2018): The scope of earth-observation to improve the consistency of the SDG slum indicator. *ISPRS International Journal of Geo-Information* 7 (11), 428.
- Kulkarni, V. Y. & Sinha, P. K. (2012): Pruning of random forest classifiers: A survey and future directions. In: *ICDSE 2012. International Conference on Data Science & Engineering*, 18 - 20 Juli 2012, Piscataway, NJ, USA, 64–68.

- Kuplich, T. M., Curran, P. J. & Atkinson, P. M. (2003): Relating SAR image texture and backscatter to tropical forest biomass. In: *IGARSS 2003*. IEEE International Geoscience and Remote Sensing Symposium, 21 - 25 July 2003, Toulouse, France, 2872–2874.
- Labib, S. M., Hossain, N. & Patwary, S. H. (2018): Environmental cost of refugee crisis: Case study of Kutupalong-Balukhali Rohingya camp site: A remote sensing approach. In: *GISRUK 2018*. 26th annual GIScience Research UK conference, 17 - 20 April 2018, Leicester, UK, 1–7.
- Lachaise, M., Fritz, T., Bals, U., Bamler, R. & Eineder, M. (2012): Phase unwrapping correction with dual-baseline data for the TanDEM-X mission. In: *IGARSS 2012*. IEEE International Geoscience and Remote Sensing Symposium, 22 - 27 July 2012, Munich, Germany, 5566–5569.
- Laneve, G., Santilli, G. & Lingenfelder, I. (2007): Development of automatic techniques for refugee camps monitoring using very high spatial resolution (VHSR) satellite imagery. In: *IGARSS 2006*. IEEE International Geoscience and Remote Sensing Symposium, 31 July - 4 August 2006, Denver, USA, 841–845.
- Lang, S. (2014): *Operationelle Fernerkundungsdienste: Nutzen aktuelle "Lösungen" wirklich das gesamte Potential?: 3. Gemeinsamer Workshop der Arbeitskreise "Auswertung von Fernerkundungsdaten der DGPF e.V." und "Fernerkundung" der DGfG e.V.*, Berlin.
- Lang, S. & Füreder, P. (2015): Earth observation for humanitarian operations. *Journal for Geographic Information Science* 1, 384–390.
- Lang, S., Füreder, P., Kranz, O., Card, B., Roberts, S. & Papp, A. (2015): Humanitarian emergencies: Causes, traits and impacts as observed by remote sensing. In: Thenkabail, P. S. (Ed.): *Remote sensing of water resources, disasters, and urban studies*. CRC Press, Boca Raton, 483–512.
- Lang, S., Füreder, P. & Rogenhofer, E. (2018): Earth observation for humanitarian action. In: Al-Ekabi, C. & Ferretti, S. (Eds.): *Yearbook on Space Policy 2016: Space for sustainable development*. Springer International Publishing, Cham, 217–229.
- Langer, S., Tiede, D. & Lüthje, F. (2015): Long-term monitoring of the environmental impact of a refugee camp based on Landsat time series: The example of deforestation and reforestation during the whole lifespan of the camp Lukole, Tanzania. *Journal for Geographic Information Science* 1, 434–437.
- Laur, H., Casu, F., Bally, P., Caumont, H. & Pinto, S. (2016): The Geohazards Exploitation Platform. In: *EGU General Assembly 2016*. European Geosciences Union General Assembly, 17 – 22 April 2016, Vienna, Austria, 14672.
- Lavalle, M., Solimini, D., Pottier, E. & Desnos, Y.-L. (2008): PolInSAR for forest biomass retrieval: PALSAR observations and model analysis. In: *IGARSS 2008*. IEEE International Geoscience and Remote Sensing Symposium, 7 - 11 July 2008, Boston, MA, USA, 302–305.
- Le Toan, T., Beaudoin, A., Riom, J. & Guyon, D. (1992): Relating forest biomass to SAR data. *IEEE Transactions On Geoscience And Remote Sensing* 30 (2), 403–411.
- Lee, J.-S. (1980): Digital image enhancement and noise filtering by use of local statistics. *IEEE Transactions on Pattern Analysis and Machine Intelligence* (2), 165–168.
- Lee, J.-S. (1981): Refined filtering of image noise using local statistics. *Computer Graphics and Image Processing* 15 (4), 380–389.
- Lee, J.-S. (1983): A simple speckle smoothing algorithm for synthetic aperture radar images. *IEEE Transactions on Systems, Man, and Cybernetics* (1), 85–89.
- Lee, J.-S. (1986): Speckle suppression and analysis for synthetic aperture radar images. *Optical Engineering* 25 (5), 255636.
- Lee, J.-S., Grunes, M. R., Ainsworth, T. L., Du, L.-J., Schuler, D. L. & Cloude, S. R. (1999): Unsupervised classification using polarimetric decomposition and the complex Wishart classifier. *IEEE Transactions On Geoscience And Remote Sensing* 37 (5), 2249–2258.
- Lee, J.-S., Grunes, M. R., Schuler, D. L., Pottier, E. & Ferro-Famil, L. (2006): Scattering-model-based speckle filtering of polarimetric SAR data. *IEEE Transactions On Geoscience And Remote Sensing* 44 (1), 176–187.
- Lee, J.-S., Jurkevich, L., Dewaele, P., Wambacq, P. & Oosterlinck, A. (1994): Speckle filtering of synthetic aperture radar images: A review. *Remote Sensing Reviews* 8 (4), 313–340.
- Lee, J.-S. & Pottier, E. (2009): *Polarimetric radar imaging: From basics to applications*. CRC Press, Boca Raton.

- Lee, J.-S., Wen, J.-H., Ainsworth, T. L., Chen, K.-S. & Chen, A. J. (2009): Improved sigma filter for speckle filtering of SAR imagery. *IEEE Transactions On Geoscience And Remote Sensing* 47 (1), 202–213.
- Lee, S.-R. (2010): Overview of KOMPSAT-5 program, mission, and system. In: *IGARSS 2010*. IEEE International Geoscience and Remote Sensing Symposium, 25 - 30 July 2010, Honolulu, HI, USA, 797–800.
- Lehner, A., Naeimi, V. & Steinnocher, K. (2017): Sentinel-1 for urban areas-comparison between automatically derived settlement layers from Sentinel-1 data and Copernicus high resolution information layers. In: *GISTAM 2017*. International Conference on Geographical Information Systems Theory, Applications and Management, 27 - 28 April 2017, Porto, Portugal.
- Lehner, B., Verdin, K. & Jarvis, A. (2008): New global hydrography derived from spaceborne elevation data. *Transactions American Geophysical Union* 89 (10), 93–94.
- Lei, L., Perissin, D. & Qin, Y. (2013): Change detection with spaceborne InSAR technique in Hong Kong. In: *IGARSS 2013*. IEEE International Geoscience and Remote Sensing Symposium, 21 - 26 July 2013, Melbourne, Australia, 338–341.
- Leidman, E., Humphreys, A. & Cramer, B. G. et al. (2018): Acute malnutrition and anemia among Rohingya children in Kutupalong camp, Bangladesh. *JAMA* 319 (14), 1505–1506.
- Lessard-Fontaine, A., Soupart, M. & Laborderie, S. de (2015): Supporting Ebola combat with satellite images: The MSF perspective. *Journal for Geographic Information Science*, 445–448.
- Li, H., Gong, M., Wang, Q., Liu, J. & Su, L. (2016): A multiobjective fuzzy clustering method for change detection in SAR images. *Applied Soft Computing* 46, 767–777.
- Li, Z., Liu, J. & Xu, C. (2004): Error analysis in InSAR data processing. *Wuhan Daxue Xuebao (Xinxi Kexue Ban)* 29 (1), 72–76.
- Liao, M., Jiang, L., Lin, H., Huang, B. & Gong, J. (2008): Urban change detection based on coherence and intensity characteristics of SAR imagery. *Photogrammetric Engineering & Remote Sensing* 74 (8), 999–1006.
- Ließ, M., Glaser, B. & Huwe, B. (2012): Uncertainty in the spatial prediction of soil texture. *Geoderma* 170, 70–79.
- Lillesand, T. M., Kiefer, R. W. & Chipman, J. W. (2008): *Remote sensing and image interpretation*, 6. ed. Wiley, Hoboken, NJ.
- Lin, X., Zhang, R. & Shen, J. (2012): A template-matching based approach for extraction of roads from very high-resolution remotely sensed imagery. *International Journal of Image and Data Fusion* 3 (2), 149–168.
- Lindsey, E. O., Natsuaki, R. & Xu, X. et al. (2015): Line - of - sight displacement from ALOS - 2 interferometry: Mw 7.8 Gorkha earthquake and Mw 7.3 aftershock. *Geophysical Research Letters* 42 (16), 6655–6661.
- Lischer, S. K. (2005): *Dangerous sanctuaries: Refugee camps, civil war, and the dilemmas of humanitarian aid*. Cornell University Press, Ithaca.
- Lisini, G., Salentinig, A., Du, P. & Gamba, P. E. (2018): SAR-based urban extents extraction: From ENVISAT to Sentinel-1. *IEEE Journal of Selected Topics in Applied Earth Observations and Remote Sensing* 11 (8), 2683–2691.
- Lisle, D. de, Iris, S., Arsenault, E., Smyth, J. & Kroupnik, G. (2018): Radarsat constellation mission status update. In: *EUSAR 2018*. 12th European Conference on Synthetic Aperture Radar, 04 - 07 June 2018, Aachen, Germany, 1–5.
- Liu, H., Zhao, Z. & Jezek, K. C. (2004): Correction of positional errors and geometric distortions in topographic maps and DEMs using a rigorous SAR simulation technique. *Photogrammetric Engineering & Remote Sensing* 70 (9), 1031–1042.
- Liu, J., Heiskanen, J., Aynekulu, E., Maeda, E. & Pellikka, P. (2016): Land cover characterization in west Sudanian savannas using seasonal features from annual Landsat time series. *Remote Sensing* 8 (5), 365.
- Liu, J. G., Black, A., Lee, H., Hanaizumi, H. & Moore, J. (2001): Land surface change detection in a desert area in Algeria using multi-temporal ERS SAR coherence images. *International Journal of Remote Sensing* 22 (13), 2463–2477.

- Liu, L., Schaefer, K. M., Chen, A. C., Gusmeroli, A., Zebker, H. A. & Zhang, T. (2015): Remote sensing measurements of thermokarst subsidence using InSAR. *Journal of Geophysical Research: Earth Surface* 120 (9), 1935–1948.
- Lodhi, M. A., Echavarria, F. R. & Keithley, C. (1998): Using remote sensing data to monitor land cover changes near Afghan refugee camps in northern Pakistan. *Geocarto International* 13 (1), 33–39.
- Loew, A. & Mauser, W. (2007): Generation of geometrically and radiometrically terrain corrected SAR image products. *Remote Sensing of Environment* 106 (3), 337–349.
- Loheide, S. P. & Gorelick, S. M. (2007): Riparian hydroecology: A coupled model of the observed interactions between groundwater flow and meadow vegetation patterning. *Water Resources Research* 43 (7).
- Loneragan, S. (1998): The role of environmental degradation in population displacement. *Environmental change and security project report* 4 (6), 5–15.
- Long, M. W. (1983): *Radar reflectivity of land and sea*, 2. ed. Artech House, Dedham, Mass.
- Longley, C. & Maxwell, D. (2003): *Livelihoods, chronic conflict and humanitarian response: A synthesis of current practice*, London.
- Longley, P. A. (2002): Geographical information systems: Will developments in urban remote sensing and GIS lead to 'better' urban geography? *Progress in Human Geography* 26 (2), 231–239.
- Lopes, A., Nezry, E., Touzi, R. & Laur, H. (1993): Structure detection and statistical adaptive speckle filtering in SAR images. *International Journal of Remote Sensing* 14 (9), 1735–1758.
- López-García, M. J. & Caselles, V. (1991): Mapping burns and natural reforestation using Thematic Mapper data. *Geocarto International* 6 (1), 31–37.
- Louet, J. & Bruzzi, S. (1999): ENVISAT mission and system. In: *IGARSS 1999*. IEEE International Geoscience and Remote Sensing Symposium, 28 June - 2 July 1999, Hamburg, Germany, 1680–1682.
- Lu, D., Mausel, P., Brondizio, E. & Moran, E. (2004): Change detection techniques. *International Journal of Remote Sensing* 25 (12), 2365–2401.
- Lu, Z. & Dzurisin, D. (2014): InSAR observations and insights into aleutian volcanism. In: Lu, Z. & Dzurisin, D. (Eds.): *InSAR imaging of Aleutian volcanoes*. Springer, Berlin, 347–367.
- Luckman, A., Baker, J., Kuplich, T. M., Yanasse, C. & Frery, A. C. (1997): A study of the relationship between radar backscatter and regenerating tropical forest biomass for spaceborne SAR instruments. *Remote Sensing of Environment* 60 (1), 1–13.
- Ludwig, R. & Schneider, P. (2006): Validation of digital elevation models from SRTM X-SAR for applications in hydrologic modeling. *ISPRS Journal of Photogrammetry and Remote Sensing* 60 (5), 339–358.
- Lüge, T., Sudhoff, R. S., Lessard-Fontaine, A., La Borderie, S. de & Soupart, M. (2014): GIS support for the MSF Ebola response in Guinea in 2014 case study. *Geneva: Médecins Sans Frontières Operational Center*.
- Lundgren, P., Casu, F. & Manzo, M. et al. (2004): Gravity and magma induced spreading of Mount Etna volcano revealed by satellite radar interferometry. *Geophysical Research Letters* 31 (4).
- Lüneburg, E., Ziegler, V., Schroth, A. & Tragl, K. (1991): Polarimetric covariance matrix analysis of random radar targets. In: *AGARD 1991*. Electromagnetic Wave Propagation Panel Symposium on Target and Clutter Scattering and Their Effects on Military Radar Performance, 6 - 10 May 1991, Ottawa, Canada, 1–12.
- Lusch, D. P. (1999): *Introduction to microwave remote sensing*. Michigan State University, Michigan.
- Ma, L., Li, M. & Blaschke, T. et al. (2016): Object-based change detection in urban areas: The effects of segmentation strategy, scale, and feature space on unsupervised methods. *Remote Sensing* 8 (9), 761.
- Ma, Y., Wu, H. & Wang, L. et al. (2015): Remote sensing big data computing: Challenges and opportunities. *Future Generation Computer Systems* 51, 47–60.

- Maghsoudi, Y., Collins, M. J. & Leckie, D. (2011): Speckle reduction for the forest mapping analysis of multi-temporal Radarsat-1 images. *International Journal of Remote Sensing* 33 (5), 1349–1359.
- Mahabir, R., Croitoru, A., Crooks, A., Agouris, P. & Stefanidis, A. (2018): A critical review of high and very high-resolution remote sensing approaches for detecting and mapping slums: Trends, challenges and emerging opportunities. *Urban Science* 2 (1), 8.
- Malsin, J. (2017): Raqqa is in ruins and ISIS in retreat. *Time*, October 22. <http://time.com/raqqa-ruins-isis-retreat/> (04.01.2018).
- Mansourpour, M., Rajabi, M. A. & Blais, J. A. R. (2006): Effects and performance of speckle noise reduction filters on active radar and SAR images. *International Archives of Photogrammetry and Remote Sensing* 36 (1), W41.
- MapAction (2011): Field guide to humanitarian mapping. [https://mapaction.org/wp-content/uploads/2016/12/mapaction\\_field\\_guide\\_to\\_humanitarian\\_mapping.pdf](https://mapaction.org/wp-content/uploads/2016/12/mapaction_field_guide_to_humanitarian_mapping.pdf) (15.09.2018).
- Mari, S., Valentini, G. & Serva, S. et al. (2018): COSMO-SkyMed second generation system access portfolio. *IEEE Geoscience and Remote Sensing Magazine* 6 (1), 35–43.
- Márquez-Martínez, J., Cohen, J., Doody, S., Lau-Semedo, P. & Larkins, A. (2017): Next generation low cost SAR payloads: NovaSAR-S and beyond. In: *IGARSS 2017*. IEEE International Geoscience and Remote Sensing Symposium, 23 - 28 July 2017, Fort Worth, TX, USA.
- Martin, A. (2005): Environmental conflict between refugee and host communities. *Journal of Peace Research* 42 (3), 329–346.
- Martin, M. F., Margesson, R. & Vaughn, B. (2017): The Rohingya crises in Bangladesh and Burma: CRS Report R45016. <https://fas.org/sgp/crs/row/R45016.pdf> (11.08.2018).
- Martinez, J.-M. & Le Toan, T. (2007): Mapping of flood dynamics and spatial distribution of vegetation in the Amazon floodplain using multitemporal SAR data. *Remote Sensing of Environment* 108 (3), 209–223.
- Martinis, S., Kuenzer, C. & Wendleder, A. et al. (2015): Comparing four operational SAR-based water and flood detection approaches. *International Journal of Remote Sensing* 36 (13), 3519–3543.
- Martinis, S., Twele, A. & Voigt, S. (2009): Towards operational near real-time flood detection using a split-based automatic thresholding procedure on high resolution TerraSAR-X data. *Natural Hazards and Earth System Sciences* 9 (2), 303–314.
- Marx, A. & Goward, S. N. (2013): Remote sensing in human rights and international humanitarian law monitoring: Concepts and methods. *Geographical Review* 103 (1), 100–111.
- Mason, D. C. & Davenport, I. J. (1996): Accurate and efficient determination of the shoreline in ERS-1 SAR images. *IEEE Transactions On Geoscience And Remote Sensing* 34 (5), 1243–1253.
- Mason, D. C., Giustarini, L., Garcia-Pintado, J. & Cloke, H. L. (2014): Detection of flooded urban areas in high resolution Synthetic Aperture Radar images using double scattering. *International Journal of Applied Earth Observation and Geoinformation* 28, 150–159.
- Mason, D. C., Schumann, G., Neal, J. C., Garcia-Pintado, J. & Bates, P. D. (2012): Automatic near real-time selection of flood water levels from high resolution Synthetic Aperture Radar images for assimilation into hydraulic models: A case study. *Remote Sensing of Environment* 124, 705–716.
- Mason, D. C., Speck, R., Devereux, B., Schumann, G., Neal, J. C. & Bates, P. D. (2010): Flood detection in urban areas using TerraSAR-X. *IEEE Transactions On Geoscience And Remote Sensing* 48 (2), 882–894.
- Mason, D. C., Trigg, M., Garcia-Pintado, J., Cloke, H. L., Neal, J. C. & Bates, P. D. (2016): Improving the TanDEM-X digital elevation model for flood modelling using flood extents from Synthetic Aperture Radar images. *Remote Sensing of Environment* 173, 15–28.
- Massonnet, D. & Feigl, K. L. (1998): Radar interferometry and its application to changes in the earth's surface. *Reviews of Geophysics* 36 (4), 441–500.
- Massonnet, D., Rossi, M. & Carmona, C. et al. (1993): The displacement field of the Landers earthquake mapped by radar interferometry. *Nature* 364, 138 EP -.
- Matgen, P., Hostache, R., Schumann, G., Pfister, L., Hoffmann, L. & Savenije, H.H.G. (2011): Towards an automated SAR-based flood monitoring system: Lessons learned from two case studies. *Physics and Chemistry of the Earth, Parts A/B/C* 36 (7-8), 241–252.

- Mathew, D. (2005): Information technology and public health management of disasters: A model for South Asian countries. *Prehospital and Disaster Medicine* 20 (1), 54–60.
- Matsuoka, M. & Yamazaki, F. (2004): Use of satellite SAR intensity imagery for detecting building areas damaged due to earthquakes. *Earthquake Spectra* 20 (3), 975–994.
- Maxwell, J. C. (1865): A dynamical theory of the electromagnetic field. *Philosophical Transactions of the Royal Society of London* 155 (0), 459–512.
- McKeown, D. M. (1990): Toward automatic cartographic feature extraction. In: Pau, L. F. (Ed.): *Mapping and spatial modelling for navigation*. Springer, Heidelberg, 149–180.
- MDA (2016): Radarsat-2 pricing information. <https://mdacorporation.com/docs/default-source/product-spec-sheets/geospatial-services/pricelist.pdf?sfvrsn=12> (15.01.2019).
- Meier, E., Frei, U. & Nüesch, D. (1993): Precise terrain corrected geocoded images. *SAR Geocoding: Data and Systems*, 173–185.
- Meier, P. (2015): *Digital humanitarians: How big data is changing the face of humanitarian response*. Routledge, Boca Raton.
- Meier, P., Milzow, C., Kgotlhang, L. & Kinzelbach, W. (2010): Recognition of flooding patterns in the Okavango delta using ENVISAT ASAR images. In: UNESCO (Ed.): *Application of satellite remote sensing to support water resources management in Africa: Results from the TIGER Initiative*, Paris, 124–132.
- Meijerink, A. M. J., Bannert, D., Batelaan, O., Lubczynski, M. W. & Pointet, T. (2007): *Remote sensing applications to groundwater*. United Nations Educational, Scientific and Cultural Organization (UNESCO), Paris.
- Melesse, A. M., Weng, Q., Thenkabail, P. S. & Senay, G. B. (2007): Remote sensing sensors and applications in environmental resources mapping and modelling. *Sensors* 7 (12), 3209–3241.
- Merwade, V., Olivera, F., Arabi, M. & Edleman, S. (2008): Uncertainty in flood inundation mapping: Current issues and future directions. *Journal of Hydrologic Engineering* 13 (7), 608–620.
- Methmann, C. & Oels, A. (2015): From ‘fearing’ to ‘empowering’ climate refugees: Governing climate-induced migration in the name of resilience. *Security Dialogue* 46 (1), 51–68.
- Meyer, F. J. (2017): A cloud-based system for automatic hazard monitoring from Sentinel-1 SAR data. In: *AGU Fall Meeting Abstracts*. American Geophysical Union, Fall Meeting, 07 - 15 December, New Orleans, USA.
- Middleton, N. & Thomas, D. S. G. (1997): *World atlas of desertification*, 2nd ed. Arnold, London.
- Milillo, P., Riel, B., Minchew, B., Yun, S.-H., Simons, M. & Lundgren, P. (2016): On the synergistic use of SAR constellations’ data exploitation for earth science and natural hazard response. *IEEE Journal of Selected Topics in Applied Earth Observations and Remote Sensing* 9 (3), 1095–1100.
- Misra, T., Rana, S. S. & Desai, N. M. et al. (2013): Synthetic Aperture Radar payload on-board RISAT-1: Configuration, technology and performance. *Current Science*, 446–461.
- Mitcham, C. & Muñoz, D. (2010): Humanitarian engineering. *Synthesis Lectures on Engineers, Technology, and Society* 5 (1), 1–87.
- Mitchard, E. T. A. & Flintrop, C. M. (2013): Woody encroachment and forest degradation in sub-Saharan Africa's woodlands and savannas 1982–2006. *Philosophical Transactions of the Royal Society of London* 368 (1625), 20120406.
- Mitchard, E. T. A., Saatchi, S. S. & Lewis, S. L. et al. (2011): Measuring biomass changes due to woody encroachment and deforestation/degradation in a forest-savanna boundary region of central Africa using multi-temporal L-band radar backscatter. *Remote Sensing of Environment* 115 (11), 2861–2873.
- Mitchard, E. T. A., Saatchi, S. S. & White, L. J. T. et al. (2012): Mapping tropical forest biomass with radar and spaceborne LiDAR in Lopé National Park, Gabon: Overcoming problems of high biomass and persistent cloud. *Biogeosciences* 9 (1), 179–191.
- Mitchard, E. T. A., Saatchi, S. S. & Woodhouse, I. H. et al. (2009): Using satellite radar backscatter to predict above-ground woody biomass: A consistent relationship across four different African landscapes. *Geophysical Research Letters* 36 (23), 409.

- Mittermayer, J., Wollstadt, S., Prats-Iraola, P. & Scheiber, R. (2014): The TerraSAR-X Staring Spotlight mode concept. *IEEE Transactions On Geoscience And Remote Sensing* 52 (6), 3695–3706.
- Mladenova, I. E., Jackson, T., Bindlish, R. & Hensley, S. (2013): Incidence angle normalization of radar backscatter data. *IEEE Transactions On Geoscience And Remote Sensing* 51 (3), 1791–1804.
- Moghaddam, M. & Saatchi, S. S. (1995): Analysis of scattering mechanisms in SAR imagery over boreal forest: Results from BOREAS '93. *IEEE Transactions On Geoscience And Remote Sensing* 33 (5), 1290–1296.
- Monaco, J. E. (2014): *Supporting timely humanitarian assistance / disaster response decisions through geospatial intelligence and GIS tools: AY 2014-001*. United States Army Command and General Staff College, Fort Leavenworth.
- Monier, C. (2009): Goz Beida: Monthly report. [https://www.unicef.org/wcaro/wcaro\\_chad-UNICEFMonthly\\_Report\\_Nov\\_09.pdf](https://www.unicef.org/wcaro/wcaro_chad-UNICEFMonthly_Report_Nov_09.pdf) (31.01.2017).
- Monju, A. N. (2017): New reports says Bangladesh island chosen to relocate Rohingyas 'fit for habitation'. *BD News*, February 25. <https://bdnews24.com/bangladesh/2017/02/25/new-government-report-finds-bangladesh-island-chosen-to-relocate-rohingyas-as-fit-for-habitation> (11.08.2018).
- Montclos, M.-A. P. d. & Kagwanja, P. M. (2000): Refugee camps or cities? The socio-economic dynamics of the Dadaab and Kakuma camps in Northern Kenya. *Journal of Refugee Studies* 13 (2), 205–222.
- Moreira, A., Bachmann, M. & Balzer, W. et al. (2018): Tandem-L: Project status and main findings of the phase B1 study. In: *IGARSS 2018*. IEEE International Geoscience and Remote Sensing Symposium, July 22–27, Valencia, Spain.
- Moreira, A., Krieger, G. & Hajnsek, I. et al. (2004): TanDEM-X: A TerraSAR-X add-on satellite for single-pass SAR interferometry. In: *IGARSS 2004*. IEEE International Geoscience and Remote Sensing Symposium, 20 - 24 September 2004, Anchorage, USA, 1000–1003.
- Morena, L. C., James, K. V. & Beck, J. (2004): An introduction to the Radarsat-2 mission. *Canadian Journal of Remote Sensing* 30 (3), 221–234.
- Moser, G. & Serpico, S. B. (2006): Generalized minimum-error thresholding for unsupervised change detection from SAR amplitude imagery. *IEEE Transactions On Geoscience And Remote Sensing* 44 (10), 2972–2982.
- Moser, G. & Serpico, S. B. (2009): Unsupervised change detection from multichannel SAR data by Markovian data fusion. *IEEE Transactions On Geoscience And Remote Sensing* 47 (7), 2114–2128.
- Moser, L., Probeck, M. & Ramminger, G. et al. (2017): Sentinel-based evolution of copernicus land services on continental and global scale. In: *WorldCover 2017*. ESA WorldCover, 14 - 16 March 2017, Frascati.
- MSF (2014): Ethiopia: Critical conditions for South Sudanese refugees in Gambella: 09 July 2014. <https://www.msf.org.uk/article/ethiopia-critical-conditions-south-sudanese-refugees-gambella> (04.11.2018).
- Mulder, F., Ferguson, J., Groenewegen, P., Boersma, K. & Wolbers, J. (2016): Questioning big data: Crowdsourcing crisis data towards an inclusive humanitarian response. *Big Data & Society* 3 (2), 2053951716662054.
- Mulder, V. L., Bruin, S. de, Schaepman, M. E. & Mayr, T. R. (2011): The use of remote sensing in soil and terrain mapping: A review. *Geoderma* 162 (1–2), 1–19.
- Müller, M. F., Yoon, J., Gorelick, S. M., Avisse, N. & Tilmant, A. (2016): Impact of the Syrian refugee crisis on land use and transboundary freshwater resources. *Proceedings of the National Academy of Sciences of the United States of America* 113 (52), 14932–14937.
- Musa, Z. N., Popescu, I. & Mynett, A. (2015): A review of applications of satellite SAR, optical, altimetry and DEM data for surface water modelling, mapping and parameter estimation. *Hydrology and Earth System Sciences* 19 (9), 3755–3769.

- Ndyeshumba, P. (2000): The use of remote sensing for environmental impact assessment and determination of the area affected by refugees in Ngara district north western Tanzania. *International Archives of Photogrammetry and Remote Sensing* 33 (B7/3; PART 7), 981–984.
- Neckel, N., Braun, A., Kropáček, J. & Hochschild, V. (2013): Recent mass balance of the Purogangri Ice Cap, central Tibetan Plateau, by means of differential X-band SAR interferometry. *The Cryosphere* 7 (5), 1623.
- Neumann, M., Saatchi, S. S., Ulander, L. M. H. & Fransson, J. E. S. (2011): Parametric and non-parametric forest biomass estimation from PolInSAR data. In: *IGARSS 2011. IEEE International Geoscience and Remote Sensing Symposium*, 24 - 29 July 2011, Vancouver, BC, Canada, 420–423.
- Newell, R. G. & Stavins, R. N. (2000): Climate change and forest sinks: Factors affecting the costs of carbon sequestration. *Journal of Environmental Economics and Management* 40 (3), 211–235.
- Nezry, E., Leysen, M. & de Grandi, G. (1995): Speckle and scene spatial statistical estimators for SAR image filtering and texture analysis: Some applications to agriculture, forestry, and point targets detection. In: Franceschetti, G., Oliver, C. J., Shiue, J. C. & Tajbakhsh, S. (Eds.): *SPIE 2584. Synthetic Aperture Radar and Passive Microwave Sensing*, 25 - 28 September 1995, Paris, France, 110–120.
- Nguyen, D. (2012): Comparison of elevation derived from insar data with dem from topography map in Son Dong, Bac Giang, Viet Nam. In: *COSPAR 2012. 39th COSPAR Scientific Assembly*, 14–22 July 2012, Mysore, India, 1365–1377.
- Nicole, W. (2015): The WASH approach: Fighting waterborne diseases in emergency situations. *Environmental Health Perspectives* 123 (1), A6.
- Ninomiya, Y., Fu, B. & Cudahy, T. J. (2005): Detecting lithology with Advanced Spaceborne Thermal Emission and Reflection radiometer (ASTER) multispectral thermal infrared “radiance-at-sensor” data. *Remote Sensing of Environment* 99 (1–2), 127–139.
- Nisha de Silva, F. (2001): Providing spatial decision support for evacuation planning: A challenge in integrating technologies. *Disaster Prevention and Management: An International Journal* 10 (1), 11–20.
- Nishidai, T. (1993): Early results from ‘Fuyo-1’ Japan's Earth Resources Satellite (JERS-1). *International Journal of Remote Sensing* 14 (9), 1825–1833.
- Nizalapur, V., Madugundu, R. & Jha, C. S. (2011): Coherence-based land cover classification in forested areas of Chattisgarh, Central India, using environmental satellite-advanced synthetic aperture radar data. *Journal of Applied Remote Sensing* 5 (1), 59501.
- NPC (2006): Population and housing census of the Federal Republic of Nigeria: Housing characteristics and amenities. Priority tables (LGA) - Volume II. <http://catalog.ihsn.org/index.php/catalog/3340/download/48520> (03.10.2018).
- Nuhu, A. & Kwenin, H. (2016): Displacement tracking matrix: Round 10 report - June 2016. [https://reliefweb.int/sites/reliefweb.int/files/resources/01\\_IOM%20DTM%20Nigeria\\_Round%20OX%20Report\\_20160630.pdf](https://reliefweb.int/sites/reliefweb.int/files/resources/01_IOM%20DTM%20Nigeria_Round%20OX%20Report_20160630.pdf) (28.05.2018).
- Nuhu, A. & Kwenin, H. (2017): Displacement tracking matrix: Round 19 report - September 2017. [https://reliefweb.int/sites/reliefweb.int/files/resources/01%20DTM%20Nigeria%20Round%20XIX%20Report%20September%202017\\_0.pdf](https://reliefweb.int/sites/reliefweb.int/files/resources/01%20DTM%20Nigeria%20Round%20XIX%20Report%20September%202017_0.pdf) (28.05.2018).
- Nunziata, F. & Migliaccio, M. (2013): On the COSMO-SkyMed PingPong mode to observe metallic targets at sea. *IEEE Journal of Oceanic Engineering* 38 (1), 71–79.
- OCHA (2016): Ethiopia weekly humanitarian bulletin: 16 May 2016. <https://www.humanitarianresponse.info/en/node/125848> (15.11.2018).
- OCHA (2017): Ethiopia: Gambela region administrative map: 17 August 2017. <https://reliefweb.int/map/ethiopia/ethiopia-gambela-region-administrative-map-17-aug-2017> (15.10.2018).
- OCHA (2018): Joint response plan for Rohingya humanitarian crisis: March - December 2018. <https://www.unocha.org/sites/unocha/files/JRP%20for%20Rohingya%20Humanitarian%20Crisis%202018.PDF> (12.11.2018).
- Oddone, A., Costantini, M., Pietranera, L., Ciappa, A., Grandoni, D. & Nicolosi, P. (2015): Use of COSMO-SkyMed data for innovative and operational applications. In: *IGARSS 2015. IEEE*

- International Geoscience and Remote Sensing Symposium, 26 - 31 July 2015, Milan, Italy, 215–218.
- Oliver, C. J. (2000): Rain forest classification based on SAR texture. *IEEE Transactions On Geoscience And Remote Sensing* 38 (2), 1095–1104.
- Olshen, R. A. (2016): Radio Detection And Ranging (RADAR). In: Olshen, R. A. (Ed.): *Remote Sensing from Air and Space, Second Edition*. Society of Photo-Optical Instrumentation Engineers (SPIE), Bellingham.
- Olthof, I. & Tolszczuk-Leclerc, S. (2018): Comparing Landsat and Radarsat for current and historical dynamic flood mapping. *Remote Sensing* 10 (5), 780.
- Omar, H., Misman, M. A. & Kassim, A. R. (2017): Synergetic of PALSAR-2 and Sentinel-1A SAR polarimetry for retrieving aboveground biomass in dipterocarp forest of Malaysia. *Applied Sciences* 7 (7), 675.
- Onana, V. P., Ngono, J. M., Trebossen, H., Rudant, J. P. & Tonye, E. (2001): Coastline detection in SAR images using texture analysis in textural or geometrical multi-resolution. In: *IGARSS 2001*. IEEE International Geoscience and Remote Sensing Symposium, 9 - 13 July 2001, Sydney, NSW, Australia.
- Ordu, G. E.-O. (2017): Trends and patterns of Boko Haram terrorist and militants' aggression in Nigeria. *Aggression and Violent Behavior* 37, 35–41.
- OSM (2018): 2014 West Africa Ebola response. [https://wiki.openstreetmap.org/wiki/2014\\_West\\_Africa\\_Ebola\\_Response](https://wiki.openstreetmap.org/wiki/2014_West_Africa_Ebola_Response) (07.11.2018).
- Otsu, N. (1979): A threshold selection method from gray-level histograms. *IEEE Transactions on Systems, Man, and Cybernetics* 9 (1), 62–66.
- Ozden, A., Faghri, A., Li, M. & Tabrizi, K. (2016): Evaluation of Synthetic Aperture Radar satellite remote sensing for pavement and infrastructure monitoring. *Procedia Engineering* 145, 752–759.
- Pailou, P., Schuster, M. & Tooth, S. et al. (2009): Mapping of a major paleodrainage system in eastern Libya using orbital imaging radar: The Kufrah River. *Earth and Planetary Science Letters* 277 (3-4), 327–333.
- Palen, L., Soden, R., Anderson, T. J. & Barrenechea, M. (2015): Success & scale in a data-producing organization: The socio-technical evolution of OpenStreetMap in response to humanitarian events. In: *CHI 2015*. 33rd annual ACM conference on human factors in computing systems, 18 - 23 April 2015, Seoul, Republic of Korea, 4113–4122.
- Papp, A. & Barclay, L. (2018): The field, its needs and new technologies. In: Al-Ekabi, C. & Ferretti, S. (Eds.): *Yearbook on Space Policy 2016: Space for sustainable development*. Springer International Publishing, Cham, 231–236.
- Paradella, W. R., dos Santos, A. R., Veneziani, P. & Morais, M. C. de (2017): Synthetic Aperture Radar for geological applications in the moist tropics: Experiences from the Brazilian Amazon region. *Revista Brasileira de Geociências* 30 (3), 538–542.
- Paradella, W. R., dos Santos, A. R., Veneziani, P., Sant'Anna, M. V. & Morais, M. C. de (2014): Geological investigation using Radarsat-1 images in the tropical rain forest environment of Brazil. *Canadian Journal of Remote Sensing* 26 (2), 82–90.
- Patel, S., Sliuzas, R. & Mathur, N. (2015): The risk of impoverishment in urban development-induced displacement and resettlement in Ahmedabad. *Environment and Urbanization* 27 (1), 231–256.
- Patino, J. E. & Duque, J. C. (2013): A review of regional science applications of satellite remote sensing in urban settings. *Computers, Environment and Urban Systems* 37, 1–17.
- Patra, S., Ghosh, S. & Ghosh, A. (2011): Histogram thresholding for unsupervised change detection of remote sensing images. *International Journal of Remote Sensing* 32 (21), 6071–6089.
- Pearce, W. A. (1985): Cloud shadow effects on remote sensing. *IEEE Transactions On Geoscience And Remote Sensing* (5), 634–639.
- Pedersen, J. P., Seljelv, L. G., Strøm, G. D., Follum, O. A., Andersen, J. H. & Wahl, T. (1995): Oil spill detection by use of ERS SAR data—from R&D towards pre-operational early warning detection service. In: Guyenne, T. D. (Ed.): *ESASP 1996*. Second ERS Applications Workshop, 6 - 8 December, London, UK, 181.

- Peduto, D., Nicodemo, G., Maccabiani, J. & Ferlisi, S. (2017): Multi-scale analysis of settlement-induced building damage using damage surveys and DInSAR data: A case study in The Netherlands. *Engineering Geology* 218, 117–133.
- Peduzzi, P., Dao, H., Herold, C. & Mouton, F. (2009): Assessing global exposure and vulnerability towards natural hazards: The Disaster Risk Index. *Natural Hazards and Earth System Sciences* 9 (4), 1149–1159.
- Peltzer, G., Crampé, F. & Rosen, P. A. (2001): The Mw 7.1, Hector Mine, California earthquake: Surface rupture, surface displacement field, and fault slip solution from ERS SAR data. *Comptes Rendus de l'Académie des Sciences-Series IIA-Earth and Planetary Science* 333 (9), 545–555.
- Peña, S. A. & Abdelsalam, M. G. (2006): Orbital remote sensing for geological mapping in southern Tunisia: Implication for oil and gas exploration. *Journal of African Earth Sciences* 44 (2), 203–219.
- Pentland, B. T., Hærem, T. & Hillison, D. (2011): The (n)ever-changing world: Stability and change in organizational routines. *Organization Science* 22 (6), 1369–1383.
- Perissin, D. (2018): *Sarproz software*.
- Perissin, D. & Ferretti, A. (2007): Urban-target recognition by means of repeated spaceborne SAR images. *IEEE Transactions On Geoscience And Remote Sensing* 45 (12), 4043–4058.
- Perissin, D., Ferretti, A. & Prati, C. (2006): Spaceborne SAR anatomy of a city. In: Osten, W. (Ed.): *Fringe 2005: The 5th International Workshop on Automatic Processing of Fringe Patterns*. Springer, Berlin.
- Perski, Z. (1998): Applicability of ERS-1 and ERS-2 InSAR for land subsidence monitoring in the Silesian coal mining region, Poland. *International Archives of Photogrammetry and Remote Sensing* 32, 555–558.
- Pesaresi, M. & Gerhardinger, A. (2011): Improved textural built-up presence index for automatic recognition of human settlements in arid regions with scattered vegetation. *IEEE Journal of Selected Topics in Applied Earth Observations and Remote Sensing* 4 (1), 16–26.
- Pickett, S. T. A., Cadenasso, M. L. & Benning, T. L. (2003): Biotic and abiotic variability as key determinants of savanna heterogeneity at multiple spatiotemporal scales. In: Du Toit, J. T. (Ed.): *The Kruger experience: Ecology and management of savanna heterogeneity*. Island Press, Washington D.C., 22–40.
- Pierce, J. R. (1974): *Almost all about waves*. MIT Press, Cambridge, Mass.
- Pierce, L., Kellndorfer, J., Ulaby, F. T. & Norikane, L. (1996): Practical SAR orthorectification. In: *IGARSS 1996*. IEEE International Geoscience and Remote Sensing Symposium, 27–31 May 1996, Lincoln, NE, USA, 2329–2331.
- Pierdicca, N., Pulvirenti, L., Chini, M., Guerriero, L. & Candela, L. (2013): Observing floods from space: Experience gained from COSMO-SkyMed observations. *Acta Astronautica* 84, 122–133.
- Pinker, S. (2012): *The better angels of our nature: Why violence has declined*. Penguin Books, New York, Toronto, London.
- Plank, S. (2014): Rapid damage assessment by means of multi-temporal SAR: A comprehensive review and outlook to Sentinel-1. *Remote Sensing* 6 (6), 4870–4906.
- Pohl, C., Munro, D. & van Genderen, J. L. (1997): Enhanced image analysis through multilevel data fusion techniques. In: Kadar, I. (Ed.): *AeroSense 1997: Signal processing, sensor fusion, and target recognition VI*. 11th International Symposium on Aerospace/Defense Sensing, Simulation and Controls, 20 - 25 April 1997, Orlando, FL, USA, 32.
- Poland, M. (2006): InSAR captures rifting and volcanism in East Africa. *Alaska Satellite Facility News & Notes* 3, 2.
- Polidori, L. (1995): Quality specifications for radar derived digital elevation models. In: *IGARSS 1995*. IEEE International Geoscience and Remote Sensing Symposium, 10 - 14 July 1995, Firenze, Italy, 208–209.
- Polidori, L., Caillault, S. & Canaud, J.-L. (1995): Change detection in radar images: Methods and operational constraints. In: *IGARSS 1995*. IEEE International Geoscience and Remote Sensing Symposium, 10 - 14 July 1995, Firenze, Italy, 1529–1531.

- Porfiri, M., Ferro-Famil, L. & Nicolas, J.-M. (2015): Building profile reconstruction using TerraSAR-X data time-series and tomographic techniques. In: *Multi-Temp 2015*. 2015 8th International Workshop on the Analysis of Multitemporal Remote Sensing Images (Multi-Temp), 22 - 24 July 2015, Annecy, France, 1–4.
- Porter, G. (2002): Living in a walking world: Rural mobility and social equity issues in sub-Saharan Africa. *World Development* 30 (2), 285–300.
- Potin, P., Rosich, B. & Miranda, N. et al. (2018): Sentinel-1 constellation mission operations status. In: *IGARSS 2018*. IEEE International Geoscience and Remote Sensing Symposium, July 22–27, Valencia, Spain, 1547–1550.
- Pottier, E. & Ferro-Famil, L. (2009): Exploitation of ALOS PALSAR SAR full-polarimetry data to the mapping of an African region. *Geoscience and Remote Sensing Symposium* (2), II9–II12.
- Poullis, C. & You, S. (2010): Delineation and geometric modeling of road networks. *ISPRS Journal of Photogrammetry and Remote Sensing* 65 (2), 165–181.
- Prati, C., Ferretti, A. & Perissin, D. (2010): Recent advances on surface ground deformation measurement by means of repeated space-borne SAR observations. *Journal of Geodynamics* 49 (3-4), 161–170.
- Prati, C. & Rocca, F. (1992): Focusing SAR data with time-varying Doppler centroid. *IEEE Transactions On Geoscience And Remote Sensing* 30 (3), 550–559.
- Preiss, M. & Stacy, N. J. S. (2006): *Coherent change detection: Theoretical description and experimental results*, Edinburgh, Australia.
- Prins, E. (2008): Use of low cost Landsat ETM+ to spot burnt villages in Darfur, Sudan. *International Journal of Remote Sensing* 29 (4), 1207–1214.
- Pulvirenti, L., Pierdicca, N., Chini, M. & Guerriero, L. (2011): An algorithm for operational flood mapping from Synthetic Aperture Radar (SAR) data using fuzzy logic. *Natural Hazards and Earth System Sciences* 11 (2), 529.
- Qi, Z., Yeh, A. G.-O., Li, X. & Lin, Z. (2012): A novel algorithm for land use and land cover classification using Radarsat-2 polarimetric SAR data. *Remote Sensing of Environment* 118, 21–39.
- Quinn, J. A., Nyhan, M. M., Navarro, C., Coluccia, D., Bromley, L. & Luengo-Oroz, M. (2018): Humanitarian applications of machine learning with remote-sensing data: Review and case study in refugee settlement mapping. *Philosophical Transactions of the Royal Society of London* 376 (2128).
- Rahman, M. Z. (2018): Livelihoods of Rohingyas and their Impacts on deforestation. In: Tani, M. & Rahman, M. A. (Eds.): *Deforestation in the Teknaf Peninsula of Bangladesh: A study of political ecology*. Springer, Singapore, 113–125.
- Ramchurn, S. D., Huynh, T. D. & Wu, F. et al. (2016): A disaster response system based on human-agent collectives. *Journal of Artificial Intelligence Research* 57.
- Ramsey, E., Lu, Z., Suzuoki, Y., Ragoonwala, A. & Werle, D. (2011): Monitoring duration and extent of storm-surge and flooding in western coastal Louisiana marshes with Envisat ASAR data. *IEEE Journal of Selected Topics in Applied Earth Observations and Remote Sensing* 4 (2), 387–399.
- Raney, R. K. & Wessels, G. J. (1988): Spatial considerations in SAR speckle consideration. *IEEE Transactions On Geoscience And Remote Sensing* 26 (5), 666–672.
- Ranson, K. J. & Sun, G. (1994): Mapping biomass of a northern forest using multifrequency SAR data. *IEEE Transactions On Geoscience And Remote Sensing* 32 (2), 388–396.
- Ratha, D., De, S., Celik, T. & Bhattacharya, A. (2017): Change detection in polarimetric SAR images using a geodesic distance between scattering mechanisms. *IEEE Geoscience and Remote Sensing Letters* 14 (7), 1066–1070.
- REACH (2017): Maiduguri city - As of June 2017. <https://reliefweb.int/map/nigeria/reference-map-nigeria-borno-state-maiduguri-city-june-2017> (14.10.2018).
- Reale, D., Nitti, D. O., Peduto, D., Nutricato, R., Bovenga, F. & Fornaro, G. (2011): Postseismic deformation monitoring with the Cosmo SkyMed constellation. *IEEE Geoscience and Remote Sensing Letters* 8 (4), 696–700.

- Redwood-Campbell, L. J., Sekhar, S. N. & Persaud, C. R. (2014): Health care workers in danger zones: A special report on safety and security in a changing environment. *Prehospital and Disaster Medicine* 29 (5), 503–507.
- Ren, S., Cao, X., Wei, Y. & Sun, J. (2015): Global refinement of random forest. In: *CVPR 2015. IEEE Conference on Computer Vision and Pattern Recognition*, 7 - 12 June 2015, Boston, MA, 723–730.
- Richards, J. A. (2009): *Remote sensing with imaging radar*. Springer, Berlin, Heidelberg.
- Rignot, E., Way, J., Williams, C. & Viereck, L. (1994): Radar estimates of aboveground biomass in boreal forests of interior Alaska. *IEEE Transactions On Geoscience And Remote Sensing* 32 (5), 1117–1124.
- Rishmawi, K. & Prince, S. (2016): Environmental and anthropogenic degradation of vegetation in the Sahel from 1982 to 2006. *Remote Sensing* 8 (11), 948.
- Rivoal, M. & Haselip, J. A. (2017): The true cost of using traditional fuels in a humanitarian setting. Case study of the Nyarugusu refugee camp, Kigoma region, Tanzania: UNEP DTU Partnership Working Paper Series Volume 3. [http://orbit.dtu.dk/files/157400638/LD\\_2017\\_TheTrueCostOfUsingTraditionalFuels\\_Rivoal\\_Haselip.pdf](http://orbit.dtu.dk/files/157400638/LD_2017_TheTrueCostOfUsingTraditionalFuels_Rivoal_Haselip.pdf) (15.02.2019).
- Robinson, C., Saatchi, S. S., Neumann, M. & Gillespie, T. (2013): Impacts of spatial variability on aboveground biomass estimation from L-band radar in a temperate forest. *Remote Sensing* 5 (3), 1001–1023.
- Romero Lankao, P. (2010): Water in Mexico City: What will climate change bring to its history of water-related hazards and vulnerabilities? *Environment and Urbanization* 22 (1), 157–178.
- Rosin, P. L. & Ioannidis, E. (2003): Evaluation of global image thresholding for change detection. *Pattern Recognition Letters* 24 (14), 2345–2356.
- Rossi, M., Rembold, F., Bolognesi, M., Nori, M., Mureithi, S. & Nyberg, G. (2018): Mapping land enclosures and vegetation cover changes in the surroundings of Kenya's Dadaab refugee camps with very high resolution satellite imagery. *Land Degradation & Development* 19 (4), 494.
- Rubenstein, L. S. & Bittle, M. D. (2010): Responsibility for protection of medical workers and facilities in armed conflict. *The Lancet* 375 (9711), 329–340.
- Rudari, R., Beckers, J. & Angeli, S. de et al. (2016): Impact of modelling scale on probabilistic flood risk assessment: The Malawi case. *E3S Web of Conferences* 7 (5), 4015.
- Rutinwa, B. (2017): The end of asylum? The changing nature of refugee policies in Africa. In: Lambert, H. (Ed.): *International refugee law*. Routledge, London, 35–64.
- Saatchi, S. S., Marlier, M., Chazdon, R. L., Clark, D. B. & Russell, A. E. (2011): Impact of spatial variability of tropical forest structure on radar estimation of aboveground biomass. *Remote Sensing of Environment* 115 (11), 2836–2849.
- Saint-Jean, R., Singhroy, V. & Khalifa, S. M. (2014): Geological Interpretation of Integrated SAR Images in the Azraq Area of Jordan. *Canadian Journal of Remote Sensing* 21 (4), 511–517.
- Sander, P. (2007): Lineaments in groundwater exploration: A review of applications and limitations. *Hydrogeology Journal* 15 (1), 71–74.
- Sanders, B. F. (2007): Evaluation of on-line DEMs for flood inundation modeling. *Advances in Water Resources* 30 (8), 1831–1843.
- Sandwell, D. T., Myer, D., Mellors, R., Shimada, M., Brooks, B. & Foster, J. (2008): Accuracy and resolution of ALOS interferometry: Vector deformation maps of the Father's Day intrusion at Kilauea. *IEEE Transactions On Geoscience And Remote Sensing* 46 (11), 3524–3534.
- Santoro, M. & Wegmüller, U. (2014): Multi-temporal synthetic aperture radar metrics applied to map open water bodies. *IEEE Journal of Selected Topics in Applied Earth Observations and Remote Sensing* 7 (8), 3225–3238.
- Sato, M., Feng, X. & Takahashi, K. (2008): 3D subsurface SAR for humanitarian demining. *7th European Conference on Synthetic Aperture Radar (EUSAR)*, 1–4.
- Scarr, S., Cai, W., Foo, W. & Wu, J. (2017): Bangladesh's island solution. *Thomson Reuters*, September 07. <http://fingfx.thomsonreuters.com/gfx/rngs/MYANMAR-ROHINGYA/010050PD1KP/index.html> (11.08.2018).

- Schaber, G. G., McCauley, J. F. & Breed, C. S. (1997): The use of multifrequency and polarimetric SIR-C/X-SAR data in geologic studies of Bir Safsaf, Egypt. *Remote Sensing of Environment* 59 (2), 337–363.
- Schaeffer, A. (2016): UNOSAT: 15 years of humanitarian mapping. <http://cds.cern.ch/record/2229079> (18.01.2018).
- Scheuchl, B., Caves, R., Cumming, I. G. & Staples, G. (2001): Automated sea ice classification using spaceborne polarimetric SAR data. IEEE 2001 International. *Geoscience and Remote Sensing Symposium* 7, 3117–3119.
- Schillaci, C., Braun, A. & Kropáček, J. (2012): Terrain analysis and landform recognition. In: Cook, S. J., Clarke, L. E. & Nield, J.M. (Eds.): *Geomorphological techniques: Online edition*, London, 1–18.
- Schmitt, A., Sieg, T., Wurm, M. & Taubenböck, H. (2018): Investigation on the separability of slums by multi-aspect TerraSAR-X dual-co-polarized high resolution spotlight images based on the multi-scale evaluation of local distributions. *International Journal of Applied Earth Observation and Geoinformation* 64, 181–198.
- Schmullius, C. & Evans, D. L. (1997): Review article Synthetic aperture radar (SAR) frequency and polarization requirements for applications in ecology, geology, hydrology, and oceanography: A tabular status quo after SIR-C/X-SAR. *International Journal of Remote Sensing* 18 (13), 2713–2722.
- Schöpfer, E., Spröhnle, K. & Kranz, O. et al. (2017): Towards a multi-scale approach for an earth observation-based assessment of natural resource exploitation in conflict regions. *Geocarto International* 32 (10), 1139–1158.
- Schotten, C. G.J., van Rooy, W. W.L. & Janssen, L. L.F. (1995): Assessment of the capabilities of multi-temporal ERS-1 SAR data to discriminate between agricultural crops. *International Journal of Remote Sensing* 16 (14), 2619–2637.
- Schuler, D. L., Lee, J.-S. & de Grandi, G. (1996): Measurement of topography using polarimetric SAR images. *IEEE Transactions On Geoscience And Remote Sensing* 34 (5), 1266–1277.
- Schultz, L. A., Molthan, A., Nicoll, J. B., Bell, J. R., Gens, R. & Meyer, F. J. (2017): Integration of Synthetic Aperture Radar imagery and derived products into severe weather disaster response. In: *AGU Fall Meeting Abstracts*. American Geophysical Union, Fall Meeting, 07 - 15 December, New Orleans, USA, IN22B-04.
- Schumann, G. & Di Baldassarre, G. (2010): The direct use of radar satellites for event-specific flood risk mapping. *Remote Sensing Letters* 1 (2), 75–84.
- Schumann, G., Hostache, R. & Puech, C. et al. (2007): High-resolution 3D flood information from radar imagery for flood hazard management. *IEEE Transactions On Geoscience And Remote Sensing* 45 (6), 1715–1725.
- Schwabisch, M., Matschke, M., Knopfle, W. & Roth, A. (1995): Quality assessment of InSAR-derived DEMs generated with ERS tandem data. In: *IGARSS 1995*. IEEE International Geoscience and Remote Sensing Symposium, 10 - 14 July 1995, Firenze, Italy, 802–804.
- Schwarz, B., Pestre, G. & Tellman, B. et al. (2018): Mapping floods and assessing flood vulnerability for disaster decision-making: A case study remote sensing application in Senegal. In: Mathieu, P.-P. & Aubrecht, C. (Eds.): *Earth observation open science and innovation*. Springer International Publishing, Cham, 293–300.
- Schwarz, G., Espinoza-Molina, D. & Datcu, M. (2008): Adapting multilooking for joint radiometrical and geometrical SAR image enhancement. *Polarization* 2, 2.1.
- Schweitzer, P. N. (1995): Monthly average polar sea-ice concentration: U.S. Geological Survey digital data series. <https://geology.usgs.gov/tools/metadata/training/examples/dds27.html> (05.12.2018).
- Sen, G. (2017): Bangladesh and the Rohingya: Implications of refugee re-location to Thengar Char island. [https://idsa.in/idsacomments/bangladesh-and-the-rohingya\\_gsen\\_280217](https://idsa.in/idsacomments/bangladesh-and-the-rohingya_gsen_280217) (06.08.2018).
- Sengupta, S. & Fountain, H. (2018): The biggest refugee camp braces for rain: ‘This is going to be a catastrophe’: More than half a million Rohingya refugees face looming disaster from floods and landslides when the first storms of the monsoon season hit their camp in Bangladesh.

- 14.03.2018. <https://www.nytimes.com/2018/03/14/climate/bangladesh-rohingya-refugee-camp.html> (10.09.2018).
- Serra, J. & Soille, P. (2012): *Mathematical morphology and its applications to image processing*. Springer Science & Business Media, Dordrecht.
- Sheng, Y. & Xia, Z. G. (1996): A comprehensive evaluation of filters for radar speckle suppression. In: *IGARSS 1996*. IEEE International Geoscience and Remote Sensing Symposium, 27-31 May 1996, Lincoln, NE, USA, 1559-1561.
- Shimada, M., Itoh, T. & Motooka, T. et al. (2014): New global forest/non-forest maps from ALOS PALSAR data (2007-2010). *Remote Sensing of Environment* 155, 13-31.
- Shook, E., Bowlick, F. J. & Kemp, K. K. et al. (2018): Cyber literacy for GIScience: Toward formalizing geospatial computing education. *The Professional Geographer*, 1-18.
- Shugar, D. H., Rabus, B. T. & Clague, J. J. (2010): Elevation changes (1949-1995) of Black Rapids Glacier, Alaska, derived from a multi-baseline InSAR DEM and historical maps. *Journal of Glaciology* 56 (198), 625-634.
- Siegert, F. & Ruecker, G. (2000): Use of multitemporal ERS-2 SAR images for identification of burned scars in south-east Asian tropical rainforest. *International Journal of Remote Sensing* 21 (4), 831-837.
- Singh, L. P., van Westen, C. J., Ray, P. C. & Pasquali, P. (2005): Accuracy assessment of InSAR derived input maps for landslide susceptibility analysis: A case study from the Swiss Alps. *Landslides* 2 (3), 221-228.
- Singhroy, V., Slaney, R., Lowman, P., Harris, J. & Moon, W. (2014): Radarsat and radar geology in Canada. *Canadian Journal of Remote Sensing* 19 (4), 338-351.
- Sinha, S., Jeganathan, C., Sharma, L. K. & Nathawat, M. S. (2015): A review of radar remote sensing for biomass estimation. *International Journal of Environmental Science and Technology* 12 (5), 1779-1792.
- Skolnik, M. I. (1980): *Introduction to radar systems*, 2<sup>nd</sup> edn. McGraw-Hill, Boston, Mass.
- Skriver, H., Nielsen, A. A., Canty, M. J. & Conradsen, K. (2017): Change detection in multitemporal polarimetric SAR images. In: *11th ASAR workshop*. Earth Observation Summit 2017, 20 - 22 June 2017, Montreal, Canada.
- Slater, J. & Brown, R. (2000): Changing landscapes: Monitoring environmentally sensitive areas using satellite imagery. *International Journal of Remote Sensing* 21 (13-14), 2753-2767.
- Small, D. (2011): Flattening Gamma: Radiometric terrain correction for SAR imagery. *IEEE Transactions On Geoscience And Remote Sensing* 49 (8), 3081-3093.
- Small, D., Miranda, N. & Meier, E. (2009a): A revised radiometric normalisation standard for SAR. In: *IGARSS 2009*. IEEE International Geoscience and Remote Sensing Symposium, 12 - 17 July 2009, Cape Town, South Africa, IV-566-IV-569.
- Small, D., Miranda, N. & Meier, E. (2009b): Local incidence angle considered harmful. In: *CEOS SAR Cal/Val*. CEOS SAR Calibration & Validation Workshop, 17 - 19 November 2009, Pasadena, California, 17-19.
- Small, D. & Schubert, A. (2008): Guide to ASAR geocoding. *University of Zurich* (1).
- Smillie, I. (2001): Capacity building and the humanitarian enterprise. In: Smillie, I. (Ed.): *Patronage or partnership: Local capacity building in humanitarian crises*. Kumarian Press, Bloomfield, 1-7.
- Smirl, L. (2008): Building the other, constructing ourselves: Spatial dimensions of international humanitarian response. *International Political Sociology* 2 (3), 236-253.
- Smith, S. E., El-Shamy, I. & Abd-El Monsef, H. (1997): Locating regions of high probability for groundwater in the Wadi El-Arish Basin, Sinai, Egypt. *Journal of African Earth Sciences* 25 (2), 253-262.
- Soh, L.-K. & Tsatoulis, C. (1999): Texture analysis of SAR sea ice imagery using gray level co-occurrence matrices. *IEEE Transactions On Geoscience And Remote Sensing* 37 (2), 780-795.
- Soille, P., Burger, A. & Marchi, D. de et al. (2018): A versatile data-intensive computing platform for information retrieval from big geospatial data. *Future Generation Computer Systems* 81, 30-40.

- Solbø, S. & Solheim, I. (2005): Towards operational flood mapping with satellite SAR. In: Lacoste, H. & Ouwehand, L. (Eds.): *SP-572. Envisat & ERS Symposium*, 6 - 10 September 2004, Salzburg, Austria.
- Song, S. H. & Kwag, Y. K. (2011): Geo-location error correction for synthetic aperture radar image. In: *AP SAR 2011. 3rd International Asia-Pacific Conference on Synthetic Aperture Radar*, 26 - 30 September 2011, Seoul, Korea, 1–4.
- Souksavanh, O. (2018): Faulty construction, heavy rain cause dam to flood Lao villages: Translated by Roseanne Gerin. 20.09.2017. <https://www.rfa.org/english/news/laos/faulty-construction-heavy-rain-cause-dam-to-flood-lao-villages-09202017151556.html> (10.09.2018).
- Southworth, J., Zhu, L. & Bunting, E. et al. (2014): Changes in vegetation persistence across global savanna landscapes, 1982–2010. *Journal of Land Use Science* 11 (1), 7–32.
- Spann, M. & Wilson, R. (1985): A quad-tree approach to image segmentation which combines statistical and spatial information. *Pattern Recognition* 18 (3-4), 257–269.
- Spiegel, P. B., Checchi, F., Colombo, S. & Paik, E. (2010): Health-care needs of people affected by conflict: Future trends and changing frameworks. *The Lancet* 375 (9711), 341–345.
- Spröhnle, K., Fuchs, E.-M. & Pelizari, P. A. (2017): Object-based analysis and fusion of optical and SAR satellite data for dwelling detection in refugee camps. *IEEE Journal of Selected Topics in Applied Earth Observations and Remote Sensing* 10 (5), 1780–1791.
- Stabel, E. & Löffler, E. (2003): Optimised mapping of flood extent and floodplain structures by radar EO-methods. In: *Fringe 2003. Proceedings of Fringe Workshop*, Frascati, Italy.
- Stängel, M., Tiede, D., Lüthje, F., Füreder, P. & Lang, S. (2014): Object-based image analysis using VHR satellite imagery for monitoring the dismantling of a refugee camp after a crisis: The case of Lukole, Tanzania. *Journal for Geographic Information Science*, 45–48.
- Stasolla, M. & Gamba, P. E. (2009): Humanitarian aids using satellite technology. In: Olla, P. (Ed.): *Space technologies for the benefit of human society and earth*. Springer Netherlands, Dordrecht, 431–451.
- Stephens, G. & Matson, M. (1993): Monitoring the Persian Gulf war with NOAA AVHRR data. *International Journal of Remote Sensing* 14 (7), 1423–1429.
- Stern, R. J. & Abdelsalam, M. G. (1996): The origin of the great bend of the Nile from SIR-C/X-SAR imagery. *Science* 274 (5293), 1696–1698.
- Sudmanns, M., Augustin, H., Tiede, D., Lang, S. & Cavallaro, A.-M. (2018a): EO-Compass: Granule statistics for Sentinel-2 images. <http://eo-compass.zgis.at> (15.10.2018).
- Sudmanns, M., Tiede, D., Augustin, H. & Lang, S. (2019): Assessing global Sentinel-2 coverage dynamics and data availability for operational Earth observation (EO) applications using the EO-Compass. *International Journal of Digital Earth*, 1–17.
- Sudmanns, M., Tiede, D., Lang, S. & Baraldi, A. (2018b): Semantic and syntactic interoperability in online processing of big Earth observation data. *International Journal of Digital Earth* 11 (1), 95–112.
- Sudmanns, M., Tiede, D., Wendt, L. & Baraldi, A. (2017): Automatic ex-post flood assessment using long time series of optical Earth observation images. *Journal for Geographic Information Science* 1, 217–227.
- Suhrke, A. (1994): Environmental degradation and population flows. *Journal of International Affairs*, 473–496.
- Sui, D., Goodchild, M. F. & Elwood, S. (2013): Volunteered geographic information, the exaflood, and the growing digital divide. In: Sui, D. Z., Elwood, S. & Goodchild, M. F. (Eds.): *Crowdsourcing geographic knowledge: Volunteered Geographic Information (VGI) in Theory and Practice*. Springer, Heidelberg, 1–12.
- Sulik, J. J. & Edwards, S. (2010): Feature extraction for Darfur: Geospatial applications in the documentation of human rights abuses. *International Journal of Remote Sensing* 31 (10), 2521–2533.
- Sun, G., Ranson, K. J., Guo, Z., Zhang, Z., Montesano, P. & Kimes, D. (2011): Forest biomass mapping from lidar and radar synergies. *Remote Sensing of Environment* 115 (11), 2906–2916.

- Suzuki, R., Kim, Y. & Ishii, R. (2013): Sensitivity of the backscatter intensity of ALOS PALSAR to the above-ground biomass and other biophysical parameters of boreal forest in Alaska. *Polar Science* 7 (2), 100–112.
- Svoray, T. & Shoshany, M. (2010): SAR-based estimation of areal aboveground biomass (AAB) of herbaceous vegetation in the semi-arid zone: A modification of the water-cloud model. *International Journal of Remote Sensing* 23 (19), 4089–4100.
- Tachiiri, K. x. & Ohta, I. (2004): Assessing impact of a large-sized refugee camp on the local vegetation condition with remote sensing: A case study of Kakuma, Kenya. In: *IGARSS 2004*. IEEE International Geoscience and Remote Sensing Symposium, 20 - 24 September 2004, Anchorage, USA, 1547–1550.
- Tadono, T., Ishida, H., Oda, F., Naito, S., Minakawa, K. & Iwamoto, H. (2014): Precise global DEM generation by ALOS PRISM. *ISPRS Annals of Photogrammetry, Remote Sensing and Spatial Information Sciences* II-4, 71–76.
- Tammaing, P. (2011): Sustainability in humanitarian action: Basis of a panel discussion: "Sustainable Humanitarian Action: Bridging relief to development". 31st International Conference of the Red Cross And Red Crescent. <https://daraint.org/wp-content/uploads/2011/12/Sustainability-in-humanitarian-action.pdf> (20.11.2018).
- Tapete, D. & Cigna, F. (2017): InSAR data for geohazard assessment in UNESCO world heritage sites: State-of-the-art and perspectives in the Copernicus era. *International Journal of Applied Earth Observation and Geoinformation* 63, 24–32.
- Tapete, D., Cigna, F., Masini, N. & Lasaponara, R. (2013): Prospection and monitoring of the archaeological heritage of Nasca, Peru, with ENVISAT ASAR. *Archaeological Prospection* 20 (2), 133–147.
- Tarchi, D., Casagli, N., Moretti, S., Leva, D. & Sieber, A. J. (2003): Monitoring landslide displacements by using ground - based synthetic aperture radar interferometry: Application to the Ruinon landslide in the Italian Alps. *Journal of Geophysical Research: Solid Earth* 108 (B8).
- Taubenböck, H. & Kraff, N. J. (2014): The physical face of slums: A structural comparison of slums in Mumbai, India, based on remotely sensed data. *Journal of Housing and the Built Environment* 29 (1), 15–38.
- Taubenböck, H. & Kraff, N. J. (2015): Das globale Gesicht urbaner Armut? Siedlungsstrukturen in Slums. In: Taubenböck, H., Wurm, M., Esch, T. & Dech, S. (Eds.): *Globale Urbanisierung: Perspektive aus dem All*. Springer, Berlin, 107–119.
- Taubenböck, H., Wurm, M. & Netzband, M. et al. (2011): Flood risks in urbanized areas: Multi-sensoral approaches using remotely sensed data for risk assessment. *Natural Hazards and Earth System Sciences* 11, 431–444.
- Teeuw, R. M., Leidig, M., Saunders, C. & Morris, N. (2013): Free or low-cost geoinformatics for disaster management: Uses and availability issues. *Environmental Hazards* 12 (2), 112–131.
- Tesauro, M., Berardino, P., Lanari, R., Sansosti, E., Fornaro, G. & Franceschetti, G. (2000): Urban subsidence inside the city of Napoli (Italy) observed by satellite radar interferometry. *Geophysical Research Letters* 27 (13), 1961–1964.
- Thenkabail, P. S., Hanjra, M. A., Dheeravath, V. & Gumma, M. (2010): A holistic view of global croplands and their water use for ensuring global food security in the 21st century through advanced remote sensing and non-remote sensing approaches. *Remote Sensing* 2 (1), 211–261.
- Thenkabail, P. S., Knox, J. W. & Ozdogan, M. et al. (2012): Assessing future risks to agricultural productivity, water resources and food security: How can remote sensing help? *Photogrammetric Engineering & Remote Sensing* 78 (8), 773–782.
- Tholey, N., Allenbach, B., Clandillon, S., Fella, K., de Fraipont, P. & Yésou, H. (2011): Emergency response service: over ten years of Rapid Mapping at SERTIT. In: *ESA GMES 2011*. 2nd Earth Observation GMES Operational Capacity Workshop, 17 - 18 March 2011, Sofia, Bulgaria.
- Thu, P. M. & Populus, J. (2007): Status and changes of mangrove forest in Mekong Delta: Case study in Tra Vinh, Vietnam. *Estuarine, Coastal and Shelf Science* 71 (1-2), 98–109.
- Tian, X., Yan, M. & van der Tol, C. et al. (2017): Modeling forest above-ground biomass dynamics using multi-source data and incorporated models: A case study over the qilian mountains. *Agricultural and Forest Meteorology* 246, 1–14.

- Tiede, D., Füreder, P., Lang, S., Hölbling, D. & Zeil, P. (2013): Automated analysis of satellite imagery to provide information products for humanitarian relief operations in refugee camps: From scientific development towards operational services. *Photogrammetrie-Fernerkundung-Geoinformation* 2013 (3), 185–195.
- Tiede, D., Krafft, P., Füreder, P. & Lang, S. (2017): Stratified template matching to support refugee camp analysis in OBIA workflows. *Remote Sensing* 9 (4), 326.
- Tiede, D., Lang, S., Hölbling, D. & Füreder, P. (2010): Transferability of OBIA rulesets for IDP camp analysis in Darfur. *The International Archives of the Photogrammetry, Remote Sensing and Spatial Information Sciences* 38.
- Tolomei, C., Salvi, S., Boncori, J. M. & Pezzo, G. (2015): InSAR measurement of crustal deformation transients during the earthquake preparation processes: A review. *Bollettino di Geofisica Teorica ed Applicata* 56 (2).
- Tomás, R., Garcia-Barba, J. & Cano, M. et al. (2012): Subsidence damage assessment of a gothic church using differential interferometry and field data. *Structural Health Monitoring* 11 (6), 751–762.
- Tomás, R., Romero, R. & Mulas, J. et al. (2014): Radar interferometry techniques for the study of ground subsidence phenomena: A review of practical issues through cases in Spain. *Environmental Earth Sciences* 71 (1), 163–181.
- Torres, R., Snoeij, P. & Geudtner, D. et al. (2012): GMES Sentinel-1 mission. *Remote Sensing of Environment* 120, 9–24.
- Touzi, R. (2002): A review of speckle filtering in the context of estimation theory. *IEEE Transactions On Geoscience And Remote Sensing* 40 (11), 2392–2404.
- Touzi, R. (2016): Polarimetric target scattering decomposition: A review. In: *IGARSS 2016*. IEEE International Geoscience and Remote Sensing Symposium, 10 - 15 July 2016, Beijing, China, 5658–5661.
- Tragl, K. (1990): Polarimetric radar backscattering from reciprocal random targets. *IEEE Transactions On Geoscience And Remote Sensing* 28 (5), 856–864.
- Tralli, D. M., Blom, R. G., Zlotnicki, V., Donnellan, A. & Evans, D. L. (2005): Satellite remote sensing of earthquake, volcano, flood, landslide and coastal inundation hazards. *ISPRS Journal of Photogrammetry and Remote Sensing* 59 (4), 185–198.
- Trinder, J. C. & Wang, Y. (1998): Automatic road extraction from aerial images. *Digital Signal Processing* 8 (4), 215–224.
- Tronin, A. A. (2006): Remote sensing and earthquakes: A review. *Physics and Chemistry of the Earth, Parts A/B/C* 31 (4–9), 138–142.
- Tsyganskaya, V., Martinis, S., Marzahn, P. & Ludwig, R. (2018): SAR-based detection of flooded vegetation: A review of characteristics and approaches. *International Journal of Remote Sensing* 39 (8), 2255–2293.
- Turner, S. (2016): What is a refugee camp? Explorations of the limits and effects of the camp. *Journal of Refugee Studies* 29 (2), 139–148.
- Twele, A., Cao, W., Plank, S. & Martinis, S. (2016): Sentinel-1-based flood mapping: A fully automated processing chain. *International Journal of Remote Sensing* 37 (13), 2990–3004.
- Ulaby, F. T., Batlivala, P. & Dobson, M. C. (1978): Microwave backscatter dependence on surface roughness, soil moisture, and soil texture: Part I: Bare Soil. *IEEE Transactions on Geoscience Electronics* 16 (4), 286–295.
- Ulaby, F. T., Moore, R. K. & Fung, A. K. (1981): *Microwave remote sensing: Active and passive: Volume I: Microwave remote sensing fundamentals and radiometry*. Addison-Wesley, Reading, Mass.
- Ulaby, F. T., Moore, R. K. & Fung, A. K. (1986): *Microwave remote sensing: Active and passive: Volume II: Radar remote sensing and surface scattering and emission theory*. Artech House, Norwood, Mass.
- Ulaby, F. T., Moore, R. K. & Fung, A. K. (1990): *Microwave remote sensing: Active and passive: Volume III: From theory to applications*, Reprint ed. Artech House, Norwood, Mass.
- UNHCR (2005): Sudan/Chad update: Highlights. Update 15. <http://www.unhcr.org/430f47762.pdf> (31.01.2017).

- UNHCR (2007): *Handbook for emergencies*. United Nations High Commissioner for Refugees, Geneva, Switzerland.
- UNHCR (2013): *Statistical yearbook 2012: Annex A*. Table 15: Major locations and demographic composition of populations of concern to UNHCR, Geneva, Switzerland.
- UNHCR (2014): WASH guidelines on camp closure. <http://wash.unhcr.org/download/unhcr-wash-guidelines-on-camps-closure/> (08.09.2018).
- UNHCR (2015): Ethiopia: South Sudan emergency response in Gambella region: Who does what where (3W). 03 June 2015. <https://data2.unhcr.org/fr/documents/download/30227> (15.08.2018).
- UNHCR (2018a): Figures at a glance: December 2018. <https://www.unhcr.org/figures-at-a-glance.html> (01.12.2018).
- UNHCR (2018b): Forced displacement in 2017: Global trends. <https://www.unhcr.org/statistics/unhcrstats/5b27be547/unhcr-global-trends-2017.html> (01.12.2018).
- UNHCR (2018c): Global appeal 2018-2019. <https://www.unhcr.org/publications/fundraising/5a0c05027/unhcr-global-appeal-2018-2019-full-report.html> 01.12.2018.
- UNHCR (2018d): Kenya, Dadaab: Operational update. 01-15 April 2018. <https://reliefweb.int/sites/reliefweb.int/files/resources/15%20April%20Dadaab%20Bi-weekly%20Operational%20Update.pdf> (21.08.2018).
- UNHCR (2018e): *UNHCR WASH manual: Practical guidance for refugee settings*, 4<sup>th</sup> edn., Geneva, Switzerland.
- UNICEF (2017): Ethiopia humanitarian situation report #15: Reporting period 06 - 20 September 2017. <https://reliefweb.int/report/ethiopia/unicef-ethiopia-humanitarian-situation-report-15-reporting-period-06-20-september> (15.11.2018).
- UNITAR (2013): UNOSAT announces new manager: March 2013. <http://www.unitar.org/unosat-announces-new-manager> (11.12.2018).
- UNITAR (2017a): Damage assessment in Kutupalong refugee camp, Palong Khali Union, Bangladesh: UNOSAT product ID 2605. 07.06.2017. [http://www.unitar.org/unosat/node/44/2605?utm\\_source=unosat-unitar&utm\\_medium=rss&utm\\_campaign=maps](http://www.unitar.org/unosat/node/44/2605?utm_source=unosat-unitar&utm_medium=rss&utm_campaign=maps) (21.01.2019).
- UNITAR (2017b): Damage density of Ar Raqqa, Ar Raqqa governorate, Syria: UNOSAT product ID 2742. 28.11.2017. <http://www.unitar.org/unosat/map/2742> 04.01.20018.
- UNITAR (2018a): Dam collapse, Sanamxay, Attapeu, Lao People Democratic Republic. Potentially affected villages along Vang Ngao River and Xe Kong River: UNOSAT product ID 2832. 31.07.2018. [http://unosat-maps.web.cern.ch/unosat-maps/LA/FL20180723LAO/UNOSAT\\_Settlements\\_XePianXeNamnoyDam\\_FL20180723LAO.pdf](http://unosat-maps.web.cern.ch/unosat-maps/LA/FL20180723LAO/UNOSAT_Settlements_XePianXeNamnoyDam_FL20180723LAO.pdf) (15.09.2018).
- UNITAR (2018b): Evolution satellite detected water extent over Sanamxay District, Attapeu Province, Lao People Democratic Republic: UNOSAT product ID 2828. 26.07.2018. [http://www.unitar.org/unosat/node/44/2828?utm\\_source=unosat-unitar&utm\\_medium=rss&utm\\_campaign=maps](http://www.unitar.org/unosat/node/44/2828?utm_source=unosat-unitar&utm_medium=rss&utm_campaign=maps) (10.09.2018).
- UNITAR (2018c): Satellite detected water extent as of 27 July 2018 over Sanamxay District, Attapeu Province, Lao PDR: UNOSAT product ID 2834. 03.08.2018. [http://www.unitar.org/unosat/node/44/2834?utm\\_source=unosat-unitar&utm\\_medium=rss&utm\\_campaign=maps](http://www.unitar.org/unosat/node/44/2834?utm_source=unosat-unitar&utm_medium=rss&utm_campaign=maps) (10.09.2018).
- UNITAR (2018d): Satellite detected water extent as of 30 July 2018 over Samakxay District, Attapeu Province, Lao PDR: UNOSAT product ID 2835. 07.08.2018. [http://www.unitar.org/unosat/node/44/2835?utm\\_source=unosat-unitar&utm\\_medium=rss&utm\\_campaign=maps](http://www.unitar.org/unosat/node/44/2835?utm_source=unosat-unitar&utm_medium=rss&utm_campaign=maps) (10.09.2018).
- UNITAR (2018e): Time series Evolution flood satellite detected waters 13 - 29 July 2018: UNOSAT product ID 2830. 30.07.2018. [http://www.unitar.org/unosat/node/44/2830?utm\\_source=unosat-unitar&utm\\_medium=rss&utm\\_campaign=maps](http://www.unitar.org/unosat/node/44/2830?utm_source=unosat-unitar&utm_medium=rss&utm_campaign=maps) (10.09.2018).

- Urquhart, A. & Tichel, L. (2018): *Global humanitarian assistance report 2018*. Development Initiatives Ltd, Bristol, UK.
- Vajedian, S. & Motagh, M. (2018): Coseismic displacement analysis of the 12 November 2017 Mw 7.3 Sarpol-e Zahab (Iran) earthquake from SAR Interferometry, burst overlap interferometry and offset tracking. *ISPRS Annals of Photogrammetry, Remote Sensing and Spatial Information Sciences* 4 (3), 205–209.
- van Aalst, M. K. (2006): The impacts of climate change on the risk of natural disasters. *Disasters* 30 (1), 5–18.
- van den Noortgate, J. & Maes, P. (2010): *Public health engineering in precarious situations: Manual intended for the setting up of public health programmes in disadvantaged areas, particularly in refugee and displaced persons camps, and in health structures*, 2<sup>nd</sup> edn.
- van der Meer, F. D., van der Werff, H. M. A. & van Ruitenbeek, F. J. et al. (2012): Multi- and hyperspectral geologic remote sensing: A review. *International Journal of Applied Earth Observation and Geoinformation* 14 (1), 112–128.
- van Zandt, S., Peacock, W. G., Henry, D. W., Grover, H., Highfield, W. E. & Brody, S. D. (2012): Mapping social vulnerability to enhance housing and neighborhood resilience. *Housing Policy Debate* 22 (1), 29–55.
- van Zyl, J. (1992): Application of Cloude's target decomposition theorem to polarimetric imaging radar data. In: Mott, H. & Boerner, W.-M. (Eds.): *SPIE 1748. Radar Polarimetry*, 19 July 1992, San Diego, CA, 184.
- van Zyl, J. (2001): The Shuttle Radar Topography Mission (SRTM): A breakthrough in remote sensing of topography. *Acta Astronautica* 48 (5-12), 559–565.
- van Zyl, J., Chapman, B. D., Dubois, P. & Shi, J. (1993): The effect of topography on SAR calibration. *IEEE Transactions On Geoscience And Remote Sensing* 31 (5), 1036–1043.
- van Zyl, J. & Kim, Y. (2011): *Synthetic Aperture Radar polarimetry*. John Wiley & Sons, Inc, Hoboken, NJ, USA.
- van Zyl, J., Kim, Y. & Arii, M. (2008): Requirements for model-based polarimetric decompositions. In: *IGARSS 2008. IEEE International Geoscience and Remote Sensing Symposium*, 7 - 11 July 2008, Boston, MA, USA, 417- 420.
- Vasile, G., Trouve, E., Lee, J.-S. & Buzuloiu, V. (2006): Intensity-driven adaptive-neighborhood technique for polarimetric and interferometric SAR parameters estimation. *IEEE Transactions On Geoscience And Remote Sensing* 44 (6), 1609–1621.
- Vassileva, M., Giulio-Tonolo, F., Riccardi, P., Lecci, D., Boccardo, P. & Chiesa, G. (2017): Satellite SAR interferometric techniques in support to emergency mapping. *European Journal of Remote Sensing* 50 (1), 464–477.
- Verburg, P. H., Koomen, E., Hilferink, M., Pérez-Soba, M. & Lesschen, J. P. (2012): An assessment of the impact of climate adaptation measures to reduce flood risk on ecosystem services. *Landscape ecology* 27 (4), 473–486.
- Verjee, F. (2005): *The application of geomatics in complex humanitarian emergencies*. The George Washington University, Washington DC.
- Verjee, F. (2007): *An assessment of the utility of GIS-based analysis to support the coordination of humanitarian assistance*. Dissertation. The George Washington University, Washington DC.
- Verjee, F. & Gachet, A. (2007): 3.1 mapping water potential: The use of WATEX to support UNHCR refugee camp operations in eastern Chad. *Perspectives on Social Vulnerability* 94.
- Vicente-Guijalba, F., Duro, J. & Notarnicola, C. et al. (2017): Assessing hypertemporal Sentinel-1 coherence maps for land cover monitoring. In: *MultiTemp 2017. 9th International Workshop on the Analysis of Multitemporal Remote Sensing Images (MultiTemp)*, 27 - 29 June 2017, Bruges, Belgium, 1–3.
- Viera, A. J. & Garrett, J. M. (2005): Understanding interobserver agreement: The kappa statistic. *Fam Med* 37 (5), 360–363.
- Villard, L. & Le Toan, T. (2015): Relating P-Band SAR intensity to biomass for tropical dense forests in hilly terrain:  $\gamma$  0 or t0? *IEEE Journal of Selected Topics in Applied Earth Observations and Remote Sensing* 8 (1), 214–223.

- Voigt, S., Giulio-Tonolo, F. & Lyons, J. et al. (2016): Global trends in satellite-based emergency mapping. *Science* 353 (6296), 247–252.
- Voigt, S., Kemper, T., Riedlinger, T., Kiefl, R., Scholte, K. & Mehl, H. (2007): Satellite image analysis for disaster and crisis-management support. *IEEE Transactions On Geoscience And Remote Sensing* 45 (6), 1520–1528.
- Voisin, A., Krylov, V. A., Moser, G., Serpico, S. B. & Zerubia, J. (2013): Classification of very high resolution SAR images of urban areas using copulas and texture in a hierarchical Markov random field model. *IEEE Geoscience and Remote Sensing Letters* 10 (1), 96–100.
- Wakuma Abaya, S., Mandere, N. & Ewald, G. (2009): Floods and health in Gambella region, Ethiopia: A qualitative assessment of the strengths and weaknesses of coping mechanisms. *Global Health Action* 2.
- Walsh, N. P. (2017): Inside the Raqqa jail where ISIS held their betrayers. *CNN*, October 20. <https://edition.cnn.com/2017/10/20/middleeast/inside-raqqas-isis-jail/index.html> (15.01.2018).
- Walsh, N. P., van Heerden, D. & Abdelaziz, S. (2017): Satellite captures rare snapshot of life in Raqqa. *CNN*, April 25. <https://edition.cnn.com/2017/04/25/middleeast/raqqa-satellite-images/index.html> (15.01.2018).
- Wang, L. & Qu, J. J. (2009): Satellite remote sensing applications for surface soil moisture monitoring: A review. *Frontiers of Earth Science in China* 3 (2), 237–247.
- Wang, T.-L. & Jin, Y.-Q. (2012): Postearthquake building damage assessment using multi-mutual information from pre-event optical image and postevent SAR image. *IEEE Geoscience and Remote Sensing Letters* 9 (3), 452–456.
- Wang, W., Yang, X. & Yao, T. (2012): Evaluation of ASTER GDEM and SRTM and their suitability in hydraulic modelling of a glacial lake outburst flood in southeast Tibet. *Hydrological Processes* 26 (2), 213–225.
- Ward, D. P., Petty, A. & Setterfield, S. A. et al. (2014): Floodplain inundation and vegetation dynamics in the Alligator Rivers region (Kakadu) of northern Australia assessed using optical and radar remote sensing. *Remote Sensing of Environment* 147, 43–55.
- Warren, S., Hahn, C., London, J., Chervin, R. & Jenne, R. (1986): *Global distribution of total cloud cover and cloud type amounts over land*. UCAR/NCAR, NCAR Library.
- Wasowski, R. J. (1991): Some ethical aspects of international satellite remote sensing. *Photogrammetric Engineering & Remote Sensing* 57, 41–48.
- Wegmüller, U. (1999): Automated terrain corrected SAR geocoding. In: *IGARSS 1999*. IEEE International Geoscience and Remote Sensing Symposium, 28 June - 2 July 1999, Hamburg, Germany, 1712–1714.
- Wegmüller, U., Santoro, M., Werner, C. L., Strozzi, T., Wiesmann, A. & Lengert, W. (2009): DEM generation using ERS-ENVISAT interferometry. *Journal of Applied Geophysics* 69 (1), 51–58.
- Wegmüller, U., Wiesmann, A., Strozzi, T. & Werner, C. L. (2002): ENVISAT ASAR in disaster management and humanitarian relief. *Geoscience and Remote Sensing Symposium*, 2282–2284.
- Wei, L., Kumar, N., Lolla, V. N., Keogh, E. J., Lonardi, S. & Ratanamahatana, C. (2005): Assumption-free anomaly detection in time series. In: *SSDBM 2005*. 17th international conference on Scientific and statistical database management, 27 - 29 June 2005, Santa Barbara, 237–242.
- Weigand, M. (2017): *SAR image feature analysis for slum detection in megacities*. Master thesis. Universität Augsburg.
- Weinstein, A. (2017): US-led coalition takes Raqqa's Grand Mosque away from ISIS. *Business Insider*, September 05. <http://www.businessinsider.de/us-led-coalition-takes-raqqas-grand-mosque-away-from-isis-2017-9?r=US&IR=T> (15.01.2018).
- Weiss, T. G. (1999): Principles, politics, and humanitarian action. *Ethics & International Affairs* 13, 1–22.
- Weiss, T. G. & Collins, C. (2018): *Humanitarian challenges and intervention*, 2<sup>nd</sup> edn. Routledge, Boulder.
- Wells, J., Sinda, S. H. & Haddar, F. (1998): Housing and building materials in low-income settlements in Dar es Salaam. *Habitat International* 22 (4), 397–409.

- Wendt, L., Hilberg, S. & Robl, J. et al. (2015): Using remote sensing and gis to support drinking water supply in refugee/IDP camps. *Journal for Geographic Information Science* 1, 449–458.
- Wendt, L., Hilberg, S., Robl, J., Dirnberger, D., Strasser, T. & Braun, A. (2014): Hydrogeological remote sensing protocol: Deliverable 5.1 of EO4HumEn. Internal project document (ID: 840081).
- Weng, Q., Quattrochi, D. & Gamba, P. E. (Eds.) (2018): *Urban remote sensing*. CRC Press, Boca Raton.
- Wentz, F. J. (2013): SSM/I version-7 calibration report, remote sensing systems, Santa Rosa, CA.
- Werner, C. L., Hensley, S., Goldstein, R. M., Rosen, P. A. & Zebker, H. A. (1993): Techniques and applications of SAR interferometry for ERS-1: Topographic mapping, change detection, and slope measurement. In: *ESA ERS-1 1993*. First ERS-1 Symposium on Space at the Service of Our Environment, 4 - 6 November 1993, Cannes, 205–210.
- Werner, D. (2018): ICEYE achieves the ‘impossible’ with miniature radar satellite. 22.05.2018. <https://spacenews.com/qa-iceye-achieves-the-impossible-with-miniature-radar-satellite/> (15.01.2019).
- Werninghaus, R. & Buckreuss, S. (2010): The TerraSAR-X mission and system design. *IEEE Transactions On Geoscience And Remote Sensing* 48 (2), 606–614.
- Wessel, B. (2013): TanDEM-X ground segment DEM products specification document: Public document TD-GS-PS-0021. <https://tandemx-science.dlr.de> (01.09.2018).
- Westerhoff, R., Huizinga, J., Kleuskens, M., Burren, R. & Casey, S. (2010): Operational satellite based flood mapping using the Delft-FEWS System. In: *LPS 2010*. ESA Living Planet Symposium, 28 June 2010 - 2 July 2010, Bergen, Norway.
- Westra, L. (2013): *Environmental justice and the rights of ecological refugees*. Earthscan, London, New York.
- WFP (2012): Road assessment mission: Gambella - Metar - Burbe - Pugnido - Gog - Mizan - Raad - Boma - Jimma. 13 June 2012. [https://logcluster.org/sites/default/files/documents/Logistics-Cluster\\_South-Sudan\\_Ethiopia--SS-Road-Assessment](https://logcluster.org/sites/default/files/documents/Logistics-Cluster_South-Sudan_Ethiopia--SS-Road-Assessment) (15.08.2018).
- White, R. G. (1991): Change detection in SAR imagery. *International Journal of Remote Sensing* 12 (2), 339–360.
- Whitmeyer, S. J., Nicoletti, J. & Paor, D. G. de (2010): The digital revolution in geologic mapping. *GSA Today* 20 (4/5), 4–10.
- Wiek, A., Farioli, F., Fukushi, K. & Yarime, M. (2012): Sustainability science: Bridging the gap between science and society. *Sustainability Science* 7 (1), 1–4.
- Williamson, I. P., Enemark, S., Wallace, J. & Rajabifard, A. (2010): *Land administration for sustainable development*. ESRI Press Academic, Redlands, California.
- Wilson, K. B. (1992): Enhancing refugees' own food acquisition strategies. *Journal of Refugee Studies* 5 (3-4), 226–246.
- Wisner, B. (2007): *At risk: Natural hazards, people's vulnerability and disasters*, 2. ed., repr. Routledge, London.
- Witmer, F. D. W. (2015): Remote sensing of violent conflict: Eyes from above. *International Journal of Remote Sensing* 36 (9), 2326–2352.
- Witmer, F. D. W. & O'Loughlin, J. (2009): Satellite data methods and application in the evaluation of war outcomes: Abandoned agricultural land in Bosnia-Herzegovina after the 1992-1995 conflict. *Annals of the Association of American Geographers* 99 (5), 1033–1044.
- Wolde, D. (2016): *Factors affecting the performance of humanitarian logistics: The case of IRC ethiopia*. Master thesis. Addis Ababa University.
- Wolz, C. & Park, N. (2006): Evaluation of ReliefWeb. <https://www.alnap.org/help-library/evaluation-of-reliefweb> (15.12.2018).
- Woodcock, C. E. & Strahler, A. H. (1987): The factor of scale in remote sensing. *Remote Sensing of Environment* 21 (3), 311–332.
- World Meteorological Organization (2018): Kidal - Mali: WMO station number: 61214. [ftp://ftp.atdd.noaa.gov/pub/GCOS/WMO-Normals/TABLES/REG\\_\\_I/M1/61214.TXT](ftp://ftp.atdd.noaa.gov/pub/GCOS/WMO-Normals/TABLES/REG__I/M1/61214.TXT) (12.07.2018).
- Wu, C. (1976): A digital system to produce imagery from SAR data. In: *Systems design driven by sensors*, 18 - 20 October 1976, Pasadena, USA.

- Wu, S.-s., Qiu, X. & Le Wang (2005): Population estimation methods in GIS and remote sensing: A review. *GIScience & Remote Sensing* 42 (1), 80–96.
- Wulder, M. A., White, J. C. & Goward, S. N. et al. (2008): Landsat continuity: Issues and opportunities for land cover monitoring. *Remote Sensing of Environment* 112 (3), 955–969.
- Wurm, M. & Taubenböck, H. (2018): Detecting social groups from space: Assessment of remote sensing-based mapped morphological slums using income data. *Remote Sensing Letters* 9 (1), 41–50.
- Wurm, M., Taubenböck, H., Weigand, M. & Schmitt, A. (2017): Slum mapping in polarimetric SAR data using spatial features. *Remote Sensing of Environment* 194, 190–204.
- Xia, Z. G. & Sheng, Y. (1996): Radar speckle: Noise or information? In: *IGARSS 1996*. IEEE International Geoscience and Remote Sensing Symposium, 27–31 May 1996, Lincoln, NE, USA, 48–50.
- Xian, G. (2010): *Remote sensing applications for the urban environment*. CRC Press, Boca Raton.
- Xie, Y., Sha, Z. & Yu, M. (2008): Remote sensing imagery in vegetation mapping: A review. *Journal of plant ecology* 1 (1), 9–23.
- Xinyuan, W., Huadong, G., Yueming, C. & Liangsong, Z. (2004): On paleodrainage evolution in mid-late Epipliocene based on radar remote sensing in northeastern Ejin Banner, Inner Mongolia. *Journal of Geographical Sciences* 14 (2), 235–241.
- Xiong, B., Chen, Q., Jiang, Y. & Kuang, G. (2012): A threshold selection method using two SAR change detection measures based on the Markov random field model. *IEEE Geoscience and Remote Sensing Letters* 9 (2), 287–291.
- Xu, Y., Maitland, C. & Tomaszewski, B. (2015): Promoting participatory community building in refugee camps with mapping technology. In: *CTD 2015*. Seventh International Conference on Information and Communication Technologies and Development, 15 - 18 May 2015, Singapore, 67–71.
- Yague-Martinez, N., Eineder, M., Cong, X. Y. & Minet, C. (2012): Ground displacement measurement by TerraSAR-X image correlation: The 2011 Tohoku-Oki earthquake. *IEEE Geoscience and Remote Sensing Letters* 9 (4), 539–543.
- Yamaguchi, Y., Moriyama, T., Ishido, M. & Yamada, H. (2005): Four-component scattering model for polarimetric SAR image decomposition. *IEEE Transactions On Geoscience And Remote Sensing* 43 (8), 1699–1706.
- Yamazaki, F. (2001): Applications of remote sensing and GIS for damage assessment. *Structural Safety and Reliability*, 1–12.
- Yamazaki, F., Yano, Y. & Matsuoka, M. (2005): Visual damage interpretation of buildings in Bam city using quickbird images following the 2003 Bam, Iran, earthquake. *Earthquake Spectra* 21 (S1), 329–336.
- Yameogo, G., Sawadogo, S. K., Bastide, B., Belem, M. & Ouédraogo, I. (2004): *Méthodologie de collecte des données de la biomasse herbacée et ligneuse: Impact environnemental du PNGT2: suivi du couvert végétal*, Ouagadougou.
- Ye, X., Kaufmann, H. & Guo, X. F. (2004): Landslide monitoring in the Three Gorges area using D-InSAR and corner reflectors. *Photogrammetric Engineering & Remote Sensing* 70 (10), 1167–1172.
- Yousif, O. & Ban, Y. (2017): A novel approach for object-based change image generation using multitemporal high-resolution SAR images. *International Journal of Remote Sensing* 38 (7), 1765–1787.
- Yu, Y. & Acton, S. T. (2004): Automated delineation of coastline from polarimetric SAR imagery. *International Journal of Remote Sensing* 25 (17), 3423–3438.
- Zarocostas, J. (2010): Authorities investigate possible misuse of medical aid supplies in Haiti. *BMJ: British Medical Journal (Online)* 340.
- Zebker, H. A. & Villasenor, J. (1992): Decorrelation in interferometric radar echoes. *IEEE Transactions On Geoscience And Remote Sensing* 30 (5), 950–959.
- Zeil, P. & Lang, S. (2009): Do have clients a role in validation? In: Corbane, C., Broglia, M., Carrion, D., Lemoine, G. & Pesaresi, M. (Eds.): *VALgEO 2009*. International workshop on validation of geo-information products for crisis management, 23 - 25 November, Ispra, Italy, 143–147.

- Zhai, W., Shen, H., Huang, C. & Pei, W. (2016): Fusion of polarimetric and texture information for urban building extraction from fully polarimetric SAR imagery. *Remote Sensing Letters* 7 (1), 31–40.
- Zhang, H., Deng, Y. & Wang, R. et al. (2016): Spaceborne/stationary bistatic SAR imaging with TerraSAR-X as an illuminator in staring-spotlight mode. *IEEE Transactions On Geoscience And Remote Sensing* 54 (9), 5203–5216.
- Zhang, Y. & Kerle, N. (2008): Satellite remote sensing for near-real time data collection. In: Zlatanova, S. & Li, J. (Eds.): *Geospatial information technology for emergency response*. CRC Press, London, 91–118.
- Zhu, X. X. & Bamler, R. (2010): Very high resolution spaceborne SAR tomography in urban environment. *IEEE Transactions On Geoscience And Remote Sensing* 48 (12), 4296–4308.
- Zhu, X. X., Tuia, D. & Mou, L. et al. (2017): Deep learning in remote sensing: A comprehensive review and list of resources. *IEEE Geoscience and Remote Sensing Magazine* 5 (4), 8–36.
- Zink, M., Bachmann, M. & Brautigam, B. et al. (2014): TanDEM-X: The new global DEM takes shape. *IEEE Geoscience and Remote Sensing Magazine* 2 (2), 8–23.
- Zink, M., Moreira, A. & Bachmann, M. et al. (2017): The global TanDEM-X: A unique data set. In: *IGARSS 2017*. IEEE International Geoscience and Remote Sensing Symposium, 23 - 28 July 2017, Fort Worth, TX, USA.
- Zlatanova, S. & Li, J. (Eds.) (2008): *Geospatial information technology for emergency response*. CRC Press, London.

## Appendix

### Appendix 1 Results of the online survey among technically-oriented staff employed in the humanitarian domain

Taken from Braun (2018b), 20 participants, anonymously submitted answers, lists below in no particular order.

#### Question 1: What organization do you work for?

MSF (7x); Amnesty International (2x); ICRC (2x); UN-Habitat (2x); International Aid Services (2x); Austrian Red Cross; ITHACA; Consultant in Remote Sensing & GIS; Groundwater Relief; Humanitarian OSM team Uganda.

#### Question 2: Please name your position and occupation

Senior adviser; Special advisor in remote sensing; GIS technical advisor; technical engineer; CEO; Country manager; GIS technical focal point/coordination; GIS & satellite imagery analyst; programme manager, project management and design of evaluations; Deputy Country Director, IWRM Specialist; GIS and remote sensing analyst; GIS unit; GIS referent / technical advisor / learning & development / roster management; GIS officer; GIS specialist; GIS (spatial analysis, data collection, mapping); GIS Specialist; web mapping manager; HLP officer; GIS junior;

#### Question 3: Please rate the following data sources

*Table 27: Survey on the degree of familiarity with different geospatial data sources*

	never heard of	heard of	occasionally used	already used several times	frequently used	total (n)
Vector data (Shapefiles, KML/KMZ, GeoJSON...)	0 %	0 %	0 %	10 %	90 %	20
GPS points or routes (locations, transects, outlines, ...)	0 %	0 %	0 %	20 %	80 %	20
Statistical data with a spatial component	0 %	15 %	5 %	40 %	40 %	20
Optical satellite imagery (e.g. Landsat, WorldView, SPOT, ...)	0 %	0 %	10 %	10 %	80 %	20
Data collected in the field (measurements, surveys, samples, ...)	0 %	0 %	15 %	10 %	75 %	20
Digital maps or digitized analogue maps	0 %	0 %	20 %	25 %	55 %	20
Digital elevation models (e.g. SRTM, ASTER GDEM, ...)	0 %	0 %	25 %	10 %	65 %	20
Optical aerial imagery (images of flight campaigns)	0 %	15 %	35 %	30 %	20 %	20
Radar satellite imagery (e.g. TerraSAR-X, Sentinel-1, ...)	0 %	25 %	50 %	15 %	10 %	20

**Question 4: Please check all points that apply to you regarding radar satellite imagery***Table 28: Survey on the opinion of radar remote sensing in a humanitarian context*

I'm not interested at all.	0 %
It is not related to my current occupation or expertise.	5 %
I am curious or interested.	90 %
I don't have the technical expertise to use it.	40 %
I don't have the time to learn or get into it.	35 %
Optical imagery seems more applicable to me.	10 %

*Table 29: Optional comments on the use of radar remote sensing in a humanitarian context*

Radar is new to me and while I have been successful looking at flooded mine areas, I do not have that much time to investigate further.
On some application (soil or vegetation water content) or some weather condition (frequent cloud cover), radar imageries could provide complementary or primary information.
I am curious as it is very complementary of optical sensor due to frequency, and cloud penetration. However, we need more expertise to understand and work with the signals
I use it often, but I would like to explore its application in the different fields of Earth Observations
I would like to use radar imagery more, see the high potential in the use of radar imagery for humanitarians
We are interested in using radar data, especially to overcome the problem of cloud cover during rainy season. Also, to produce DTM and so on.
I use it sometime as well but less (mainly for topo)

**Question 5: Which of the following properties or applications of radar imagery seem attractive to you or your organization (multiple choice)?**

*Table 30: Potential of radar imagery as seen by staff in the humanitarian domain*

Independency from cloud cover and daylight	90 %
Mapping water bodies and other resources	80 %
Damage assessment in emergency situations	75 %
High spatial resolution (e.g. 1 meter)	70 %
Provision of images at regular intervals (e.g. for monitoring purposes)	60 %
Mapping landcover / land-use and its dynamics	55 %
Provision of images at specifically defined dates (tasking)	50 %
Measurement of topography or ground motion at the centimeter scale	50 %
Capability to penetrate materials (e.g. canopies, soils, ...)	50 %
Provision of data at no cost at all	45 %
Large spatial coverage (> 250 km in one image)	45 %
Assisting search for groundwater	45 %
Cheaper than optical imagery	30 %
Input for operational routines (automated tasks at different dates or in different areas)	20 %

*Table 31: Optional comments on the benefits of radar images*

Measuring water levels in lakes..... Mapping changes in soil/geology
I am not particularly well versed on the technical side of radar imagery (or remote sensing in general). So, lots of these sound useful to me but I need to be educated on the limitations and appropriate usage of radar data. It's very easy to grab data and go in humanitarian settings without properly understanding where you should be cautious using it.

## Appendix 2 Comparison of SAR imaging modes

Table 32: Comparison of SAR imaging modes and their spatial properties

Satellite	Band	Mode with abbreviation <sup>1</sup>	Polarization <sup>2</sup>	Spatial resolution [m] <sup>3</sup>	Spatial extent (range) <sup>4</sup> [km]	Source
Seasat	L	STD Standard	Single (HH)	25	100	<a href="#">ESA</a>
ERS-1/ERS-2	C	SM StripMap	Single (HH)	20	100	<a href="#">ESA</a>
ERS-1/ERS-2	C	WV Wave	Single (HH)	30	5	<a href="#">ESA</a>
JERS-1	L	STD Standard	Single (HH)	18	75	<a href="#">JAXA</a>
ENVISAT	C	IM Image	Single (HH / VV)	30	100	<a href="#">ESA</a>
ENVISAT	C	AP Alternate Polarization	Dual (HH+HV / VV+VH / HH+VV)	30	100	<a href="#">ESA</a>
ENVISAT	C	WS WideSwath	Single (HH / VV)	150	400	<a href="#">ESA</a>
ENVISAT	C	WV Wave	Single (HH / VV)	150	5	<a href="#">ESA</a>
ENVISAT	C	GM Global Monitoring	Single (HH / VV)	4000	1000	<a href="#">ESA</a>
RADARSAT-1	C	F Fine	Single (HH)	8	50	<a href="#">CSA</a>
RADARSAT-1	C	S Standard	Single (HH)	25	100	<a href="#">CSA</a>
RADARSAT-1	C	W Wide	Single (HH)	30	150	<a href="#">CSA</a>
RADARSAT-1	C	SN ScanSAR Narrow	Single (HH)	50	300	<a href="#">CSA</a>
RADARSAT-1	C	SW ScanSAR Wide	Single (HH)	100	500	<a href="#">CSA</a>
RADARSAT-1	C	EH Extended High	Single (HH)	25	75	<a href="#">CSA</a>
RADARSAT-1	C	EL Extended Low	Single (HH)	35	170	<a href="#">CSA</a>
ALOS PALSAR	L	FBS Fine Beam Single	Single (HH / VV)	7.5	50	<a href="#">JAXA</a>
ALOS PALSAR	L	FBD Fine Beam Dual	Dual (HH+HV / VV+VH)	15	50	<a href="#">JAXA</a>
ALOS PALSAR	L	SC ScanSAR	Single (HH / VV)	100	300	<a href="#">JAXA</a>
ALOS PALSAR	L	PLR Polarimetric	Quad (HH+HV+VH+VV)	50	50	<a href="#">JAXA</a>
ALOS-2	L	SL Spotlight	Single or Dual (HH+HV / VV+VH)	1	25	<a href="#">JAXA</a>
ALOS-2	L	SM1 StripMap 1	Single or Dual (HH+HV / VV+VH)	3	55	<a href="#">JAXA</a>
ALOS-2	L	SM2 StripMap 2	Single or Dual (HH+HV / VV+VH)	6	55	<a href="#">JAXA</a>

## Appendix

ALOS-2	L	SM2 StripMap 2	Full (HH+HV+VH+VV), circular	6	40	<a href="#">JAXA</a>
ALOS-2	L	SM3 StripMap 3	Single or Dual (HH+HV / VV+VH)	10	70	<a href="#">JAXA</a>
ALOS-2	L	SC ScanSAR	Single or Dual (HH+HV / VV+VH)	100	350	<a href="#">JAXA</a>
ALOS-2	L	SCW ScanSAR Wide	Single or Dual (HH+HV / VV+VH)	60	460	<a href="#">JAXA</a>
RADARSAT-2	C	S Standard	Dual (HH+HV / VV+VH / HH+VV)	25	100	<a href="#">CSA</a>
RADARSAT-2	C	W Wide	Dual (HH+HV / VV+VH / HH+VV)	25	150	<a href="#">CSA</a>
RADARSAT-2	C	F Fine	Dual (HH+HV / VV+VH / HH+VV)	10	50	<a href="#">CSA</a>
RADARSAT-2	C	SN ScanSAR Narrow	Dual (HH+HV / VV+VH / HH+VV)	50	300	<a href="#">CSA</a>
RADARSAT-2	C	SW ScanSAR Wide	Dual (HH+HV / VV+VH / HH+VV)	100	500	<a href="#">CSA</a>
RADARSAT-2	C	QPS Polarimetry Standard	Full (HH+HV+VH+VV), circular	25	25	<a href="#">CSA</a>
RADARSAT-2	C	QPF Polarimetry Fine	Full (HH+HV+VH+VV), circular	10	25	<a href="#">CSA</a>
RADARSAT-2	C	SL Spotlight	Single (HH/VV)	1-2	18	<a href="#">CSA</a>
RADARSAT-2	C	UF UltraFine	Single (HH/VV)	3	20	<a href="#">CSA</a>
RADARSAT-2	C	MLF Multi-Look Fine	Single (HH/VV)	10	50	<a href="#">CSA</a>
TerraSAR-X	X	ST Staring Spotlight	Single (HH/VV)	0.6	3	<a href="#">Airbus</a>
TerraSAR-X	X	HS High Resolution	Single, Dual	1.2	5	<a href="#">Airbus</a>
TerraSAR-X	X	SL Spotlight	Single, Dual	1.7	10	<a href="#">Airbus</a>
TerraSAR-X	X	SM StripMap	Single (HH/VV)	3.5	30	<a href="#">Airbus</a>
TerraSAR-X	X	SM StripMap	Dual (HH+HV / VV+VH / HH+VV)	3.5	15	<a href="#">Airbus</a>
TerraSAR-X	X	SC ScanSAR	Single (HH/VV)	18.5	150	<a href="#">Airbus</a>
TerraSAR-X	X	SCW Wide ScanSAR	Single (HH/VV)	40	200	<a href="#">Airbus</a>
COSMO-SkyMed	X	SL Spotlight	Single (HH/VV)	1	10	<a href="#">ASI</a>
COSMO-SkyMed	X	SL Spotlight	Dual (HH+HV / VV+VH / HH+VV)	0.8	10	<a href="#">ASI</a>
COSMO-SkyMed	X	SM StripMap	Dual (HH+HV / VV+VH / HH+VV)	3	40	<a href="#">ASI</a>
COSMO-SkyMed	X	SM StripMap	Dual Burst	20	30	<a href="#">ASI</a>
COSMO-SkyMed	X	SM StripMap	Full (HH+HV+VH+VV), circular	3	15	<a href="#">ASI</a>
COSMO-SkyMed	X	SC ScanSAR	Single (HH/VV)	20	100	<a href="#">ASI</a>
COSMO-SkyMed	X	SC ScanSAR	Dual (HH+HV / VV+VH / HH+VV)	20	200	<a href="#">ASI</a>
RISAT-1	C	HRS High Resolution Spotlight	Single, Dual, Circular	1	10	<a href="#">NRSC</a>

Appendix

RISAT-1	C	FRS-1 Fine Resolution StripMap	Single, Dual, Circular	2-3	25	<a href="#">NRSC</a>
RISAT-1	C	FRS-2 Fine Resolution StripMap	Full (HH+HV+VH+VV), circular	4-9	25	<a href="#">NRSC</a>
RISAT-1	C	MRS Medium Resolution ScanSAR	Single, Dual, Circular	8-23	115	<a href="#">NRSC</a>
RISAT-1	C	CRS Coarse Resolution ScanSAR	Single, Dual, Circular	8-55	223	<a href="#">NRSC</a>
RISAT-2	X	SM StripMap	Single (HH/HV/VH/VV)	3	10	<a href="#">ESA</a>
RISAT-2	X	SC ScanSAR	Single (HH/HV/VH/VV)	8	50	<a href="#">ESA</a>
RISAT-2	X	SL Spotlight	Single (HH/HV/VH/VV)	1	10	<a href="#">ESA</a>
RISAT-2	X	M Mosaic	Single (HH/HV/VH/VV)	1.8	10	<a href="#">ESA</a>
Kompsat-5	X	SL Spotlight	Single (HH)	1	5	<a href="#">KARI</a>
Kompsat-5	X	SM StripMap	Single (HH)	3	30	<a href="#">KARI</a>
Kompsat-5	X	SC ScanSAR	Single (HH)	20	100	<a href="#">KARI</a>
Sentinel-1	C	SM StripMap	Dual (HH+HV / VV+VH)	5	80	<a href="#">ESA</a>
Sentinel-1	C	IW Interferometric Wide Swath	Dual (HH+HV / VV+VH)	10	250	<a href="#">ESA</a>
Sentinel-1	C	EW Extra Wide Swath	Dual (HH+HV / VV+VH)	100	400	<a href="#">ESA</a>
PAZ	X	SL Spotlight	Single (HH/VV)	1	5	<a href="#">ESA</a>
PAZ	X	SL Spotlight	Dual (HH+HV / VV+VH / HH+VV)	2	10	<a href="#">ESA</a>
PAZ	X	SM StripMap	Single (HH/VV)	3	15	<a href="#">ESA</a>
PAZ	X	SM StripMap	Dual (HH+HV / VV+VH / HH+VV)	6	30	<a href="#">ESA</a>
PAZ	X	SC ScanSAR	Single (HH/VV)	16	100	<a href="#">ESA</a>

Notes:

- <sup>1</sup> Names and abbreviations of the modes according to the product descriptions given in the column 'Source'.
- <sup>2</sup> Dashes (/) indicate that the polarizations are mutually exclusive, the plus sign (+) indicates that more polarizations are possible at the same time.
- <sup>3</sup> Pixel size is not necessarily the original spatial resolution and depends on incidence angle and multi-looking. Smallest possible resolution is given in all cases.
- <sup>4</sup> Range can also vary according to sensor configurations. Mean values are taken to keep the table readable.

### Appendix 3 Time of operation of selected SAR missions

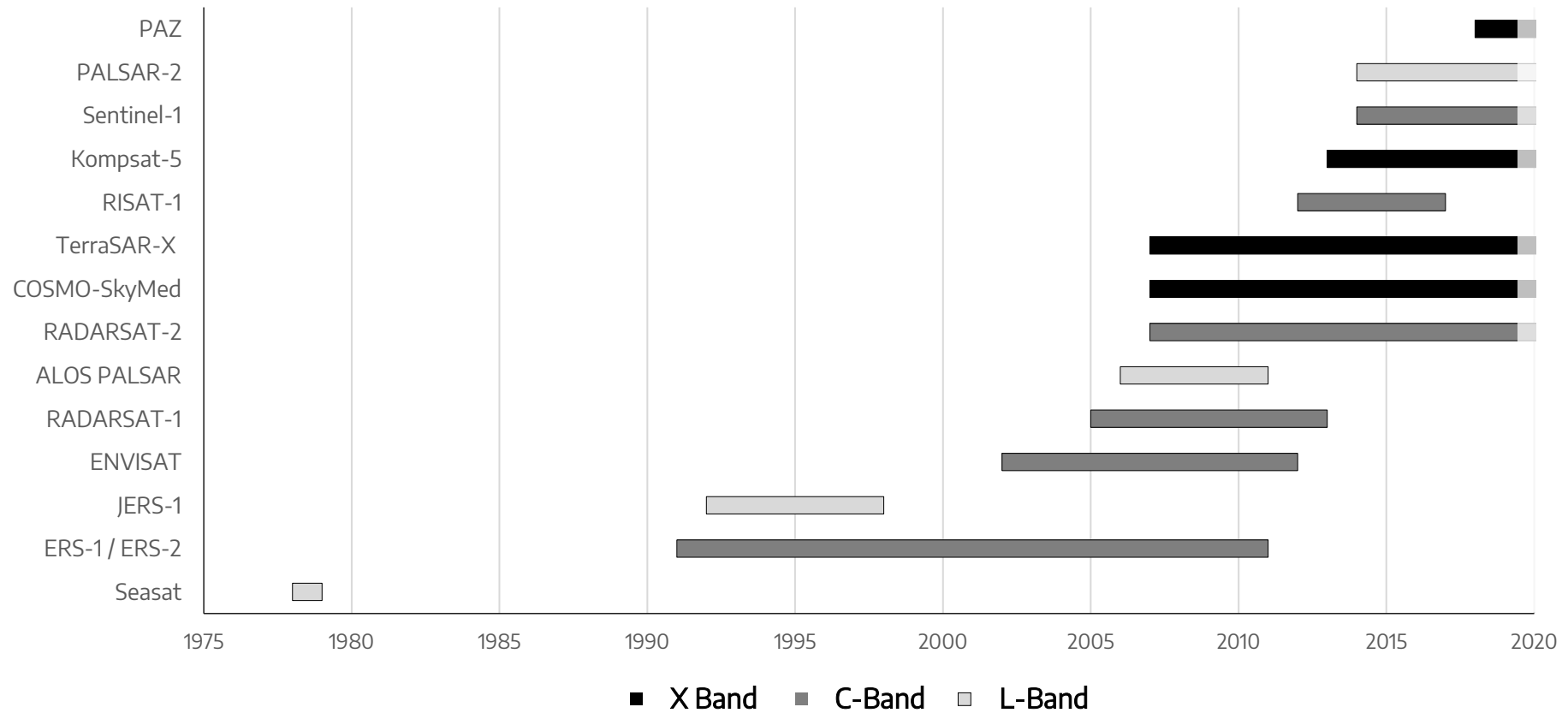


Figure 101: Temporal operation time of SAR satellite missions

Note: Military satellites are not included, because they are irrelevant in this context (not usable for humanitarian organizations).  
 Examples are SAR-Lupe (Germany), Almaz, (Russia), RISAT-2 (India) or TecSAR (Israel).

## Appendix 4 Pre-processed TerraSAR-X image

This image was radiometrically calibrated, multi-looked, speckle-filtered, terrain corrected for distortions on backscatter and pixel location and geocoded to WGS84 as described in chapter 2.3. The color composite shows the information content of both HH and VV polarization (section 2.2.4). While backscatter of both polarizations is comparably similar in most parts of the scene, differences are evident in the urban areas and the grasslands in the northwest of the scene

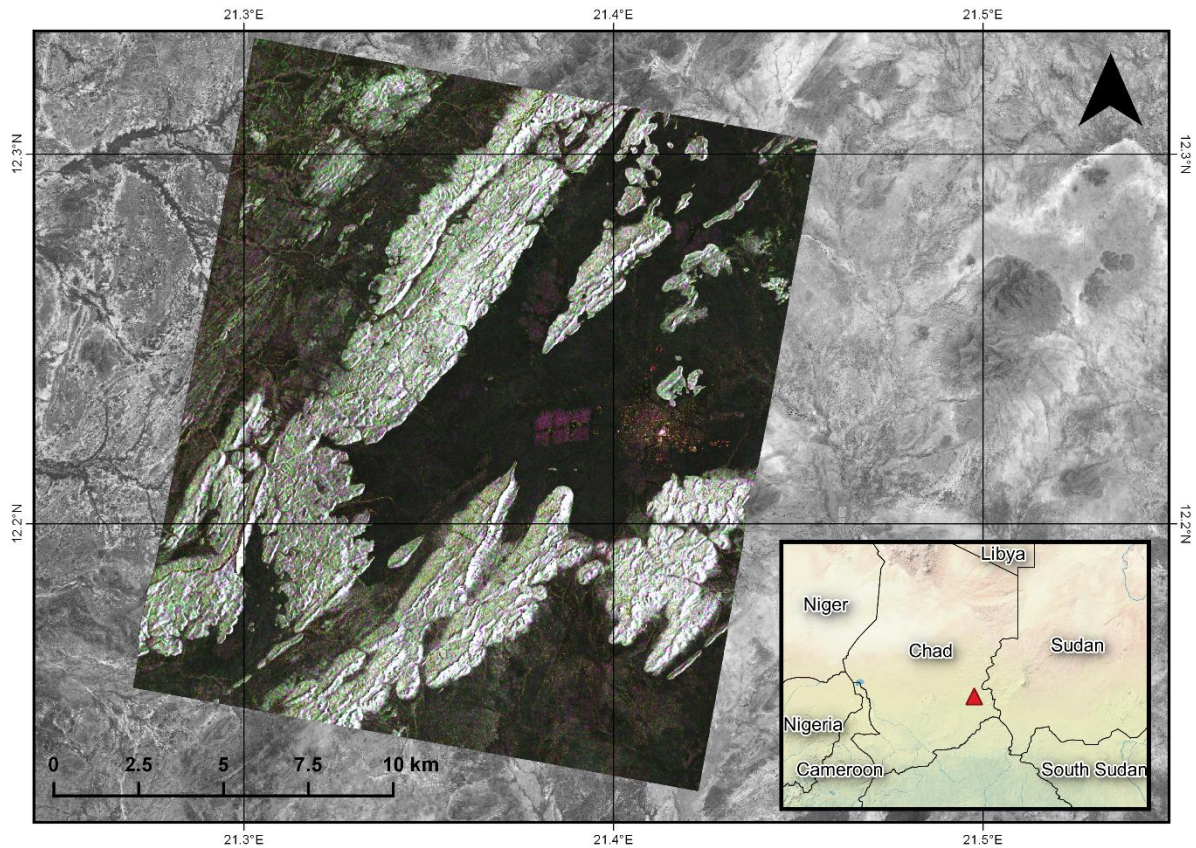
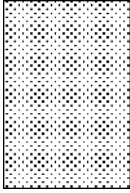
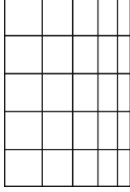
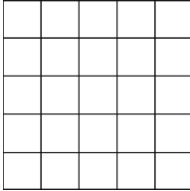
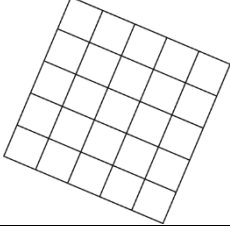
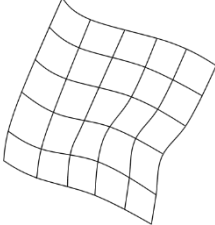


Figure 102: Pre-processed TerraSAR-X image of Djabal refugee camp, eastern Chad  
 RGB composite: red=HH, green=VV, blue=HH/VV

## Appendix 5 Product levels of SAR imagery

Table 33: Product levels of SAR imagery

#	Product level	Geometry	Properties
<b>0</b>	Raw  Abbreviations: Level 0		<ul style="list-style-type: none"> <li>– raw signal after range compression</li> <li>– data has to be focused by a SAR processor before it can be analyzed, (Bamler 1992; Prati &amp; Rocca 1992)</li> <li>– pixels do not yet represent backscatter intensity</li> <li>– not usable in common software packages</li> </ul>
<b>1</b>	Slant Range Complex  Abbreviations: SLC / SSC / L1.1 / IMS		<ul style="list-style-type: none"> <li>– most commonly ordered / delivered product</li> <li>– slant range: uneven pixel spacing</li> <li>– contains intensity and phase information</li> <li>– data is not yet geocoded / projected to a coordinate reference system</li> </ul>
<b>2</b>	Ground Range Detected  Abbreviations: MGD / GRD / MLI / PRI / L1.5 / IMP		<ul style="list-style-type: none"> <li>– ground range: even pixel spacing</li> <li>– pixel represents equal areas on ground</li> <li>– generated by multi-looking</li> <li>– no longer contains phase information (as required for radar interferometry)</li> <li>– data is not geocoded / projected</li> </ul>
<b>3a</b>	Geocoded Ellipsoid Corrected  Abbreviations: GEC / L2.0		<ul style="list-style-type: none"> <li>– data is geocoded into a coordinate reference system</li> <li>– projected onto flat earth (constant ellipsoid height)</li> <li>– suitable for areas without topography or imagery of sea surfaces</li> </ul>
<b>3b</b>	Geocoded Terrain Corrected  Abbreviations: GTC / EEC / L2.1 / Ortho		<ul style="list-style-type: none"> <li>– data is geocoded into a coordinate reference system and projected onto actual terrain surface using a DEM</li> <li>– no more foreshortening or layover effects but radiometric distortions can still be present (section 2.2.1)</li> <li>– more commonly used than #3a</li> </ul>

## Appendix 6 Editing date of OpenStreetMap data

The following website allows to compare the date at which a feature in OSM was modified at last:

<https://is-osm-uptodate.frafra.eu/>

It also shows the update frequency of single entities. In the following examples, the colors indicate the editing date, ranging from 2012 (red) to 2018 (blue) for selected parts of the city of Maiduguri (accessed on 14.10.2018).

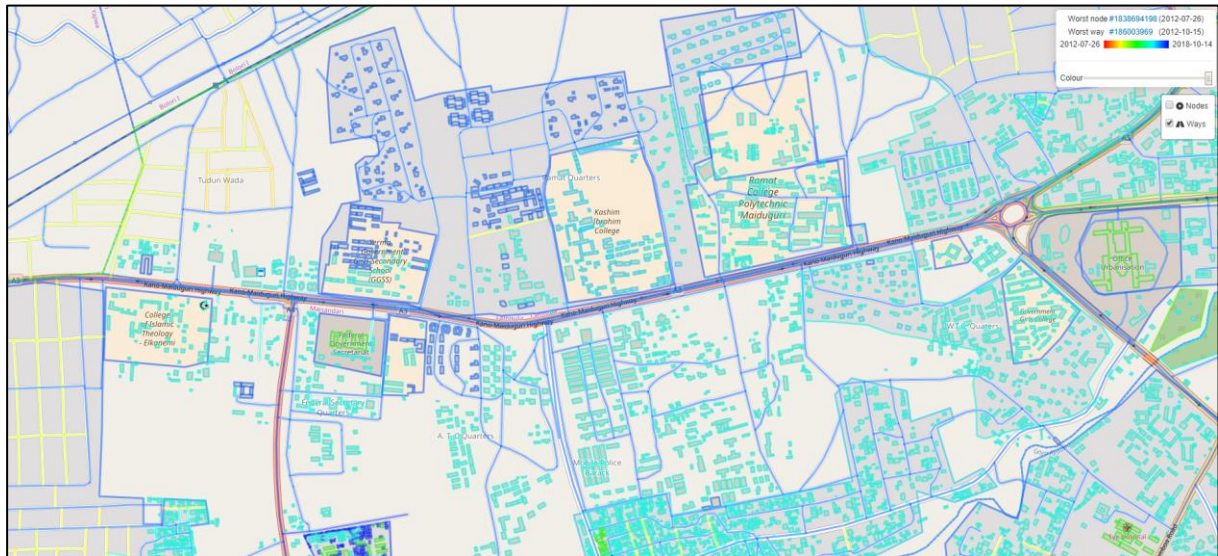


Figure 103: OpenStreetMap data in Maiduguri of different editing date

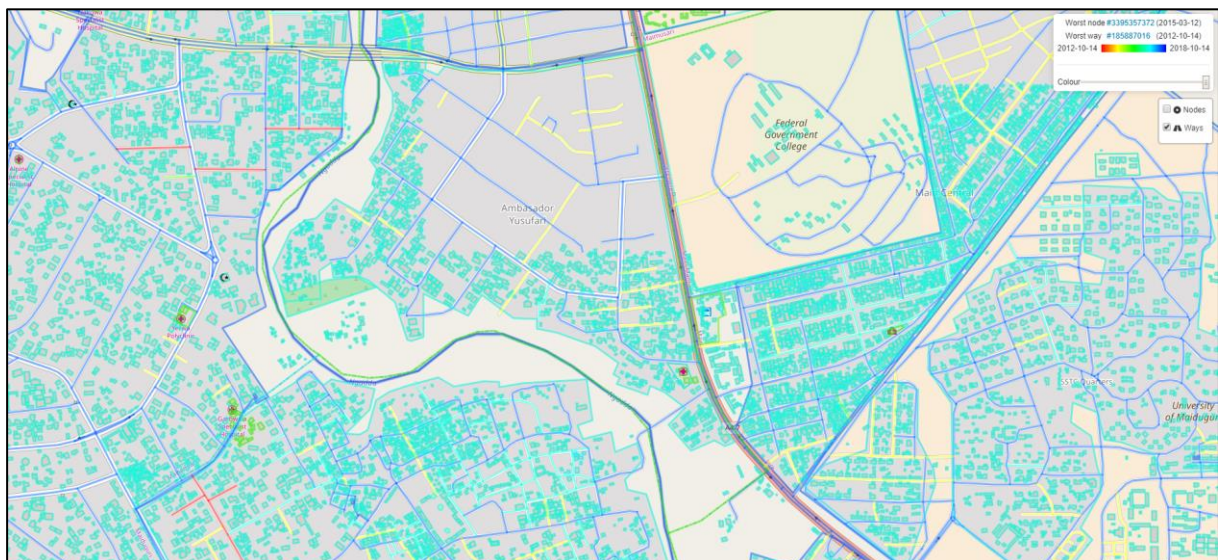


Figure 104: OpenStreetMap data in Maiduguri of different spatial completeness

# Appendix 7 Sentinel-1 coverage by the end of 2018

## Coverage Map s1a\_csar\_grdh\_iw

Coverage until 2018-11-09  
Total number of images: 476697

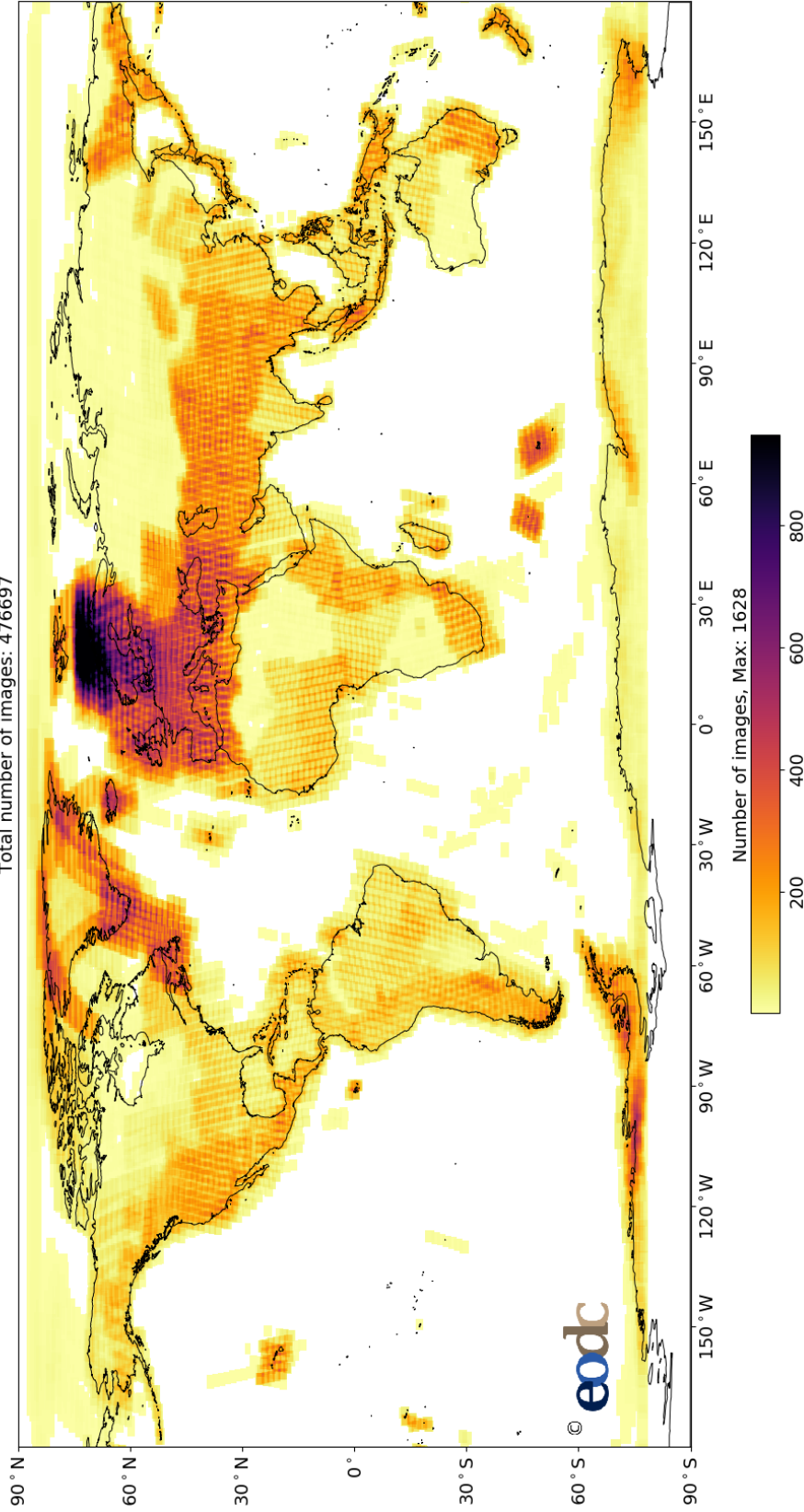


Figure 105: Number of Sentinel-1 GRD products acquired in IW mode  
Source: <https://eomex.eodc.eu/cm> (EODC 2018)

# Appendix 8 Changes in camp Kutupalong highlighted by very high-resolution TerraSAR-X data in StripMap mode

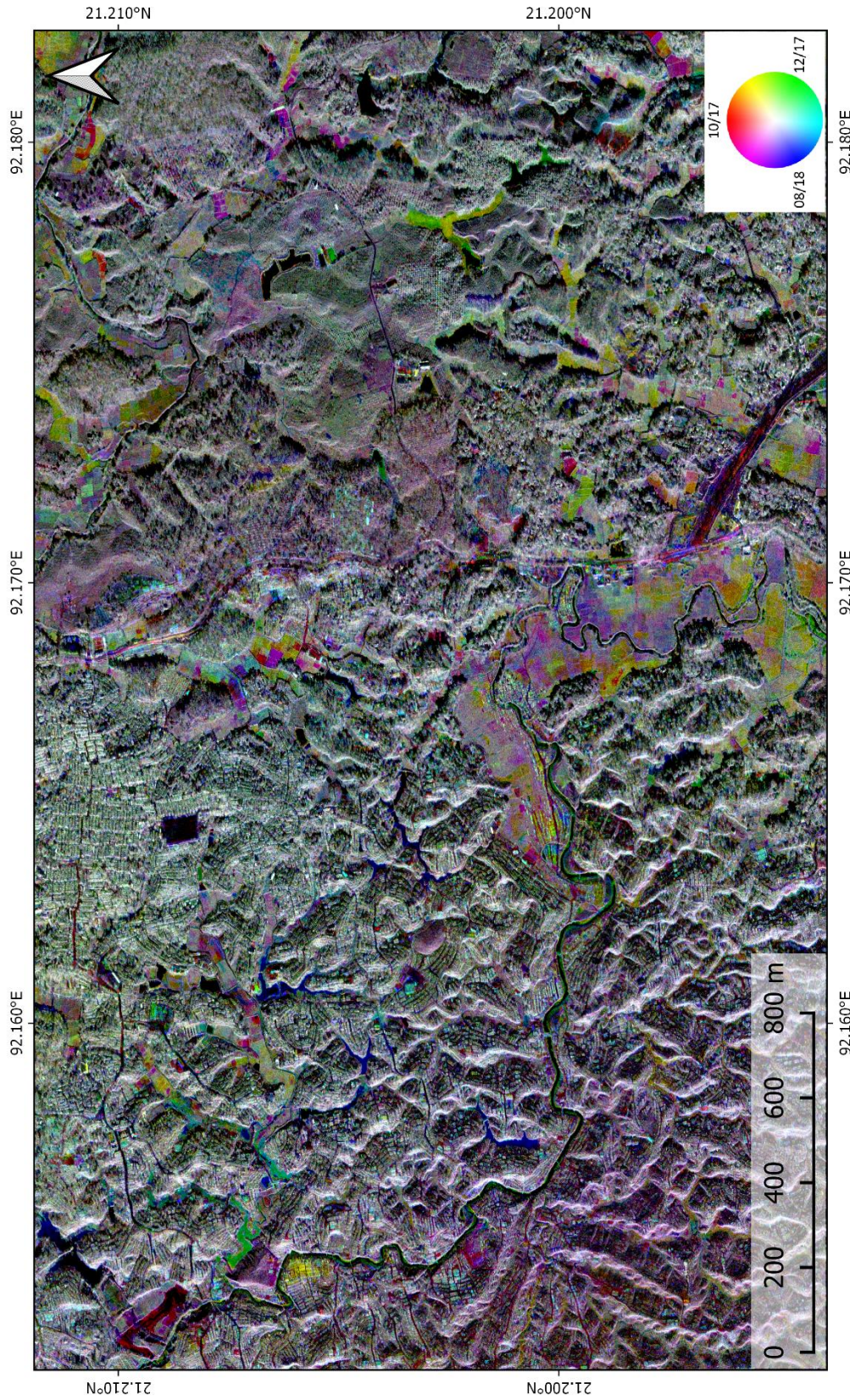
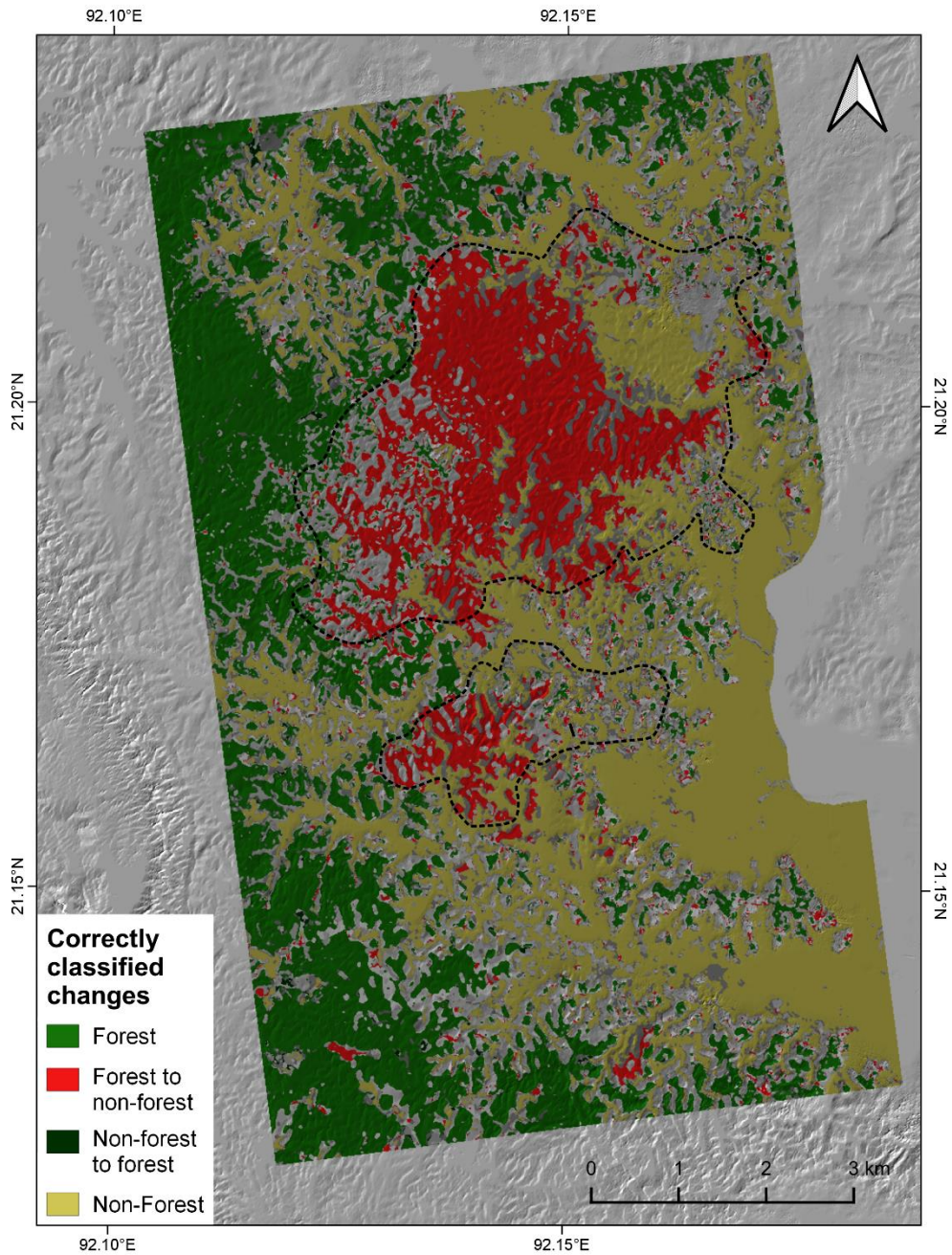


Figure 106: Changes in camp Kutupalong identified by VHR SAR color composites  
Red: 30.09.2017, green: 27.12.2017, blue: 04.08.2018

## Appendix 9 Forest change in camp Kutupalong, Bangladesh



*Figure 107: Accuracy map of the supervised forest classification for December 2016 and 2017. Grey pixels within the study area indicate incorrectly derived changes caused by errors in the binary forest classification within one or both investigated periods. Grey dashed lines indicate the extent of the camp at the end of February 2018.*

## Appendix 10 Google Earth Engine code for temporal averaging

```

// Define collection and center point
var sentinel1 = ee.ImageCollection('COPERNICUS/S1_GRD');
var center = ee.Geometry.Point([-10.1320, 8.5640]);

// Create a buffer of 15 km around center point
var area = center.buffer(15000);

// Reduce collection to IW products acquired in ascending mode
var vv = sentinel1
  .filter(ee.Filter.listContains('transmitterReceiverPolarisation', 'VV'))
  .filter(ee.Filter.eq('instrumentMode', 'IW'))
  .select('VV')
  .filter(ee.Filter.eq('orbitProperties_pass', 'ASCENDING'))
  .filterBounds(area);

// select all images available between 2014 and 2018
var S1_all = vv.filterDate(ee.Date('2014-01-01'), ee.Date('2018-12-31'));

// Convert the collection to a list and print the number of images.
var size = S1_all.toList(500).length();
print('Number of images (all): ', size);

// Create temporal average
var S1_all_mean = S1_all.mean();

// Add average to the map and zoom to area of interest
Map.addLayer(S1_all_mean.clip(area), {min: [-12], max: [-3]}, 'mean', 1);
Map.centerObject(S1_all_mean.clip(area));

// Export the temporal average as GeoTiff to GoogleDrive
Export.image.toDrive({
  image: S1_all_mean.clip(area),
  description: 'Gueckedou_average',
  scale: 10,
  folder: "S1",
  region: area
});

```

# Appendix 11 Infrastructure map with flood marks

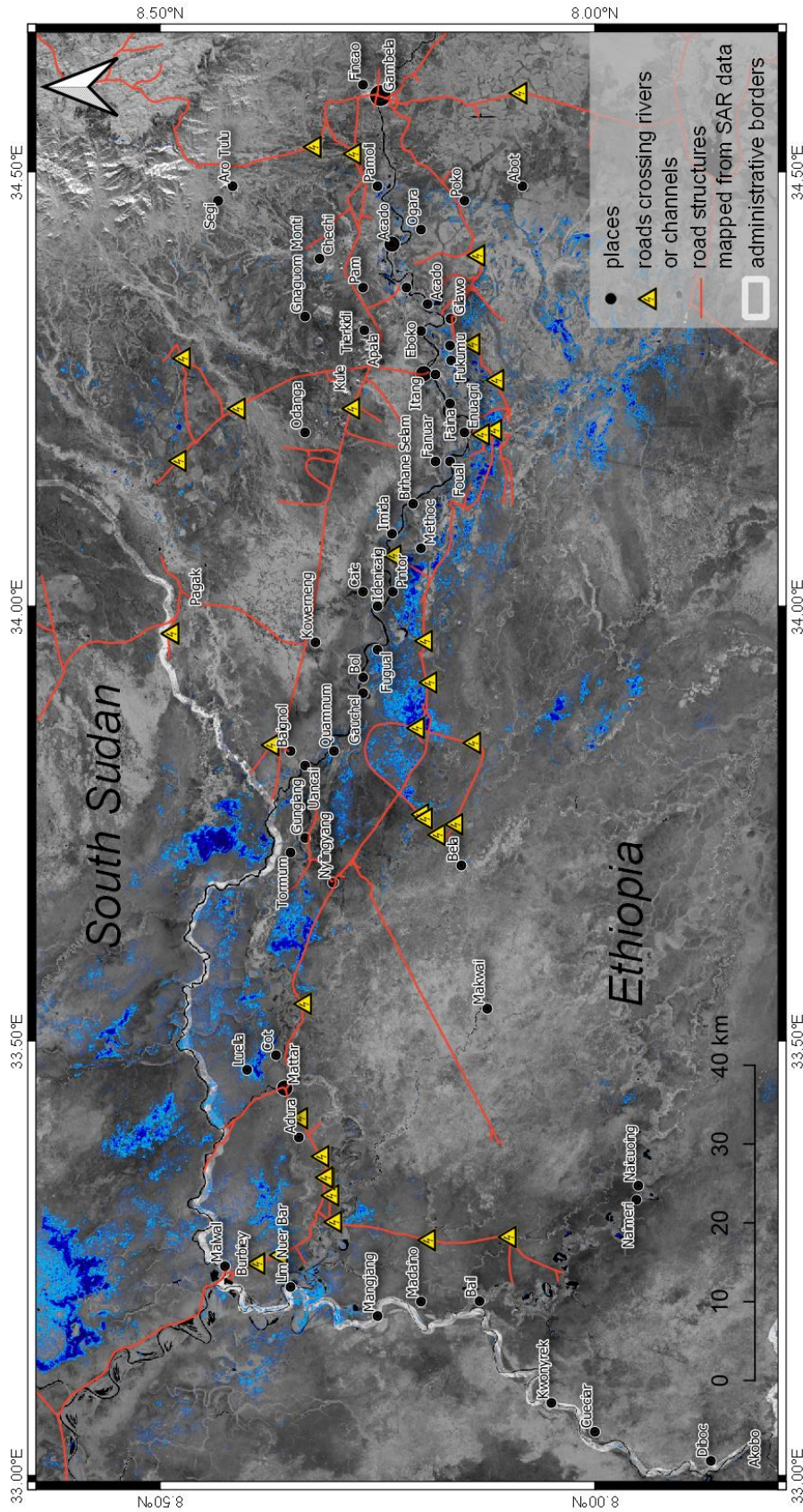


Figure 108: Road infrastructure and flood extents for Gambella, Ethiopia  
Blue areas indicate flood extents of the floods reported in May 2016 and September 2017.

# Appendix 12 Rural settlements in a polarimetric SAR image

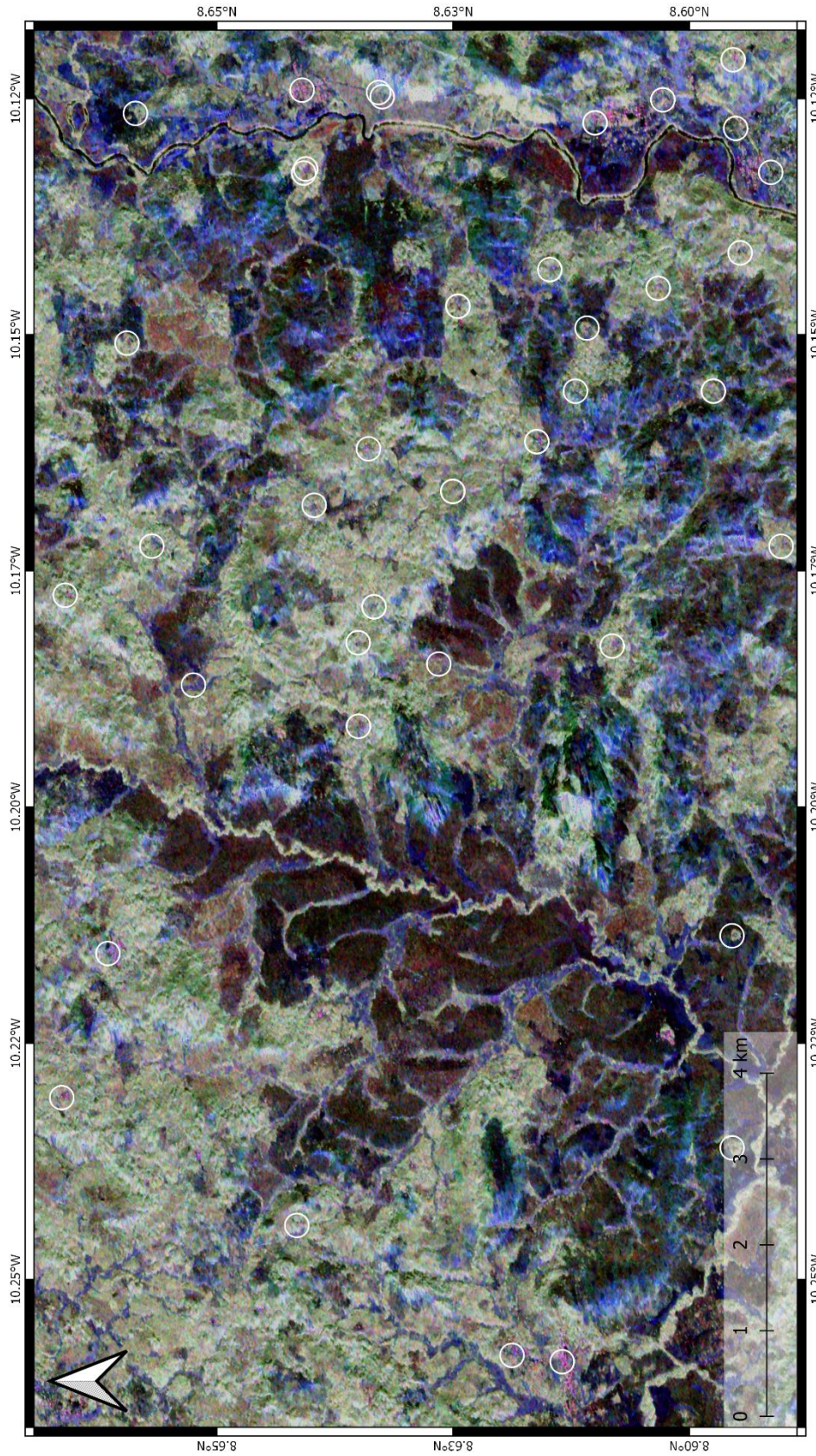


Figure 109: Polarimetric image of the rural areas around Guéckédou, Guinea  
Pauli decomposition of ALOS-2 (22.04.2016): red: dihedral scattering, green: volume scattering, blue: surface scattering.  
Note how settlements (white circles from OSM data) are marked in red hues because of the high contribution of double bounce to the RGB.

# Appendix 13 Topographic map

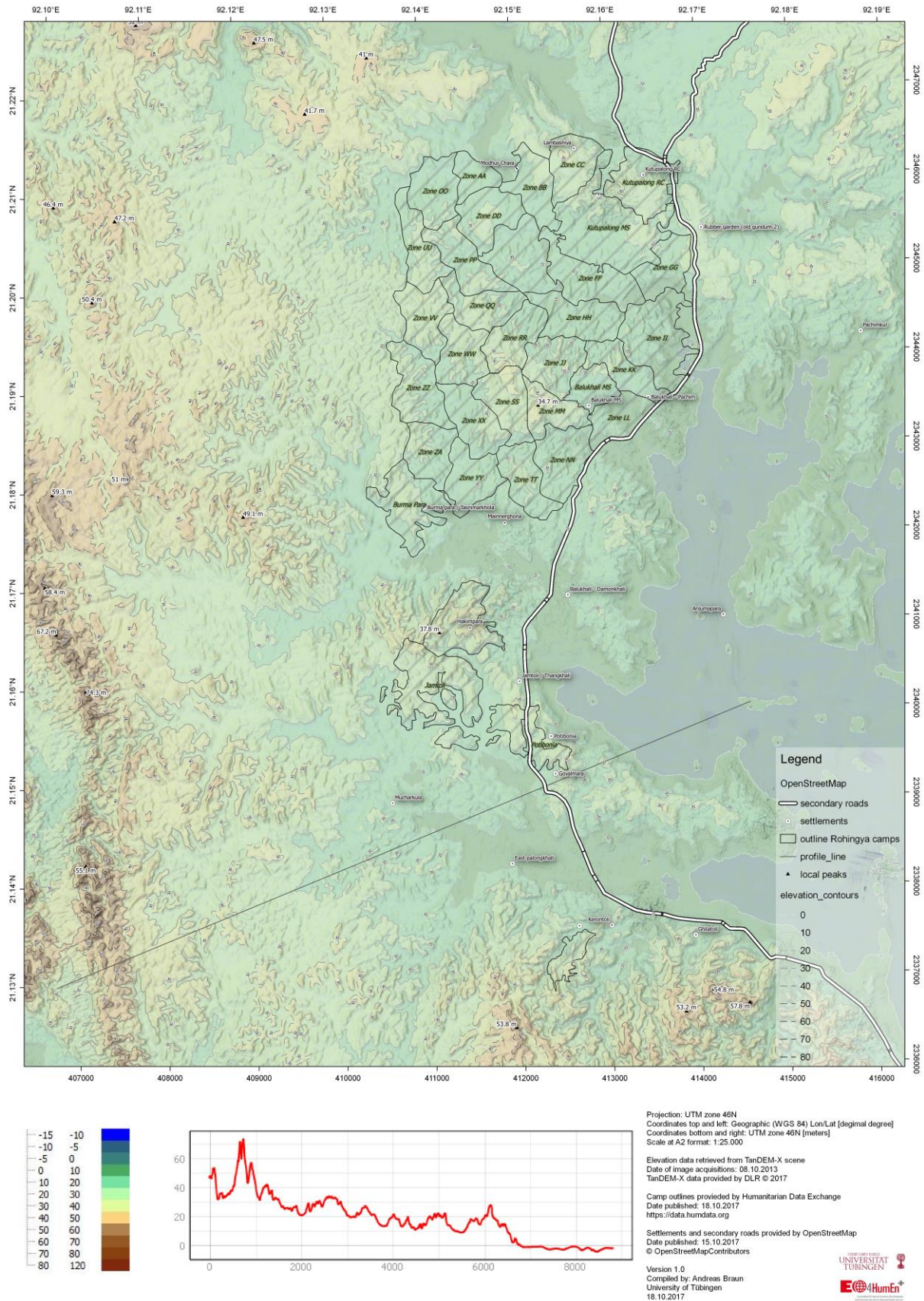


Figure 110: Topographic Map of Kutupalong as provided to MSF within EO4HumEn+ in 10/2017

## Appendix 14 Capacity development

Table 34: SAR-related capacity development in alphabetical order  
(last access to weblinks: 31.01.2019)

Name	Type	Short description
<a href="#">Advanced course on radar polarimetry</a>	Course	Lectures and practical units covering radar polarimetry, radar interferometry, polarimetric interferometry, and tomographic SAR. Hosted by the European Space Agency every two years.
<a href="#">ASF Tutorials</a>	Materials	Large collection of materials, tutorials, and videos on SAR and InSAR basics and practical applications (e.g. calibration, geocoding, displacement mapping, DEM generation, land-use mapping, glacier velocity tracking) provided by the Alaska Satellite Facility (ASF).
<a href="#">A tutorial on synthetic aperture radar</a>	Reading	A 38-page introduction on SAR, its principles, characteristics, and possible applications compiled by the DLR. Openly published within the IEEE Geoscience and Remote Sensing Magazine (GRSM).
<a href="#">Copernicus RUS</a>	Materials Webinars	Research and user support within the Copernicus program to promote the uptake of Copernicus data (e.g. Sentinel-1) by users and to facilitate research and development among its users by providing data, expert support, computing facilities, lectures, and trainings.
<a href="#">Echoes In Space</a> (formerly SAR-EDU)	Online course Materials	Self-paced learning based videos, tutorials, and community discussions, covering the history and geometry of spaceborne radar imagery, as well as land, water and hazard applications. Developed by Friedrich-Schiller-Universität Jena and EOS-Jena, assisted by the European Space Agency.
<a href="#">Eduspace</a>	Materials	Introduction to remote sensing for secondary school students and their teachers to enter the field of earth observation based on comprehensible materials, satellite images and case studies (including SAR), provided by the European Space Agency.
<a href="#">EO4Society</a>	Courses	Central platform of the European Space Agency to announce and host on-site trainings and webinars on different topics remote sensing for scientists, industry, public and private users.
<a href="#">ESA-CONAE de Formación SAR en bandas L/C/X</a>	Course	Lectures and practical units on radar basics, sensors, and applications, hosted by the Argentinian Comisión Nacional de Actividades Espaciales (CONAE) in cooperation with ESA.

Appendix

<a href="#">ESA land training</a>	Course	Lectures and practical units covering remote sensing of land applications, including multi-temporal radar analysis, surface deformation with persistent scatterers, forest applications with PolInSAR, and SAR-based flood and vegetation mapping. Hosted annually by the European Space Agency.
<a href="#">ESA Tiger / Dragon</a>	Course	Capacity development activities provided by ESA in cooperation with African and Asian partners to tackle regional challenges of global change (water scarcity, environmental hazards, resource management), based on methods of earth observation.
<a href="#">ESA TPM-19</a>	Reading	Open three-part textbook on radar interferometry compiled by ESA. Covering principles (Ferretti et al. 2007c), practical (Ferretti et al. 2007a), and mathematical (Ferretti et al. 2007b) aspects.
<a href="#">GEOS 657</a>	Online course	Lectures and practical units covering all aspects of microwave remote sensing, with a special focus on radar interferometry. Duration of 15 weeks. Includes close supervision, assignments and group projects. Developed by the University of Alaska Fairbanks.
<a href="#">MIT STEM course</a>	Materials	Technically-oriented introduction to radar systems developed by the Massachusetts Institute of Technology (MIT) with a focus on signal processing.
<a href="#">NASA ARSET</a>	Online course Materials	ARSET (Applied Remote Sensing Training) is a collection of online trainings organized by NASA. The topics cover introductory and advanced topics of earth observation, including special courses on radar remote sensing and on monitoring and meeting the UN sustainable development goals.
<a href="#">NASA Earthdata Webinar Series</a>	Webinars	Webinars on different topics of earth observation provided by NASA, including access and use of SAR data (presented by the Alaska Satellite Facility).
<a href="#">NRCAN Tutorial</a>	Materials	Extensive collection of educational materials on SAR polarimetry created by the Canada Centre for Mapping and Earth Observation and Natural Resources Canada.
<a href="#">radartutorial.eu</a>	Materials	Comprehensive and clearly structured materials on radar technologies (including SAR) compiled by C. Wolff. Available in several languages and provided under a Creative Commons license (BY-SA).
<a href="#">REDD+ training</a>	Course Materials	On-site trainings and workshops on forest mapping and use of Sentinel-1 data within the REDD+ project funded by the Regional Development European Fund (FEDER).
<a href="#">SAR Tutor</a>	Materials	Educational materials on radar basics and SAR remote sensing provided by the Fraunhofer Institute of Optronics, System Technologies and Image Exploitation (IOSB) with a modular structure and interactive learning modules (login: student, pw: student).

## Appendix 15 Acquisition costs for VHR SAR imagery

Table 35: Acquisition costs for the tasking of VHR SAR images for the ten largest refugee camps

#	Camp and hosting country	Population (estimated)	Area [km <sup>2</sup> ]	TerraSAR-X				CosmoSkyMed		Radarsat-2		
				SM, 3 m (50x30 km)	SL, 2 m (10x10 km)	HS, 1 m (10x5 km)	ST, 0.25 m (4x2.5 km)	SM, 5 m (40x40 km)	SL, 1 m (10x10 km)	SL, 1 m (18x8 m)	UF, 3 m (20x20 m)	MLF, 3 m (50x50)
1	Kutupalong, Bangladesh	885,000	17	2,950 €	4,250 €	5,950 €	13,900 €	3,000 €	6,000 €	4,000 €	3,600 €	5,200 €
2	Bidibidi, Uganda	285,000	18	2,950 €	4,250 €	5,950 €	13,900 €	3,000 €	6,000 €	4,000 €	3,600 €	5,200 €
3	Dadaab, Kenya	235,000	60	2,950 €	4,250 €	11,900 €	55,600 €	3,000 €	12,000 €	8,000 €	7,200 €	5,200 €
4	Kakuma, Kenya	185,000	35	2,950 €	4,250 €	5,950 €	27,800 €	3,000 €	6,000 €	4,000 €	3,600 €	5,200 €
5	Nyarugusu, Tanzania	140,000	20	2,950 €	4,250 €	5,950 €	13,900 €	3,000 €	6,000 €	4,000 €	3,600 €	5,200 €
6	Jabalia, Gaza	120,000	30	2,950 €	4,250 €	5,950 €	20,850 €	3,000 €	6,000 €	4,000 €	3,600 €	5,200 €
7	Zaatari, Jordan	84,000	10	2,950 €	4,250 €	5,950 €	6,950 €	3,000 €	6,000 €	4,000 €	3,600 €	5,200 €
8	Yida, South Sudan	72,000	20	2,950 €	4,250 €	5,950 €	13,900 €	3,000 €	6,000 €	4,000 €	3,600 €	5,200 €
9	Katumba, Tanzania	66,000	25	2,950 €	4,250 €	5,950 €	13,900 €	3,000 €	6,000 €	4,000 €	3,600 €	5,200 €
10	Pugnido, Ethiopia	65,000	12	2,950 €	4,250 €	5,950 €	6,950 €	3,000 €	6,000 €	4,000 €	3,600 €	5,200 €
	<b>total</b>	<b>2,137,000</b>	<b>247</b>	<b>29,500 €</b>	<b>42,500 €</b>	<b>65,450 €</b>	<b>187,650 €</b>	<b>30,000 €</b>	<b>66,000 €</b>	<b>44,000 €</b>	<b>39,600 €</b>	<b>52,000 €</b>
	Price per person			0,014 €	0,020 €	0,031 €	0,088 €	0,014 €	0,031 €	0,021 €	0,019 €	0,024 €

Sources: Airbus (2014), e-geos (2017), MDA (2016).